Stability of open natural geotextiles

Evaluating the sandtightness of different natural geotextiles by means of physical modelling

by D.T. Akerboom

Stability of open natural geotextiles

Evaluating the sandtightness of different geotextiles by means of physical modelling

Master thesis

By

D.T. Akerboom

In partial fulfilment of the requirements to
obtain the degree of Master of Science at
the Delft University of Technology
Faculty of Civil Engineering and Geosciences
Department Hydraulic Engineering

Student number:	4976053	
Date:	August 8, 2024	
Thesis committee:	Dr. ir. B. (Bas) Hofland,	TU Delft (chairman)
	Prof. dr. ir M.R.A. (Marcel) van Gent,	TU Delft, Deltares
	Ir. J.P. (Jeroen) van den Bos,	TU Delft, Boskalis (supervisor)
	Ing. C. (Coen) Kuiper,	TU Delft, Witteveen+Bos
	R.W. (Robert) Pol,	Van Aalsburg B.V.

Cover: Jute geotextile (photo from Van Aalsburg)

This thesis utilized the intern OpenAI's ChatGPT of Boskalis for writing Python scripts and occasionally for improving grammar and spelling.

Preface

This thesis is the final product of my study in Hydraulic Engineering at the Faculty of Civil Engineering and Geosciences at Delft University of Technology (TU Delft). Over a period of 11 months, from September to August, my research focused on the sandtightness of natural open geotextile filters under the joint supervision of TU Delft, Boskalis, and Van Aalsburg.

I am grateful to Boskalis for allowing me to do my graduation project within their company. I am particularly thankful to Jeroen van den Bos, my daily supervisor, for his invaluable guidance throughout my research. Additionally, I would like to thank Van Aalsburg for facilitating the physical model tests in the laboratory.

I want to express my appreciation to my committee members for their supervision, particularly Bas Hofland, Coen Kuiper, and Robert Pol. The discussions, constructive criticism, and new perspectives I received from my committee members have significantly contributed to shaping my research. I would also like to express my appreciation to Marcel van Gent for joining my committee team at the last minute and providing valuable advice.

I want to extend my appreciation to Arie, Arno, Chantal, and Pieter for their assistance in conducting my tests at the TU Delft laboratory and for their support with equipment and setting up my test set-up.

Lastly, I want to thank my parents, brothers, and friends for supporting me during this period.

Daan Akerboom
Zevenhoven, August 2024

Summary

Geotextiles are widely used in civil engineering, particularly in hydraulic engineering where they serve as filters and protect sand and clay from erosion. Their primary function is to prevent the washout of fine materials from the subsoil. Geotextiles are permeable fabrics and are usually made from plastics like polypropylene and polyethylene. However, due to environmental concerns surrounding synthetic geotextiles, there is a growing interest in moving away from plastics towards natural fibers. To facilitate this transition, understanding the engineering properties of these materials is essential. This study focuses on sandtightness, aiming to make applications more feasible.

Geotextiles can reduce the total thickness of a granular filter and thereby the costs. Because a geotextile can replace multiple granular filter layers, less material is required, which also results in lower emissions. Filters can be distinguished into two categories: geometrically open and geometrically closed filters. Sand particles cannot pass through a geometrically closed filter. The sandtightness is independent of the magnitude of the hydraulic load. Open filters prevent the erosion of the base material up to a certain hydraulic load. Open geotextile filters are not common used in hydraulic engineering.

Previous research has primarily focused on synthetic geotextiles, developing formulas to predict critical filter velocities based on their properties ((Van Der Knaap et al., 1986) and ((Klein Breteler, 1988)). In contrast to these synthetic-focused studies, a study by Lemmens in 1996 on natural geotextiles, such as jute cloth, revealed a critical hydraulic gradient of 0.26, suggesting jute's potential as an alternative to synthetic materials. Despite these findings, stability criteria for natural geotextiles remain undefined, and newly developed geotextiles from natural materials have not yet been tested.

To address this gap, experiments were conducted in a flume set-up at the Fluid Mechanics Laboratory at TU Delft, using both woven and non-woven geotextiles made from natural materials such as jute, hemp, and wool. In the flow flume, a steady current was applied to a one meter long stretch of rock, closed at the top, with a geotextile-covered sand bed beneath it, allowing hydraulic gradients up to $i = 1$ to be exerted. This set-up enabled the determination of the critical load.

A total of 19 tests were conducted with 11 different configurations, involving variations with 7 different types of geotextile (4 woven jute geotextiles and 3 non-woven geotextiles made of hemp, jute, and wool). During all test steps of the 19 tests in the flow flume, measurements of water levels, pressures, and discharge were taken. Two endoscopes were installed at different locations in the filter layer, with holes drilled into two stones to secure the endoscopes. This allowed the camera to be positioned at the top of a pore, providing a view of the geotextile and detecting passing sand grains.

To determine the critical test step where the movement of base material begins, an innovative method of analyzing the erosion state was employed using endoscope images. These endoscopes are capable of detecting sand grains, allowing for the observation of erosion dynamics. In 4 of the 19 tests, the eroded sand was also suctioned after each test step to gain insight into the amount sediment transport. This indicates that even before the critical threshold level, there are small amounts of erosion immediately after increasing the hydraulic load. If the critical threshold level has not yet been reached, this erosion will return to zero during the rest of the test step. When determining the critical test step, two values were used for the critical load: a non-erosion criterion (Ho, 2007) and a criterion of 0.2 gr/s/m² (Klein Breteler, 1988), as used in previous studies to

determine the start of movement. The non-erosion criterion is qualitative, whereas the Klein Breteler criterion is quantitative. It was found that these criteria are not equivalent, with a factor of 2 to 3 difference in the critical filter velocity.

This study concluded that the critical load for sediment transport is primarily determined by the filter velocity for open natural geotextiles. This contradicts previous studies that suggest a critical hydraulic gradient for open natural geotextiles. The critical filter velocity is influenced by the geotextile's characteristics, including thickness, opening size, and water permeability. Notably, the structure of the geotextile itself significantly affects the critical filter velocity. In this study, two woven jute geotextiles (J4: 422 gr/m² and O_{90} = 516.1 µm, J5: 518 gr/m² and O_{90} = 819.0 µm) with different structures were tested. The difference in opening size between the two geotextiles is approximately a factor of 1.5. However, the geotextile with much larger openings had a 1.75 times greater critical filter velocity with a start of movement criterion of 0.2 gr/s/m². Additionally, while the grading and size of the filter layer's grains influenced the critical hydraulic gradient, they had little to no effect on the critical filter velocity, emphasizing the significance of geotextile properties in determining their performance and stability under hydraulic load.

Ultimately, based on the tests, it can be concluded that the newly developed non-wovens could be a good alternative to synthetic geotextiles when considering sandtightness under parallel flow. All three non-wovens are reasonably stable at a hydraulic gradient of $i \approx 1$, which is the maximum gradient that could be applied in our test set-up.

Recommendations for future research include testing with coarser sand, longer test durations, and synthetic counterparts for comparative analysis. Suggested improvements to the test set-up involve detailed height measurements of the sand bed and filter layer, and using high-resolution cameras for better sediment tracking. This sediment tracking by an endoscope can be improved by using a fixed pore for the endoscope for all tests. This can ensure that the pore volume is consistent across all tests and the size of the geotextile section captured in the image is also consistent. There is potential to use endoscope images for quantitative analysis of sediment transport. Further, the study emphasizes examining different flow conditions (perpendicular, and non-stationary) to enhance geotextile designs, particularly in dynamic environments like coastal revetments.

Contents

Nomenclature

Roman symbols

Symbol	Unit	Description
A	[m^2]	area
a	[s/m]	Forchheimer coefficient
B	[m]	width
b	[s^2/m^2]	Forchheimer coefficient
C_r	[-]	coefficient in Klein-Breteler formula
D_f	[m]	filter thickness
d	[m]	diameter
d_{n50}	[m]	nominal diameter exceeded by 50% of the diameters
d_x	[m]	sieve diameter, where x% of the grains has a smaller diameter
e	[-]	empirical coefficient
g	[m/s^2]	acceleration due to gravity [g = 9.81 m/s^2]
h	[m]	water depth
h_k	[m]	water level at two times the weir height, upstream of weir
I	[–]	mobility parameter
I_c	[–]	stability parameter
i	[–]	gradient
i_{cr}	[–]	critical gradient
K	[m/s]	permeability coefficient (Darcy coefficient)
k_g	[m/s]	the permeability coefficient of the geotextile, defined as $v = k_g i^m$
k_n	[m/s]	perpendicular permeability coefficient of the geotextile $v = k_n i$, $i = dh/t_g$
k_b	[m/s]	permeability coefficient of base material
L	[m]	length
m	[-]	exponent in the equation related to the permeability
m	[-]	coefficient in Klein-Breteler formula
n_f	[–]	porosity of filter material
O_{90}	[m]	size of opening which is equal to the particle of size d_{90} of the granular material which passes through the geotextile
P	[N/m^2]	pressure
Q	[m^3/s]	discharge
Re	[-]	Reynolds number
R_T	[-]	correction factor temperature
S	[$gr/s/m^2$]	material transport
t_g	[m]	thickness of geotextile
t	[s]	time
T	[°c]	temperature
U	[m/s]	streamwise velocity (in x-direction)
u_f	[m/s]	filter velocity
$u_{f,cr}$	[m/s]	critical filter velocity
V_{H50}	[m/s]	the velocity at a hydraulic height difference of 50 mm
V	[m^3]	volume
w	[m/s]	fall velocity of base material in water
W	[kg]	weight

Greek symbols

Symbol	Unit	Description
α	[−]	Forchheimer coefficient
β	[−]	Forchheimer coefficient
Δ	[−]	relative density specific submerged density of stone (= $(\rho_s-\rho_w)/\rho_w$)
ρ	[kg/m^3]	density
ρ_w	[kg/m^3]	density of water [ρ_w = 1000 kg/m^3]
ρ_s	[kg/m^3]	density of stones
τ_c	[N/m^2]	critical shear stress
ν_w	[m^2/s]	kinematic viscosity of water (= 1.09*10^{-6} m^2/s at 17 °C)
ψ	[−]	permittivity
ψ_s	[−]	Shields-parameter

Frequently used indices

Symbol	Description
b	base layer, base material
cr	critical
f	filter layer, filter material

Coordinate system

In this thesis the following coordinate system is used:

Left side = the left side looking with the flow direction
Right side = the right side looking with the flow direction

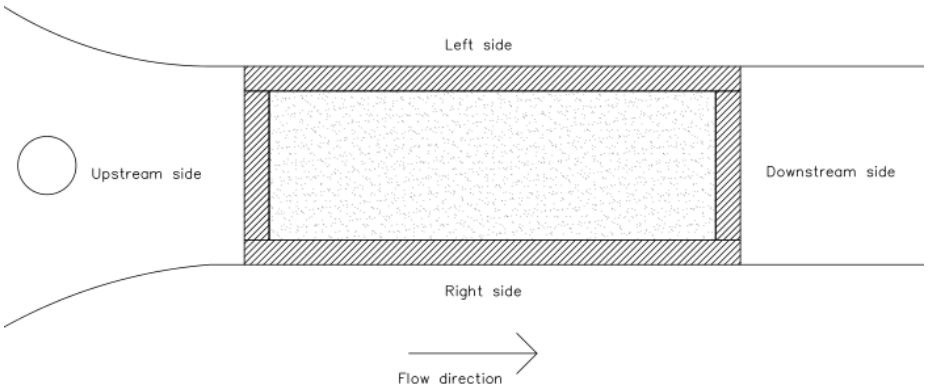

Figure 0-1: Coordinate system

1 Introduction

1.1 Background

Geotextiles are widely used in civil engineering. In hydraulic engineering they are mainly used as filters and to protect the surface against erosion. The main purpose in these situations is to prevent the fine material being washed out. Geotextiles are permeable fabrics and are usually made from plastics like polypropylene and polyethylene. Geotextiles can reduce the total thickness of a granular filter and thereby the costs. Because a geotextile can replace multiple filter layers, less material is required, which also results in lower emissions. Filters can be distinguished into two categories: geometrically open and geometrically closed filters. Sand particles cannot pass the openings in the geotextile when a geometrically sandtight geotextile is used. The sandtightness is independent of the magnitude of the hydraulic load. Open sandtight geotextiles prevent the erosion of the base material up to a certain hydraulic load.

In the past, several studies have been done on the sandtightness and properties of geotextile materials. Most studies have focused on synthetic geotextiles. For example, Klein Breteler has conducted research on the sandtightness of various geotextiles and determined a formula for the critical filter velocity. According to a study by Prambauer, there are several alternatives such as jute and coir as an alternative to synthetic geotextiles (Prambauer et al., 2019). Lemmens confirmed this in 1996 by researching the sandtightness of various natural and synthetic geotextiles in a flume with uniform flow conditions. He determined the critical gradient of various natural geotextiles as the head loss corresponding to the threshold at which sandy material passed through the geotextile.

Rijkswaterstaat has set itself the goal of working circularly in 2030 (Rijkswaterstaat, 2023). This means working without waste and reusing raw materials. Rijkswaterstaat has set the ambition that by 2030 at least 50% of the geotextiles to be used in water construction will be biobased (NABB, 2023). Biobased building material is material that consists of at least 70% renewable mass, determined according to EN16575:2014 (NABB, 2023). The next step is a fully circular economy by 2050. When removing geotextiles, damage often occurs, making reuse impossible. Recycling synthetic geotextiles is difficult as many different types of plastics are used and it is not yet commercially attractive to undertake (Van Dijk, 2018). The recent years have seen increasing doubts about the use of synthetic geotextiles. Exposure of a geotextile to UV radiation, oxidation, temperature, chemical agents, and biological agents can damage the geotextile and shorten its lifespan. Bai et al. (2022) has shown through practical research that exposure to solar illumination increases the risk of releasing microfibers.

This study aims to determine the sandtightness of natural fiber geotextiles under a single layer of granular material with a parallel flow. The geotextile filter construction and can be identified as an open filter. Other criteria of the geotextiles such as durability are not considered in this report.

1.2 Problem description

Using a geotextile in a filter layer can significantly reduce the thickness and cost of this layer. To create a stable open geotextile filter construction, the mobility parameter must be lower than the stability parameter. This ensures that the filter construction is stable and no erosion will occur.

The current open filter design guidelines for open geotextiles are based on scale tests performed in 1988 by Klein Breteler. He developed a formula to calculate the critical filter velocity based on the properties of the base material and geotextile (water permeability, thickness and opening size).

However, jute geotextiles have different properties than synthetic geotextiles, such as larger thickness with the same opening size and a woollier fiber structure. Currently there are no stability criteria for modern jute geotextile. Lemmens (1996) tested only one type of woven geotextile with unknown properties. Therefore, it is not possible to determine if the currently designed jute geotextiles have the same critical load. At the moment, there are several types of jute woven geotextiles and natural non-woven geotextiles on the market for which the critical load is not known. It is still uncertain whether the critical gradient (Lemmens) or critical filter velocity (Klein Breteler) is the correct approach to describe the critical load for open (natural) geotextiles.

1.3 Objective and research questions

The aim of this thesis it to expand the knowledge on the stability of natural open geotextile filters under a parallel uniform flow. By executing physical model tests and analysing the results, it will be attempted to find design criteria.

The research will be conducted using multiple research questions, the main question is the following:

What are the stability criteria for natural open geotextile filters for a situation where a single granular filter layer with geotextile experiences a flow velocity parallel to the filter structure?

The following questions are answered to come to the answer of the main question are:

Q.1. What is the critical load for open geotextile filters?
Q.2. What are the critical filter velocities of the different geotextiles under uniform parallel flow?
Q.3. How does the grading and grain size of the filter layer influence the critical hydraulic gradient and critical filter velocity?
Q.4. How does the opening size of the geotextile influence the critical hydraulic gradient and critical filter velocity?
Q.5. How does the thickness of a non-woven geotextile influence the critical hydraulic gradient and critical filter velocity?

1.4 Thesis outline

The report begins with a review of relevant literature and theoretical background of the stability of open geotextiles in chapter 2. Chapter 3 presents the model test set up, while chapter 4 presents the results of the tests. Chapter 5 presents the analysis of the test results. Chapter 6 offers the discussion of the findings. Chapter 7 serves as the concluding section, where the research objective is evaluated, and all research questions are thoroughly addressed. The final chapter, chapter 8, offers recommendations for further research.

2 Literature review

In this chapter the first phase of the design cycle is described: the problem analysis. The aim of this stage is to define the problem and find the objective of this thesis. This is accomplished by looking at the theory of the problem. In this chapter a review is given of the stability of granular open filters, the criteria of geotextiles and the stability of open geotextile filters.

2.1 Stability of granular filters

Granular filters are used to protect the subsoil against erosion and scour. There are two types of granular filter: a geometrically open filter and a geometrically closed filter.

The design of a granular filter can be based on the critical gradient in porous flow, above which grains from the base layer are no longer stable under the filter layer. The gradient is a relation between load and strength: I=DH/L, where the head difference is the load and the length as the strength

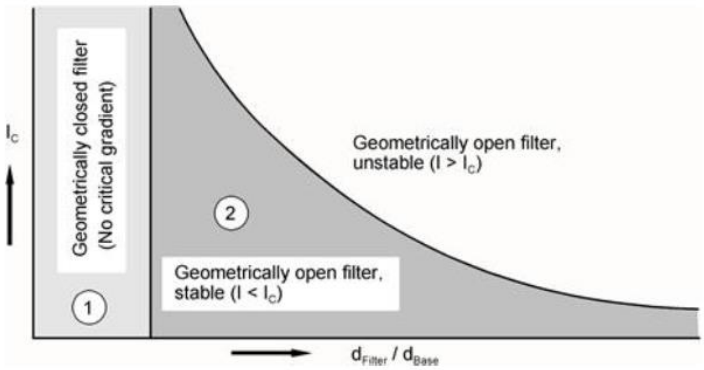

Figure 2-1: Possible design criteria for granular filters (Schiereck, 2012)

Figure 2-1 gives a graphical distinction of the two stable filter structures. The *I* can be seen as mobility parameter and I_c as a stability parameter. Geometrically closed filters are always stable, independently of the porous flow through the filter. While geometrically open filters are unstable when the mobility parameter is larger than the stability parameter. Since this study is focused on stable geometrically open filters, the geometrically closed filter and unstable open filter will only be briefly discussed.

2.1.1 Shields

Shields (1936) investigated the stability of a sand bed under uniform flow conditions. His approach takes into account the friction force caused by water on the bed. If a certain value is exceeded, the grains will start to move. The critical value of the (shear) velocity is described with the stability parameter ψ_c, the Shields parameter. This relation is shown below (Shields, 1936):

$$\psi_c = \frac{\tau_c}{(\rho_s - \rho_w)gd} = \frac{u_{*c}^2}{(\rho_s - \rho_w)gd} \tag{2.1}$$

2.1.2 Geometrically closed filter

The stability of a geometrically closed filter is determined by the geometrical properties of the filter material. The size of the grains is chosen such that the grains cannot move in the filter. Which means that the finer grains are blocked by the coarser grains (Figure 2-2). A stable and permeable filter can be designed with the following rules:

Stability criterion (Terzaghi & Peck, 1948):

$$stability: \frac{d_{f15}}{d_{b85}} < 4 \tag{2.2}$$

Permeability (CIRIA et al., 2012):

$$permeability: \frac{d_{f15}}{d_{b15}} > 1 \tag{2.3}$$

Internal stability criterion (Pilarczyk, 1988):

$$int.stability: \frac{d_{60}}{d_{10}} < 6 \tag{2.4}$$

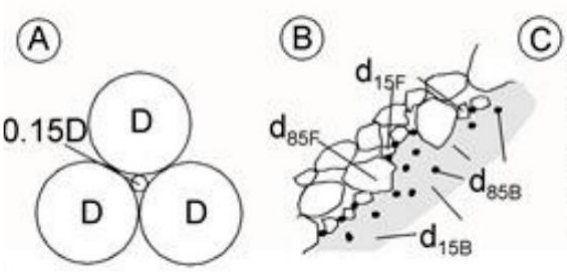

Figure 2-2: principle of geometrically closed filter (Schiereck, 2012)

2.1.3 Geometrically open filter

The material of the base layer could be transported through the filter layer when a geometrically open filter is applied. The grains of the base layer can move in and through the filter layer. There will be only erosion when the load is higher than some critical value. The filter is stable when the critical gradient is larger than the occurring gradient and unstable when the load is larger than the strength. Importantly, with an unstable open filter, some loss of material is accepted within acceptable allowed settlements.

Critical hydraulic gradient

The critical hydraulic gradient (i_{cr}) is the gradient at which base material motion sets in (De Grauw et al., 1983). The critical hydraulic gradient is a function of the base material characteristics, filter material characteristics and the flow type. The hydraulic gradient is relation between the load and strength. The head pressure is the load and the length can be interpreted as the strength (Schiereck, 2012). The filter is stable when the occurring gradient is smaller than the critical gradient. The critical gradient can be calculated with the following equation (De Grauw et al., 1983):

$$i_{cr} = \left[\frac{0.06}{n_f^{\frac{4}{3}} d_{f15}^{\frac{1}{3}}} + \frac{n_f^{\frac{5}{3}} d_{f15}^{\frac{1}{3}}}{1000 d_{b50}^{\frac{5}{3}}} \right] \cdot u_{*cr}^2 \tag{2.5}$$

The first term corresponds with the laminar term and the second term with the turbulent term. The filter velocity (u_{*cr}) for sand can be calculated with the flowing equation (De Grauw et al., 1983):

$$u_{*cr} = 1.3 d_{b50}^{0.57} + 8.3 \cdot 10^{-8} \cdot d_{b50}^{-1.2} \tag{2.6}$$

In which:

u_{*cr} = critical shear velocity of base material [m/s]
d_{b50} = diameter of bed material exceeded by 50% (mass) (m)
d_{f15} = diameter of filter material exceeded by 85% (mass) (m)
i_{cr} = critical hydraulic gradient [-]
n_f = porosity of filter material [-]

Filter velocity and Forchheimer equation

The filter velocity can be calculated with the following formula:

$$u_f = \frac{1}{A}\iint u dA = n \cdot u \quad \left(n = \frac{V_p}{V_T}\right) \tag{2.7}$$

In which *n* is the porosity and u the real velocity in the pores. The porosity, *n*, can be defined as the pore volume, V_p, dived by the total volume V_T.

After combining all square inertia and turbulence terms in one quadratic friction term and replacing the (linear) viscous gradient with a linear friction term, the Forchheimer equation appears (Van Gent, 1992):

$$\frac{1}{pg}\frac{\partial p}{\partial x} = i = au_f + bu_f|u_f| + c\frac{\partial u_f}{\partial t} \tag{2.8}$$

With:

$$a = \alpha\frac{\left(1-n_f\right)^2}{n_f^3}\frac{\upsilon_w}{g d_{n50}^2} \tag{2.9}$$

and,

$$b = \beta\frac{\left(1-n_f\right)}{n_f^3}\frac{1}{g d_{n50}} \tag{2.10}$$

For stationary flow ($\partial u_f/\partial t = 0$), equation (2.8) is the classical Forchheimer-equation. The flow through fine material is laminar. The relation between the hydraulic gradient, *i,* and the filter velocity, u_f, is linear, indicating that the relation is described by the first term of the right-hand side of Equation (2.8). For a turbulent porous flow, as in coarser material, the relation is quadratic, indicating that the second term dominates. For material ranging in between, as for gravel, both terms play a role (Schiereck, 2012).

Based on permeability measurements, Van Gent (1993) determined that a value of 1000 for alpha and a value of 1.1 for beta can be used as a first estimate ((Van Gent, 1993) and (Van Gent, 1995)).

Past study: Design rules for the interface between granular filter and base (1987)

This study determined the critical filter velocity for different base materials and filter materials. A dry sand transport of 0.2 gr/s/m, was used as critical threshold level. The critical filter velocity is defined as: "The critical filter velocity, u_{fcr} , is the maximum velocity in the filter at which the sediment motion is such that the stability of the total structure is not yet in danger. This appears, in fact, to be comparable to the criterion used by Shields." (Bezuijen et al., 1987). Based on measurements, the following design rule for the critical filter velocity under uniform flow conditions has derived (Klein Breteler, 1987) ($0.1 < d_{b50} < 1$ mm):

$$u_{f,cr} = \frac{n_f}{e}\sqrt{\psi_s \Delta g d_{b50}}\ with\ e = C_r Re^{-m}\ and\ Re = \frac{u_{f,cr} d_{f15}}{\upsilon_w} \quad (2.11)$$

This results in:

$$u_{f,cr} = \left(\frac{n_f}{C_r}\left(\frac{u_{f,cr} d_{f15}}{\upsilon_w}\right)^m \sqrt{\psi_s \Delta g d_{b50}}\right)^{\frac{1}{1-m}} \quad (2.12)$$

In which:

$u_{f,cr}$ = critical filter velocity, where u_f is the averaged velocity over the cross-section of the filter [m/s]
d_{bx} = the grain size of base material corresponding to x % by weight of finer particles [m]
d_{f15} = diameter of filter material exceeded by 85% (mass)[m]
ψ_s = Shields parameter for base material [-]
g = acceleration due to gravity [m/s²]
n_f = porosity of filter material [-]
e = $C_r Re^{-m}$ [-], (see Table 2-1)
Re = Reynolds number [-]
Δ = relative submerged density of base material = $(\rho_s - \rho_w)/\rho_w$
ρ_s = density of base material [kg/m³]
ρ_w = density of water [kg/m³]
v_w = kinematic viscosity of water [m²/s]

The coefficients ψ_c , m and C_r depend on the grain size of the base material and are given in Table 2-1.

Table 2-1: Values for the coefficients C_r and m and the shields parameter ψ_s for different values of d_{b50} (Klein Breteler, 1987)

d_{b50} [mm]	C_r [-]	m [-]	ψ_s [-]
0.10	1.18	0.25	0.110
0.15	0.78	0.20	0.073
0.20	0.71	0.18	0.055
0.30	0.56	0.15	0.044
0.40	0.45	0.11	0.038
0.50	0.35	0.07	0.036
0.60	0.29	0.04	0.035
0.70	0.22	0.00	0.034
0.80	0.22	0.00	0.034
1.00	0.22	0.00	0.035

Past study: Hydraulic load on a geometrically open filter construction (1988)
This study, by Van Os (1998), focused on the influence of the flow over a filter layer on the erosion of the base layer. He did this by installing a height-adjustable caisson above a filter construction so that a gap is created between the filter construction and the caisson (Figure 2-3). This allows to measure the amount of erosion of the base layer and the pore velocity in the filter layer. After reaching a depth of 1.5 times the grain diameter of the filter material, the average and standard deviation of the pore velocity do not decrease further in the filter layer. The amount of erosion under a thick filter layer is smaller than under a thin filter layer. This can be explained by the large distance between the base layer and flow at the top of the filter layer that a grain of sand has to travel.

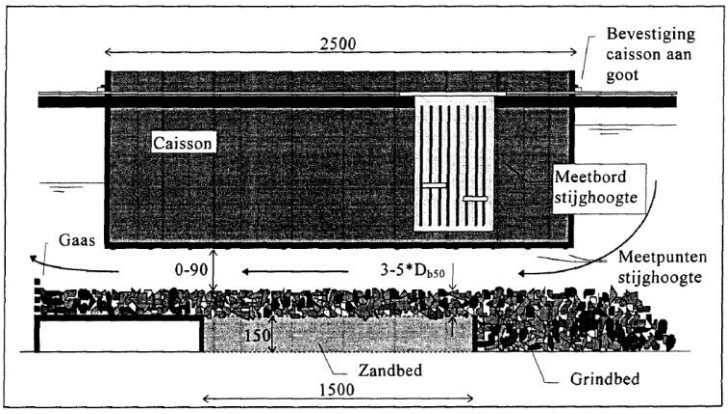

Figure 2-3: Test set-up used by Van Os (Van Os, 1998)

Tests were done with two filter layer thicknesses: 3*d_{f50} (60 mm) and 5*d_{f50} (100 mm). if the caisson is placed directly on the filter (gap height = 0), the critical gradient for motion at the interface between filter and sand is almost the same for both filter layer thicknesses (5.3% for 3*d_{f50} and 5.4% for 5*d_{f50}). This means that there is hardly any influence of the filter thickness. Because with a gap height of 0 cm there is no influence of the flow over the filter structure, the flow through the filter is constant over the height. With increasing gap height, the velocity above the filter layer increases rapidly for a given gradient. The critical gradient decreases with increasing gap height. The thickness of the filter clearly plays a role in the value of the critical gradient. A thicker filter results in a larger critical gradient when a there is velocity above the filter layer. According to a study of Klar (2005) the damping in the filter layer occurs mainly in the first 4 to 5 times the nominal diameter of the granular material.

2.2 Geotextiles

Geotextiles are common used as filters in hydraulic engineering. There are two main types of geotextiles (CUR, 1993):

- Woven; woven geotextile made from yarns or strips, where these semi-finished products have an ordered structure.
- Non-woven: mechanically, chemically or thermally bonded fibers characterized by a random orientation of the fibers.

By applying a geotextile, far fewer layers of stones are needed to make a stable filter. A geotextile is very useful when there is less space and can be cost effective for large project. Figure 2-4 shows a granular filter design and a filter design with a geotextile.

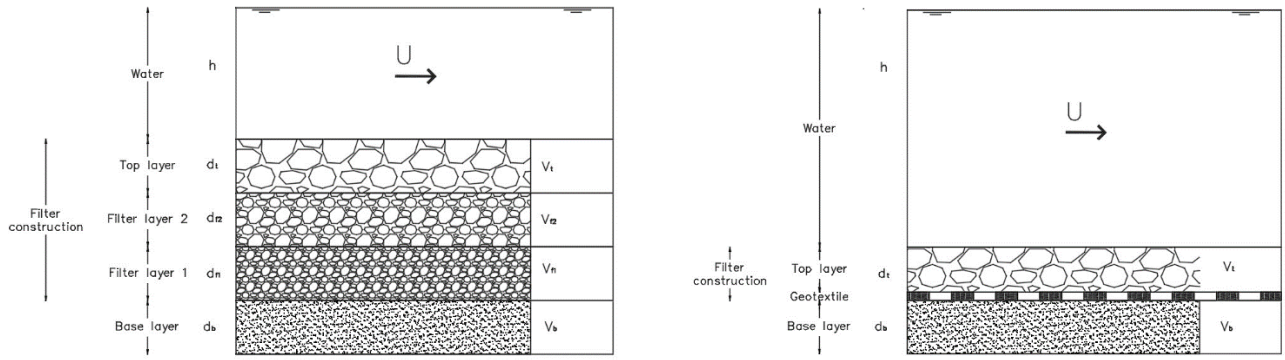

Figure 2-4: Granular filter (left) and geotextile filter (right)

2.2.1 Hydraulic load on bed and banks

The two main flow directions for filters are (Figure 2-5):

- Perpendicular flow
- Parallel flow

With a flow parallel to the interface, the gradient is defined in the filter layer, with a flow perpendicular to the interface, the gradient is defined in the base material.

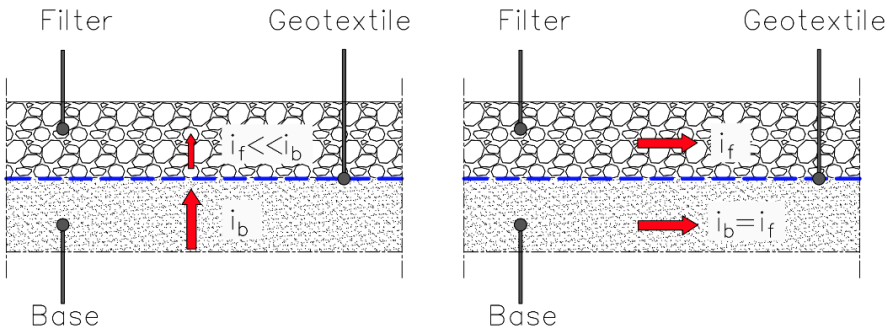

Figure 2-5: Perpendicular and parallel flow in granular filter (adapted from (CUR bouw & infra, 2009))

Parallel flow

Parallel flows in filters can be caused by the flow in rivers, flows behind outflow structures, but flows due to shipping can also occur as a result of:

- Return flow
- Propeller wash

The main flow in the filter layer is parallel to the geotextile. The local flow has a component in the vertical direction caused by the presence of the rock, because the water flows around these obstacles.

Perpendicular flow

A perpendicular flow dominates when the groundwater table within a dike is higher than the outside water level, water will flow out from the dike (Figure 2-6). This will result in a large perpendicular component. Like the groundwater level. Perpendicular currents can be caused by a water level depression caused by a passing ship (Bezuijen & Kohler, 1996) or a rapid drop in the water level in a river due to a decrease in discharge.

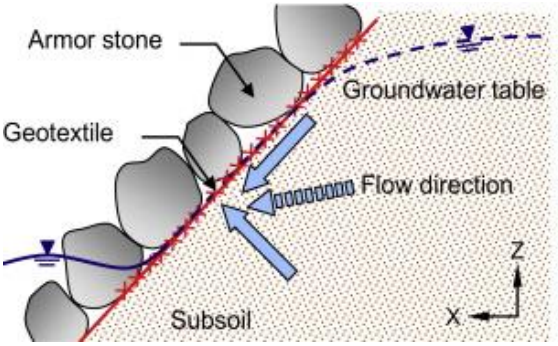

Figure 2-6: Flow perpendicular to the surface (Faure et al., 2010)

2.2.2 Materials of geotextiles

Geotextiles can be made of synthetic fibers or natural fibers. Natural fibers can be made from materials like jute, coconut, hemp and wool.

Synthetic geotextile

Currently, almost all geotextiles used in hydraulic engineering are made of polypropylene or polyethylene. These two raw materials have been widely used in recent decades since the rise of plastic. Before this invention, natural materials were mainly used for geotextiles. Synthetic geotextiles are relatively light and cheap. In recent years, more and more questions have arisen about the environmental impact of synthetic geotextiles. Prolonged solar radiation contact damages geotextiles and reduces their lifetime, which results in the crushing of materials and the release of microfibers (Carneiro et al., 2019).

Jute

The jute fibers that are needed for making a geotextile are mostly obtained from the bast of the species Corchorus olitorius. After harvesting, the jute fibers are extracted from the stalk by retting. These fibers mainly consist of cellulose and lignin (Abdullah, 2013). The tensile strength of jute is 20% higher in wet condition than in dry condition. Jute is a biobased material and biodegradable under natural conditions. This is in contrast to biobased plastics made from polylactide (PLA) that are only biodegradable through industrial composting conditions.

2.2.3 Design criteria geotextiles

There are two main criteria for designing a geotextile: retention and permeability criteria (Moraci et al., 2022). Several additional considerations are required for a suitable design of geotextile filters. Anti-clogging, survivability and durability are mentioned in literature (PIANC, 2011). The two main criteria must be specified for every case where a geotextile is located between the granular armour layer and the sandy base material. If there is a big difference in grain size between the sandy base material and the armour layer, an extra filter layer between these two layers must be placed. This is shown in Figure 2-7.

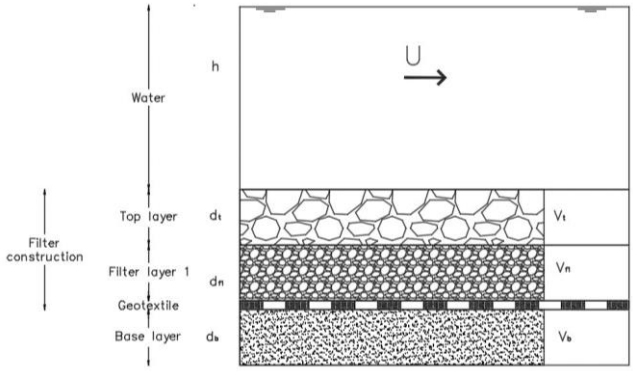

Figure 2-7: Geotextile filter with 2 granular layers

Retention criteria

The sandtightness of a geotextile filter depends on the relation between the properties of the base material and the openings in the geotextile. According to EN12956, the openings of the textile can be characterized by doing a reserve sieve test of the base material. The particle size distribution of the sandy base material is determined after washing through a single layer of textile used as a sieve,

without load. The characteristic opening size, O_{90} or O_{95}, corresponds for example with the d_{90} of the passed fraction.

A common used stability rule for a geometrically closed geotextile filter is (CUR, 1993):

$$\frac{O_{90}}{D_{b90}} \leq 2 \tag{2.13}$$

In many situations, some loss of fine material is not detrimental to the functioning of the filter, since a small layer under the geotextile can act as part of the total filter system (Figure 2-8). The finer parts are washed through the textile and the coarser particles act as a filter for the remaining soil.

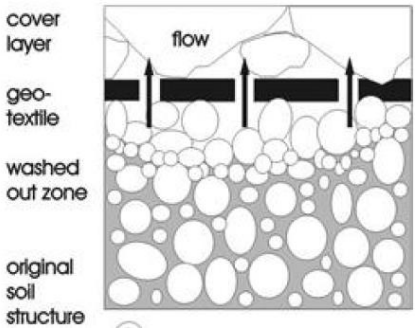

Figure 2-8: Migration of fine particles (Schiereck, 2012)

Permeability criteria

To ensure that there is no pressure build-up under the geotextile, the permeability of the geotextile should be larger than the permeability of the subsoil. A simple rule of thumb is that the permeability of the geotextile should be 10 times larger than that of the subsoil. The permeability of the geotextile can be measured using Darcy's law at the same way as that of soil. The permittivity parameter is often used to characterize the permeability of a geotextile:

$$P = \frac{u_f}{\Delta h} = \frac{k_n}{t_g} \tag{2.14}$$

In which is Δh is the head difference, u_f is the filter velocity, t_g is the thickness of the geotextile and k the "normal" permeability coefficient. P can be seen as the permeability per m thickness of the geotextile. The minimum water permeability of a geotextile depends on the soil and can be calculated with the values from Table 2-2 and the formula below:

$$k_g \geq C_m \times k_b \tag{2.15}$$

Table 2-2: Permeability of different soil types (CUR bouw & infra, 2009)

Soil type	C_m **[-]**	d_{b50} **[mm]**	k_b **[m/s]**
Clay	100	$< 2*10^{-3}$	$10^{-10} – 10^{-8}$
Silt	100	$2*10^{-3} – 63*10^{-3}$	$10^{-8} – 10^{-6}$
Sand	10	$63*10^{-3} – 2$	$10^{-6} – 10^{-3}$
Gravel	10	2 – 63	$10^{-3} – 10^{-1}$

Other criteria

In addition to the two important criteria, there are also a few other criteria for geotextiles. One of these criterion is blocking. Blocking occurs when large particles seal the openings in the textile. This can decrease the permeability significantly.

Clogging is the trapping fine particles in the opening of the textile leading to a decrease of permeability. This can happen when water is contaminated with chemicals, e.g. Iron. Clogging is a time-dependent process. Clogging mainly occurs with non-woven geotextiles.

Another criterion is serviceability. This criterion is aimed at the installation of the geotextile. Damage of the textile during installation is not allowed. The textile must be resistant for placing the cover layers. According to CUR 174, the maximum drop height of the stones is limited and depends on the rock grading. If this height is exceeded, a protective layer of gravel must be applied. The lifetime of a geotextile is influenced by various factors, including UV radiation, oxidation, temperature chemical agents and biological agents (CUR building & infrastructure, 2012) (Bai et al., 2022). The environmental conditions are important for geotextiles.

2.2.4 Stability of open geotextiles

Open geotextiles prevent the erosion of the subsoil up to a certain hydraulic load. This load is described by the (pressure potential) gradient, i, or the filter velocity u_f (discharge per unit flow area), in the filter layer on top of the geotextile. The erosion mechanism of sand grains under a geotextile is basically the same as the erosion mechanism on the bottom of a river. In both cases there is a shear stress, induced by the flow near the bottom, which causes a horizontal force (and vertical lift force) on the particles. At a certain flow velocity, the flow-induced force (shear stress) exceeds the friction and gravity forces, leading to the start of transport. We consider a situation as presented in Figure 2-9, with a geotextile on a subsoil of sand and under a layer of rock to describe the physical processes involved in the behaviour of the subsoil under a geotextile. The main flow in the rock layer is assumed to be parallel to the geotextile. In spite of this, the local flow has a component in the vertical direction caused by the presence of the rock, because the water flows around these obstacles. This also happens near the geotextile, where the water flows through the geotextile, picks up sand grains and transports them into the rock layer. This transport mechanism can only take place if the hydrodynamic forces on the sand grains allow the initial transportation and, furthermore, if the mesh width of the geotextile is large enough to let the particles pass (Pilarczyk, 2000).

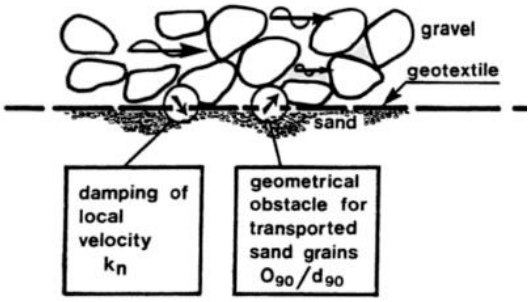

Figure 2-9: Erosion mechanism (Klein Breteler & Verheij, 1990)

The diagram in Figure 2-10 visualizes the transport mechanism and shows the aspects influencing the transport. The depicted mechanism indicates that the geotextile decreases the hydraulic load on the sand interface.

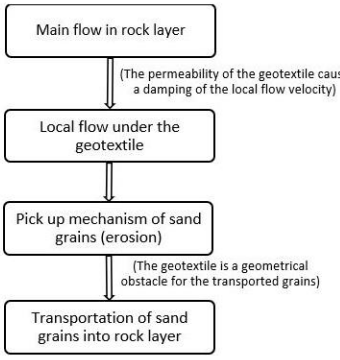

Figure 2-10: Various stages in transport (Klein Breteler & Verheij, 1990)

2.2.4.1 Past studies on the stability of synthetic open geotextiles under parallel flow

In the past, multiple studies have been done on the critical gradients and critical filter velocities of synthetic open geotextiles.

Design criteria for Geotextiles beyond the sandtightness requirement (1986)

This study, by Van Der Knaap et al. (1986), focused on the hydraulic gradients and filter velocities of different geotextiles. A transport rate of 0.15 gr/s/m was chosen as criterion for the threshold of sediment transport. This value was chosen for the following reason: "This criterion roughly corresponds with the criterion used by Shields." (Van Der Knaap et al., 1986). Two tests were executed with the same geotextile (Table 2-3) but different filter diameters (T3: d_{f50}=24 mm and T4: d_{f50} =14.3 mm). This results in nearly the same critical filter velocity for both tests but a 40% lower critical gradient. Based on the test results, an empirical formula has been formulated to calculate the critical filter velocity:

$$u_{f,cr} = \left(4\left(\frac{d_{b90}}{O_{90}}\right)\left(\frac{v_{*cr}}{k_n}\right)^{\frac{1}{2m}} + \frac{n_f}{k}\right)\sqrt{\psi_s \Delta g d_{b50}} \qquad (2.16)$$

In which:

$u_{f,cr}$ = critical filter velocity [m/s]
d_{bx} = grain size of base material corresponding to x % by weight of finer particles [m]
O_{90} = pore size of geotextile corresponding to the average diameter of the sand standardized fraction, of which 90 % remains on the geotextile [m]
t_g = thickness of geotextile [m]
ψ_s = Shields parameter for base material [-]
g = acceleration due to gravity [m/s²]
k_n = filter velocity through geotextile without sand or gravel [m/s]
k = permeability of gravel [m/s]
m = exponent in the equation related to the permeability [-]
n_f = porosity of filter material [-]
Δ = relative submerged density of base material = $(\rho_s - \rho_w)/\rho_w$
ρ_s = mass density of sand [kg/m³]
ρ_w = mass density of water [kg/m³]
v_{*cr} = critical shear velocity the Shields parameter [m/s] (=$\sqrt{\psi_s \Delta g d_{b50}}$)

Table 2-3: The critical filter velocity, $u_{f,cr}$, related to geotextile and subsoil characteristics (Van Der Knaap et al., 1986)

Test	Geotextile							Base material		Filter		Parameters			results	
	number	type	O_{90} [mm]	O_{98} [mm]	t_g [mm]	k_n [mm/s]	m [-]	d_{b50} [mm]	d_{b90} [mm]	d_{f50} [mm]	n_f [-]	$\frac{O_{90}}{d_{b90}}$	$\frac{t_g}{d_{b90}}$	$\left(\frac{w}{k_n}\right)^{\frac{1}{m}}$	$u_{f,cr}$ [mm/s]	i_{cr} [-]
3	N66373	G	0.52	0.55	0.68	5.0	1.0	0.15	0.22	24	0.42 - 0.43	2.36	-	-	52	0.22
4	N66373	G	0.52	0.55	0.68	5.0	1.0	0.15	0.22	14.3	0.42 - 0.43	2.36	-	-	49	0.32

Sandtightness of geotextiles as a function of hydraulic load (1988)

In this research conducted by Klein Breteler (1988), various geotextiles were tested for their sandtightness. The filter velocity was gradually increased, and the migration of subsoil particles was measured to determine the critical filter velocity at which subsoil erosion occurred. After each test step, the average sand transport was measured by suctioning the sedimented sand downstream from the model section, drying it, and weighing it. A transport rate of 0.2 gr/s/m was used as the threshold criterion for sediment transport.

Klein Breteler observed that the method of increasing the critical load has a significant effect on the size of the sand transport. When the filter velocity is increased in several large steps, the sand transport is clearly larger than when the same filter velocity is reached in small steps. It was also observed that with a constant filter velocity, the sand transport decreases significantly.

To validate the assumption that erosion is primarily influenced by the filter velocity, three tests (T5, T8, and T10) were conducted using the same sand and geotextile but with different filter materials. The results of these tests (Table 2-4) showed that the critical filter velocity varied within the margin of test accuracy (51, 53, and 49 mm/s respectively), while the critical gradient varied significantly (23%, 24%, and 33% respectively).

Additionally, a test (T16) was performed using the same geotextile but with finer sand. This resulted in a decrease in the critical filter velocity by 33% to 35 mm/s compared to test 8. More tests results are shown in appendix A.2.

Table 2-4: Important test results (Klein Breteler, 1988)

Test	Geotextile							Base material		Filter		Parameters			results	
	number	type	O_{90} [mm]	O_{98} [mm]	t_g [mm]	k_n [mm/s]	m [-]	d_{b50} [mm]	d_{b90} [mm]	d_{f15} [mm]	n_f [-]	$\frac{O_{90}}{d_{b90}}$	$\frac{t_g}{d_{b90}}$	$\left(\frac{w}{k_n}\right)^{\frac{1}{m}}$	$u_{f,cr}$ [mm/s]	i_{cr} [-]
T5	N66373	G	0.52	0.55	0.68	5.0	1.0	0.15	0.22	20	0.42 - 0.43	2.4	3.1	1.8	51	0.23
T8	N66373	G	0.52	0.55	0.68	5.0	1.0	0.15	0.22	20	0.42 - 0.43	2.4	3.1	1.8	53	0.24
T10	N66373	G	0.52	0.55	0.68	5.0	1.0	0.15	0.22	11	0.42 - 0.43	2.4	3.1	1.8	49	0.33*
T16	N66373	G	0.52	0.55	0.68	5.0	1.0	0.096	0.13	20	0.42 - 0.43	4.0	5.2	1.0	35	0.13
* a value of 0.49 was mentioned in the report of 1988, but this value is not in accordance with the data in table 1 of the report																

The empirical formula of van der Knaap et al. (1986), is adapted with the test results. The influence of the geotextile thickness is introduced and the permeability parameter is changed:

$$u_{f,cr} = \left(12\left(\frac{t_g}{d_{b90}}\right)\left(\frac{d_{b90}}{O_{90}}\right)^4\left(\frac{w}{k_g}\right)^{\frac{1}{2m}} + \frac{n}{e}\right)\sqrt{\psi_s \Delta_b g d_{b50}} \qquad (2.17)$$

In which:

$u_{f,cr}$ = critical filter velocity [m/s]
d_{bx} = the grain size of base material corresponding to x % by weight of finer particles [m]
d_{f15} = diameter of filter material exceeded by 85% (mass)[m]
O_{90} = the pore size of geotextile corresponding to the average diameter of the sand standardized fraction, of which 90 % remains on the geotextile [m]
t_g = thickness of geotextile [m]
ψ_s = Shields parameter for base material [-]
g = acceleration due to gravity [m/s²]
k_g = the permeability coefficient of the geotextile, defined as $v_g = k_g i_g$ [m/s]
m = the exponent in the equation related to the permeability [-]
n_f = porosity of filter material [-]
e = $C_r Re^{-m}$ [-], (see Table 2-1)
Re = Reynolds number = $u_{f,cr} d_{f15}/v_w$ [-]
Δ = relative submerged density of base material = $(\rho_s - \rho_w)/\rho_w$ [-]
ρ_s = density of base material [kg/m³]
ρ_w = density of water [kg/m³]
v_w = kinematic viscosity of water [m²/s], (see Table A-1)
w = fall velocity of base material in water [m/s] =

$$\frac{\Delta g d_{b15}^2}{18 v_w} \quad \text{if } d_{b15} \le 0.1 \text{ mm}$$

$$\frac{10v}{d_{b15}}\left(\sqrt{\left(1+\frac{\Delta g d_{b15}^3}{100 v_w^2}\right)}-1\right) \quad \text{if } d_{b15} > 0.1 \text{ mm}$$

The formula is derived from a small number of tests with woven geotextiles on a subsoil of fine sand and therefore should not be used outside the range: $0.1 < d_{b50} < 0.2$ mm.

The formula shows that the critical filter velocity mainly depends on the d_{b90}/O_{90} ratio. The structure of the fabric affects the critical filter velocity. A tape fabric can withstand a larger hydraulic load than a mesh netting geotextile with an equal O_{90}. To account for this, the permeability of the geotextile has been added to the formula. The test results show that a certain mesh netting geotextile prevents erosion up to the same critical filter velocity as a tape fabric with approximately 20 to 40% larger openings.

Using the above formula, Klein Breteler has derived a design graph (Figure 2-11) for a gradient parallel to the interface of the filter with a filter layer of granular material.

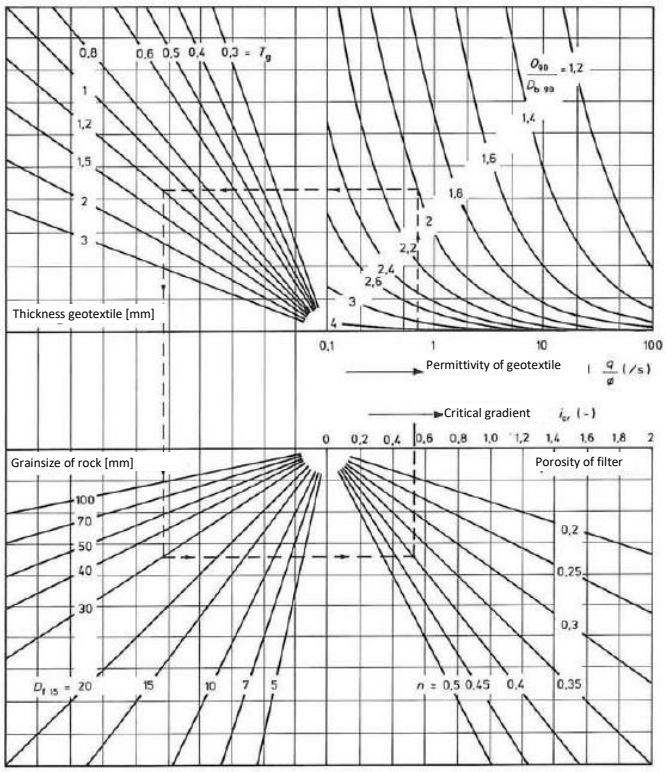

Figure 2-11: Determination of the critical gradient (only valid for woven geotextiles on non-cohesive sand with $0.1 < d_{b50} < 0.2$ mm) (adapted from (CUR, 1993))

Performance of geotextiles on clay and fine sand in bed and bank protections (1994)

In this study, research was conducted on the impact of the thickness of non-wovens on the critical loading for non-woven geotextiles on clay. Tests were performed with two geotextiles to determine the critical loading, where 3 layers of geotextile were stacked on top of each other. For the geotextile S201, this resulted in a much greater filter velocity than with a single layer (Table 2-5). However, with the geotextile PHB3, the opposite effect was observed.

Table 2-5: Influence of thickness on critical load non-woven geotextiles (Klein Breteler et al., 1994)

Test	Subsoil	Geotextile					Filter		results	
		number	type	O_{90} [mm]	t_g [mm]	k_n [mm/s]	d_{f15} [mm]	n_f [-]	$u_{f,cr}$ [m/s]	i_{cr} [-]
11	Medium clay < 2 µm: 22% d_{50} = 42 µm d_{90} = 100 µm	PHB3	nw	0.183	1.3	4.2	55		0.46	2.8
12		PHB3	nw	0.183	1.3	4.2	55		0.32	1.5
13		PHB3	nw	0.183	4	-	55		0.28	1.2
16	Poor clay < 2 µm: 20% d_{50} = 130 µm d_{90} = 400 µm	S201	nw	0.161	3.3	5.1	55		0.27	1.1
17		S201	nw	0.161	10	-	55		0.54	3.8

Applied geotextile research (1995)

In this study, by Van Der Meulen and Smith (1995), the critical filter velocity and critical gradient of various geotextiles were investigated on clay and fine sand. During the experiments, the concentration was measured in g/L. These concentration measurements were converted into a transport rate using the filter velocity, the flow area of the tunnel, and the effective width of the geotextile. A transport rate of 0.2 gr/s/m was used as the threshold criterion for sediment transport.

In this study, it was observed that increasing the load resulted in a significant increase in the concentration signal during the first 1 to 2 minutes. After this short period, the signal slightly decreased and remained constant until the next increase. The reason for the initial increase and subsequent decrease in the concentration signal may be attributed to the washout of easily erodible particles. The particles which have the stronger resistance are not eroded and stay in place, whereas the weakest are eroded.

The study found that the thickness of a non-woven geotextile with a thickness less than 5 mm on a sandbed (appendix A.4) influenced the critical gradient and critical filter velocity. However, this conclusion is only partially based on tests conducted with geotextiles with a small O_{90}, which can be considered as geometrically closed.

The critical gradient was found to depend on the grain size of the filter, while the critical filter velocity showed no dependence on it. The influence of the cohesion of clay on the critical gradient is stronger than the influence of the different geotextile parameters provided that the geotextile is geometrically open. More tests results are shown in appendix A.4.

Table 2-6: The critical filter velocity, $u_{f,cr}$, related to geotextile and subsoil characteristics (Van Der Meulen & Smith, 1995)

Test	Geotextile						Base material		Filter		results	
	number	type	O_{90} [mm]	t_g [mm]	k_n [mm/s]	m [-]	d_{b50} [mm]	d_{b90} [mm]	d_{f50} [mm]	n_f [-]	$u_{f,cr}$ [mm/s]	i_{cr} [-]
105	NF180	w	0.183	0.68	1.4	0.7			75		400	2.6
302	NF180	w	0.183	0.68	1.4	0.7			22		300	Circa 6
303	NF180	w	0.183	0.68	1.4	0.7			145		320	1.5
102	S201-3	nw	0.120	2.7	5.4	0.96			75		0.35	2.2
301	S201-3	nw	0.120	2.7	5.4	0.96			8		0.2	Circa 6.5

The erosion behavior of revetment using geotextile (2007)

In this research by Ho (2007), 3 different woven geotextiles were tested to determine their critical filter velocity. He measured the turbidity during the entire test and introduced 3 different states of erosion: non-erosion state, steady erosion state and failure erosion state:

1) Non-erosion state:
   After reaching the peak water turbidity in the initial stage, if no further soil particles are washed out by water, the water turbidity will gradually decrease over time. Figure 2-12 (a) illustrates that the water turbidity eventually decreases to zero, indicating that the water outflow becomes clean without any soil particles and no soil erosion occurs. Therefore, under this condition, the soil remains in a non-erosion state.

2) Steady erosion state:
   Figure 2-12 (b) shows that the water turbidity decreases but does not reach zero after the peak turbidity. The residual turbidity remains constant over time. Additionally, by observing the soil through the observation window of the cell room, it is evident that particles are being transported by the flow. This indicates that the subsequent water outflow contains a fixed amount of soil particles. In other words, the sub-soil is being eroded, and the erosion rate remains constant under the fixed filter velocity. Therefore, it can be concluded that the soil is in a state of steady erosion.

3) Failure erosion state:
The water turbidity increases as the flow velocity increases. Figure 2-12 (c) illustrates that when the flow velocity remains constant, the water turbidity is high and exhibits irregular variations over time. This indicates that the water contains a significant amount of soil particles. Furthermore, during testing, it is observed that the soil undergoes noticeable erosion.

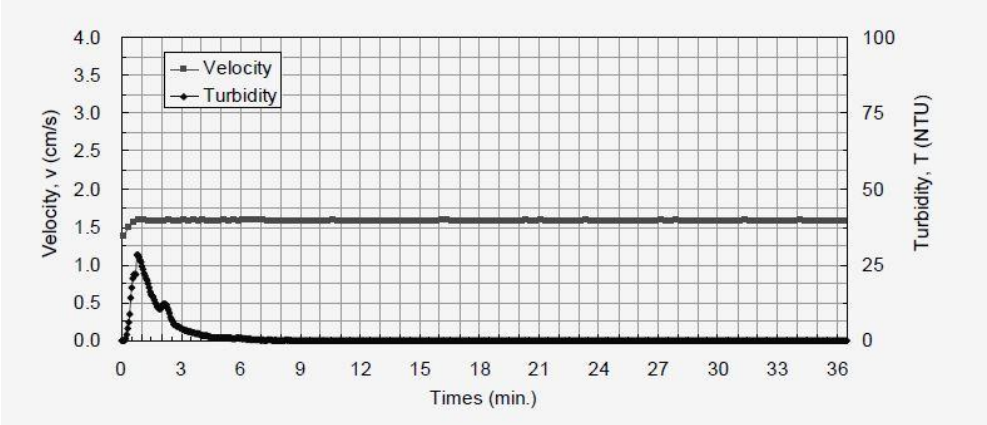

(a) Non erosion state

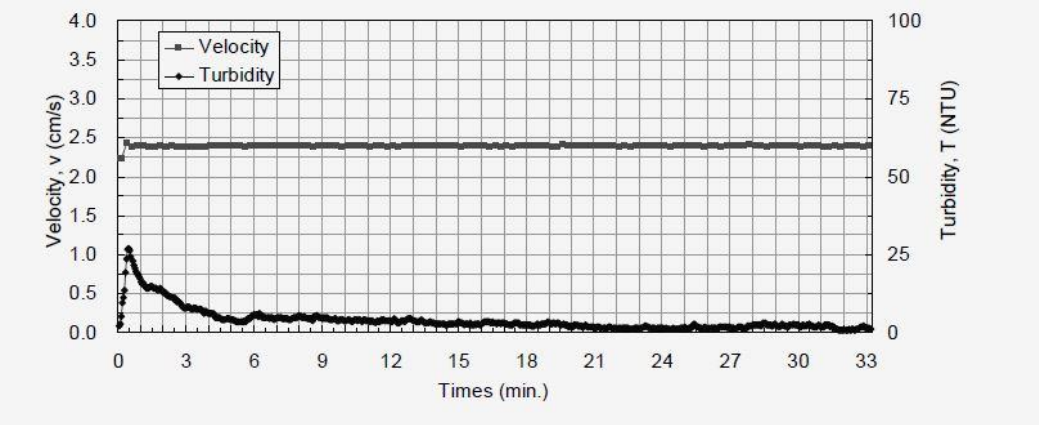

(b) Steady erosion state

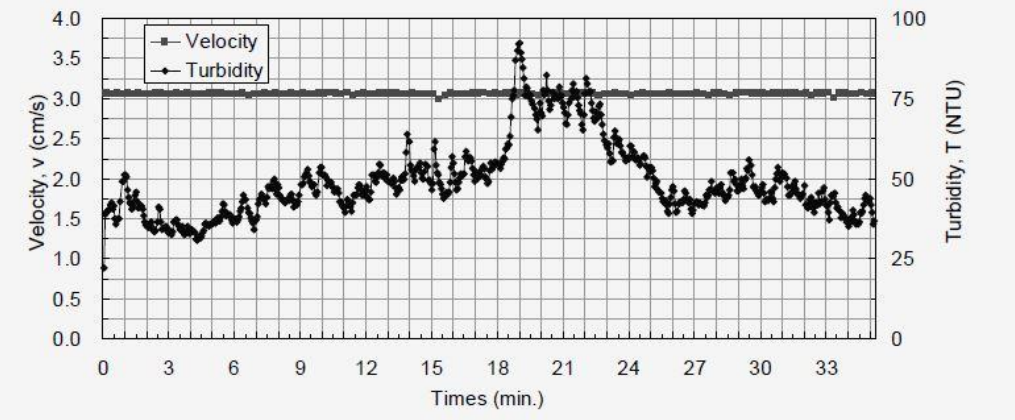

(c) Failure erosion state

Figure 2-12: Types of base material erosion states (Ho, 2007)

Looking at the turbidity during the tests, it is clearly visible that as the load increases, the turbidity also increases. If the critical filter velocity has not been reached yet, the turbidity will decrease to 0. However, if the filter velocity in the test step is larger or equal to the critical filter velocity ($u_{f,cr}$),

steady erosion will occur. The critical filter velocity is defined as the velocity when the soil begin to erode. The filter velocity when the soil situated between steady erosion and failure erosion is named the failure filter velocity ($u_{f,f}$). Figure 2-13 shows an example of the variation of water turbidity and the flow velocity with time. The same pattern can also be observed when no geotextile is present (Figure 2-14).

Ho reasoned that the sudden increase in hydraulic load washed away the soil particles that adhered to the surface of the filter material or deposited in the water pipe, caused the transient increase of water turbidity.

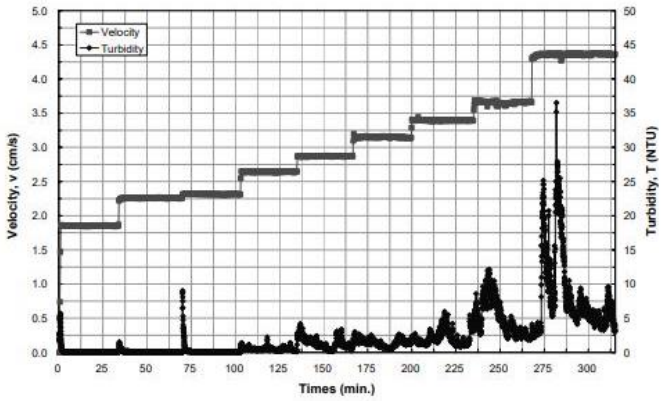

Figure 2-13: The variation of turbidity and filter velocity with time with geotextile, $u_{f,cr}$= 2.6 cm/s (Ho, 2007)

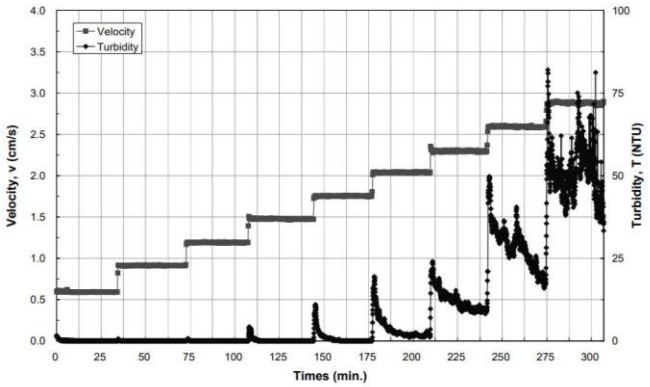

Figure 2-14: The variation of turbidity and filter velocity with time without geotextile, $u_{f,cr}$= 2.0 cm/s (Ho, 2007)

2.2.4.2 Past studies on the stability of natural open geotextiles under parallel flow

In the past, multiple studies have been done on the critical gradients of natural open geotextiles.

Lemmens (1996)

Lemmens (1996) was one of the first who executed model test to find the critical gradient of various natural materials. A water level difference was made with a caisson in the middle of a sand bed (Figure 2-15). By increasing the water level until there is a significant transport of sandy base material through the geotextile, the critical gradient can be determined for each fiber. The start of sand transport was determined visually.

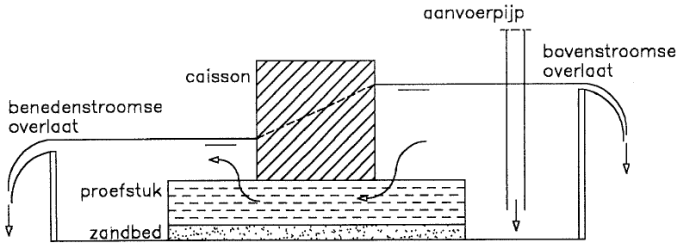

Figure 2-15: Test set-up of Lemmens (Lemmens, 1996)

Lemmens found that a jute geotextile with 4cm woodpulp can withstand nearly the same gradient as a synthetic geotextile (see Table 2-7). A single jute geotextile has a critical gradient of 26% which is much lower than a synthetic geotextile. This value is much higher than the other tested natural materials. Looking at sandtightness, jute could potentially be a good alternative for bed protections. Lemmens has tested one type of jute geotextile.

Table 2-7: Critical gradients for various types of filters (Lemmens, 1996)

Nr.	**Type of fabric**	i_{cr} **[%]**	**Eroded sand [kg]**
1	None (Classical fascine mattress)	7	24.6
2	Synthetic geotextile (not penetrable for roots)	59	Nearly zero
3	Synthetic geotextile (penetrable for roots)	16	0.1
4	Reed (classical filter cloth in fascine mattress)	18	0.9
5	Coconut fibre cloth	12	4.9
6	Coconut fibre cloth filled with 4 cm of woodpulp	14	0.75
7	Jute cloth	26	0.3
8	Jute cloth filled with 4 cm of woodpulp	56*	Nearly zero
* Maximum gradient of test set-up			

To validate the Klein Breteler formula with other research results, the critical filter velocities of the synthetic geotextiles from Lemmens' study were calculated. These velocities were then converted into a critical gradient using the Forchheimer formula. In these calculations, assumptions have been made, and the uncertainties associated with these assumptions have also been investigated. The results are presented in appendix A.5.

Design method for open geotextiles (2023)

In this thesis by Quinten Thomas (2023), the main goal was to formulate a design method for open geotextile filters. To determine this, he developed a method to determine the actual gradients under a single granular filter layer. The actual gradient is calculated as the sum of the average gradient and the fluctuating gradient. This fluctuating gradient can be characterized by the turbulent wall pressures which are derived from the pressure spectrum measured at the top of the filter layer, as described by Blake (1970). Due to the assumption that linear damping takes place in the filter layer, the gradient can be determined at the interface of the geotextile. This hypotheses about the actual gradient has been compared with measured data sets by Van De Sande (2012) and Wolters & Van Gent (2012).

2.3 Summary- Literature review and past studies

Geotextiles play a crucial role in hydraulic engineering as filters to prevent erosion of the subsoil. There are two main types of geotextiles: woven and non-woven. Woven geotextiles are made from yarns or strips and have an ordered structure, while non-woven geotextiles are made from mechanically, chemically, or thermally bonded fibers with a random orientation.

Natural geotextiles can play a role as an alternative for synthetic geotextiles. Lemmens has conducted research into various natural materials, but some of these materials are no longer used today or were not suitable as a replacement. He find a critical gradient of 0.26 for a jute cloth and concluded that jute has potential to become a replacement of synthetic geotextiles.

A study conducted by Klein Breteler (1988) has shown that the main parameters that determine the sand retention capacity of open synthetic geotextile filters are primarily the ratio of d_{b90}/O_{90}, the permeability, and to a lesser extent, the thickness of the geotextile. Previous studies conclude that the grain size of the filter material has no or a small influence on the magnitude of the critical filter velocity. These tests were primarily executed with gradations that have a d_{f15} of approximately 20 mm. In this study, no tests were conducted with filter materials having an identical d_{f50} but different gradations (wide or narrow).

From previous studies, it is clear that there are several states in the process of erosion. Firstly, there is a peak in sand transport shortly after increasing the hydraulic load. This occurs in both a filter construction with and without a geotextile. If the critical load for the geotextile has not been reached, this peak will decrease to zero. Upon reaching the critical load, a constant sand transport will occur. If this sand transport continues for a longer period, there is a possibility that this will continue. However, due to the formation of erosion pits and a natural filter beneath the fabric, it can also decrease while maintaining a constant hydraulic load.

In previous studies, different criteria have been used to describe the start of movement of sand grains. Table 2-8, provides a summary of these criteria and the most important parameters of their test set-up.

Table 2-8: Summary of important studies and threshold criterions

Study	Duration test step	Dimensions test set-up (LxB)	Measured	Threshold criterion
Klein Breteler et al. (1986)	30 minutes	1x1 m	Dry sand after each test step [gr] which is converted to gr/s/m	0.15 gr/s/m
Klein Breteler (1988)	30 a 40 minutes	1x1 m	Dry sand after each test step [gr] which is converted to gr/s/m	0.2 gr/s/m
Van der Meulen (1994/1995)	5 minutes	0.5x0.25 m	Concentration behind after test set-up [gr/l] which is converted to gr/s/m	0.2 gr/s/m
Lemmens (1996)	20 minutes	Total sandbed: 2x0.5 m Length under caisson: 1x0.5 m	Dry sand after last test step when visually seen erosion [gr]	Visually
Ho (2007)	30 minutes	0.65x0.3 m	Turbidity [NTU] C (gr/l)=0.0101×T (NTU)	Test step when turbidity is not going to zero after initial peak

3 Model test set-up

In order to answer the research questions formulated in chapter 1, model tests are executed in a flow flume.

3.1 Test facility: flume

The tests are executed in a flume in the Fluid Mechanic Laboratory at Delft University of Technology. The flume has an overall length of 14.30 m, a height of 0.40 m and a width of 0.40 m. The maximum discharge is about 80 l/s.

Figure 3-1: Flume with test set-up in the Hydraulic Engineering Laboratory

3.2 Material properties

The tests are executed with one type of base material, 3 different types of filter material and 7 different geotextiles.

3.2.1 Base material

The tests are executed with a sandbed of relative fine sand. The dimensions of the used base material is given in Table 3-1. A sieve curve is shown in Appendix C.

Table 3-1: Dimensions and density of base material

Type	d_{b15} [mm]	d_{b50} [mm]	d_{b90} [mm]	ρ_b [kg/m^3]
M34	0.146	0.180	0.242	2650

3.2.2 Geotextiles

A total of 7 different geotextiles (4 woven (w) and 3 non-woven (nw)) were tested.

<u>Woven geotextiles</u>

Prior to this study, the thickness and opening size of the woven geotextiles were determined in a laboratory. The water permeability of the geotextiles was not yet known. This has been determined using a simple measuring set-up (see Appendix B). The jute woven fabrics are presented in Figure 3-2.

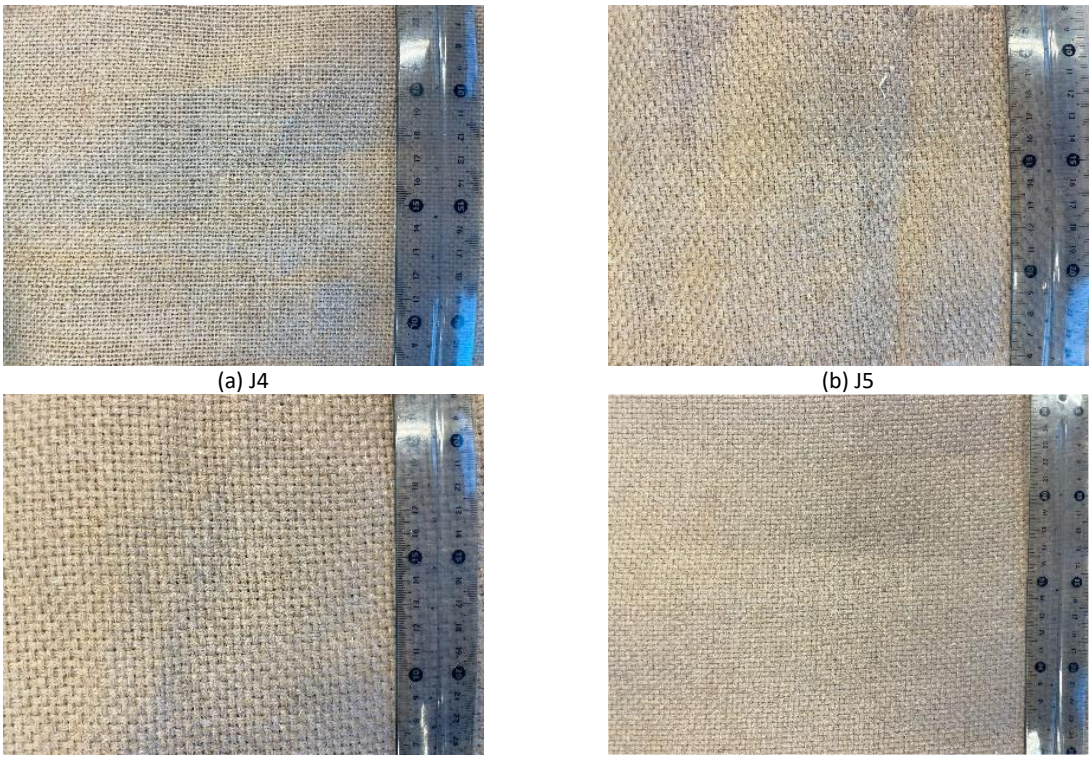

(a) J4 (b) J5

(c) J7 (d) J9

Figure 3-2: Unsaturated woven jute geotextiles (J4, J5, J7 and J9)

The table below (Table 3-2) provides an overview of the most important properties of the geotextiles. It is assumed that the parameter m is equal to 1 for all geotextiles. The parameter m is derived from the following equation: $v_g=k_g i_g^m$. When m = 1, this equation represents Darcy's flow equation.

Table 3-2: Geotextile characteristics woven geotextiles

Geotextile	Material	Type	Weight [gr/m^2]	O_{90} [µm]	t_g [mm]	k_g [mm/s]	m [-]
J4	Jute	Woven	422	516.1	1.45	0.83*	1
J5	Jute	Woven	518	819.0	1.77	0.90*	1
J7	Jute	Woven	-	-	2.01**	0.52*	1
J9	Jute	Woven	963	283.2	2.23	0.075*	1
* Tested with a simplified test set-up ** Measured with calliper							

Non-woven geotextiles

Three tests were done with non-wovens made from natural materials. These three materials are hemp, wool and recycled jute. The fibers of these materials are mechanically bonded at a support of jute. This was done to make a stronger geotextile. The three non-woven geotextiles are presented in Figure 3-3.

(a) Hemp on jute

(b) Jute on Jute

(c) Wool on jute

Figure 3-3: Non-woven geotextiles (unsaturated)

The tests with the non-woven geotextiles were conducted with the support of jute on the sandbed (left side of Figure 3-4) and mechanically bonded fibers on the filter layer side (right side of Figure 3-4).

Figure 3-4: Support of jute on sandbed (left) and mechanically bonded fibers on filter layer side (right)

The table below (Table 3-3) provides an overview of the most important properties of the geotextiles. Appendix B describes how the thickness and water permeability of the fabrics were determined. The O_{90} of these geotextiles is not known.

Table 3-3: Geotextile characteristics non-woven geotextiles

Geotextile	Material	Type	Weight [gr/m^2]	O_{90} [µm]	t_g [mm]	k_g [mm/s]
Hemp on jute	Hemp on jute	Non-woven	500	-	2.58*	0.51**
Recycled jute on jute	Recycled jute on jute	Non-woven	500	-	3.41*	1.05**
Wool on jute	Wool on jute	Non-woven	500	-	2.78*	1.62**
* Measured with calliper ** Tested with a simplified test set-up						

3.2.3 Filter layer

Three types of filter materials are used in this study (Figure 3-5). The dimensions of these three filter materials are presented in Table 3-4.

Table 3-4: Dimensions and density of filter material

Type	Range	d_{f15} [mm]	d_{f50} [mm]	d_{f85} [mm]	d_{fn50} [mm]	d_{f85}/d_{f15} [-]	ρ_f [kg/m^3]	Total weight [kg]	Total volume [m^3]
CP45/125 (wide)	45/125 mm	51.20	73.56	108.75	61.79	2.12	2602.09	109.086*	0.0419
40-70 mm	40/70 mm	45.13	54.44	62.38	45.73	1.38	2874.52	114.218*	0.0397
CP45/125 (narrow)	60-90 mm	62.46	73.21	87.82	61.50	1.41	2602.09	106.675*	0.0410
*Including 2 endoscope stones of basalt with total weight of 0.9732 kg and a volume of 0.339 dm^3									

(a) Grauwacke 45/125 mm (b) Basalt 40/70mm (b) Grauwacke 60/90mm

Figure 3-5: Filter materials

During all tests, two endoscope stones made of basalt material were used (Figure 3-6). Based on tests 1.1 and 2.1, it was decided to reduce the number of stones for the filter material with the grading 45/125 mm. The excessive number of stones made it a significant challenge to fit all the stones into the available space. Consequently, the large number of stones significantly reduced the size/amount of pores, which no longer matched the porosity of a filter layer when stones are dumped on a geotextile with a crane.

Details on the sieve curves and density measurements can be found in Appendix C.

Figure 3-6: Endoscope stones

Using large stones in a relatively narrow flume can cause a significant portion of the flow to pass along the glass and not be evenly distributed across the entire width of the filter layer. This phenomenon occurs due to the irregular shape of the large stones, which have minimal contact with the wall and provide relatively little resistance to the flow along both glass walls. Consequently, this fails to accurately simulate real-world conditions, and the impact on the experimental results can be substantial, varying with the width of the flume. To mitigate this issue, several stones were cut in half, as depicted in Figure 3-7. These halved stones were then positioned with their flat sides against the glass, as illustrated in Figure 3-8. This arrangement helps achieve a more uniform distribution of flow across the width of the flume.

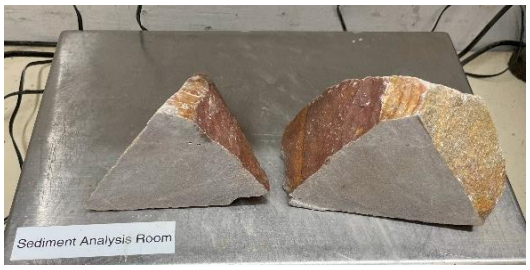

Figure 3-7: Stone through the middle


Figure 3-8: Cut stone placed against the side

3.3 Test set-up with main flow parallel to the geotextile

The stability of an open geotextile structure under parallel flow conditions is investigated through a flume experiment. To generate parallel flow through the stones and establish a hydraulic gradient, a caisson is strategically placed in the flume right at the inlet opening. This placement creates a differential in water levels across the front and back of the sandbed, inducing flow through both the filter layer and the sandbed. This set-up is illustrated in Figure 3-9.

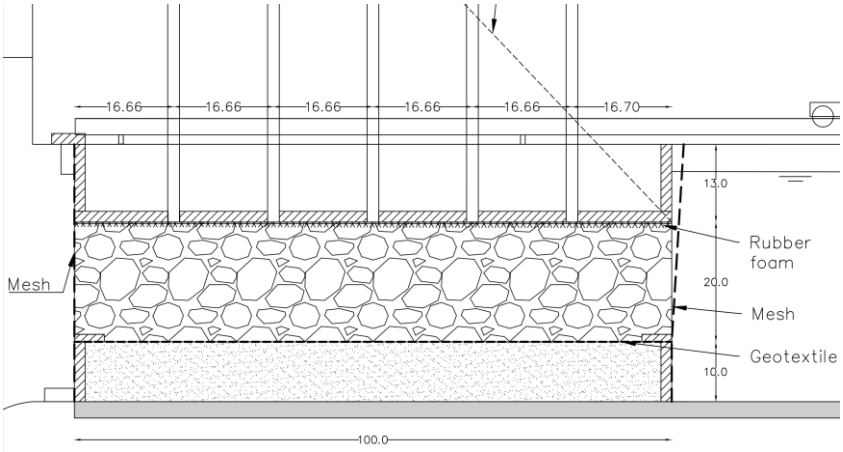

Figure 3-9: Cross-section of test set-up (the flow direction is from left to right)


Figure 3-10: Close up of test set-up (the flow direction is from right to left)

3.3.1 Construction

As shown in Figure 3-11, a filter construction has been set-up in a flume. The filter structure consists of a base layer, comprising a 10 cm thick layer of sand, with a geotextile and a filter layer on top. The base layer of sand is enclosed by 10 cm high and 1.8 cm thick wooden beams, measuring 1 meter in length and 40 cm in width. The geotextile is secured to these wooden beams using wooden slats and screws. The filter layer is fixed on both sides with a mesh to prevent the stones from being carried away by the flow, allowing for the formation of a square filter layer.

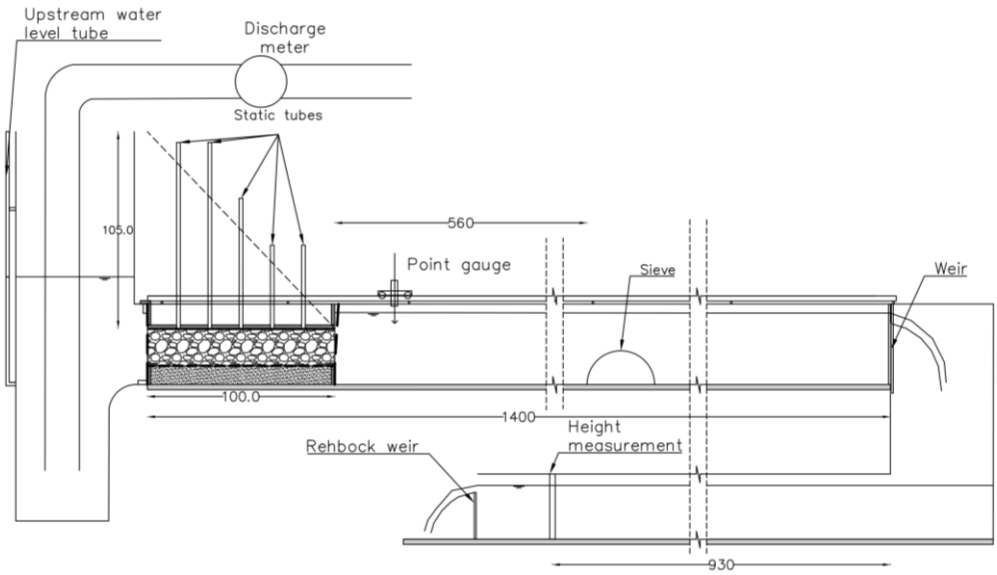

Figure 3-11: Design model test set-up

The caisson used in the experiment measures 1 meter in length and 13 cm in height, allocating a space of 20 cm in height for the filter layer. To improve the connection between the caisson and the filter layer, a 5 cm thick layer of rubber foam is applied, effectively filling the gap between the stones and the bottom of the caisson. The difference made by applying versus not applying the rubber foam between the stones and the bottom of the caisson is shown in the photos below (Figure 3-12).

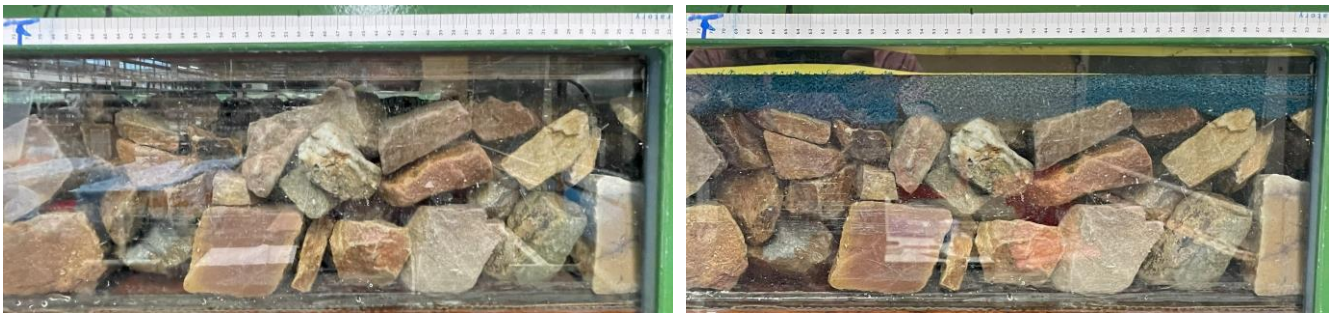

Figure 3-12: Filter layer without rubber foam (left) and filter layer with rubber foam (right)

A sieve, depicted in Figure 3-13, has been positioned approximately 5.6 meters downstream from the filter construction within the flume. This sieve is designed as a semicircle with a diameter of 36 cm. Prior to the main tests, several preliminary tests were conducted to ascertain whether the sieve's mesh was fine enough to capture even the smallest particles of the sandy base material. The primary function of this sieve is to prevent the dispersion of eroded sand throughout the entire length of the flume.

Figure 3-13: Sieve in the flume

3.3.2 Details test section

Two detailed cross-sections of the test section are illustrated in Figure 3-14 and Figure 3-15. These cross-sections clearly show the layering within the filter construction. The details reveal how the geotextile being tested is securely clamped between two wooden slats. The upper slat is firmly attached to the base layer structure using screws, ensuring stability. To minimize the flow between the flume's wall and the caisson, and primarily to channel it through the filter layer, compriband is used along the side of the caisson. Additionally, a rubber strip is utilized to create a watertight seal between the caisson and the top of the flume wall, preventing any leakage that could compromise the test's integrity.

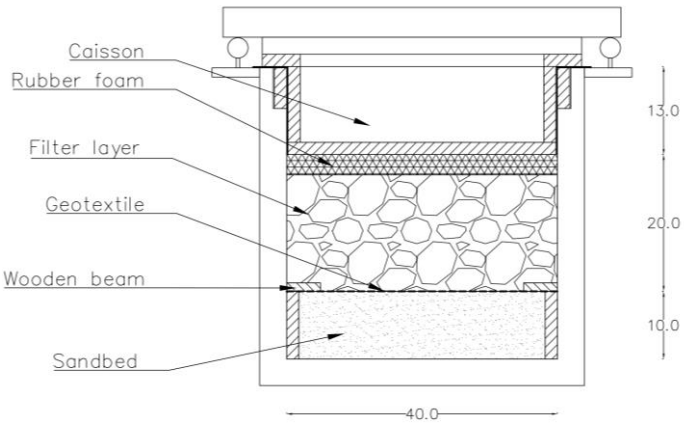

Figure 3-14: Front view test set-up (dimensions in cm)

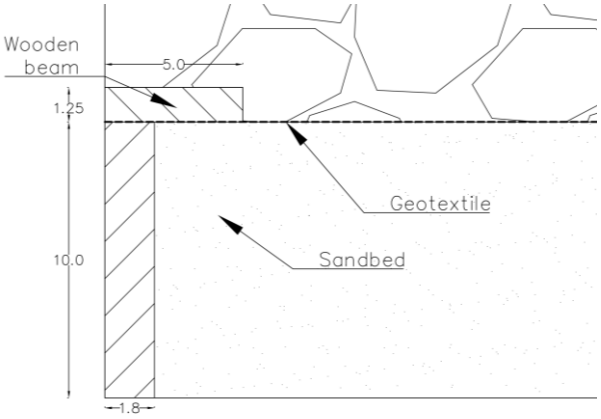

Figure 3-15: Detail fixation of geotextile (dimensions in cm)

3.4 Measurements

To determine the critical gradient or filter velocity at which the base material begins to move, it is essential to measure water levels, pressures under the caisson, and discharge. The measurement methods for determining the transport of base material, water levels, discharge, and pressure fluctuations under the caisson will be explained in the following paragraphs.

3.4.1 Water levels

The water levels at both sides of the caisson are measured. The water level at the inflow side is determined by measuring the water level of a static tube (Figure 3-16) by a tape measure and the water level at the downstream side of the structure is measured with a point gauge (Figure 3-17). During each test step, the water levels are measured twice once the preset water level has reached a constant value.

Figure 3-16: Static tube on upstream side

Figure 3-17: Point gauge on downstream side

3.4.2 Pressures

To monitor the hydraulic head profile beneath the caisson, 5 static tubes have been installed in the bottom of the caisson (Figure 3-18). These static tubes are all mounted at approximately 16.66 cm center-to center from eachother and 20 cm from the sides of the flume. This pressure distribution determines the gradient across the filter construction. The locations of the static tubes are presented in Figure 3-19. Every test step the pressures are measured twice once the preset water level has reached a constant value.

Figure 3-18: Static tubes

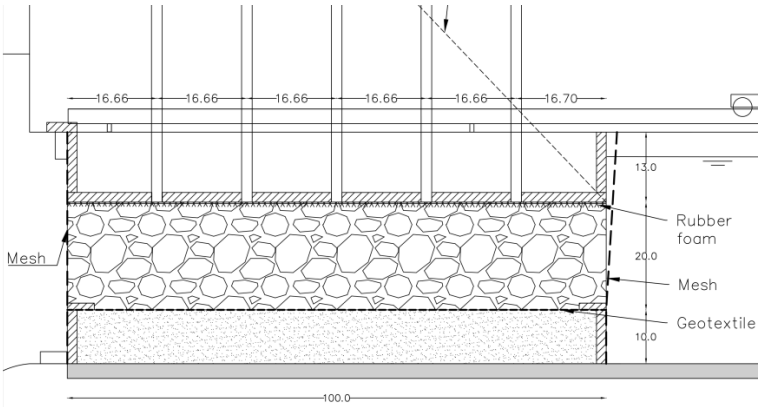

Figure 3-19: Dimensions static tubes

3.4.3 Water temperature

During every test, the temperature of the water was measured. This temperature was around 17 degrees Celsius during each test.

3.4.4 Discharge

The discharge in the inflow pipe can be directly monitored using the valve recorder (Proline Prosonic Flow 91W). In addition to the valve recorder, the Rehbock weir was employed to measure the discharge, positioned at the end of the water return beneath the flume (Figure 3-20). Both the valve recorder and the Rehbock sensor produce analog signals as their outputs. To make these signals usable for measurement purposes, all sensors were connected to a Data Acquisition (DAQ) module (Figure 3-21). This DAQ module was responsible for converting the analog signals into digital signals, which were subsequently read by a computer. The data was analyzed using the DASYlab software and recorded every 2 seconds.

Figure 3-20: Rehbock weir

Figure 3-21: DAQ module

The height sensor of the Rehbock weir was calibrated by measuring the water level with a pointer gauge at the water level sensor. The measured values are then correlated with the measured voltages of the sensor, as detailed in Table 3-5. The water level above the Rehbock weir is directly associated with a specific discharge, a relationship that is defined by equation (3.1). Before conducting the tests, the voltage signal from the valve recorder was adjusted so that the discharge could be accurately determined using the calibration formula provided in Table 3-5. According to the calibration data from the valve recorder supplied by the manufacturer, the valve recorder produces precise discharge measurements when the flow velocity in the inflow pipe exceeds 0.3 m/s, a rate that corresponds to a discharge of approximately 10 L/s. The calibration graphs are available in Appendix E.

For tests 5.1 and 6, the discharge measurements from the Rehbock weir and the discharge meter were not automatically logged but were manually read and recorded at each test step. Utilizing this data, the discharge graphs were reconstructed through interpolation, providing a comprehensive overview of the discharge rates throughout these tests.

Table 3-5: Calibration equations

Measuring purpose	Calibration	Unit
Rehbock	h_k = (Rehbock voltage -3.5209)/ 0.02675	mm
Valve recorder	Q = (Valve voltage-2.0)*10	l/s

The measured water level before the Rehbock weir can be converted into a discharge value:

$$Q = B_{reh} \times m' \times \frac{2}{3} \times h_e \times \sqrt{\frac{2}{3} g \times h_e}\,, \text{with } h_e = h_k + 0.0011 \text{ and } m' = 1.045 + 0.141 \times \frac{h_e}{a} \quad (3.1)$$

Where:

Q = discharge [m^3/s]
B_{reh} = width of Rehbock weir = 0.445 m
a = height of Rehbock weir = 0.250 m
h_k = measured water height above weir [m]

3.5 Erosion measurements

During the tests 3 different methods are used to determine the start of movement of the different tests. The used methods are described below.

Hall sensor

A Hall sensor, accompanied by two associated magnets (each with a diameter of 5mm and a width of 25mm), has been installed beneath the geotextile to monitor its subsidence. Prior to initiating the tests, the Hall sensor was calibrated. The calibration graph is provided in Appendix E. Following calibration, the Hall sensor was waterproofed and affixed to a wooden block (Figure 3-22). This set-up guarantees that the sensor maintains a consistent position, precisely 5 cm above the bottom of the flume, throughout the duration of the tests.

Figure 3-22: Hall sensor

Endoscope inside the filter layer

To analyze the dynamics within the filter layer, two endoscope cameras were placed into the filter layer, as shown in Figure 3-23. A hole was drilled into a stone, and the cameras were then secured with clay in these holes. For each test, the cameras were strategically positioned at distances of 50 cm and 75 cm from the upstream side, in the center of the flume, as depicted in Figure 3-24. The frame rate of the cameras varied between tests, ranging from 15 to 30 frames per second.

During the installation of the filter layer, the endoscopes were manually positioned above a pore. Consequently, their position, in terms of both height and exact location, varied with each test. This variance in positioning prevents an exact comparison of the images captured across different tests.

Figure 3-23: Endoscope camera's

Figure 3-24: Positioning endoscope

The images captured by the installed endoscopes are of high enough quality to observe the movement of individual sand grains. It is also clearly visible that there are distinct moments when a significant amount of sediment is rapidly released from beneath the geotextile, as illustrated in Figure 3-25. Additionally, the process of filling the flume was recorded for several tests. This was done to determine, in retrospect, whether and to what extent erosion occurred during the flume filling process.

Figure 3-25: View at 02:58:53 (left), view at 03:04:33 (middle) and view at 03:50:21 (right), test 3.1

During the experiments, there were multiple instances where the software intended to save the camera videos experienced malfunctions. This led to either corrupt files or videos not being saved at all. Some of the videos are unusable due to air bubbles present in front of the camera lens and in one instance, even a plastic film that has adhered to the clay used to secure the camera in the stone.

Photos with camera of phone

During several tests, photos of the flume's bottom behind the test structure were taken after each test step. This approach facilitates a visual assessment of the quantity of sediment released from the test set-up during a given test step. Furthermore, it enables the use of image processing techniques to determine the hydraulic load at which start of sediment movement begins.

Suctioning the sediment behind the structure

The sediment eroded during each test step was suctioned using a garden hose through a siphoning process, which created a flow through the hose (Figure 3-26). The end of the hose was securely connected to a basin, under which a sieve was placed (Figure 3-26). The mesh of the sieve was sufficiently fine to filter out all sand particles from the water effectively. After this process, both the hose and the structure were flushed with tap water to ensure that no sediment particles remained in the hose or attached to the structure.

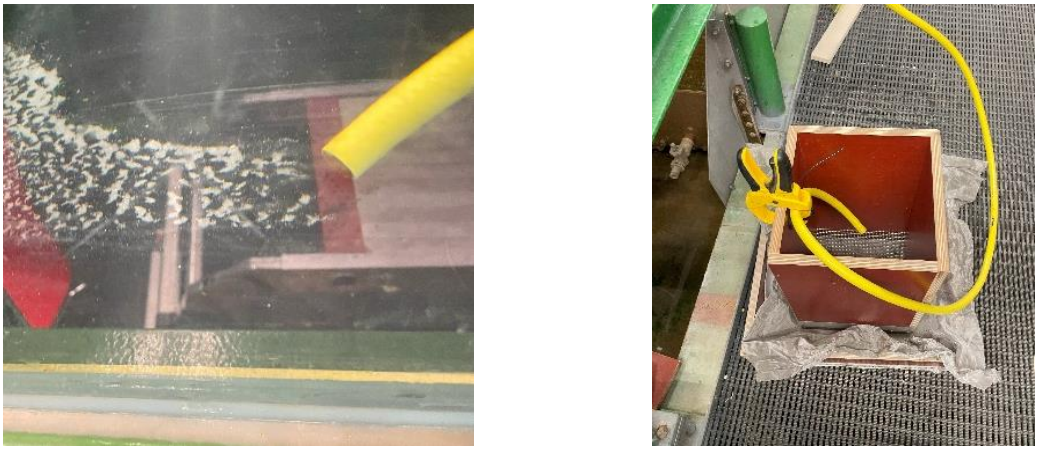

Figure 3-26 Suctioning sediment (left) and sieve construction (right)

The primary advantage of using this sediment removal method is its ability to allow the flow within the experiment to continue without interruption. Halting the flow to suction sediment could induce an initial peak in erosion upon restarting the experiment, potentially altering the outcomes. However, this approach also presents challenges, especially when trying to suction sand after surpassing the critical load. In instances of significant sediment transport, it becomes challenging to

suction all the sediment following a test step. This difficulty arises because new sediment can be released from the filter set-up during the suctioning process, settling in areas already cleared of sediment. Visual inspections have indicated that this additional sediment is minimal compared to the total amount vacuumed for that particular test step. Any small amount of sediment left will be suctioned after the subsequent test step.

After suctioning, the sediment was left to dry on the sieve before being transferred into a smaller plastic bag for weighing. The plastic bag's weight is 7.2 grams, and this is deducted from the total measured weight to determine the net weight of the dry sediment for each test step.

3.6 Testing procedure

In this section the execution of a test will be described. This consists of three parts preparation, execution and after a test.

3.6.1 Preparation of a test

The steps for the preparation of a test set-up are presented below. The test structure was built in the following order:

- Adding sand and flattening the base layer
- Placing a sandtight geotextile and fastening it with beams
- Filling the flume with water until the water level reaches one centimeter below the top of the sandbed. As a result, the filling time of the flume is significantly reduced.
- Removing the sandtight geotextile
- Placing geotextile and fastening it with beams
- Placing filter layer with endoscopes
- Placing rubber foam
- Installing and securing caisson with clamps on the flume.
- Filling the flume with water until the water level reaches some centimeters above the bottom of the caisson

In appendix D.1, a more comprehensive test protocol is provided. During tests 1.1, 2.1, 5.1, 6, 7, 10, 11, and 12, a sandtight geotextile was not used; instead, the flume was filled in one go.

3.6.2 Execution of a test

If the water level in the flume reached the preset height of the weir at the flume's end, the valve at the inflow pipe was closed. This was followed by a zero measurement to establish a base water level. After this initial measurement, the water level upstream was incrementally raised for each subsequent test step. During these steps, both the water levels and flow rates were measured and recorded twice to ensure accuracy. It is important to note that for all tests (with the exceptions of tests 5.1 and 6), the flow rate was continuously recorded, allowing for a detailed analysis of flow dynamics throughout the experiment.

3.6.3 After a test

After completing a test, the data recording and endoscopes were deactivated. The weir at the end of the flume was then lowered to facilitate the removal of all water from the flume. Once the water was completely drained, the test set-up was carefully dismantled, following the reverse order of its initial preparation. Subsequently, photographs were taken of the geotextile to document its condition post-test. After the removal of the geotextile, additional photographs were taken of the sandbed to

capture any changes or patterns of erosion. The sand that had been eroded during the test was collected from the bottom of the flume, dried, and then weighed to quantify the amount of sediment transport.

3.7 Test program

To address the research question and its sub-questions, a total of 12 different tests were conducted, divided into two phases. In the first phase, the focus was on determining the critical load for four different woven jute geotextiles, while varying various parameters of the filter construction. To understand the distinction between an open granular filter and an open geotextile filter, one test was conducted without using a geotextile. The second phase aimed at determining the critical loads for three natural non-woven geotextiles.

3.7.1 Design to experiment

To test the hypothesis that the critical filter velocity or the critical gradient constitutes the critical load for (natural) open geotextiles, a specific test set-up was designed. For this purpose, three distinct filter materials were selected based on the following criteria:

- Utilization of the largest possible stone grading that fits within the flume's constraints and is also practically applied on geotextiles.
- Selection of stone gradings that offer the maximum gradient and filter velocity achievable within the intended test set-up in the flume.
- Choice of stone gradings that show no variance in d_{f50} but differ in the porosity of the filter layer.
- The relationship between the hydraulic gradient and the filter velocity must be distinct enough to allow for a clear observation of differences in the outcomes.

Given the spatial constraints for the filter layer within the flume, a 45/125 mm grading was selected. In conjunction with the characteristics of the geotextiles, the Klein Breteler formula, traditionally applied to synthetic geotextiles, was utilized to predict the expected critical filter velocities. Utilizing the Forchheimer equation, this velocity was then translated into a hydraulic gradient to assess its practicality within the flume's limitations. A stone grading was chosen that would permit a significant measurable difference in hydraulic gradient at the same filter velocity, thereby facilitating the determination of the critical filter velocity and gradient within the proposed test set-up. Lastly, a grading with the same d_{f50} as the 45/125 mm grading but with a narrower gradation was selected. The type of grading plays a pivotal role in the pore size of the filter layer (Laan, 1996). With a narrow gradation, the presence of fewer small stones to occupy the pores results in higher porosity compared to a wide gradation. Since porosity significantly influences the hydraulic gradient, this leads to a gradient/velocity ratio that varies from that of a wide gradation.

3.7.2 Key parameters

This sub-section discusses the key parameters influencing the sandtightness of open geotextile filters, as identified in the literature review. The potentially usable design formula (equation (2.17)) is critically evaluated by varying key parameters within the test program:

- **Ratio of Geotextile Thickness to Base Material Grain Size (t_g/d_{b90}):** This examines how the physical structure of the geotextile interacts with the base material's granular size.
- **Ratio of Base Material Grain Size to Geotextile Opening Size (d_{b90}/O_{90}):** The size of the sand grains in combination with the opening size of the geotextile ensures how easily these grains can move through the geotextile.

- **Ratio of Fall Velocity to Water Permeability of Geotextile (w/k_g):** This examines the flow damping parameter of the geotextile.
- **Grain Sizes of Filter Layer:** Different sizes are tested to understand their role in the critical load (filter velocity or critical gradient) for open geotextiles

3.7.3 Test overview woven geotextiles and open granular filter

The tests executed with the woven geotextiles are presented in Table 3-6.

Table 3-6: Test program woven geotextiles

Test number	Geotextile	Base material	Filter material	
		d_{b50} [mm]	Grainsize range	Filter thickness
T1	J4	0.180	45/125 mm	200 mm
T2	J5	0.180	45/125 mm	200 mm
T3	J7	0.180	45/125 mm	200 mm
T4	J9	0.180	45/125 mm	200 mm
T5	J4	0.180	40/70 mm	200 mm
T6	J5	0.180	40/70 mm	200 mm
T7	-	0.180	40/70 mm	200 mm
T8	J4	0.180	60/90 mm	200 mm
T9	J5	0.180	60/90 mm	200 mm

Expected values woven geotextiles

To obtain an indication of the critical gradients and critical filter velocities that will occur, an estimation of the expected values for each test was calculated using the Klein Breteler and Forchheimer equation. It is crucial to acknowledge that this equation was initially developed for synthetic geotextiles, which might lead to underestimations or overestimations when applied to jute geotextiles. Moreover, there could be uncertainties regarding the measured permeability of the geotextiles. Despite these potential limitations, these estimations can still serve as a preliminary gauge to assess whether the test set-up is adequately designed to determine the critical load for the geotextiles. The calculated values are detailed in the table below (Table 3-7).

Table 3-7: Expected values and parameters with Klein Breteler formula

Test	Geotextile				Base material			Filter			Parameters			Calculated	
	number	O_{90} [mm]	t_g [mm]	k_g [mm/s]	d_{b15} [mm]	d_{b50} [mm]	d_{b90} [mm]	d_{f15} [mm]	d_{fn50} [mm]	n_f [-]	$\frac{O_{90}}{d_{b90}}$	$\frac{t_g}{d_{b90}}$	$\left(\frac{w}{k_g}\right)^{\frac{1}{m}}$	$u_{f,cr}$ [m/s]	i_{cr} [-]
T1	Jute J4	0.516	1.45	0.83*	0.146	0.180	0.242	51.2	61.79	0.40**	2.13	5.99	17.80	0.24	1.0
T2	Jute J5	0.819	1.77	0.90*	0.146	0.180	0.242	51.2	61.79	0.40**	3.38	7.31	16.41	0.07	0.09
T3	Jute J7		2.01	0.52*	0.146	0.180	0.242	51.2	61.79	0.40**		8.31	28.41		
T4	Jute J9***	0.283	2.23	0.075*	0.146	0.180	0.242	51.2	61.79	0.40**	1.33	10.51	196.96	11.25	2108.6
T5	Jute J4	0.516	1.45	0.83*	0.146	0.180	0.242	45.13	45.73	0.40**	2.43	5.99	17.80	0.24	1.35
T6	Jute J5	0.819	1.77	0.90*	0.146	0.180	0.242	45.13	45.73	0.40**	3.86	7.31	16.41	0.07	0.13
T7	-	-	-	-	0.146	0.180	0.242	45.13	45.73	0.40**	-	-	-	0.012	0.023
T8	Jute J4	0.516	1.45	0.83*	0.146	0.180	0.242	65	61.50	0.40**	2.43	6.83	17.80	0.24	1.02
T9	Jute J5	0.819	1.77	0.90*	0.146	0.180	0.242	65	61.50	0.40**	3.86	8.34	16.41	0.07	0.09

* Measured with simplified permeability test
** Assumption
*** This geotextile is a geometrically closed geotextile based on the ratio O_{90}/d_{b90}

The calculated data points from the tests with the woven jute geotextiles have been incorporated into Klein Breteler's graph (Figure 3-27). As can be observed, the tests are well-distributed across the graph. Given that these data points are spread throughout the entire range, if the measured critical

filter velocities closely match the calculated critical filter velocities, it can be concluded that the formula can be applied across the full range for natural geotextiles.

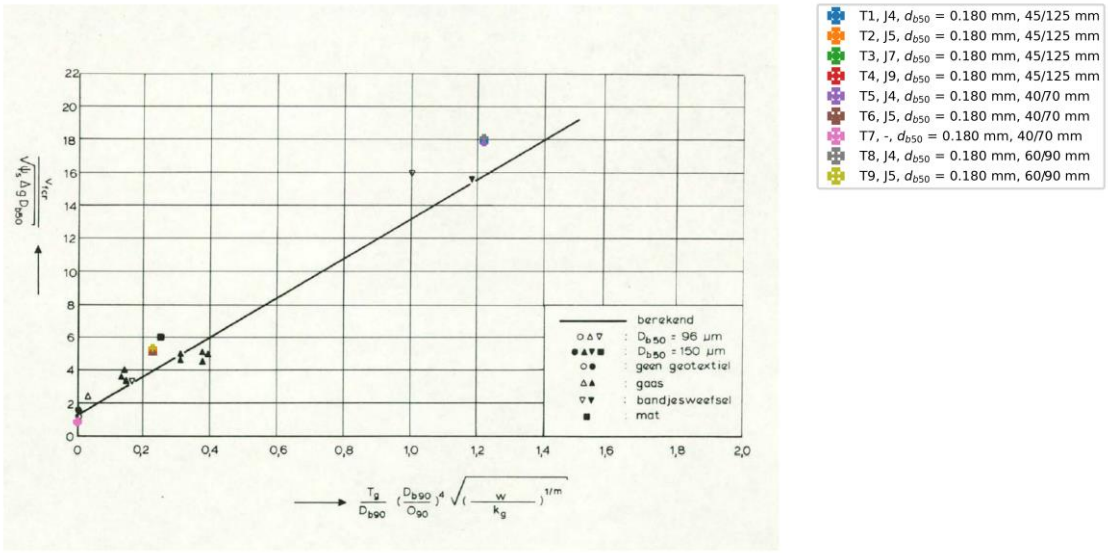

Figure 3-27: Overview of tests and datapoints from Klein Breteler (1988)

3.7.4 Test overview non-woven geotextiles

In addition to the tests conducted on woven geotextiles, three natural non-woven geotextiles are also tested to determine their critical load. The details of these tests are presented below (Table 3-8). For these non-woven geotextiles, the O_{90} value is unknown, and there currently exists no formula to estimate their critical load. These non-woven geotextiles are new to the market and have been tested to see if there is potential for further development in the future.

If the start of sediment movement is observed during any of the tests with the non-woven geotextiles, further investigations will be carried out to assess how the thickness of the geotextile affects the sandtightness of non-woven geotextiles. This investigation into the influence of geotextile thickness on sandtightness will be conducted by stacking multiple layers of the same geotextile on top of each other.

Table 3-8: Test program non-woven geotextiles

Test number	Geotextile	Base material	Filter material	
	Material geotextile	d_{b50} [mm]	Grainsize range	Filter thickness
T10	Hemp on jute (nw)	0.180	45/125 mm	200 mm
T11	Jute on jute (nw)	0.180	45/125 mm	200 mm
T12	Wool on jute (nw)	0.180	45/125 mm	200 mm

4 Test results

This chapter, along with Appendix F, presents the results of the model tests.

The chapter is divided into six sections. The first section presents the performed tests, the second section covers the porosity, the third section covers the hydraulic conditions during the tests followed by the fourth section, which explains the transport of sediment of the woven geotextiles. The fifth section describes the results of the non-woven geotextiles. The final section discusses some errors and limitations related to the measurements and model set-up.

4.1 Tests performed

This section offers a summary of all the tests conducted as part of the study. Several tests have been repeated with the same test set-up. In these tests, a version number is included after the test number (e.g., test 1.1 and 1.2). The details of each test, including its configuration, total duration, and the total amount of eroded sand, are documented in Table 4-1.

After the first two tests (tests 1.1 and 2.1) with the filter material 45/125 mm, it was decided to reduce the quantity of stones used in the filter layer. This adjustment was made because the large number of stones made it significantly challenging to fit all the stones into the available space for the filter layer. This also resulted in a constructed filter layer that did not correspond to a filter layer that made by dumping stones on a geotextile with a crane. Additionally, the ratio of filter velocity to hydraulic gradient was not sufficiently different from that of the 40/70 mm filter material. Subsequent tests with the 45/125 mm filter material were conducted with the same reduced quantity of stones.

Table 4-1: Test results woven geotextiles

Test	**Geotextile**		**Filter material**	**Duration [h]**	**Total amount of eroded sand after test [gr]**
	Type	**Woven (w)/Non-woven (nw)**			
Test 1.1	J4	woven	45/125 mm*	5.25	159
Test 1.2	J4	woven	45/125 mm*	4.25	601
Test 1.3	J4	woven	45/125 mm	5.33	907.8
Test 2.1	J5	woven	45/125 mm	6.4	124
Test 2.2	J5	woven	45/125 mm	4.75	154
Test 2.3	J5	woven	45/125 mm	6.33	191.4
Test 3.1	J7	woven	45/125 mm	4.65	459
Test 3.2	J7	woven	45/125 mm	6	315.6
Test 4	J9	woven	45/125 mm	4.15	14.8
Test 5.1	J4	woven	40-70 mm	4.8	134
Test 5.2	J4	woven	40-70 mm	4.3	195
Test 6	J5	woven	40-70 mm	7.5	76
Test 7	-	-	40-70 mm	1.8	1656
Test 8	J4	woven	60-90 mm	4.8	585
Test 9.1	J5	woven	60-90 mm	4.6	171
Test 9.2	J5	woven	60-90 mm	5.15	151.2
Test 10	Hemp on jute	non-woven	45/125 mm	3.75	17
Test 11	Jute on jute	non-woven	45/125 mm	3	7
Test 12	Wool on jute	non-woven	45/125 mm	4.0	10
*Tests 1.1 and 2.1 were conducted with a larger amount of stones compared to other tests with the filter material 45/125 mm					

4.2 Porosity

The porosity affects the pore velocity and thus the filtration rate of the filter layer. Based on the total amount of stones and the size of the spaces within the filter layer, it is possible to determine the average porosity. The size of an empty filter layer is illustrated in Figure 4-1.The primary dimensions of the filter layer are 0.2x0.4x1 meters (hxBxL). However, the slats used to secure the geotextile must be excluded from this measurement. Additionally, the mesh at the back is slightly tilted, resulting in a slightly larger volume.

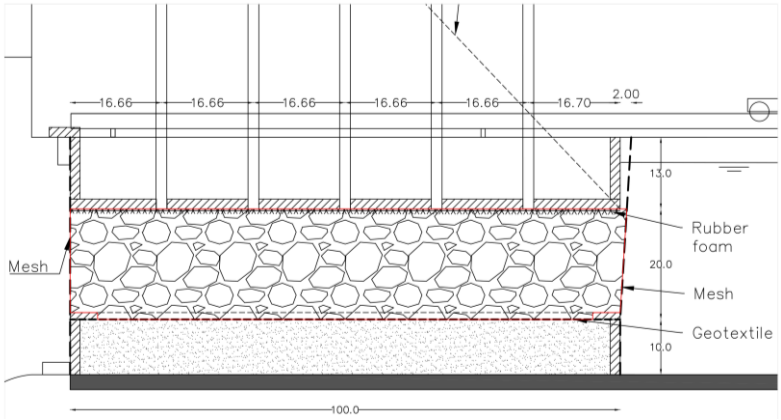

Figure 4-1: Dimensions filter layer

The volume of the geotextile is neglected in this calculation as it is approximately equal to the thickness of the rubber on the sides of the flume. The total empty volume remaining after subtracting the volume of the elements present in the filter layer (in addition to the stones) from a completely empty filter layer can be calculated using the following formula:

$$V_{net} = V_{empty} - V_{ws} \tag{4.1}$$

With:

V_{net} = volume filter layer without wooden slats [m^3]
V_{empty} = volume empty filter layer [m^3]
V_{ws} = volume of wooden slats [m^3]

With the parameters of Table 4-2, the net volume of the filter layer is calculated. This net volume is 0.0789 m³.

Table 4-2: Volumes filter layer

Parameter	Value	Unit
Volume empty filter layer	0.0805	m^3
Volume of wooden slats	0.001625	m^3

The porosity can be calculated using the following formula:

$$n_{average} = 1 - \frac{\frac{W}{\rho_f}}{V_{net}} = 1 - \frac{V_s}{V_{net}} \tag{4.2}$$

With:

$n_{average}$ = average porosity of filter material [-]
V_s = volume stones [m^3]
V_{net} = volume filter layer without wooden slats [m^3]

Using the formula above the average porosity of the different filter materials were calculated. Tests 1.1 and 2.1 were considered separately because these tests were conducted with a different amount of stones than the other tests with the 45/125 mm filter material. The results of the different average porosities of the various filter materials are shown in Table 4-3.

Table 4-3: Dimensions filter material parameters and average porosity

Test/filter material	**Volume of stones [m^3]**	**Average porosity [-]**
45/125 mm*	0.0419**	0.469
45/125 mm of test 1.1	0.0456**	0.422
45/125 mm of test 2.1	0.0428**	0.457
40/70 mm	0.0397**	0.497
60/90 mm	0.0410**	0.480
*Without tests 1.1 and 2.1 **Including 2 endoscope stones of basalt with a volume of 0.339 dm^3		

According to the theories of Knieß (1977) and Bosma (2001), the distribution of porosity within a filter layer is not uniform across its height. The porosity is larger at both the top and bottom of the layer, while in the middle, it matches the bulk porosity. The bulk porosity refers to the porosity of a filter layer within a very large container filled with stones, where the effects of the edges can be disregarded. This concept is illustrated schematically in Figure 4-2 below.

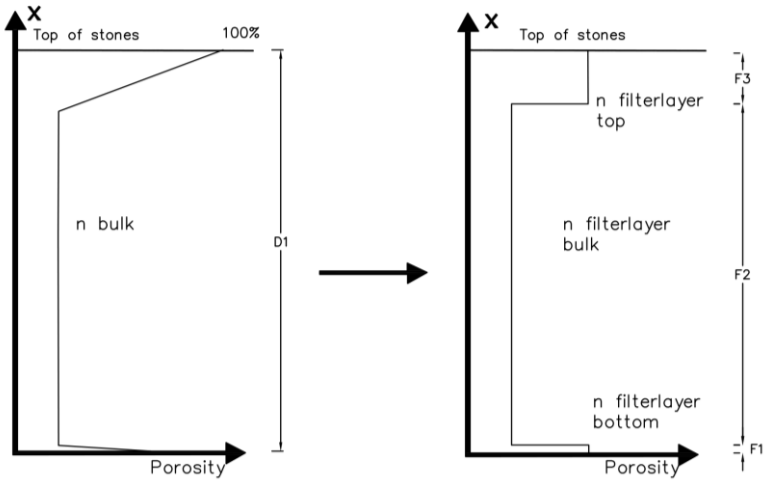

Figure 4-2: Schematization porosity distribution (adapted from (Bosma, 2001))

Using the formulas below, the different influence lengths can be calculated (Bosma, 2001):

F1: $$0.275 * d_{n50} \quad (4.3)$$

F2: $$D_1 - F_1 - F_3 \quad (4.4)$$

F3: $$0.74 * d_{n50} \quad (4.5)$$

The average porosity calculated with equation (4.2) for the entire filter layer can be used to determine the bulk porosity of the filter layer. The average porosity is equal to the equation below:

$$n_{average} = \frac{\frac{n_{bulk}+100}{2} * 0.275 d_{n50} + n_{bulk} * (D1 - (0.275 + 0.74) * d_{n50}) + \frac{n_{bulk}+100}{2} * 0.74 d_{n50}}{D1} \quad (4.6)$$

With:

$n_{average}$ = average porosity of filter material [%]
n_{bulk} = bulk porosity of filter material [%]
d_{n50} = nominal diameter exceeded by 50% of the diameters [m]
$D1$ = thickness of filter layer [m]

Table 4-4 presents the dimensions, influence lengths, and bulk porosities of the different filter materials.

Table 4-4: Dimensions filter material parameters and influence lengths

Test/filter material	**Volume of stones [m³]**	**d_{n50} [m]**	**D1 [m]**	**F1 [m]**	**F2 [m]**	**$n_{average}$ [-]**	**n_{bulk} [-]**
45/125 mm*	0.0419**	0.06179	0.2	0.0170	0.0457	0.469	0.370
45/125 mm of test 1.1	0.0456**	0.06232	0.2	0.0171	0.0461	0.422	0.313
45/125 mm of test 2.1	0.042806**	0.06228	0.2	0.0171	0.0461	0.457	0.355
40/70 mm	0.0397**	0.04573	0.2	0.0126	0.0338	0.497	0.431
60/90 mm	0.0410**	0.06150	0.2	0.0169	0.0455	0.480	0.384
*Without tests 1.1 and 2.1 **Including 2 endoscope stones of basalt with a volume of 0.339 dm³							

The average porosity ($n_{average}$) is calculated using the measured volume of stones and the known volume of the filter layer. The bulk porosity (n_{bulk}) is determined by considering the average porosity and the distribution of porosity throughout the height of the filter layer (Bosma, 2001). Applying rubber foam to the top of the filter layer reduces the average porosity. To refer to the porosity that applies to the remaining part of the filter layer when rubber foam is used, the term effective porosity (n_{eff}) is used. The determination of this effective porosity is described in section 5.1.

4.3 Hydraulic conditions

The hydraulic conditions for each test were determined using the discharge data collected through the Rehbock weir and valve recorder, along with the recorded water levels and pressures. During the tests, the hydraulic load was incrementally increased until sediment transport was observed. Importantly, all tests were carried out with a continuous flow rate, ensuring no interruptions that could potentially affect the outcomes.

4.3.1 Hydraulic head profile

The gradient across the filter structure for each test step was calculated using the water level measurements taken at both sides of the caisson. In this study, it was decided to utilize the average gradient to determine the critical hydraulic gradient. It was observed that, at certain locations, particularly at the front and back of the caisson, the local gradient can be higher than the average gradient. This primarily occurs at the front and back of the caisson. At both the front and rear, slats are attached, preventing the gradient from directly affecting the base layer. Despite deviations from the average gradient in some tests, it is used for the following reasons (Van Os, 1998):

- As the flow velocity increases, the water levels in the static tubes begin to exhibit fluctuations, leading to less precise average water level readings. By opting for the average

gradient, the influence of these fluctuations on the gradient determination is minimized compared to using the local gradient.

- If the local gradient is greater than the average, the erosion will also be stronger in that area. However, the erosion is determined over the entire filter construction. Since the amount of eroded material is related to the gradient, the gradient must also be taken over the entire filter construction.

In most tests, the water pressure measurement points form a linear alignment with the pressures, reinforcing the decision to refer to the average gradient when discussing the critical hydraulic gradient. An illustrative example of the hydraulic head profile across the caisson is provided in Figure 4-3.

The hydraulic gradient is calculated using the following formula:

$$i = \frac{\Delta h}{L} \tag{4.7}$$

Where *Δh* represents the water level difference between the inflow side and the outflow side, and *L* is the length between the inflow side and the outflow points. This length is equal to the length of the caisson and measures 1 meter. Detailed information regarding the hydraulic gradient for each test step across all tests is provided in Appendix F.1.

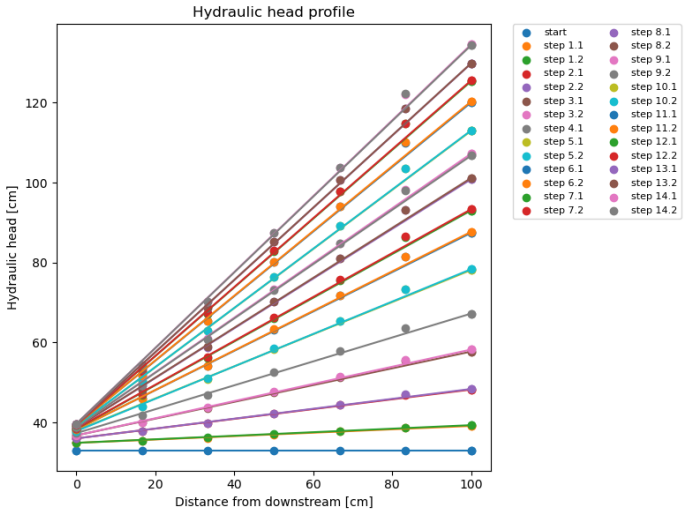

Figure 4-3: Hydraulic head profile test 3.1, the first and last points indicate the inflow and outflow points, while the five intermediate points correspond to the five static tubes

4.3.2 Discharge

After analyzing the discharge measurements, it was concluded that the discharge readings from the Rehbock weir and the discharge meter were not consistent. Based on the manual calibration measurement of the Rehbock weir, it was determined that the Rehbock weir provides more accurate readings than the discharge meter within the discharge range relevant to the tests conducted. Consequently, the Rehbock weir's discharge data were used to calculate the filter velocity, while the valve recorder's signal was utilized to ascertain the duration of each test step. To generate a larger hydraulic gradient across the filter structure, the weir at the flume's end was lowered during several tests. This adjustment led to a reduction in water level behind the filter structure, thereby enabling a larger hydraulic gradient. These adjustments are identifiable as brief spikes in the discharge graph of the Rehbock weir (Around 3:00 hour in Figure 4-4).

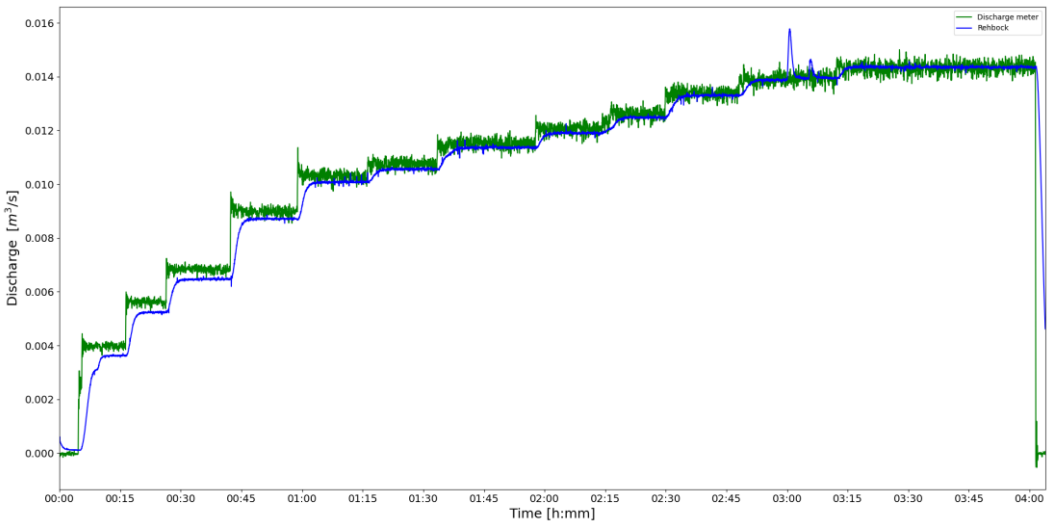

Figure 4-4: Discharge graph test 12

The discharge graph from both measuring instruments during the calibration test, which took place without any test set-up in the flume, is provided in Appendix E. The discharge graph of test 1.3 is shown in Figure 4-5. The discharge for a specific test step was calculated by averaging the discharge values once they stabilized following a hydraulic load increase at the start of a test step. Appendix F.1 contains the recorded discharge for each test step across all tests. A minor dip in the Rehbock weir's discharge curve at the conclusion of each test step signifies the period of sediment removal behind the test set-up. Throughout this sediment removal process, the readings from the discharge meter remained constant.

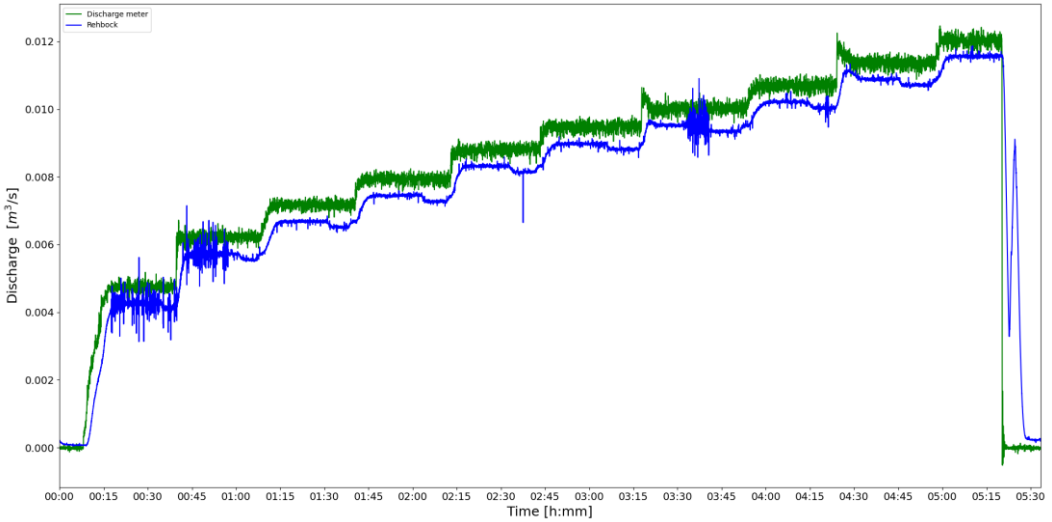

Figure 4-5: Discharge graph test 1.3

4.3.3 Filter velocity

The filter velocity is an average velocity for the entire filter layer. The actual velocity in the pores is higher. The filter velocity has been calculated by the discharge measured by the Rehbock weir divided by the flow area of the filter layer.

$$u_f = \frac{Q}{A_C} \tag{4.8}$$

Where Q represents the discharge per unit time, A_c is the flow cross section area (Figure 4-6).

Since a closed 'filter box' is used, there is almost a constant filter velocity across the depth. When flow occurs above a filter layer, the flow is not constant across the depth.

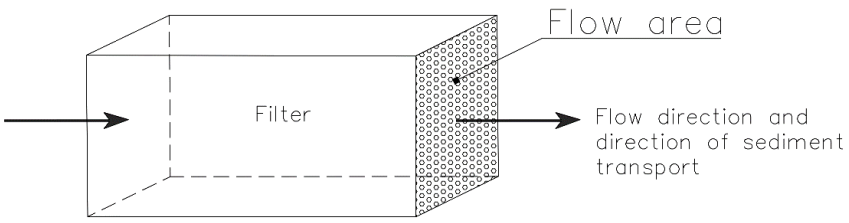

Figure 4-6: Flow area (adapted from (Klein Breteler & Den Adel, 1992))

During all tests, a 5 cm thick rubber foam was placed on top of the filter layer to obstruct the flow between the bottom of the caisson and the stones. This measure effectively seals the pores at the top of the filter layer, thereby eliminating edge effects at this location. Due to the substantial thickness of the rubber foam, the top 5 cm of the filter layer is either covered by foam rubber or by stones. Consequently, the effective height of the filter layer available for water flow is reduced by 5 cm from the maximum height between the geotextile and the bottom of the caisson. Additionally, the flow area is also reduced by the two wooden slats on both sides. In Figure 4-7, the used flow area is outlined in red. Appendix F.1 contains the calculated filter velocity for each test step across all tests.

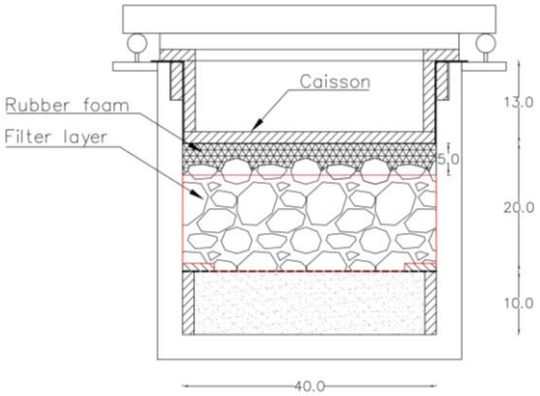

Figure 4-7: Cross section flow area (dimensions in cm)

An example of the filter velocity during a test is shown in Figure 4-8.

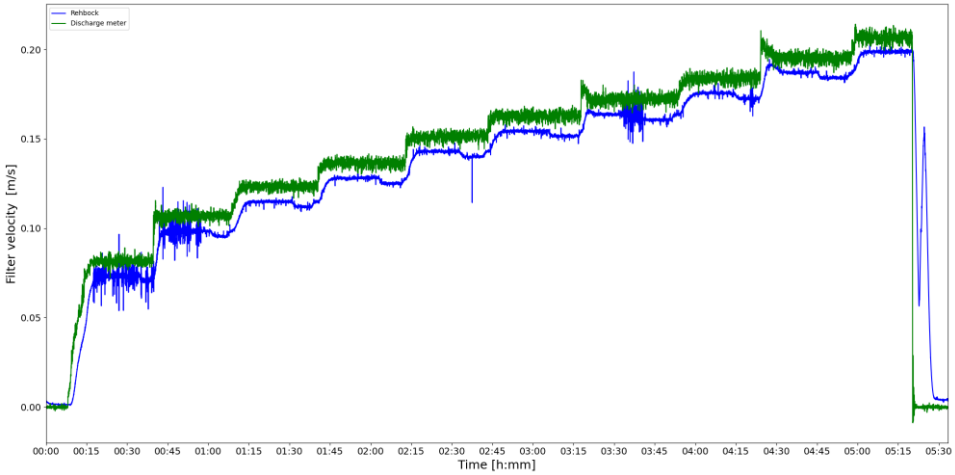

Figure 4-8: Filter velocity test 1.3

4.3.4 Duration of one time step

The duration of each test step is determined by identifying the start and end times for the step. The start time is specifically defined as the moment when the water level upstream of the test set-up is heightened, while the end time is identified as the point at which the water level is raised for the subsequent test step. This is visualized in Figure 4-9. The duration was obtained through a Python analysis, followed by a final manual correction to rectify any discrepancies or errors. Detailed information regarding the time duration for each test step across all tests is documented in Appendix F.1.

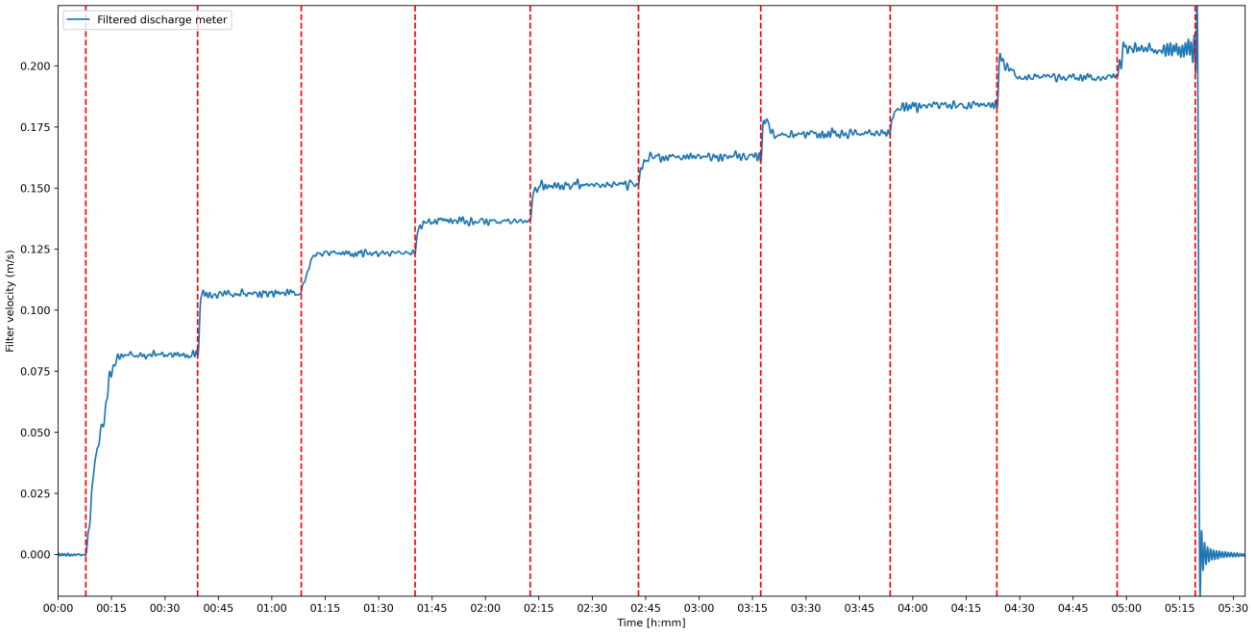

Figure 4-9: Time step duration for test 1.3

4.4 Sediment transport woven geotextiles

In the past, various criteria have been used to define the start of sand grain movement. These criteria are discussed in sub-section 4.4.1. Subsequently, these two different criteria were used to determine the start of movement. The following four methods were applied to analyze the start of movement:

- Measurement of erosion below the geotextile by Hall sensor (sub-section 4.4.2)
- Qualitative classification based on erosion state (measured with endoscope) (sub-section 4.4.3)
- Indirect measurement of sand transport after each test step based on image analysis (sub-section 4.4.4)
- Quantitative classification based on direct measurement of sand transport for each test step (sub-section 4.4.5)
- Quantitative analysis of endoscope images for each test step (particle count) (sub-section 4.4.6)

4.4.1 Classification of start of movement of sand grains

This study focuses on identifying the hydraulic load at the start of movement of the base material, known as the critical load, which could be determined by either the filter velocity or the hydraulic gradient. Determining this point precisely is challenging. The criterion adopted in this study is that as soon as a significant amount of erosion is observed, this condition is recognized as the critical load. At this particular test step, the average gradient across the caisson is considered as the critical

gradient, while the average filter velocity during this step is identified as the critical filter velocity. This point is described as a non-erosion criterion. Up to this established point, minimal or no sediment transport occurs through the geotextile. In his research, Klein Breteler (1988) utilized a value of 0.2 gr/s/m to describe the start of movement. Adapting this value to the width (1 meter) of the test set-up (Figure 4-10) used in this study results in a threshold criterion value of 0.2 gr/s/m².

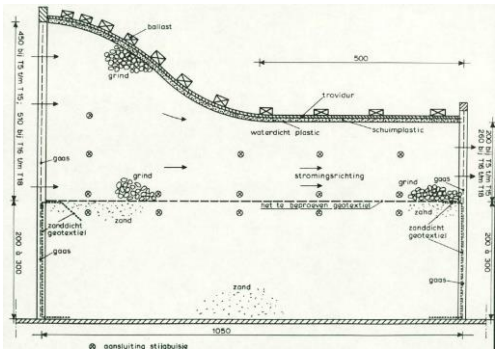

Figure 4-10: Test set-up Klein Breteler (Klein Breteler, 1988)

Erosion mechanisms with and without a geotextile

Erosion mechanisms vary significantly depending on the presence of geotextile between the filter layer and subsoil. Without geotextile, erosion progresses through three stages (Figure 4-11). Initially, when the flow velocity is below the critical filter velocity, the subsoil remains stable, and no erosion occurs. Once the velocity exceeds this critical threshold, erosion begins at a steady, low rate until it reaches a specific threshold, known as $u_{f,f}$. Beyond this point, the erosion rate rapidly increases, leading to significant base material transport.

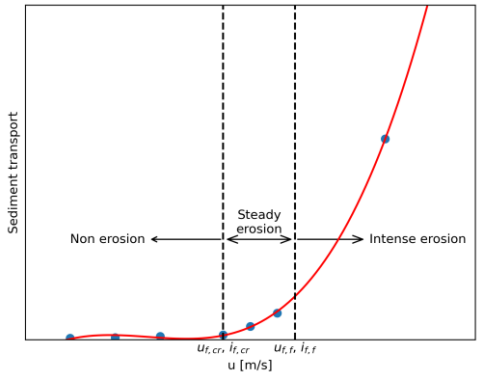

Figure 4-11: Erosion mechanisms without geotextile (Ho, 2007)

With geotextile, the erosion mechanism is more complex and includes four stages, as outlined by Ho (2007). The first two stages mirror those without geotextile. However, once the critical load exceeds the failure velocity, the geotextile allows fine particles to wash out, increasing the soil erosion rate (Figure 4-12). This results in the formation of a natural filter layer during erosion, accompanied by headward erosion. If headward erosion and downstream deposition continue, the erosion rate stabilizes and remain constant. If headward erosion stops and a stable natural filter layer forms, the erosion rate decreases. These findings are supported by Ho (2007) and Klein Breteler (1988). The presence of geotextile can stabilize the erosion process by facilitating the formation of a natural filter layer.

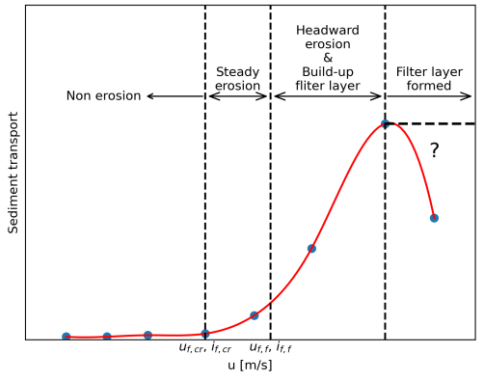

Figure 4-12: Erosion mechanisms with geotextile (Ho, 2007)

4.4.2 Hall sensor

A Hall sensor has been employed to measure the settlement resulting from erosion underneath the geotextile. The data gathered from these sensors reveal that detecting the start of movement presents a significant challenge, as depicted in Figure 4-13. The phenomenon of erosion within the sand bed does not occur uniformly across the whole sand bed. Instead, it is contingent upon the local flow patterns, which are, in turn, influenced by the specific arrangement of stones within the filter layer. As erosion becomes more pronounced, it spreads across the entire sand bed, leading to the settlement of the geotextile. However, the initial formation of erosion channels and pits does not necessarily align with the sensor's installed location. This variability in erosion patterns complicates the task of detecting critical moments of significant sand transport. Consequently, the Hall sensor will not be used to determine the start of movement.

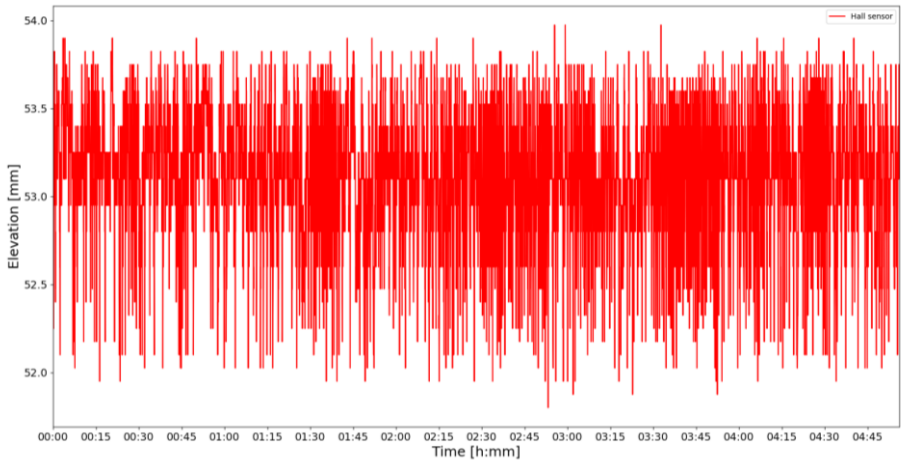

Figure 4-13: Results Hall sensor test 3.1

4.4.3 Determining the start of movement with video processing of endoscopes images

Using video processing techniques, a Python script was developed to count the number of sand particles passing per video frame captured by the two endoscopes. An illustration of this process is shown in Figure 4-14. Through this method, an estimation of the intensity of sand particle transport per unit of time is achieved, allowing for the correlation of transport states, as described by Ho (2007), with different test steps. The count of particles per frame has been converted into a count of particles per second, with the moving average calculated based on the number of particles per second.

It is important to note that the count does not differentiate between unique particles per second, leading to a potential overestimation of the actual number of particles per second, particularly at lower flow rates. This is because the same particle can appear in more than one video frame. Consequently, it is not feasible to directly translate the particle counts from the graph into a precise quantity of sediment per test step.

Additionally, the count is influenced by the movement of loose geotextile threads, which can be misidentified as particles. Although the script attempts to account for moving threads, complete elimination is not possible. However, upon visual inspection of the videos, it has been assessed that such occurrences are minimal and do not significantly impact the observation of visible erosion states during a test step.

Figure 4-14: Still of video processing test 9.2

In the two graphs presented below (Figure 4-15 and Figure 4-16), the number of particles is depicted by red lines. A moving average of the number of particles is represented in orange. Additionally, the filter velocity as measured by the discharge meter is plotted in these figures. Although this measurement does not precisely indicate the filter velocity, it effectively underscores the moments when the hydraulic load was increased. The first graph originates from the endoscope positioned in the middle of the test set-up (50cm), while the second graph is derived from the endoscope located 75cm from the start of the caisson.

In the first test step, an initial erosion peak is observed shortly after the critical load is increased (marking a new test step), which then decreases to almost zero for the remainder of the test step. Ho (2007) also identified this pattern as the non-erosion state. This peak is also present during test step 2, but here, the peak does not completely return to zero, indicating a "steady transport" state. The trend for test step 3 also shows a declining pattern but does not fully decrease to zero. However, the magnitude of the line suggests that significantly more sediment transport occurred during this test step compared to test step 2. Starting from test step 4, it is evident that continuous erosion transpires throughout the entire test step, marking a state of ongoing erosion that persists until the end of the test.

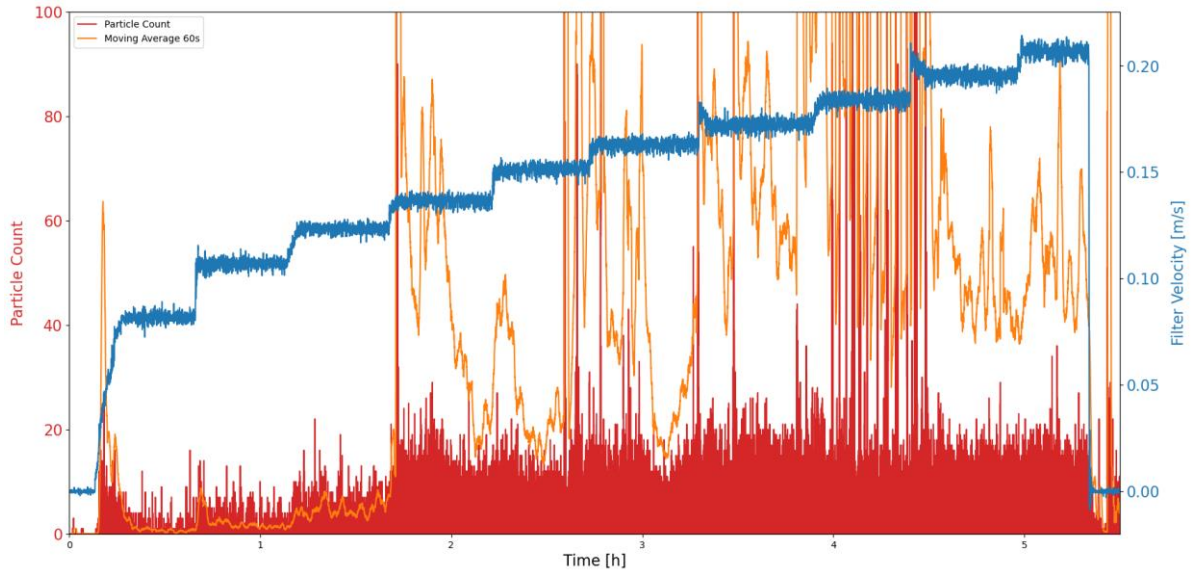

Figure 4-15: Sand particles per frame and moving average vs. time, test 1.3 camera 50cm

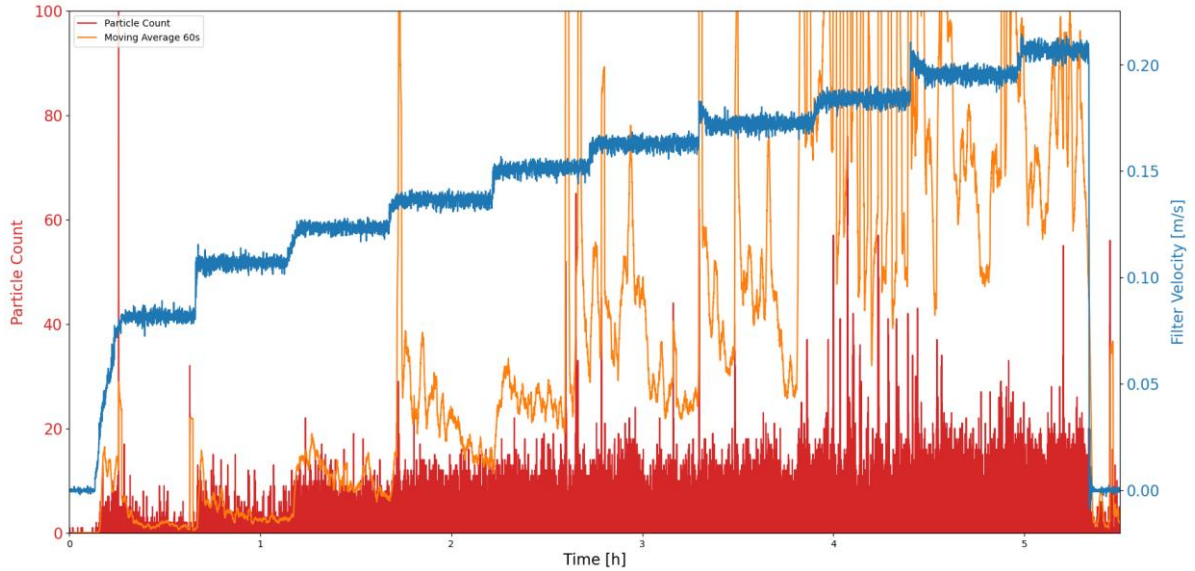

Figure 4-16: Sand particles per frame and moving average vs. time, test 1.3 camera 75cm

For every test that yielded useful camera images, a similar graph was created and is presented in Appendix F. These graphs facilitate the determination of the erosion state for each test step. In some tests, the duration of test steps was too short to accurately assess whether the number of particles approached zero. To address this and still quantify these test steps, it was decided that a visible declining trend towards zero would be classified as a non-erosion state. Through the classification of different erosion states, it becomes possible to identify at which test step the start of movement occurs. Consequently, the critical gradient and critical filter velocity for each test are determined based on these observations. For some tests, the crucial test step cannot be determined based on endoscope measurements. However, for these tests, the test steps where a clear erosion state is visible have been determined. The erosion state corresponding to each test step is shown in Appendix F.1.

4.4.4 Determining the start of movement with image processing

During the experiment, the sand eroded from the base layer and transported through the geotextile settles behind the test set-up. To estimate the relative amount of base material present on the surface of the flume behind the structure, a Python-based analysis is employed.

The process for determining the relative amount of gravel at the surface involves converting color images into black and white images. In these converted images, the sand is represented as white, and the bottom of the flume appears black. This conversion process encompasses several steps:

1. Each photograph is initially warped to ensure a consistent orientation across all images.

2. Following this warping, in the resulting images, sand is depicted as light gray to nearly white, while the surface of the flume appears as dark gray.

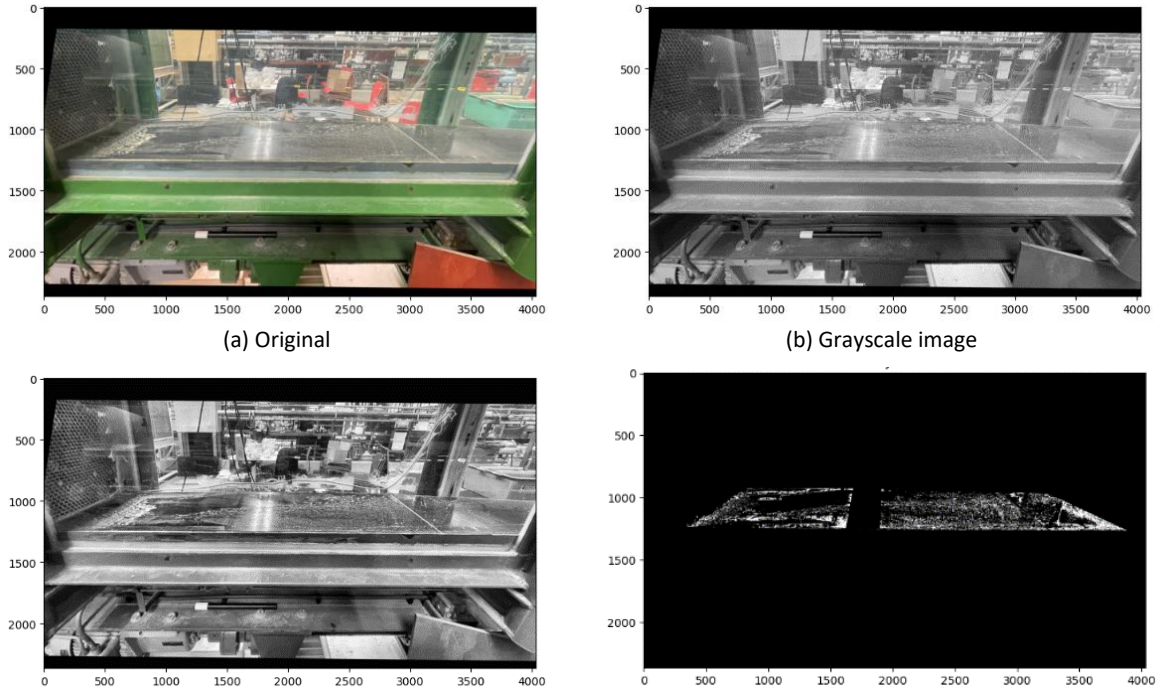

(a) Original (b) Grayscale image

(c) Grayscale image with CLAHE (d) Grayscale image without reflection area

Figure 4-17: Example images of the flume surface showing, the original (a) and grayscale image (b), grayscale image after CLAHE (c) and the grayscale image without reflection area (d)

The second step in the image conversion process aims to enhance the contrast of the image to minimize the effects of shadows from the walls using Contrast Limited Adaptive Histogram Equalization (CLAHE). Following this contrast enhancement, each photo is visually inspected to determine the threshold value at which the sand on the bottom of the flume is accurately selected, while also identifying areas affected by the reflection of lights to exclude from the calculation. For each image, three ranges of threshold values are utilized to detect different aspects of the sand distribution:

1) 200<x<255, in this range, the larger mounds of sand are mainly detected.

2) 180<x<200, in this range, areas with many loose grains of sand close to each other are mainly detected.

3) 145<x<180, In this range, the detection focuses on loosely scattered grains at the bottom of the flume. The areas identified within this threshold have the highest uncertainty due to the influence of

shadows, reflections, and the sharpness of the photos. As sand transport and flow velocity increase, the number of pixels within this range tends to decrease during the test.

Based on these threshold values, pixels falling within the specified ranges are rendered white, while all other pixels are turned black (as shown in Figure 4-18). By calculating the ratio of white pixels to the total number of pixels in the selected area of the flume, the density or amount of sand in this section can be determined. This analysis was conducted for the initial steps of each test.

In the image still a number of disturbances are present:

- Small spots due to shadows of parts of the flume
- White kit between the different bottom plates

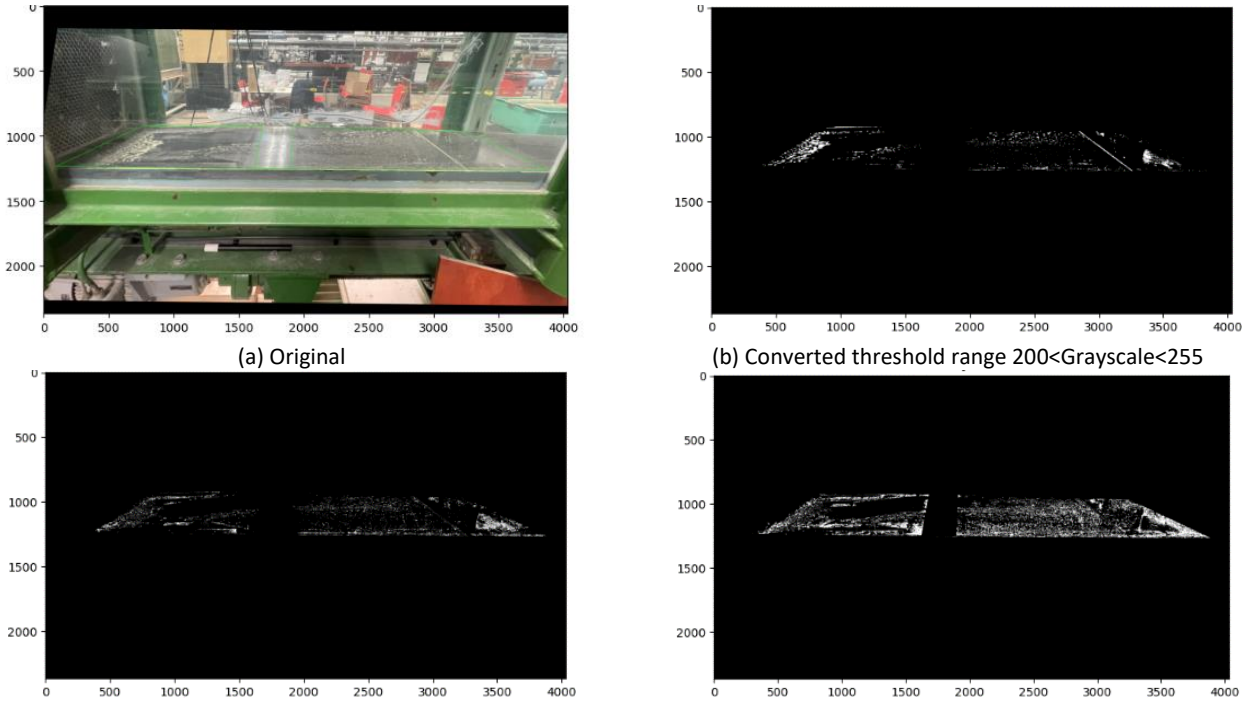

(a) Original

(b) Converted threshold range 200<Grayscale<255

(c) Converted threshold range 180<Grayscale<200

(d) Converted threshold range 145<Grayscale<180

Figure 4-18: Example images of the flume surface showing, the original (a), threshold range 200<Grayscale<255, (b), threshold range 180<Grayscale<200 (c) and threshold range 145<Grayscale<180 (d)

Compartment 1 refers to the section of the flume that lies between the test set-up and the first subsequent wall support, as illustrated in the previously mentioned photo. Compartment 2 is the part of the flume situated between the next two wall supports. This spatial arrangement is depicted in Figure 4-19, providing a clear visual representation of the compartment numbering within the flume.

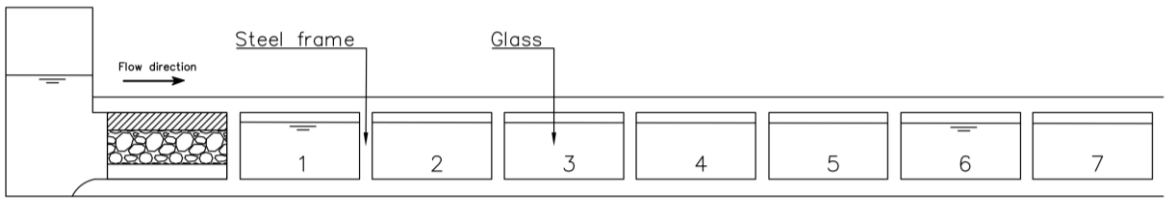

Figure 4-19: Sideview flume with compartment numbering

By plotting the density of sand for the various test steps within compartments 1 and 2 against the filter velocity for each test step, it is possible to create a graph. This graph serves to visually represent

the quantity of sand that has accumulated behind the structure over the course of the testing phases, as shown in Figure 4-20. Based on visual observations, the ranges 200-255 and 180-200 have been combined and represented as a single line in the graph.

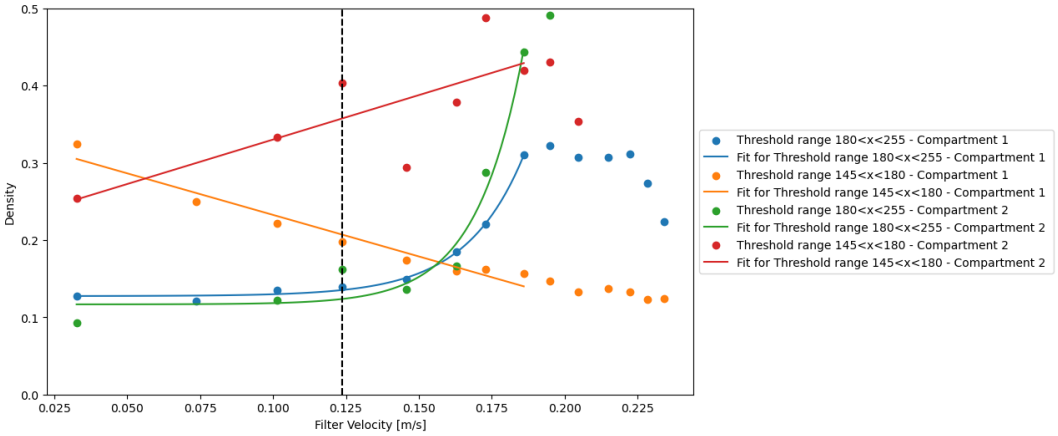

Figure 4-20: Graph of amount of sand behind structure test 3.1

The graph mentioned above offers insights into the test step at which the start of movement of sand grains begins. Nonetheless, the precision of these results does not suffice to accurately quantify the exact amount of eroded sediment per time step. This limitation in precision can be partly attributed to a phenomenon observed at higher flow rates, wherein sediment particles are washed over each other, causing some of the sediment to be transported from compartment 1 to compartment 2. While this method yields a reasonably good estimation of the moment when movement begins, it will not be utilized further to determine the start of movement due to its inherent limitations.

4.4.5 Determining the average sediment transport

Four tests (tests 1.3, 2.3, 3.2, and 9.2) were conducted, where the sediment was suctioned from the bottom of the flume after each test step. The amount of dried material measured after each test step has been converted to an average material transport per second per square meter using the following formula:

$$S\ [gr/s/m^2] = \frac{W}{A_e * t} \tag{4.9}$$

Where W is the mass of dry sand, A_e is the area of sediment erosion surface and t is the test step duration. As shown in Figure 4-21, the soil erosion surface is 0.90 m × 0.30 m = 0.27 m^2. In the figure below (Figure 4-21), the sediment erosion surface area is visualized.

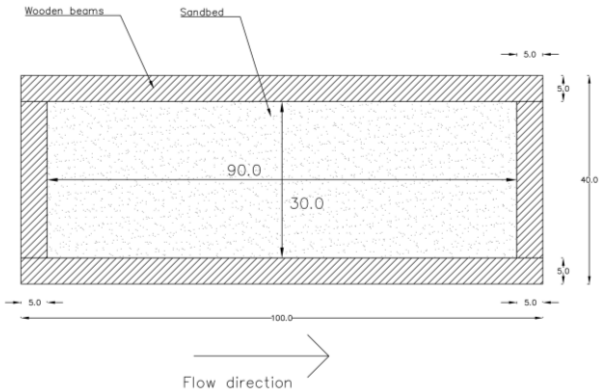

Figure 4-21: Area of soil erosion surface (dimensions in cm)

4.4.6 Determining the average particle transport

Based on the endoscope images described in sub-section 4.4.3, the number of particles per frame was counted. These counts were subsequently converted into the number of particles per second. It is important to note that the script used does not count the number of unique particles per second.

To determine if a transport graph could be generated based on the particle count, the integral of the moving average line for each test step was calculated. This value was then divided by the test step duration. The preceding process is summarized in the formula below:

$$P\ [average\ amount\ particles/s] = \frac{\int_{t_1}^{t_2} moving\ average\ line}{\Delta t} \tag{4.10}$$

The moving average line, represented in orange such as Figure 5-11, is a function of the moving average. t_1 is the start time of the test step, t_2 is the end time of the test step, and Δt is the test step duration (t_1 - t_2).

The value obtained using the above formula represents the average number of particles per second for the entire test step. Since a low filter velocity causes a particle to be counted in multiple frames per second, this leads to an overestimation of the number of particles.

The measurements from the endoscope images provide an amount of sediment passing through a specific ray (Figure 4-22) in the filter layer, while the measured sand transport is expressed in units of grams per second per square meter (gr/s/m²).

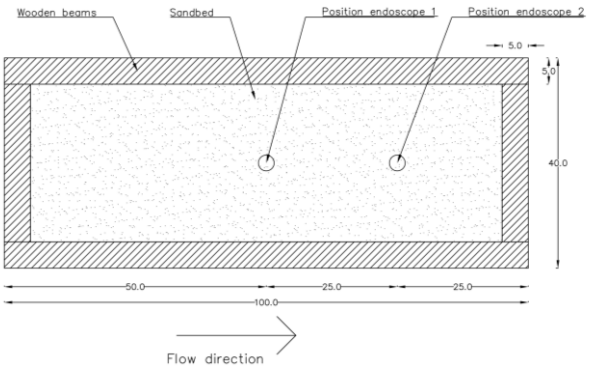

Figure 4-22: Positions of endoscopes

4.4.7 Summary methods to determine the critical test step and results critical load

Based on the results of the different methods discussed in the above sub-sections, it can be concluded that there are two good methods to determine the critical test step:

- Qualitative assessment based on endoscope measurements and Ho's classification

- Quantitative assessment based on measured weighed transport and Klein Breteler criterion of 0.2 gr/s/m^2 (only for tests 1.3, test 2.3, test 3.2 and test 9.2).

In the table presented below (Table 4-5), the results of the tests conducted with natural woven geotextiles are presented. This table includes the key results for each test, such as the critical filter velocity, critical gradient, duration of the test, and the total amount of eroded sand. A total of 16 tests were carried out with 9 different configurations.

For some tests, the crucial test step cannot be determined based on endoscope measurements. This has been indicated with a question mark.

Table 4-5: Test results woven geotextiles non-erosion criterion

Test	Geotextile	Filter material	Test step	$u_{f,cr}$ [m/s]	i_{cr} [-]	Duration [h]
Test 1.1	J4	45/125 mm	7	≈ 0.106	≈ 0.29	5.25
Test 1.2	J4	45/125 mm	2	≈ 0.101	≈ 0.21	4.25
Test 1.3	J4	45/125 mm	2	≈ 0.098	≈ 0.19	5.33
Test 2.1	J5	45/125 mm		≈ ?	≈ ?	6.4
Test 2.2	J5	45/125 mm	4	≈ 0.126	≈ 0.31	4.75
Test 2.3	J5	45/125 mm	3	≈ 0.132	≈ 0.26	6.33
Test 3.1	J7	45/125 mm	3	≈ 0.101	≈ 0.21	4.65
Test 3.2	J7	45/125 mm	3	≈ 0.102	≈ 0.21	6
Test 4	J9	45/125 mm		>0.21	> 0.95	4.15
Test 5.1	J4	40-70 mm		≈ ?	≈ ?	4.8
Test 5.2	J4	40-70 mm	2	≈ 0.090	≈ 0.17	4.3
Test 6	J5	40-70 mm		≈ ?	≈ ?	7.5
Test 7	-	40-70 mm	3	≈ 0.017	≈ 0.02	1.8
Test 8	J4	60-90 mm	2	≈ 0.097	≈ 0.14	4.8
Test 9.1	J5	60-90 mm		≈ ?	≈ ?	4.6
Test 9.2	J5	60-90 mm	3	≈ 0.132	≈ 0.26	5.15

The table above clearly shows that in the tests with the same geotextile but different filter materials, the critical filter velocity is nearly the same, even though there is a significant difference in the critical gradient.

4.5 Sediment transport non-woven geotextiles

The tests with the non-woven geotextiles show that the test facility cannot achieve sufficient gradient/filter velocity to cause these geotextiles to reach the start of movement (Figure 4-23).

Figure 4-23: Geotextile wool on jute after test (left) and sandbed after test wool on jute (right)

The discharge graphs obtained from the Rehbock weir distinctly indicate the moments during the tests when the weir was lowered to facilitate a larger hydraulic gradient. This adjustment is evident from the peaks in the discharge graph of the Rehbock weir, which are not mirrored in the data captured by the discharge meter. In addition, the images captured by the endoscopes during these tests have been analyzed to ascertain whether, despite the minimal amount of eroded sediment, sediment transport was still occurring. The graph presented below (Figure 4-24) clearly demonstrates

that sediment transport was present during the first 5 test steps This transport of material is likely caused by sand that was still present on the stones at the beginning of the test and sand that was released during the manipulation of the sandbed and the placement of the geotextile. Following these initial steps, a constant line slightly above 0 is observable in the graph. The reason this line does not exactly align with zero is primarily due to the presence and movement of sand particles and small stone particles on the fabric. The outcomes of the tests involving non-woven geotextiles are documented in Table 4-6.

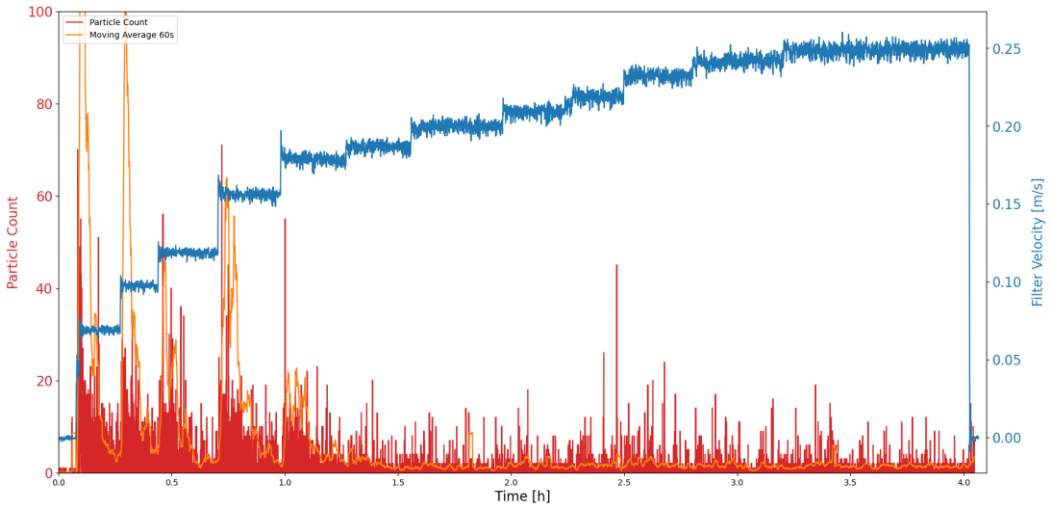

Figure 4-24: Sand particles per frame and moving average vs. time, test 12 (wool on jute) camera 50cm

Table 4-6: Test results non-woven geotextiles

Test	Geotextile	Filter material	$u_{f,cr}$ [m/s]	i_{cr} [-]	Duration [h]	Total amount of eroded sand [gr]
Test 10	Hemp on jute	45/125 mm	>0.20	>0.98	3.75	17
Test 11	Jute on jute	45/125 mm	>0.22	>0.98	3	7
Test 12	Wool on jute	45/125 mm	>0.21	>0.99	4.0	10

4.6 Model effects and uncertainties

The used test set-up is a simplified representation of the reality. Simplifications within the physical model may result in inaccuracies or distorted representations of processes. This section will discuss effect that do not occur in reality, model effects, and the uncertainties of the set-up.

4.6.1 Model effects

Wall effects

The walls of the flume, being made of glass, are completely flat. This characteristic, in combination with the shape of the stones, leads to larger pore openings at the sides of the filter layer compared to those in the middle. During the construction of the filter layer, considerable effort was made to minimize these larger pore openings at the glass walls. As part of this effort, some of the large stones from the 45/125 mm filter layer were cut in half to mitigate the effect at the sides. Furthermore, the top of the caisson is entirely smooth, which could potentially influence the flow dynamics. To minimize the effect of the caisson's smooth surface, rubber foam has been applied, enhancing the overall set-up's ability to simulate natural conditions more accurately.

Positioning of stones

The impact of the hydraulic load on the geotextile is significantly influenced by the characteristics of the filter material, with porosity/pore size and stone positioning being crucial factors. In the tests that were carried out, variations in how the stones were positioned became particularly noticeable. The broad grading of the 45/125 mm filter material facilitated a wide variety of stone positions and pore sizes. To ensure that the caisson could be securely pressed against the edges of the flume, it was imperative that no stones protruded above the bottom of the caisson. Consequently, it was sometimes necessary to reposition several stones in the filter layer to maintain an equal number of stones per test.

When manually placing stones within a rectangular box, there is an inherent tendency to arrange the stones too orderly, particularly along the sides. This overly neat stacking can result in a reduction in porosity, affecting the overall effectiveness of the filter layer. This careful consideration of stone positioning and the effort to maintain uniformity across tests highlight the complexity of replicating natural conditions within a controlled experimental set-up.

In and outflow effects

The inflow and outflow of water into and from the filter layer can significantly influence the flow dynamics, thereby affecting the hydraulic gradients near the entrance and exit points of the test set-up. To mitigate these effects on the sand bed and ensure a more uniform flow pattern, wooden slats have been strategically installed at both the front (inflow side) and back (outflow side) of the test set-up.

Placement of endoscopes

The presence of two endoscopes within the filter layer represents an atypical element not usually found in standard geotextile filter construction applications. To mitigate their potential impact on the experimental results, a decision was made to install the cameras within a stone, thereby minimizing their influence on the surrounding environment. The only minor effect on the results comes from the cables of the endoscopes. These cables were strategically routed upwards via the shortest path possible and then directed just beneath the rubber foam towards the back of the test set-up.

It is important to note that the distance between the endoscope and the geotextile varies across tests. This variability can lead to differences in the number of particles counted by the endoscopes, as the perspective and field of view of the cameras change depending on their positioning relative to the geotextile.

4.6.2 Uncertainties transport of base material measurements

The amount of sediment measured per test step and at the end of each test is subject to uncertainties from the model set-up and the measurement methods.

<u>Uncertainties in measurements of transport of tase material:</u>

- Sand that was partially transported during the filling of the flume and washed out under different flow conditions.
- Material from the stones if there is residual material on them.
- The method of suctioning the sediment from the bottom of the flume.

Filling of the Flume:

During the process of filling the flume, erosion of sand from the filter layer can occur. Despite filling the flume at a controlled flow rate, the initial opening of the valve can result in a relatively high flow velocity over the geotextile, leading to minor erosion of the base material.

Effects of Jute Threads on Erosion:

The woolly structure of the threads of jute/natural geotextiles means that sediment eroded from beneath the geotextile is not always immediately transported to the rear of the test set-up, especially at low flow rates. During the installation and filling of the flume, a small amount of sediment always lands on the geotextile. There may also be a small amount of sediment present on the stones. Some of this sediment, due to the woolly structure, is not immediately transported to the rear of the test set-up during the filling of the flume and the first test step. Consequently, it is not possible to trace whether the sediment that ends up behind the test set-up during the first test steps was actually eroded during these steps. As a result, sand eroded from beneath the geotextile may end up behind the test set-up in the next test step and thus be counted in that step.

Tests with geotextiles where the start of movement is not achieved also illustrate this issue. The graph showing the number of particles per second indicates that the geotextile is "clean" only after 4/5 test steps. This observation suggests that the sediment captured during the initial test steps is partly derived from the installation of the geotextile or originates from the stones.

Suctioning sediment during tests:

All experiments were conducted under a continuous flow regime, without any interruptions. Consequently, sediment continued to be released from the test set-up while sediment from the flume's bottom was being suctioned away. In test steps characterized by minimal erosion, the quantity of sediment being suctioned is comparatively low. However, in steps experiencing significant erosion, the amount of sediment released could still be considerable.

As the suctioning process was underway, it was possible for sediment to settle on areas of the flume floor from which sediment had already been removed. Once sediment was suctioned from the entire bottom of the flume, a final, rapid suction action was executed in an attempt to remove as much sediment as possible. Despite these efforts, some sediment might not have been suctioned up completely and would remain on the flume floor. This residual sediment was then removed during the suctioning process of the subsequent test step.

Qualification of erosion state

Although the best attempts were made to define the erosion state for every test step as accurate as possible, the visual observations and interpretations of the graphs still are a source of subjectivity.

4.6.3 Uncertainties of measurements

In the analysis of experimental data, there are two primary types of inaccuracies that can arise: measurement errors and uncertainties in the analysis of the data. These inaccuracies have the potential to significantly impact the results of calculations, potentially leading to variations in the interpretation of experimental outcomes. An overview of the various sources of errors and uncertainties is provided in Table 4-7. It is crucial to acknowledge that despite diligent efforts to estimate these uncertainties as precisely as possible, a certain level of subjectivity is inherent in the determination of errors.

Table 4-7: Absolute error in measured parameters

Variable	Absolute error	Unit
Pointer gauge	1	mm
Tape measure	1	mm
Rehbock weir	1	mm
d_{f50}	$0.05 \cdot d_{f50}$	mm
d_{b50}	$0.05 \cdot d_{b50}$	mm
t_g **(lab)**	$0.03 \cdot t_g$	mm
t_g **(caliper)**	$0.1 \cdot t_g$	mm
k_g	$0.2 \cdot k_g$	mm/s
ρ_w	5	kg/m^3
ρ_s	100	kg/m^3
ρ_b	$0.001 \cdot \rho_b$	kg/m^3

Flow area

The size of the flow area impacts the filter velocity. In this study, the decision was made not to account for the volume of rubber foam within the flow area. This choice results in a smaller flow area compared to scenarios where the foam's volume is included, consequently leading to an increased filter velocity. The filter velocity determined here represents the maximum possible velocity, in contrast to situations where the foam rubber's volume is considered, which would utilize the minimum filter velocity. Additionally, the rounding of stones resting against the flume's glass tends to cause an overestimation of the foam rubber's surface area rather than an underestimation of the total volume of foam rubber.

4.6.4 Start-up and settings

At the beginning of each test, the flume was gradually filled with water to reduce the potential for erosion during the filling process. Once the water level attained the preset height of the weir located at the end of the flume, the valve was closed, and a baseline (zero) measurement was recorded. The water level/discharge on the upstream side was controlled by a valve, which required manual adjustments for each test step, as illustrated in Figure 4-25. This manual process of adjusting the valve introduces challenges in precisely reaching the predetermined water level for each test step. As a result, there have been occasions where the water level either surpassed the intended height or took an extended period to stabilize at the correct water level.

Figure 4-25: Valve of inflow pipe

5 Analysis

This chapter presents a comprehensive analysis of the test results from Chapter 4. Initially, the porosity of each test is determined. Following this, the Forchheimer coefficients are analyzed to provide insights into the flow characteristics through the filter material. The transport of the base material is then examined to determine the point at which movement of the base material starts. An analysis is subsequently conducted to determine the critical load for open natural geotextiles. Additionally, the impact of pore size on the critical load is evaluated, assessing how the dimensions of the openings in the geotextile influence the material's resistance to hydraulic load. The results are then compared with the previous study by Lemmens, and the measurements from the endoscope images are analyzed to create a sediment transport graph. Finally, the measured critical hydraulic loads from the experiments are compared with the pre-calculated critical loads, offering a comparison between expected and observed outcomes.

5.1 Porosity

The porosities of the different filter materials calculated in Section 4.2 are influenced by the application of rubber foam at the top of the filter layer. Consequently, we will refer to this adjusted measurement as the effective porosity (n_{eff}). The application of rubber foam reduces the effective porosity because it is placed at the location in the filter layer where the highest porosity is typically found, according to Bosma's (2001) theory (Figure 5-1).

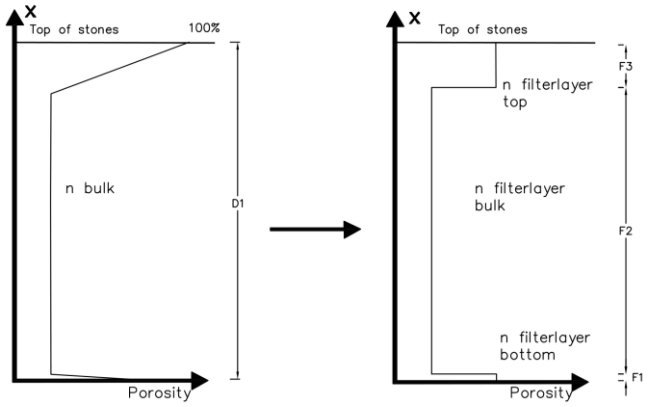

Figure 5-1: Schematization porosity distribution (adapted from (Bosma, 2001))

The effective porosity of the filter layer when applying rubber foam to the top of the filter layer can be calculated using the equation below:

$$n_{eff} = \frac{\int_0^{0.275d_{n50}} \frac{n_{bulk}+100}{0.275d_{n50}} * X + 100dx + \int_{0.275d_{n50}}^{D1-0.74d_{n50}} n_{bulk}\,dx + \int_{D1-0.74d_{n50}}^{D_1-h_{RF}} \frac{100-n_{bulk}}{0.74d_{n50}} * X + 100 - \frac{100-n_{bulk}}{0.74d_{n50}} * D1dx}{D1-h_{RF}} \quad (5.1)$$

With:

n_{eff} = effective porosity of filter material [-]
n_{bulk} = bulk porosity of filter material
d_{n50} = nominal diameter exceeded by 50% of the diameters [m]
$D1$ = thickness of filter layer [m]
h_{RF} = height of rubber foam [m]

Using equation (5.1), the effective porosity was calculated for average rubber foam thicknesses of approximately 2 cm, 3 cm, and 4 cm. The results are presented in Table 5-1.

Table 5-1: Dimensions filter material parameters and influence lengths

Test/filter material	**Volume of stones [m³]**	**d_{n50} [m]**	**n_{bulk} [-]**	**n_{eff} with h_{RF} =0cm [-]**	**n_{eff} with h_{RF} =2cm [-]**	**n_{eff} with h_{RF} =3cm [-]**	**n_{eff} with h_{RF} =4cm [-]**
45/125 mm*	0.0419	0.06179	0.370	0.469	0.425	0.412	0.405
45/125 mm of test 1.1	0.0456	0.06232	0.313	0.422	0.374	0.359	0.352
45/125 mm of test 2.1	0.042806	0.06228	0.355	0.457	0.412	0.398	0.391
40/70 mm	0.0397	0.04573	0.431	0.497	0.460	0.453	0.453
60/90 mm	0.0410	0.06150	0.384	0.480	0.437	0.424	0.418
*Without tests 1.1 and 2.1							

From the analysis of the thickness of the rubber foam (Appendix C.3.1), it has been concluded that the average thickness of the rubber foam is approximately 3 cm. The porosities of the various filter materials at this rubber foam thickness will be used in this study.

5.2 Forchheimer coefficients

Forchheimer has established a relationship between the hydraulic gradient across the filter material and the filter velocity within the filter material, as described in sub-section 2.1.3. This relationship is:

$$i = au_f + bu_f^2 \tag{5.2}$$

The experimental relationship between the hydraulic gradient and the filter velocity for each test has been established, with an illustrative example depicted in Figure 5-2. Based on this experimental data, the model constants 'a' and 'b' for the Forchheimer equation are derived. These constants, when combined with the filter material's specific characteristics such as porosity, d_{fn50}, and the viscosity of the water, enable the application of the Forchheimer equation to estimate the Alpha (α) and Beta (β) values.

The amount of rubber foam present at the top of the filter layer influences the porosity. To illustrate how this porosity affects the Alpha and Beta values, these parameters have been determined for all three calculated porosities. The Alpha and Beta values for each test are provided in Appendix F.2.

From the analysis, it has been concluded that the average thickness of the rubber foam is approximately 3 cm. At this thickness, the average Alpha and Beta values are 3900 and 1.11, respectively. Prior to the tests, calculations were made with assumed values of 1000 for Alpha and 1.1 for Beta. The test results now indicate that the initial assumption for Alpha was too low, whereas the assumption for Beta was accurate.

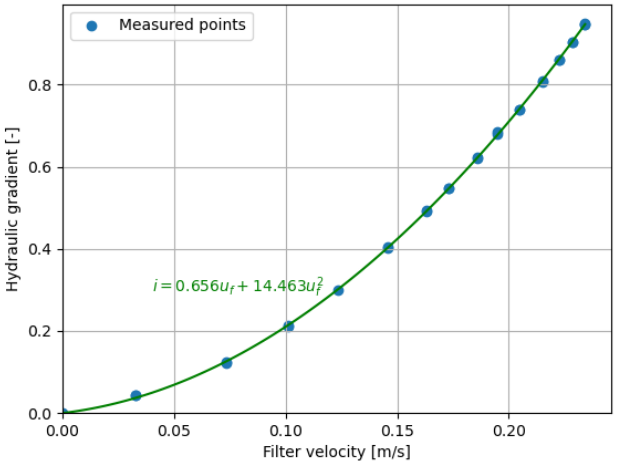

Figure 5-2: Relation between hydraulic gradient and filter velocity test 3.1

5.2.1 Ratio hydraulic gradient and filter velocity

By using 3 types of filter materials, the ratio between the hydraulic gradient and the filter velocity will differ. Below, a graph (Figure 5-3) is shown with the ratios of each test step of all the different tests. These ratios clearly show that not every test with the same filter material also has the same ratio.

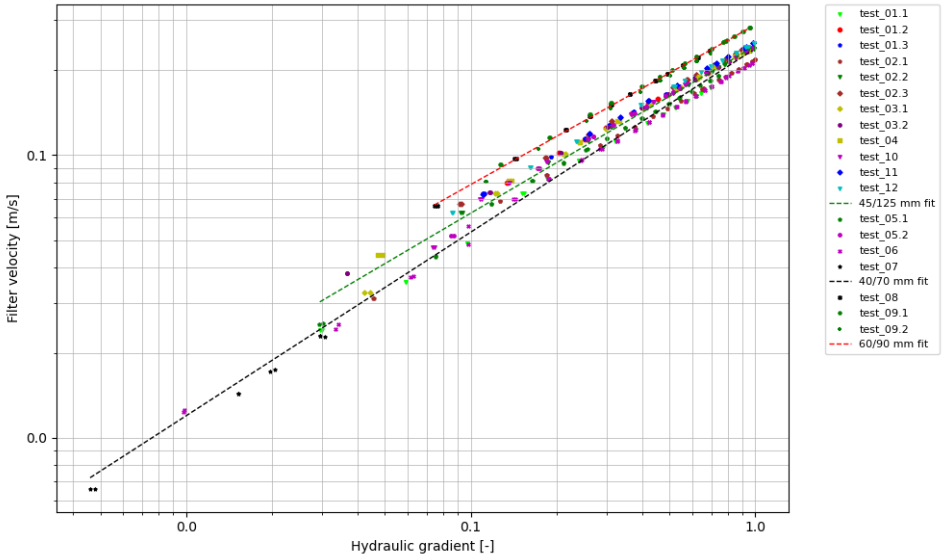

Figure 5-3: Ratio hydraulic gradient and filter velocity

5.3 Transport of base material

The diagrams in Figure 5-4 and Figure 5-5 depict relationship between the filter velocity and the transport of base material. The amount of sediment measured per test step has been recalculated into a transport rate, expressed in grams per second per square meter (gr/s/m²). In both figures, a trend line has been drawn through the data points to highlight the observed trend. For each test, this trend line is extended to reach the threshold criterion of 0.2 gr/s/m², as established by Klein Breteler (1988).

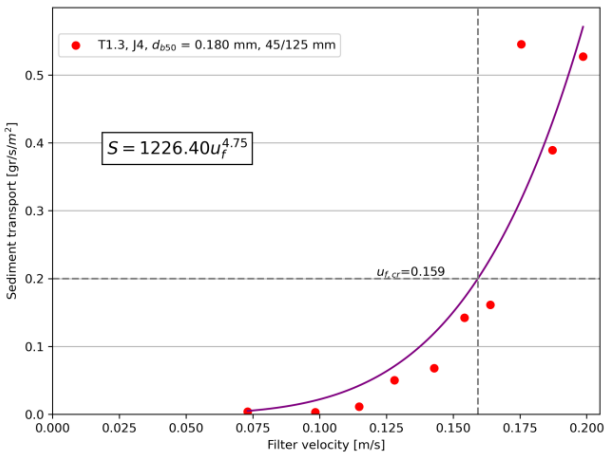

Figure 5-4: Transport of base material vs. filter velocity, test 1.3

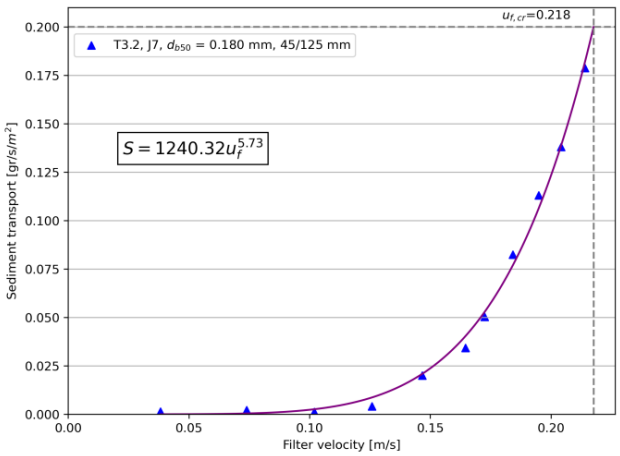

Figure 5-5: Transport of base material vs. filter velocity, test 3.2

The two figures below (Figure 5-6 and Figure 5-7) depict the measured transport of base material of tests 2.3 and 9.2. Both tests were conducted using the same geotextile but with different types of filter material. The d_{f50} of both filter materials was nearly equal, however, a wide grading was used during test 2.3, and a narrow grading was used in test 9.2.

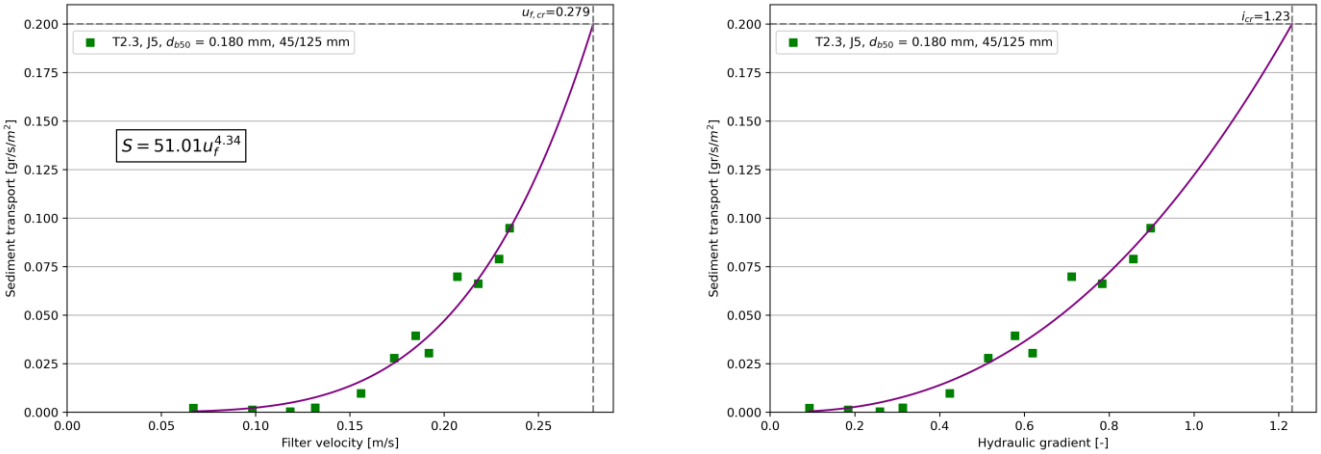

Figure 5-6: Transport of base material vs. filter velocity and transport of base material vs hydraulic gradient, test 2.3

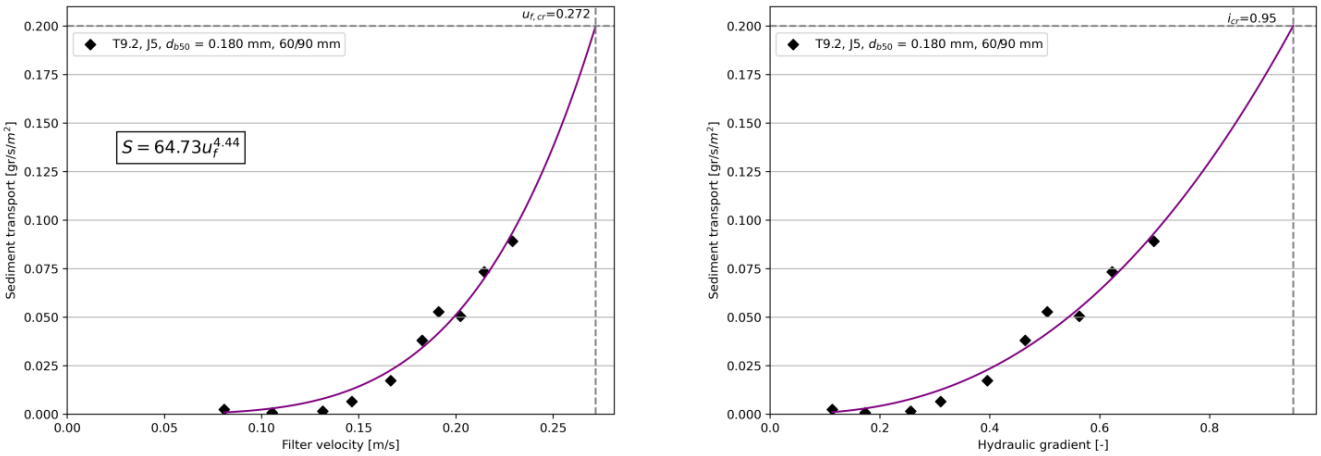

Figure 5-7: Transport of base material vs. filter velocity and transport of base material vs. hydraulic gradient, test 9.2

5.4 Critical load for open (natural) geotextiles

Based on the results obtained above, it can be determined whether the critical load for open (natural) is the critical filter velocity or hydraulic gradient. The distinct filter materials used in the experiments lead to varying ratios of filter velocity to hydraulic gradient across tests. If the start of movement in both tests is triggered at the same value for a particular type of load, it indicates that this load type is responsible for the start of movement.

In Figure 5-8, the average sand transport per test phase for tests 2.3 and 9.2 is graphed against both filter velocity and hydraulic gradient. The same geotextile, J5, was used in these tests, but with different stone gradations. Test 2.3 utilized a stone grading of 45/125 mm, whereas test 9.2 employed a grading with a similar median diameter (d_{f50}) but a narrower gradation. During the fourth test step of both experiments, the hydraulic gradient remained nearly identical (approximately 0.31), yet the filter velocities differed (0.132 m/s for test 2.3 and 0.147 m/s for test 9.2). Notably, sediment transport occurs in test 9.2 but nearly no sediment transport is measured in test 2.3.

This observation suggests that while the hydraulic gradient remained similar, the differing filter velocities between the two tests influenced the start and magnitude of sediment transport. This highlights the potential impact of filter velocity and stone grading on sediment movement, indicating a complex interaction between hydraulic conditions and material characteristics in determining the critical load for sediment transport.

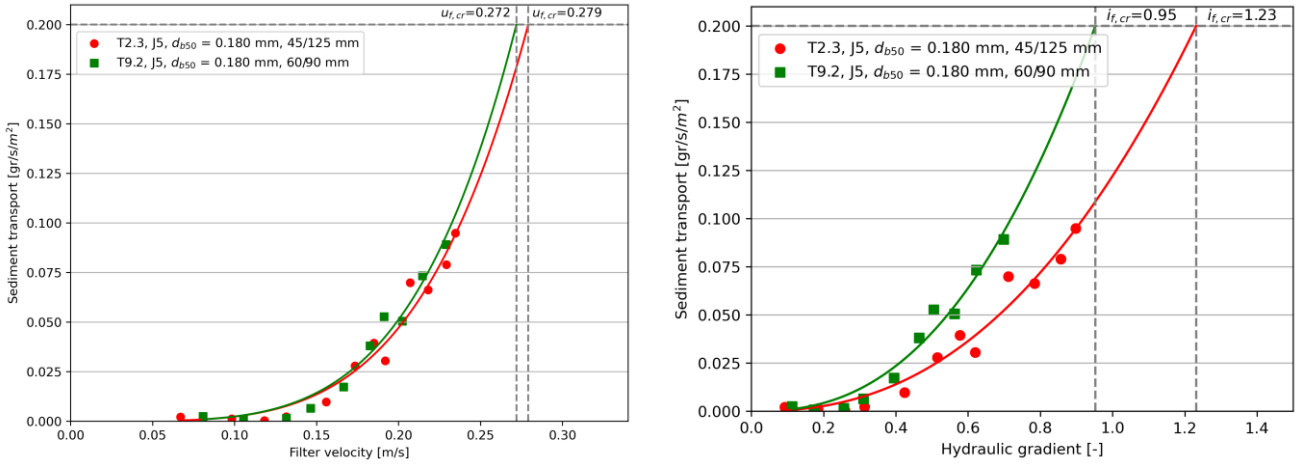

Figure 5-8: Transport of base material vs. filter velocity and transport of base material vs. hydraulic gradient, tests 2.3 and 9.2

The figure above also includes the trend lines extended to Klein Breteler's threshold criterion for both tests. The difference in critical filter velocity between the two tests is only 0.007 m/s, while there is a significant difference in the critical gradient.

In the table below (Table 5-2), the results of the critical filter velocity of the two different threshold criteria for the four tests are shown.

Table 5-2: Test results of two threshold criteria

Test	**Geotextile**	**Filter material**	**Non-erosion criterion**		**Criterion: 0.2 gr/s/m²**	
			$u_{f,cr}$ **[m/s]**	i_{cr} **[-]**	$u_{f,cr}$ **[m/s]**	i_{cr} **[-]**
Test 1.3	J4	45/125 mm	≈ 0.098	≈ 0.19	≈ 0.159	≈ 0.46
Test 2.3	J5	45/125 mm	≈ 0.132	≈ 0.31	≈ 0.279	≈ 1.23
Test 3.2	J7	45/125 mm	≈ 0.102	≈ 0.21	≈ 0.218	≈ 0.83
Test 9.2	J5	60/90 mm	≈ 0.132	≈ 0.26	≈ 0.272	≈ 0.95

5.5 Influence of openings size on critical load

The literature reveals that the d_{b90}/O_{90} ratio is currently used as the most important indicator for the sandtightness of open geotextiles (Klein Breteler, 1988). To illustrate this, the sediment transport of the geotextiles J4 ((O_{90} = 516.1 µm) and J5 (O_{90} = 819.0 µm) is plotted against the filter velocity and hydraulic gradient in the figure below (Figure 5-9). Figure 5-9 shows that the geotextile J5 can withstand a larger hydraulic load than the tested geotextile J4, despite its opening size being almost 50% larger.

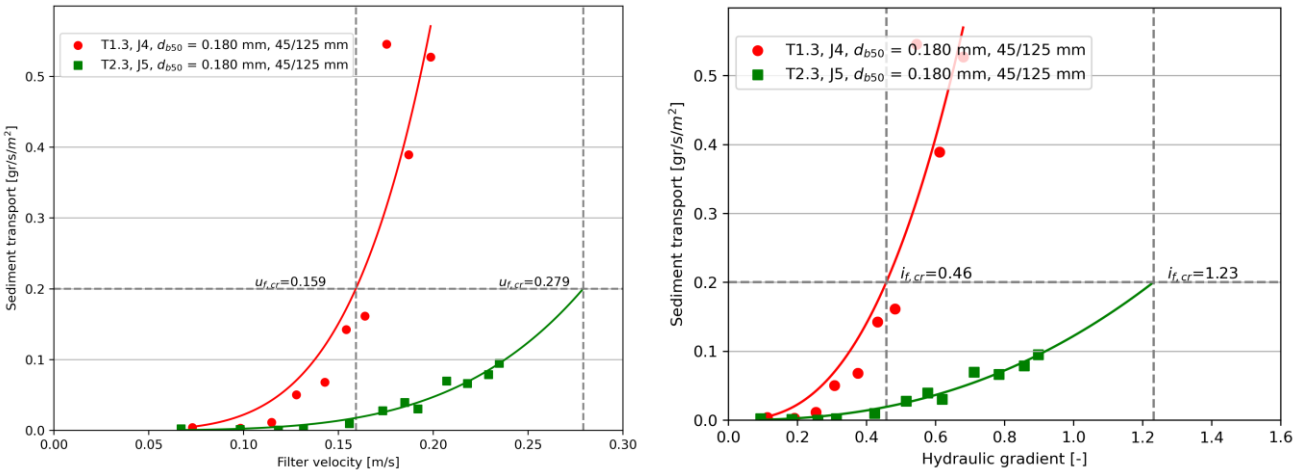

Figure 5-9: Transport of base material vs filter velocity and transport of base material vs hydraulic gradient, tests 1.3 and 2.3

5.6 Comparison with Lemmens

Lemmens (1996) determined only the critical gradient for one jute geotextile, with a value of 0.26. By converting this value to a critical filter velocity, a good comparison can be made between the geotextile tested by Lemmens and the geotextiles tested in this study. The critical filter velocity of the woven jute geotextile can be calculated as follows:

$$i = 0.26 = au_{f,cr} + bu_{f,cr}|u_{f,cr}| \quad (5.3)$$

Lemmens (1996) conducted his experiments using fine sand and a filter layer with stones ranging from 80 to 200 mm in size. Along the flume wall, a stone grading of 30-40 mm was applied. Some parameters were not mentioned in Lemmens's research, leading to certain assumptions. All dimensions of the base and filter material parameters are included in Table 5-3.

Table 5-3: Dimensions base and filter material parameters

Parameter	Value	Unit
d_{fn50}	140**	mm
n_f	0.4*	-
v_w	$1.09*10^{-6}$ (at 17 °C)*	m^2/s
α	1000***	-
β	1.1***	-

* Assumption
** Assumption made with (Laan, Het gebruik van steen in waterbouwkundige constructies, 1996)
*** Assumption made with (Van Gent, 1993) and (Van Gent, 1995)

Using these values in combination with equations (2.9) and (2.10), the coefficients *a* and *b* are found to be 0.03 s/m and 7.51 s²/m², respectively. Consequently, the critical filter velocity in the filter layer $u_{f,cr}$ can be computed, resulting in a critical velocity of 0.183 m/s for the jute geotextile.

$$u_{f,cr} = 0.183\ [m/s] \tag{5.4}$$

During Lemmens' (1996) test, a complex erosion pattern was also observed, where a small amount of sand was released in the earlier steps and a larger amount in the later steps. A total of 300 grams was eroded during the entire test, assuming that this was almost entirely eroded in the last test step of 1 hour.

Lemmens used a sand bed of 50 cm on both the inflow and outflow sides, with a caisson of 1 meter in between. No erosion occurred on the downstream side, and approximately 25 cm eroded on the upstream side. The erodible width was approximately 35 cm, which is the distance between the sandtight geotextile attached to both sides of the flume. This results in an erodible area of approximately 0.44 m² (1.25 m x 0.35 m). Consequently, approximately 0.19 grams per second per square meter (gr/s/m²) was eroded.

5.7 Sediment transport graph with endoscope measurements

The figures below display both the average number of particles per second per test step versus the filter velocity and the measured amount of eroded base material at the end of each test step, as calculated in section 5.3. The particle measurements are derived from images captured by an endoscope positioned 75 cm from the inflow point. At lower filter velocities, a particle may appear in multiple frames per second, leading to an overestimation of the particle count. Therefore, these data points are excluded from the fit applied to the various data points. As the filter velocity increases, the likelihood of double-counting the same sand particle within a second decreases.

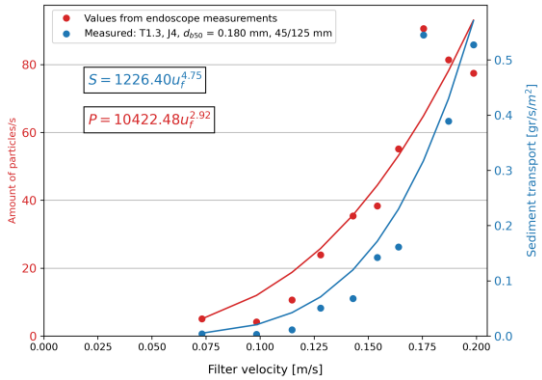

Figure 5-10: Transport of base material vs. filter velocity, test 1.3

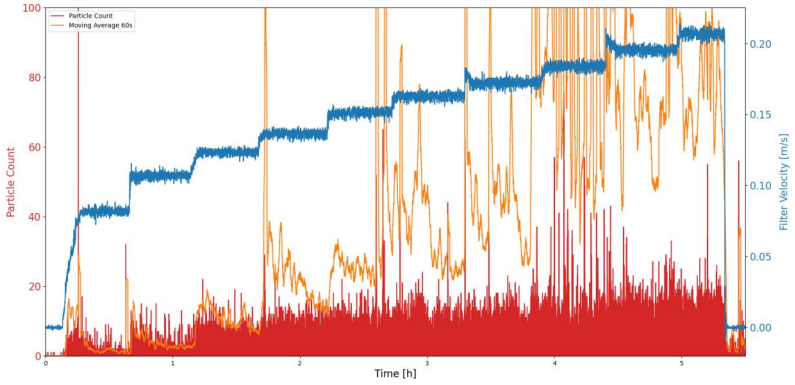

Figure 5-11: Sand particles per frame and moving average vs. time, test 1.3 camera 75cm

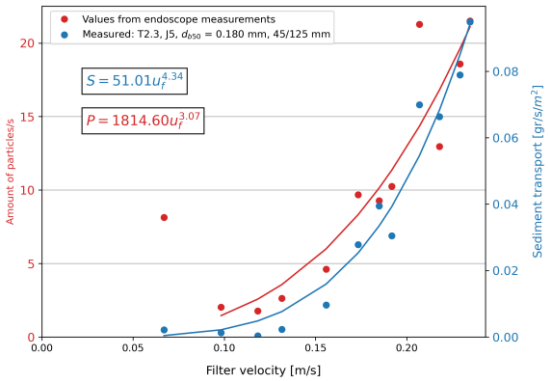

Figure 5-12: Transport of base material vs. filter velocity, test 2.3

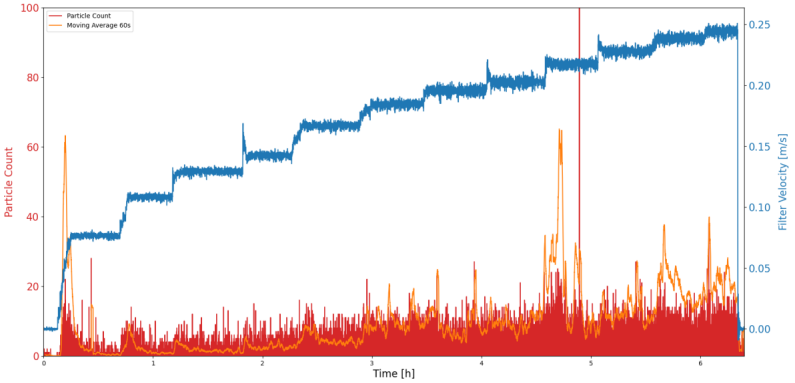

Figure 5-13: Sand particles per frame and moving average vs. time, test 2.3 camera 75cm

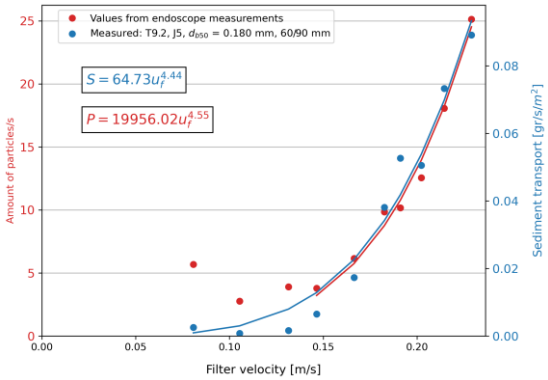

Figure 5-14: Transport of base material vs. filter velocity, test 9.2

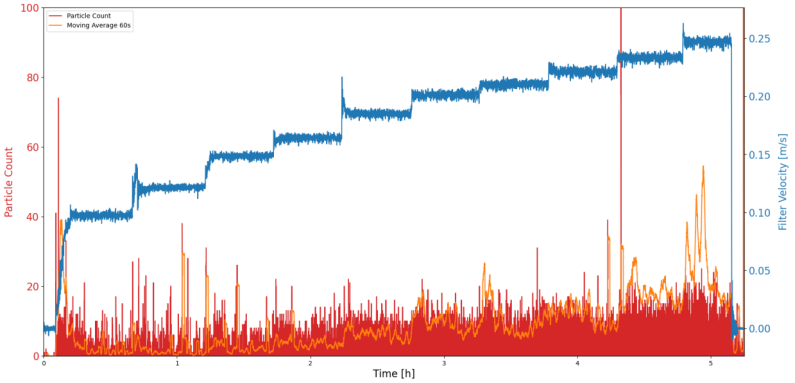

Figure 5-15: Sand particles per frame and moving average vs. time, test 9.2 camera 75cm

The above graphs can also be created using the measurements from the endoscope at a distance of 50 cm from the inflow point. These are shown in the figures below.

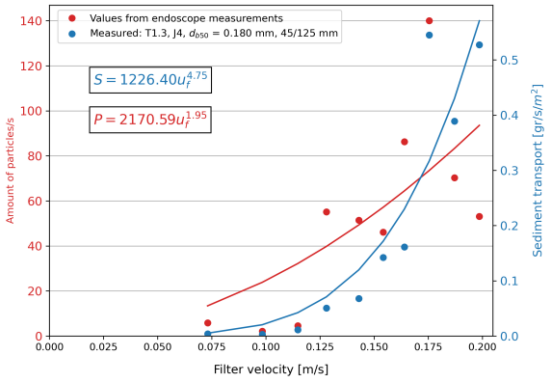

Figure 5-16: Transport of base material vs. filter velocity, test 1.3

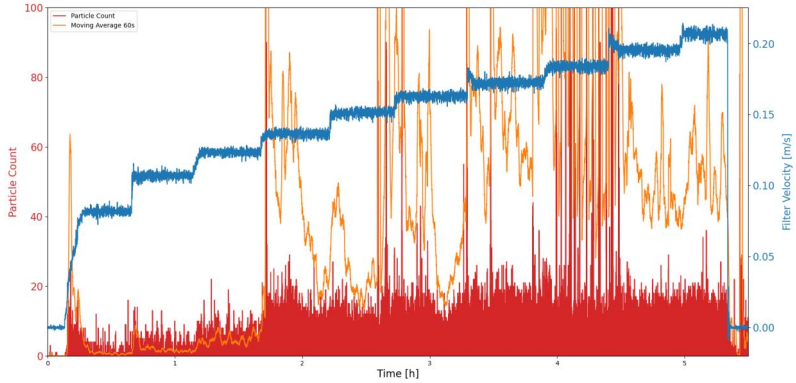

Figure 5-17: Sand particles per frame and moving average vs. time, test 1.3 camera 50cm

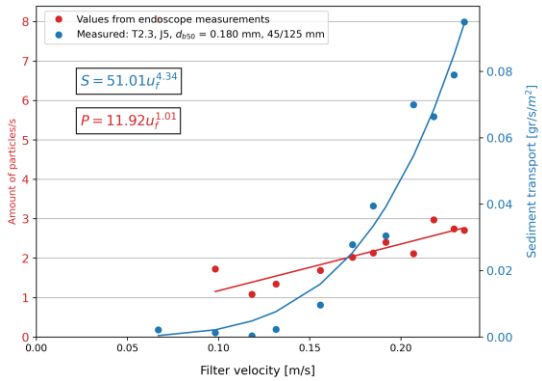

Figure 5-18: Transport of base material vs. filter velocity, test 2.3

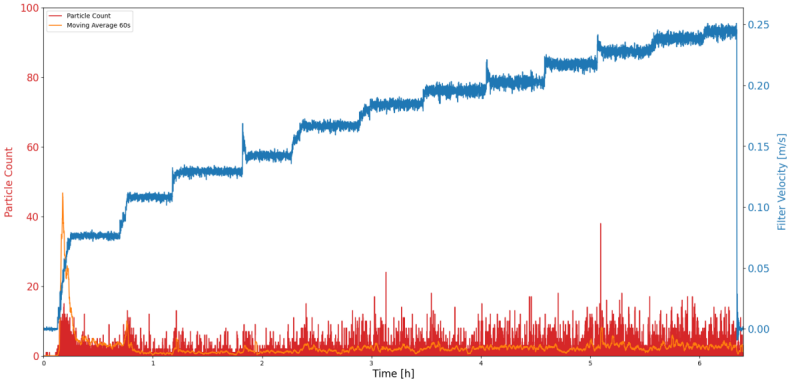

Figure 5-19: Sand particles per frame and moving average vs. time, test 2.3 camera 50cm

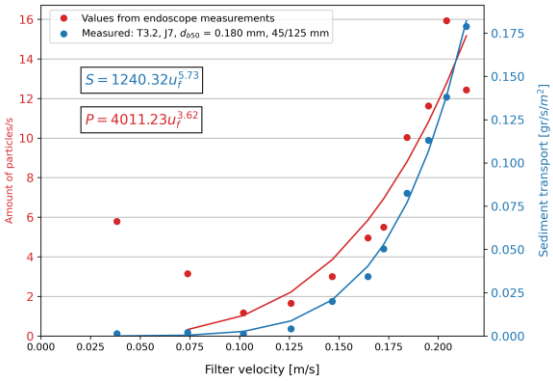

Figure 5-20: Transport of base material vs. filter velocity, test 3.2

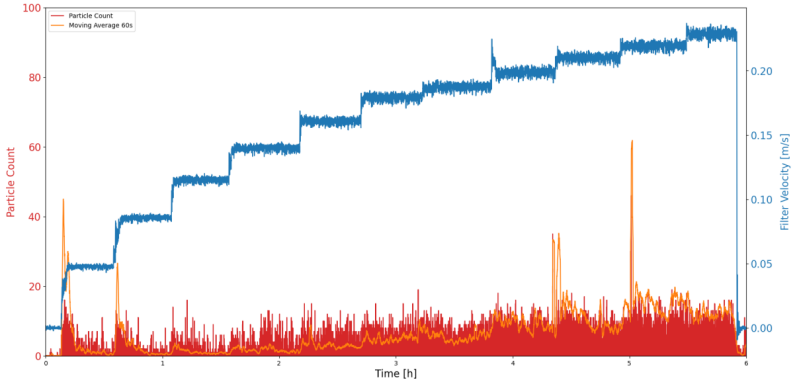

Figure 5-21: Sand particles per frame and moving average vs. time, test 3.2 camera 50cm

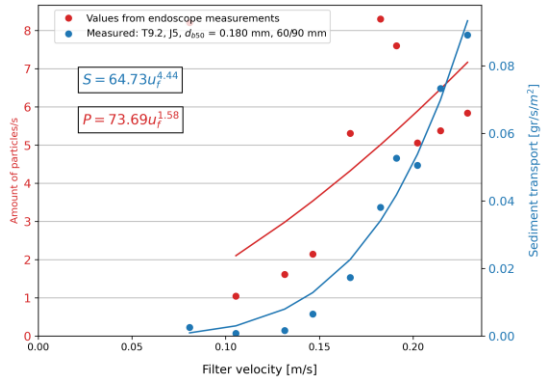

Figure 5-22: Transport of base material vs. filter velocity, test 9.2

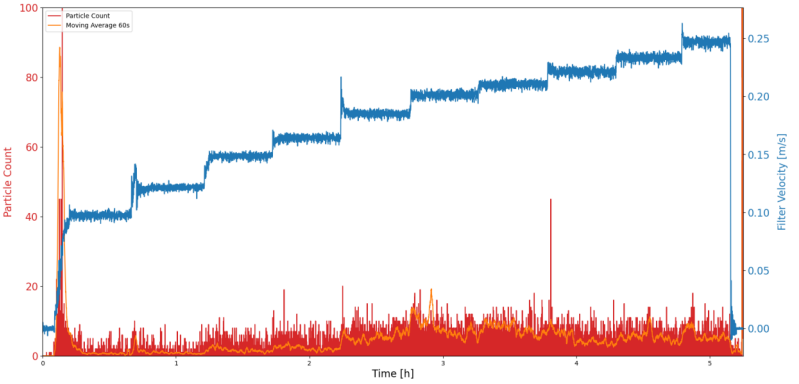

Figure 5-23: Sand particles per frame and moving average vs. time, test 9.2 camera 50cm

The results show that there is a better fit with the images from the endoscope at 75 cm from the inflow point than with the measurements from the endoscope at 50 cm.

There may be a correlation between the unit of measured sand transport and the results obtained based on the endoscope images. This correlation can be described with the formula below:

$$S = a \times P \tag{5.5}$$

Where S is the sand transport in gr/s/m^2, a the ratio coefficient and P the particle transport in one pore in the filter layer in average amount of particles/s.

Python has automatically scaled the y-axes of both measurements by taking the highest value in the graph. In the table below (Table 5-4), the values of the y-axes obtained from the endoscope images at a distance of 75 cm from the inflow point and the measured amount of sand transport for the three tests are presented. The same table also shows the ratio coefficient for these three tests. Based on the ratios from these three tests, it appears that there is an average ratio of 222 between these two different measurement methods.

Table 5-4: Transport measurements of both methods and the results of the ratio between them

Test	**Geotextile**	**Filter material**	***S* transport**	***P* transport**	***a***
			[gr/s/m²]	**[average amount of particles/s]**	**[-]**
Test 1.3	J4	45/125 mm	0.5	83	166
Test 2.3	J5	45/125 mm	0.08	22	275
Test 9.2	J5	60/90 mm	0.08	18	225
Average					222

5.8 Validity of the original Klein Breteler (1988) formula/comparison synthetic geotextile

Before conducting the experiments, the Klein Breteler (1988) formula was utilized to predict the critical filter velocities for various geotextiles. This step was essential to evaluate if the formula could accurately estimate the critical velocity of natural geotextiles as well. To validate the formula's applicability, the calculated critical velocities were then compared with critical filter velocities observed during the tests. The results are given in Table 5-5.

Table 5-5: Calculated and measured values with Klein Breteler formula

Test	Geotextile				Base material			Filter			Parameters			Calculated		Measured 0.2 gr/s/m²	
	Type	O_{90} [mm]	t_g [mm]	k_g [mm/s]	d_{b15} [mm]	d_{b50} [mm]	d_{b90} [mm]	d_{f15} [mm]	d_{fn50} [mm]	n_f [-]	$\frac{O_{90}}{d_{b90}}$	$\frac{t_g}{d_{b90}}$	$\left(\frac{w}{k_g}\right)^{\frac{1}{m}}$	$u_{f,cr}$ [m/s]	i_{cr} [-]	$u_{f,cr}$ [m/s]	i_{cr} [-]
T1	J4	0.516	1.45	0.83*	0.146	0.180	0.242	51.2	61.79	0.41	2.13	5.99	17.00	0.24	1.0	0.159	0.46
T2	J5	0.819	1.77	0.90*	0.146	0.180	0.242	51.2	61.79	0.41	3.38	7.31	16.76	0.07	0.09	0.279	1.23
T3	J7		2.01**	0.52*	0.146	0.180	0.242	51.2	61.79	0.41		8.31	109.28	-	-	0.218	0.83
T9	J5	0.819	1.77	0.90*	0.146	0.180	0.242	65	61.50	0.42	3.86	7.31	14.72	0.07	0.09	0.272	0.95

* Measured with simplified permeability test
** Measured with calliper

The measured results revealed that the critical filter velocity for geotextile J4 was underestimated by approximately 33% compared to its pre-calculated value. The calculation of the critical filter velocity relies on various parameters, each determined with a certain level of uncertainty. This inherent uncertainty can lead to calculated values that are either slightly higher or lower than actual outcomes.

Figure 5-24 presents both the calculated and measured critical filter velocities, alongside the experimental results from Klein Breteler (1988). The uncertainties associated with these measurements and calculations are depicted through error bars on the graph. A significant discrepancy is observed between the calculated and measured critical filter velocities for geotextile J5, with the criterion used by Klein Breteler also highlighted. Notably, the pre-calculated filter velocity is almost four times smaller than the critical filter velocity determined by the trend line.

Klein Breteler (1988) included water permeability in the formula, taking into account the structure of the fabric (whether tape fabric or mesh netting) in the equation. This incorporation aims to enhance the accuracy of predicting critical filter velocities, especially in light of the structural differences between various geotextiles. Despite these efforts, the notable deviation between calculated and

measured values underscores the challenges in accurately predicting geotextile performance solely based on pre-calculated parameters.

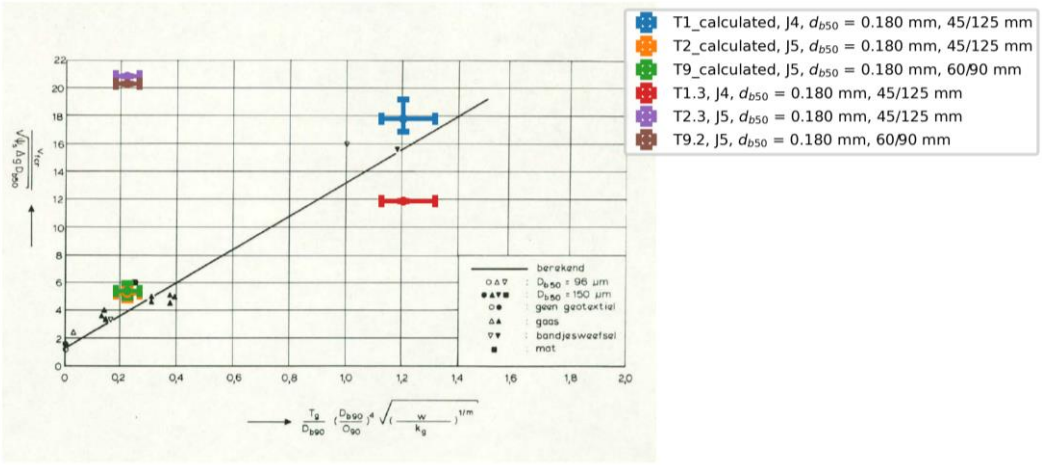

Figure 5-24: Calculated and measured points

6 Discussion

In this chapter, the findings of this study are discussed.

6.1 Porosity

The effective porosity calculated in section 5.1 is the best possible approximation of the actual porosity. This effective porosity takes into account:

- The volume of material placed in the volume of the test section (average porosity)
- Edge effects that result in a non-uniform distribution of porosity across the test section (less porosity in the middle, more towards the outer edges)
- The influence of the rubber foam at the top edge, which blocks part of the pore volume

However, the actual porosity during different tests may deviate from the calculated value. The random placement of stones and the edge effects of the flume can impact the actual porosity. Additionally, the amount of rubber foam at the top of the filter layer influences the porosity. Although an average height was used for all tests, this height can still vary per test, leading to variations in porosity from one test to another.

6.2 Forchheimer coefficients

The Forchheimer coefficients (*a* and *b*) have been determined using the experimental relationship between the hydraulic gradient and the filter velocity. However, there is a margin of error in determining both the gradient and the filter velocity, leading to possible deviations from the established values. These coefficients were ultimately converted into Alpha (α) and Beta (β) values using the Forchheimer equation, taking into account the particle size of the filter material, porosity, and viscosity. The Alpha and Beta values at a rubber foam thickness of 3 cm are approximately 3900 and 1.11, respectively.

Determining the volume of rubber foam is a factor of uncertainty. The amount of rubber foam, as seen in the results in Table 5-1, has a significant impact on the porosity and thus on the Forchheimer coefficients (Table F-20). The volume of the stones was determined using the total weight of the stones and their density. This determined density could also vary, resulting in a larger or smaller volume of stones.

6.3 Transport of base material

The sediment collected after each test step behind the test set-up was converted into an erosion rate of grams per second per square meter. The parameters used for this conversion have uncertainties:

- Duration of test step
- Collected number of grams
- Square meters of erodible surface

For each test step, both the start and the end were determined. The start of a test step was marked by the beginning of increasing the hydraulic load, and the end by the next increase in critical load for the following test step. Since the hydraulic load is increased by manually opening the valve, the duration to reach the new water level is not the same for every test step. As a result, there is a slight deviation in how long the constant hydraulic load lasted for each test step.

Since the sediment was suctioned after each test step, but the flow was not stopped, erosion continued to occur during the suctioning. This eroded sediment also ended up in places where all the sediment had already been suctioned. After the entire surface from the sieve to the filter construction was covered, a quick suction stroke was made to suck up the majority of it. However, it was not possible to suction all the material. Therefore, between stopping the suctioning and the next increase in hydraulic load, erosion still occurs, but this amount of sediment is accounted for in the following test step.

For the calculation of the erodible surface area of the test set-up, it was assumed to be the area between the slats. However, during test 1.3, erosion also occurred under these slats. Klein Breteler (1988) did not use slats but instead used a section of sand-tight geotextile at both the front and back of his test set-up. As a result, erosion was not possible at these locations, but the area of these geotextiles was not taken into account when converting the criteria from gr/s/m to gr/s/m^2. If this adjustment had been made, the criterion would have been slightly higher than the 0.2 gr/s/m^2 criterion currently used.

6.4 Determining start of movement with video processing

Endoscopic images were taken of 2 pores within the filter layer. The size of the pore, in conjunction with the "openness" of the channels leading to it significantly influence the transportation of sand grains through the pore. Additionally, the count of sand grains observed in a pore is affected by the height and position of the camera, which can change during the clamping of the caisson, potentially skewing the observed data. For instance, a shift in the camera's position might result in an image partially obscured by a stone, reducing the visible area of the geotextile and, consequently, the number of particles counted.

To assess whether the rate of sand grains per second offers a reliable measure for identifying the start of sediment movement, Figure 6-1 and Figure 6-2, present graphs of average sediment transport and the rate of particles per second, respectively. A comparison of these graphs indicates that the start of movement is observable from the particle rate graph. Specifically, the graph for test 1.3 shows a marked increase in erosion during test step 8, aligning with the measured sediment erosion for that phase. Moreover, initial erosion peaks in the first two test steps highlight that each incremental increase in test conditions leads to an initial surge of erosion, even before reaching the critical load. However, these peaks cannot be directly compared to the sediment erosion between steps due to the low flow velocities and the limitation of the current analysis software, which counts the number of particles per second without distinguishing between unique particles. This limitation often results in an overestimation of the particle count, a problem that decreases at higher flow velocities as the likelihood of repeatedly detecting the same particle decreases. Therefore, the graph primarily provides insights into the erosion pattern throughout the test rather than specifying the exact quantity of eroded sediment.

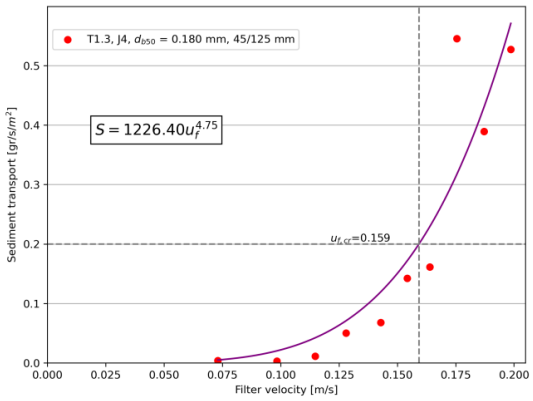

Figure 6-1: Transport of base material vs. filter velocity, test 1.3

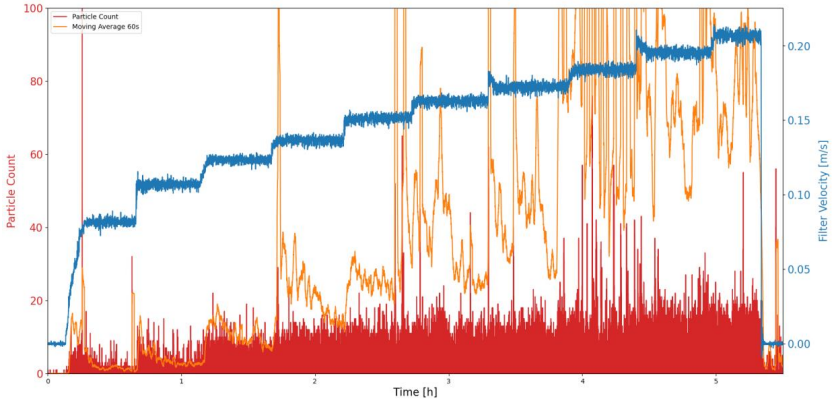

Figure 6-2: Sand particles per frame and moving average vs. time, test 1.3 camera 75cm

The graph below clearly shows that despite the limitations of the analysis method, a coherent erosion pattern can still be established for test 3.2.

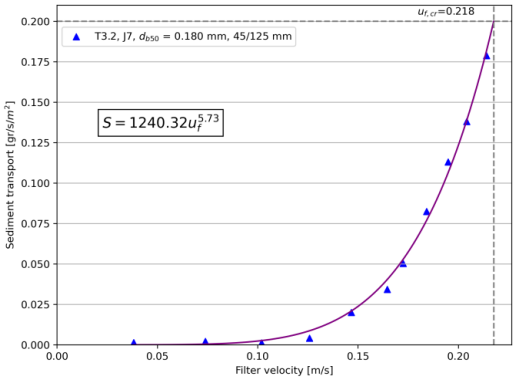

Figure 6-3: Transport of base material vs. filter velocity, test 3.2

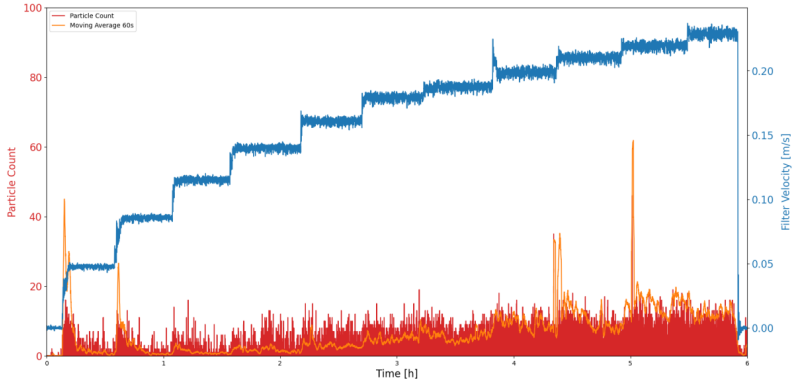

Figure 6-4: Sand particles per frame and moving average vs. time, test 3.2 camera 50cm

6.5 Critical load

The results from tests using the same geotextile but with different filter materials showed minor differences in the critical filter velocities at both start of movement criteria. These variances can partly be attributed to the step size used to increase the water level on the upstream side, and they also fall within the tests' margin of error. The filter velocity was not measured directly but was determined with the discharge and flow area, suggesting that the actual filter velocity might have been slightly lower than estimated. Despite these uncertainties, the difference in hydraulic gradient is so significant that the start of movement indeed occurs at a specific critical filter velocity.

Given this context, the critical load for open geotextiles being the critical filter velocity implies that the critical hydraulic gradient identified by Lemmens (1996) for a jute geotextile does not serve as a suitable value for stability calculations in the case of open jute geotextiles. Furthermore, a significant benefit for future model experiments with open geotextiles is that each geotextile will require only a single test to determine its critical filter velocity. With the knowledge from prior studies on translating hydraulic gradient into filter velocity, it becomes feasible to ascertain the maximum hydraulic gradient for each filter material type.

6.6 Openings size on critical load

The analysis presented in Chapter 5 regarding geotextiles indicates that the d_{b90}/O_{90} ratio does not consistently align with the expectation that a smaller O_{90} value would enable a geotextile to withstand a higher hydraulic load. This suggests that the structure of the geotextile itself may play a significant role in its critical load. Klein Breteler (1988) noted in his research that a tape fabric geotextile could withstand higher filter velocities than a mesh netting geotextile with an identical O_{90} value. The test results from Klein Breteler indicate that a certain mesh netting geotextile prevents erosion up to the same critical filtration velocity as a tape fabric geotextile with openings that are approximately 20% to 40% larger, assuming they have the same thickness. A tape fabric geotextile has relatively few openings compared with a mesh netting geotextile. The number of openings affects permeability, but more importantly, it influences the contraction of flow lines in the presence of a vertical gradient component (Klein Breteler, 1988).

In a study conducted by Van Der Meulen and Smith in 1995, the O_{90}/t_g ratio was explored to ascertain whether it could accurately describe the impact of a geotextile's structure on its critical load when used with clay. However, this study did not reveal a consistent trend that suggested a decrease in critical load corresponding with an increase in the O_{90}/t_g value for clay.

The structures of geotextiles J4, J5, and J7, in dry condition, are depicted in the subsequent figure (Figure 6-5). It is clear from the figure that the structure of these geotextiles varies. Geotextile J4 is characterized by a relatively high number of openings, but they are "small". Conversely, geotextile J5 has fewer openings, but have “large” and “small” ones. Test results demonstrate that, despite J5 having larger openings, it performs better than the J4 geotextile. This observation confirms that the structure significantly influences the critical load. A comparison between geotextiles J4 and J7 reveals that while both have a similar structure, J7 has considerably fewer holes. Although the O_{90} value of this geotextile may not be known, based on the test results, it can be concluded that this geotextile can withstand a higher hydraulic load than geotextile J4. The results show that the size and number of openings in the geotextile primarily influence the magnitude of the critical load at a criterion of 0.2 gr/s/m².

Given the current set of test results, no definitive conclusions can be established about the influence of the structure to the critical load. It is conceivable that factors such as the number of openings per unit area or the percentage of open area (POA) might offer a more effective parameter to integrate the structure of a geotextile into a potential design formula.

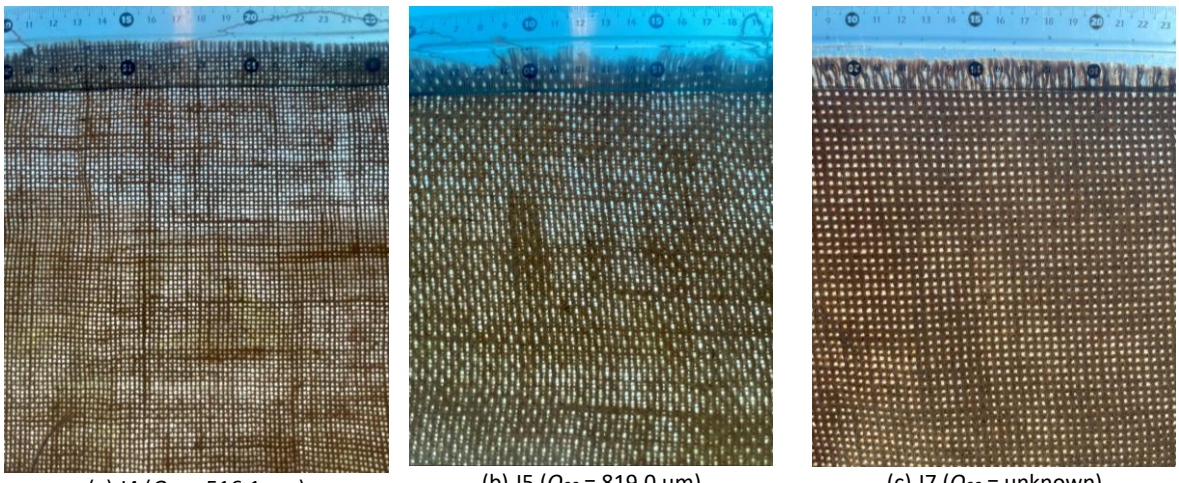

(a) J4 (O_{90} = 516.1 µm) (b) J5 (O_{90} = 819.0 µm) (c) J7 (O_{90} = unknown)

Figure 6-5: Structure of jute geotextiles J4, J5 and J7 (unsaturated)

6.7 Comparison with Lemmens

Lemmens determined a critical hydraulic gradient of 0.26 for a jute fabric. This hydraulic gradient was converted into a critical filter velocity using the Forchheimer equation. Several assumptions with uncertainties were made during this conversion. The critical filter velocity was found to be approximately 0.18 m/s. Assuming that all the collected material was eroded in the last test step, this means the erosion rate is approximately 0.19 gr/s/m².

Lemmens also indicated in his study that determining the critical gradient for the jute geotextile was much more challenging than for other tested materials. Small amounts of sand were observed behind the test set-up in the test steps before the critical test step. However, these quantities are not known but could potentially influence the erosion rate. If these amounts collectively represent a relatively large percentage of the total eroded sediment, the erosion rate would significantly decrease.

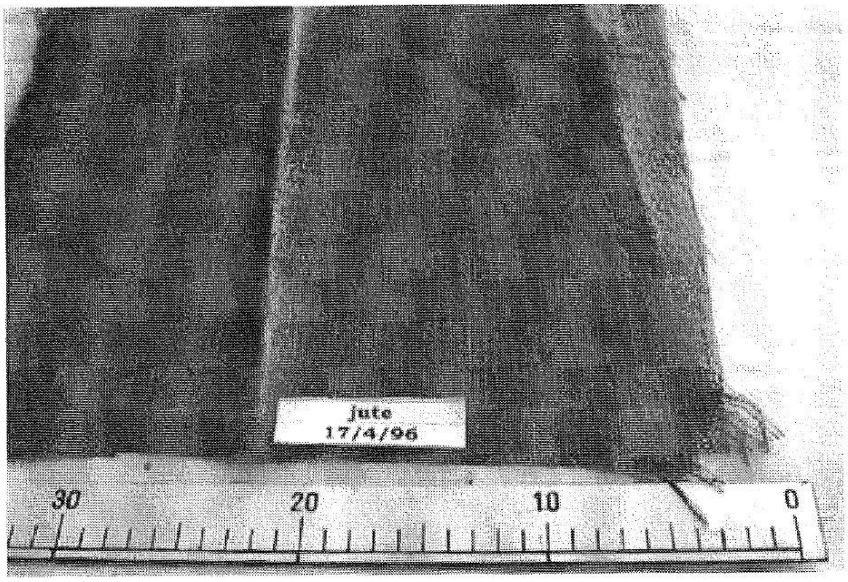

Figure 6-6: Jute geotextile (Lemmens, 1996)

Above, the jute geotextile tested by Lemmens is shown (Figure 6-6). This is a relatively finely woven geotextile with an unknown opening size. Consequently, this geotextile appears to most closely resemble the J4 geotextile (422 gr/m² and O_{90} of 516.1 µm). During test step 7 of test 1.3, the erosion rate was 0.16 gr/s/m² with a filter velocity of 0.164 m/s. The filter velocity of this geotextile thus aligns reasonably well with the critical value determined by Lemmens for the tested jute geotextile in his study.

6.8 Start of movement criterion

Klein Breteler (1988) adopted a criterion of 0.2 grams per second per square meter (gr/s/m²) for all his experiments to delineate the start of movement. This benchmark has been extensively applied in various studies by the Hydraulic Laboratory. This definition was selected over determining the velocity at which "the first particle is seen to move," because it is both reproducible and operational. Additionally, it is noted that 0.0002 kg/m/s is a very small amount (Den Adel et al., 1994).

In the current series of tests, this criterion is achieved during test 1.3, and the last test step of test 3.2 nearly reaches this threshold. The images following tests 1.3 and 3.2 demonstrate noticeable erosion, particularly at the center. Should the filter velocity persist for an hour, this would amount to

roughly 720 gr/h/m². Over an extended period, such conditions could inflict considerable damage underneath the geotextile layer. Nowadays, almost only geometrically closed geotextiles are used in practise, operating under the assumption that erosion does not take place. Due to these high standards, it is questionable whether the value previously used to define the start of movement still corresponds with the current requirements.

a) Entire sandbed

b) Upstream side

c) Detail of erosion channel

Figure 6-7: Sandbed after test 1.3 (J4, 45/125 mm)

a) Sandbed seen from upstream

b) Detail of erosion channel

Figure 6-8: Sandbed after test 3.2 (J7, 45/125 mm)

6.9 Sediment transport graph with endoscope measurements

The results of the measurements with the endoscope clearly show that by counting the number of particles per frame instead of the number of unique particles per second, there is an overestimation of the particle count in the initial test steps. This overestimation decreases as the flow velocity

increases. This is also evident in the graphs, as the fit increasingly aligns with the fitted line of the measured sediment quantity.

In general, this fitted line (P=a*u_f^b) reasonably aligns with the fitted line through the measured points (S=a*u_f^b). This indicates that it is possible to calibrate the endoscope measurements with the measured sediment quantity after each test step. The conversion factor between these two different units can thus be used to translate the endoscope measurements into a sediment transport formula. The value of the conversion factor found in this study is a = 222 with a bandwidth of 50.

6.10 Comparison with Klein Breteler formula

Upon analyzing the results pre-calculated using the Klein Breteler formula, it is observed that the formula tends to overestimate for geotextile J4. This overestimation could be attributed to the fact that the 1988 study by Klein Breteler tested only two geotextiles, with the data points on both the x-axis and y-axis being close to those of geotextile J4. However, it is crucial to note that both geotextiles tested were tape fabric geotextiles, which possess a distinct structure compared to geotextile J4. A tape fabric geotextile typically features fewer openings than a mesh netting geotextile. Given the limited number of geotextiles tested in this specific region, it is plausible that the formula developed by Klein Breteler may not accurately reflect the behavior of mesh netting geotextiles in this region of the formula, leading to an overestimation for geotextiles like J4 in this region.

7 Conclusion

This chapter summarizes the findings of the research and addresses the research questions presented in the introduction. The research questions will be addressed first, followed by the main research question.

1. What is the critical load for open geotextile filters?

It is unclear if u_f (Klein Breteler, 1988) or i (Lemmens, 1996) best describes the loads on the geotextile for filter stability. Klein Breteler initially showed, through a limited amount of tests using relatively small stones as filter material, that the critical filter velocity is the critical load for open geotextile filters. To extend this validation to include larger stones and various stone gradations, and to provide a more robust foundation through additional testing, new experiments were conducted. These involved different types of filter materials, including two with the same median diameter (d_{f50}) but with distinct gradations—one widely graded and the other narrowly. Based on the average sand transport measurements from tests 2.3 and 9.2, along with measurements of earlier studies, it can be conclusively stated that the filter velocity is the relevant load parameter for describing the start of movement for open geotextiles. This is also the expected physical outcome. In the Shields stability relation, velocity is used rather than a hydraulic gradient. Morrison (1950) also describes that the drag force term (u^2) is dominant over the flow acceleration term for small sand particles.

2. What are the critical filter velocities of the different geotextiles under uniform parallel flow?

In the context of this study, two criteria were used to define the critical filter velocity: one being the velocity below which “non-erosion” is observed, and the other being a historically utilized velocity to describe the start of movement (0.2 gr/s/m^2). The "non-erosion" critical filter velocity is equal to the filter velocity at which, if exceeded, continuous sand transport occurs. If the filter velocity is below this value, the sub-soil remains stable. Through the conducted tests, the critical filter velocities for various geotextiles have been ascertained. These results are presented in Table 7-1. The results show that the critical filter velocity for the Klein Breteler criterion is about 2 to 3 times higher than the critical filter velocity with the non-erosion criterion. The critical filter velocities for the non-woven geotextiles and the woven J9 geotextile are all larger than 0.20 m/s.

Table 7-1: Test results of two threshold criteria

Test	**Geotextile**		**Filter material**	**Criterion: Non-erosion**		**Criterion: 0.2 gr/s/m^2**	
	Type	**O_{90} [µm]**		**$u_{f,cr}$ [m/s]**	**i_{cr} [-]**	**$u_{f,cr}$ [m/s]**	**i_{cr} [-]**
Test 1.3	J4	516.1	45/125 mm	≈ 0.098	≈ 0.19	≈ 0.159	≈ 0.46
Test 2.3	J5	819.0	45/125 mm	≈ 0.118	≈ 0.26	≈ 0.279	≈ 1.23
Test 3.2	J7	-	45/125 mm	≈ 0.102	≈ 0.21	≈ 0.21	≈ 0.83
Test 4	J9	283.2	45/125 mm	>0.21	> 0.95	-	-
Test 9.2	J5	819.0	60/90 mm	≈ 0.105	≈ 0.17	≈ 0.272	≈ 0.95
Test 10	Hemp on jute	-	45/125 mm	>0.20	>0.98	-	-
Test 11	Jute on jute	-	45/125 mm	>0.22	>0.98	-	-
Test 12	Wool on jute	-	45/125 mm	>0.21	>0.99	-	-

3. *How does the grading and grain size of the filter layer influence the critical hydraulic gradient and critical filter velocity?*

To investigate the impact of grading and particle size on the filter layer's performance, this study carried out experiments using the same geotextile combined with different types of filter materials. The selected filter materials shared the same median diameter (d_{f50}) value, yet differed in their grading—one exhibited a wide grading, and the other a narrow grading. Furthermore, a smaller type of filter material was also utilized for comparison.

The findings of this research suggest that altering the grading of the filter layer leads to minimal changes in the critical filter velocity but results in significant variations in the critical hydraulic gradient. Below, in Table 7-2, both the critical filter velocity and the critical gradient are given for the 4 tests conducted. In these tests, after each test phase, the sand was removed via suction. These results demonstrate that by using a wide graded filter material, a significant higher critical gradient can be achieved than by using a narrow graded filter material. Table 7-2 indicates that J5 leads to the highest critical gradient.

Table 7-2: Test results with different filter materials

Test	**Geotextile**	**Filter material**				***Results* (0.2 gr/s/m²)**	
		Range	***Grading***	**d_{f15} [mm]**	**d_{f50} [mm]**	**$u_{f,cr}$ [m/s]**	**i_{cr} [-]**
Test 1.3	J4	45/125 mm	Wide	51.20	73.56	≈ 0.159	≈ 0.46
Test 2.3	J5	45/125 mm	Wide	51.20	73.56	≈ 0.279	≈ 1.23
Test 3.2	J7	45/125 mm	Wide	51.20	73.56	≈ 0.210	≈ 0.83
Test 9.2	J5	60/90 mm	Narrow	62.46	73.21	≈ 0.272	≈ 0.95

4. How does the opening size of the geotextile influence the critical hydraulic gradient and critical filter velocity?

Prior research has highlighted that the d_{b90}/O_{90} ratio is a critical factor for the sandtightness of open geotextiles. In Klein Breteler's formula, this ratio significantly influences the critical filter velocity. Moreover, Klein Breteler noted that tape fabric geotextiles could withstand higher filter velocities than mesh netting geotextiles with the same O_{90} value. A tape fabric geotextile has relatively fewer openings compared to a mesh netting geotextile. The findings from the tests conducted on natural geotextiles corroborate that the fabric's structure markedly affects the critical filter velocity. Specifically, the results for the woven jute geotextiles J4 (422 gr/m^2 and O_{90} of 516.1 µm) and J5 (518 gr/m^2 and O_{90} of 819.0 µm) reveal that although the opening size of J5 geotextile is almost 1.5 times that of J4 geotextile, it also has a critical filter velocity that is 1.75 times higher, based on the 0.2 gr/s/m² criterion. The results indicate that, similar to Klein Breteler (1988), the relative area of the openings or the number of openings per square meter of the geotextile affects the sandtightness.

5. *How does the thickness of a non-woven geotextile influence the critical hydraulic gradient and critical filter velocity?*

The test set-up was insufficient to reach the start of movement of the sand grains for the natural non-woven geotextiles. The critical gradients for these geotextiles were significantly higher than the maximum gradient achievable with the test set-up. Consequently, it was not possible to investigate whether the thickness of natural non-woven geotextiles affects the critical load when using sand as the base material. However, the test results indicate that the experimentally developed non-woven geotextiles are suitable for filter applications regarding sandtightness. All three geotextiles remained

stable at a gradient of approximately $i \approx 1$. Nevertheless, the tensile strength, opening size, and water permeability of these geotextiles still need to be tested before they can be applied in practice.

Main objective

What are the stability criteria for natural open geotextile filters for a situation where a single granular filter layer with geotextile experiences a flow velocity parallel to the filter structure?

The main objective of this research is to establish the stability criteria for open geotextiles under parallel flow conditions in a scenario involving a single granular filter layer. From the literature study and the results of the tests, it was determined that these are governed by the critical filter velocity. The influence of geotextile opening size, filter material properties, and the structure of the geotextile fabric are key factors in determining the geotextile's stability and sandtightness capabilities. The structure can significantly influence the sandtightness.

8 Recommendations

The present research has given new insights that enhance our understanding of open geotextile filters. During this research, new questions have been raised. In this section some recommendations for new research about open (natural) geotextile filters is given.

8.1 Application of natural geotextiles

The results of this study demonstrate that the application of natural geotextiles in practice is feasible, based on sandtightness under uniform flow conditions. The natural non-woven geotextiles and the geotextile J9 (963 g/m² fabric with an O_{90} of 200 µm) were fairly stable, with a critical filter velocity of more than 0.20 m/s under a non-erosion criterion. Considering water permeability, the non-woven wool geotextile is a good choice for use. An additional advantage is that wool is readily available in the Netherlands (Van Den Oever, 2023).

The occurring gradient on the geotextile can be calculated using the method developed by Thomas (2023). This occurring gradient can be translated into a critical filter velocity based on the size of the underlying stone layer. The challenge here is to determine the extreme values, which are dependent on large-scale turbulence and still need to be tested.

8.2 Improvements to the current test set-up

Test step duration

In certain tests conducted during this study, the duration of the test steps was insufficient to determine whether sediment transport ceases completely. Therefore, it is recommended to establish a minimum test step duration of 20 to 30 minutes for future experiments.

To gain a comprehensive understanding of the behavior differences between natural and synthetic geotextiles, particularly due to the rough and uneven nature of natural geotextiles, it is advisable to conduct preliminary tests to determine if an extension of the test step duration is necessary. Natural geotextiles, characterized by their inherently irregular surfaces, may take a longer time to reach a stable condition where peak erosion or movement subsides. Modifying the test methodology to account for this variability would enable a more precise evaluation of how quickly and effectively a geotextile can stabilize after being subjected to hydraulic stress.

Longer duration of first test steps

When analyzing the tests involving geotextiles where the start of movement has not been observed, the graph clearly shows that the quantity of particles only begins to decline to zero after several tests steps. This suggests that sand initially present on the stones at the beginning of the tests, as well as sand that settles on the geotextile after filling the flume and installing the geotextile, only starts to be removed from the geotextile after a few test stages. Extending the duration of the initial test phases in future experiments could provide a more definitive conclusion on whether the sand observed exiting the test set-up is actually associated with that specific test phase, or if it results from a delayed response detected during this phase.

Increasing of filter velocity

When slowly increasing the filter velocity, much less sand transport seems to occur than when increasing the filter velocity in large steps, this is also observed by Klein Breteler in 1988. The precise

influence of the size of this effect has not yet been further investigated. The effect of slowly increasing the velocity has a significant impact on sand transport so that the geotextile can still be used for heavy loads in places where the velocity changes slowly, but in places like propeller jets where a rapid change of velocity occurs, less so.

Height measurement of sand bed after finishing test

Before the start and after of each test, perform a height scan of the sand bed. This will allow for a better retrospective analysis of the depth and location of the erosion pits and channels. Consequently, a more detailed understanding of the damage to the sand bed can be achieved.

Height measurement of filter layer

To improve future estimations of the volume of rubber foam between the top of the filter layer and the bottom of the caisson, it is recommended to perform a complete height scan of the top of the filter layer in future studies. This approach would enable a more accurate estimation of the amount of rubber foam. With this more precise determination, the porosity and flow area can also be calculated with greater accuracy.

8.3 Further testing of (natural) geotextiles

Synthetic Geotextile:

A test should be conducted using a synthetic geotextile that has a similar thickness and pore size as its natural counterpart to enable a meaningful comparison. This will help in understanding the performance differences between natural and synthetic geotextiles under similar conditions.

Coarser Sand:

Given that the study primarily utilized relatively fine sand as the base material, it is recommended to conduct the same tests with coarser sand. The d_{b90} of this sand should be selected to ensure it still functions effectively as an open geotextile filter. This would provide insights into how geotextiles perform with different sand grainsizes.

Multiple Layered Bed Protections:

Experiments should include testing the geotextiles with a filter layer consisting of small-grained stones placed directly on the geotextile, topped with a layer of larger stones. The smaller stones reduce the filter velocity acting on the geotextile, potentially allowing the filter construction to handle larger hydraulic loads.

Flow Above Filter Material:

It is important to determine the critical filter velocity with a flow above the filter layer to assess the damping effect of the filter layer. This can help in understanding how the filter material influences the flow and its capacity to reduce the velocity effectively.

Damage Criterion:

With knowledge of the sediment transport at certain filter velocities, more targeted research can be conducted to examine the damage patterns in the sand bed at specific flow velocities. This will determine whether the level of erosion and sediment transport remains within acceptable limits.

Sieving sand

Sieving the eroded sand from various test steps can provide insight into whether, during a specific test step, only the smallest particles erode or if the largest particles are also affected. This method is crucial for assessing the potential development or presence of a natural filter during certain test steps.

Influence of structure of geotextile on critical filter velocity

From the results of this study and previous studies, it has been concluded that the structure of an open geotextile can significantly influence its sandtightness. To investigate the extent of this influence, it would be beneficial to conduct tests using the current test set-up, but with geotextiles that have different opening sizes while maintaining the same structure. These test results could also be used to explore whether, in addition to the critical O_{90}/d_{b90} ratio, another parameter or ratio could be identified to predict sandtightness. This could potentially involve examining the number of openings and the percentage of openings.

8.4 Research on damaged geotextile

During the process of installing and placing stones on the geotextile, the fabric might be damaged, or there could be manufacturing defects such as weaving errors (as indicated in the figure below). The impact of these potential issues on sediment transport is currently uncertain. This study has quantified sediment amounts for each test step in several experiments. By repeating these experiments with damaged geotextiles, it would be possible to reveal differences in transport rates. By conducting the same tests under these altered conditions, we can examine the resulting erosion profiles to determine if there is a significant variation in the quantity of sand eroded at each test step.

Figure 8-1: Weaving error

8.5 Analysis of erosion

Turbidity

Measuring the turbidity throughout the entire test to observe if a similar turbidity pattern emerges using the same set-up as in Ho's study.

Enhancement of sand grain counting with Endoscope Images

To improve the tracking and counting of sand grains in future experiments, it is recommended to use a higher-resolution camera along with colored sand. The utilization of colored sand significantly assists in identifying whether the sand grains moving through the system originated from the stones or were already present in the water system. Additionally, this approach facilitates the exclusion of

moving threads from the geotextiles, making it easier to focus on the sand grains themselves. A camera with a high frame rate can potentially also be used to determine the pore velocity.

Camera positioning:

Establishing a fixed position for the camera is crucial for consistent and accurate measurements across tests. A consistent camera position enables easier comparison of grain velocity and quantity between different test steps. This can be achieved by creating a fixed pore where the stones are glued together in a controlled manner, allowing for natural settlement if erosion occurs beneath the geotextile.

Counting and Tracking Improvements:

By maintaining the same camera position, the accuracy of the sand grain counting tool can be enhanced, minimizing the miscounting of moving threads from the geotextile. The tool's capability can also be expanded to count the number of unique particles per second. With the known volume of the pore under observation, it becomes possible to convert the number of particles per second into a concentration measurement.

Exploring Different Camera Angles:

While the view of the camera in this study focused solely on the geotextile, positioning a camera higher within the filter layer could provide additional insights. This vantage point might reveal if sediment concentration varies significantly with height, offering a more comprehensive understanding of sediment transport dynamics within the system.

Determining start of movement with image processing

Using colored sand and a fixed camera position enhances the precision and simplicity of the photo analysis process. This approach ensures that the effects of shadows and reflections from tl lighting do not impact the results. By taking photos from a consistent camera position for each compartment of the flume, it becomes feasible to calculate the total amount of sediment from each compartment. This enables the determination of the total sediment quantity for each test step.

By employing both image processing and sediment suction during a test, it is possible to compare the measured transport rate curve with the transport curve generated through image processing, to verify their correspondence.

8.6 Different types of loading

To properly design an effective bank protection, it is essential to understand both the critical load of parallel flow, perpendicular flow and non-stationary flow conditions (like waves).

Perpendicular flow

Since the sandtightness for perpendicular flow of the natural geotextiles tested in this study is not yet known, it is advisable to test these geotextiles for perpendicular flow. During these tests, variations can be made with the grain size of the sand, but combinations can also be created with, for example, a combination of a non-woven and woven geotextiles, resulting in a hybrid geotextile. During these tests, it is also possible to examine whether conducting these tests with and without a filter layer affects the performance of the stones in ensuring the fabric's threads function better when held more tightly. In 0, there is a drawing of a test set-up to determine the critical load for a perpendicular flow condition.

Non-stationary flow condition

The sandtightness of open natural geotextile filter constructions under non-stationary flow conditions, such as waves, remains an under-researched area. These dynamic environments challenge our current understanding and application of open geotextiles, especially in coastal revetments. Future research must explore the sandtightness of geotextiles when exposed to wave action to gain insights into their performance and limitations. Conducting focused studies is critical for enhancing geotextile designs.

References

Abdullah, A. (2013). *Jute Geo-textiles and environment.* Dhaka. https://www.researchgate.net/publication/312624243_Jute_Geo-_textiles_and_environment

Bai, X., Li, F., Ma, L., & Li, C. (2022). Weathering of geotextiles under ultraviolet exposure: A neglected source of microfibers from coastal reclamation. *Science of The Total Environment, 804*. https://doi.org/https://doi.org/10.1016/j.scitotenv.2021.150168

Bezuijen, A., & Kohler, H. (1996). Filter and revetment design of water imposed embankments induced by wave and draw-down loadings. *Proc. EuroGeo 1.* Maastricht.

Bezuijen, A., Klein Breteler, M., & Bakker, K. (1987). Design criteria for placed block revetments and granular filters. *Second International Conference on Coastal and Port Engineering in Developing Countries.* Beijing.

Bosma, C. (2001). *Porositeit in breuksteenconstructies.* Faculteit der Civiele Techniek en Geowetenschappen. TU Delft.

Carneiro, J. R., Almeida, P. J., & Lopes, M. d. (2019). Evaluation of the Resistance of a Polypropylene Geotextile Against Ultraviolet Radiation. *Microscopy and Microanalysis, Volume 25*, 196–202.

CIRIA, CUR, & CETMEF. (2012). *The Rock Manual. The use of rock in hydraulic engineering (2nd edition).* London: C683, CIRIA.

CUR. (1993). *CUR 161 Filters in de waterbouw.* Gouda: CUR.

CUR bouw & infra. (2009). *CUR-rapport 174 'Geokunststoffen in de waterbouw - Tweede, herziene uitgave'.* Gouda: Stichting CURNET.

CUR building & infrastructure. (2012). *CUR 243 Durability of Geosynthetics.* Gouda: Stichting CURNET.

De Grauw, A., Van Der Meulen, T., & Van Der Does de Bye, M. (1983). *Design criteria for granular filters.* Delft hydraulics Laboratory.

Den Adel, H. (1986). *Analysis of permeability measurements using.* Delft: Deltares.

Den Adel, H., Koenders, M. A., & Bakker, K. (1994). The analysis of relaxed criteria for erosion-control filters. *Canadian Geotechnical Journal, 31*, 829-840.

Faure, Y.-H., Ho, C., Chen, R.-H., Le Lay, M., & Blaza, J. (2010). A wave flume experiment for studying erosion mechanism of revetments using geotextiles. *Geotextiles and Geomembranes, 28*(4), 360-373. https://doi.org/https://doi.org/10.1016/j.geotexmem.2009.11.002

Ho, C. C. (2007). *The erosion behavior of revetment using geotextile.* Grenoble: Université Joseph-Fourier - Grenoble I.

Klar, M. (2005). *Design of an endoscopic 3-D Particle-Tracking Velocimetry system and.* Heidelberg: PhD University of Heidelberg.

Klein Breteler, M. (1987). *Taludbekleding van gezette steen - Ontwerpregels voor granulaire filters concept verslag M1795/H195 deel XXI.* Delft: Waterloopkundig Laboratorium.

Klein Breteler, M. (1988). *Zanddichtheid van geotextielen als funktie van hydraulische belasting.* Delft: Waterloopkundig laboratorium.

Klein Breteler, M., & Den Adel, H. (1992). *Interne stabiliteit van granulaire filters bij stationaire stroming.* Delft: Waterloopkundig laboratorium.

Klein Breteler, M., & Verheij, H. (1990). Erosion control by hydrodynamically sandtight geotextiles. *International Conference on Geotextiles, Geomembrane and Related Products.* The Hague.

Klein Breteler, M., Smith, G. M., & Pilarczyk, K. W. (1994). Performance of geotextiles on clay and fine sand in bed and bank protections. *International conference on Geotextiles, Geomembrames and related products.* Singapore.

Knieß, H. (1977). *Bemessung von Schüttstein-Deckwerken im Verkehrswasserbau Lose Steinschüttungen.* Bundesanstalt für Wasserbau.

Laan, G. (1996). *De relatie tussen eisen aan loskorrelige steenrtiaterialen en ontwerpparameters.* Dienst Weg en Waterbouwkunde.

Laan, G. J. (1996). *Het gebruik van steen in waterbouwkundige constructies.* TU Delft.

Lemmens, R. J. (1996). *Natuurvriendelijke verbetering van de zanddichtheid van klassieke zink- en kraagstukken. Msc Thesis* Delft: TU Delft.

Moraci, N., Bilardi, S., & Mandaglio, M. C. (2022). Factors affecting geotextile filter long-term behaviour and their relevance in design. *Geosynthetics International* (pp. 19-42). Thomas Telford Ltd. https://doi.org/https://doi.org/10.1680/jgein.21.00019

Morisson, J., O'Brien, M., Johnson, J., & Schaaf, S. (1950). The force exerted by surface waves on piles. *Journal of Petroleum Technology, 2*, 149-154.

NABB. (2023). *Nationale Aanpak Biobased Bouwen van boerenland tot bouwmateriaal.* NABB.

Narayana Sarma, G. V., Venkatappa Rao, G., & Abid, M. (1994). *Durability of jute geotextiles.* Delhi. https://library.geosyntheticssociety.org/wp-content/uploads/resources/proceedings/122021/BR74.pdf

PIANC. (2011). *The Application of geosynthetics in waterfront areas.* Bruxelles: PIANC Secrétariat Général.

Pilarczyk, K. W. (1988). *Dikes and revetments: design, maintenance and safety assessment.* Rotterdam: A.A. Balkema. https://doi.org/https://doi.org/10.1201/9781315141329

Pilarczyk, K. W. (2000). *Geosynthetics and geosystems in Hydraulic and Coastal Engineering.* Rotterdam: A.A. Balkema.

Prambauer, M., Wendeler, C., Weitzenböck, J., & Burgstaller, C. (2019). Biodegradable geotextiles – An overview of existing and potential materials,. *Geotextiles and Geomembranes, 47*(1), 48-59. https://doi.org/https://doi.org/10.1016/j.geotexmem.2018.09.006.

Rijkswaterstaat. (2023). https://www.rijkswaterstaat.nl/leefomgeving/duurzaam-werken/circulaire-economie

Schiereck, G. J. (2012). *Introduction to bed, bank and shore protection.* Delft: VSSD. https://doi.org/https://doi.org/10.1201/9781315274935

Shields, A. (1936). *Anwendung der aehnlichkeitsmechanik und der turbulenzforschung auf die geschiebebewegung. PhD Thesis* Technical University Berlin.

Terzaghi, K., & Peck, R. B. (1948). Soil Mechanics in Engineering Practice.

Thomas, Q. J. (2023). *Design method for open geotextiles.* Delft: TU Delft.

Van Den Oever, J. (2023, June 1). *Volkskrant*. https://www.volkskrant.nl/volkskrant-magazine/wat-te-doen-met-het-grote-overschot-aan-wol-in-nederland-deze-ontwerpers-redden-wol-van-de-afvalstort~b4b93e1b/

Van Der Knaap, F., Klein Breteler, M., & Van Der Meulen, T. (1986). Design criteria for geotextiles beyond the sandtightness requirement. *Third international conference on geotextiles.* Vienna: Delft Hydraulics.

Van Der Meulen, T., & Smith, G. M. (1995). *Toegepast geotextielonderzoek, Filterwerking in geotextielconstructies.* Emmeloord: Waterloopkundig Laboratorium.

Van Dijk, E. (2018). *Circulair sturen op hoogwaardig hergebruik van toegepaste en toe te passen materialen.* Rijkswaterstaat

Van Gent, M. (1992). *Formulae to describe porous flow.* Delft: TU Delft.

Van Gent, M. (1993). *Stationary and oscillatory flow through coarse porous media.* Delft: TU Delft.

Van Gent, M. (1995). Porous flow though rubble mound material. *J. of Waterway, Port, Coastal and Ocean Engineering, 121*(3), 176-181.

Van Os, P. (1998). *Hydraulische belasting op een geometrisch open filterconstructie.* Delft: TU Delft.

Witteveen + Bos. (2022). *Duurzaamheid filterlagen in oeverbeschermingsconstructies.* Deventer: Ministerie van Infrastructuur en Waterstaat.

Appendix A Critical filter velocity studies open geotextiles

A.1 Design criteria for geotextiles beyond the sandtightness requirement (1986)

Following the research, the following formula has been established:

$$u_{f,cr} = \left(4\left(\frac{d_{b90}}{O_{90}}\right)\left(\frac{u_{*cr}}{k_n}\right)^{\frac{1}{2m}} + \frac{n}{k}\right)\sqrt{\psi_s \Delta g d_{b50}} \qquad (A.1)$$

In which:

$u_{f,cr}$ = critical filter velocity [m/s]
d_{b50} = diameter of bed material exceeded by 50% (mass)[m]
d_{b90} = diameter of bed material exceeded by 10% (mass)[m]
O_{90} = the pore size of geotextile corresponding to the average diameter of the sand standardized fraction, of which 90 % remains on the geotextile [m]
t_g = thickness of geotextile [m]
ψ_s = Shields parameter for base material [-]
g = acceleration due to gravity [m/s²]
k_n = filter velocity through geotextile without sand or gravel [m/s]
k = permeability of gravel [m/s]
m = the exponent in the equation related to the permeability [-]
n_f = porosity of filter material [-]
Δ = relative submerged density of base material = $(\rho_s - \rho_w)/\rho_w$
ρ_s = density of base material [kg/m³]
ρ_w = density of water [kg/m³]
u_{*cr} = critical shear velocity the Shields parameter [m/s] (=$(\psi_s \Delta g d_{b50})^{0.5}$)

Test nr.	geo-textile	Type	O_{90}	O_{98}	T_g	k_n	k	v_{fcr}	i_{cr}	$\frac{O_{90}}{d_{90}}$
			mm	mm	mm	mm/s	m/s	mm/s	-	-
1	N66336	A	0.37	0.39	0.45	6.8	0.11	63	0.35	1.68
2	N66339	A	0.40	0.42	0.72	6.0	0.11	65	0.35	1.82
3	N66373	A	0.52	0.55	0.68	5.0	0.11	52	0.23	2.36
4	N66373	A	0.52	0.55	0.68	5.0	0.085	49	0.32	2.36
5	R425	B	0.44	0.53	1.2	1.6	0.11	140*	1.6*	2.00
6	8147	C	0.65	0.74	2.0	2.1	0.11	78	0.48	2.95
7	-	-	-	-	0	-	0.11	21	0.05	-

Figure A-1: Test results (Van Der Knaap et al., 1986)

A.2 Sandtightness of geotextiles as function of hydraulic load (1988)

Following the research, the following formula has been established:

$$u_{f,cr} = \left(12\left(\frac{t_g}{d_{b90}}\right)\left(\frac{d_{b90}}{O_{90}}\right)^4\left(\frac{w}{k_g}\right)^{\frac{1}{2m}} + \frac{n_f}{e}\right)\sqrt{\psi_s \Delta g d_{b50}} \qquad (A.2)$$

In which:

$u_{f,cr}$ = critical filter velocity [m/s]
d_{bx} = the grain size of base material corresponding to x % by weight of finer particles [m]
d_{f15} = diameter of filter material exceeded by 85% (mass)[m]

O_{90} = the pore size of geotextile corresponding to the average diameter of the sand standardized fraction, of which 90 % remains on the geotextile [m]
t_g = thickness of geotextile [m]
ψ_s = Shields parameter [-]
g = acceleration due to gravity [m/s²]
k_g = the permeability coefficient of the geotextile, defined as $v_g = k_g i_g$ [m/s]
m = the exponent in the equation related to the permeability [-]
n_f = porosity of filter material [-]
e = $C_r Re^{-m}$ [-], (see Table A-2)
Re = Reynolds number = $u_{f,cr} d_{f15}/v_w$ [-]
Δ = relative submerged density of base material = $(\rho_s - \rho_w)/\rho_w$
ρ_s = density of base material [kg/m³]
ρ_w = density of water [kg/m³]
v_w = kinematic viscosity of water [m²/s], (see Table A-1)
w = fall velocity of base material in water [m/s] = $\frac{\Delta g d_{b15}^2}{18 v_w}$ if $d_{b15} \leq 0.1$ mm

$\frac{10 v_w}{d_{b15}} \left(\sqrt{\left(1 + \frac{\Delta g d_{b15}^3}{100 v_w^2}\right)} - 1 \right)$ if $d_{b15} > 0.1$ mm

Table A-1: Temperature and viscosity (CUR bouw & infra, 2009)

Temperature [°C]	v_w [m²/s]
0	$1.8*10^{-6}$
10	$1.3*10^{-6}$
20	$1.0*10^{-6}$
30	$0.8*10^{-6}$
40	$0.7*10^{-6}$

Table A-2: Values for the coefficients C_r and m and the shields parameter ψ_s for different values of d_{b50} (Klein Breteler, 1987)

d_{b50} [mm]	C_r [-]	m [-]	ψ_s [-]
0.10	1.18	0.25	0.110
0.15	0.78	0.20	0.073
0.20	0.71	0.18	0.055
0.30	0.56	0.15	0.044
0.40	0.45	0.11	0.038
0.50	0.35	0.07	0.036
0.60	0.29	0.04	0.035
0.70	0.22	0.00	0.034
0.80	0.22	0.00	0.034
1.00	0.22	0.00	0.035

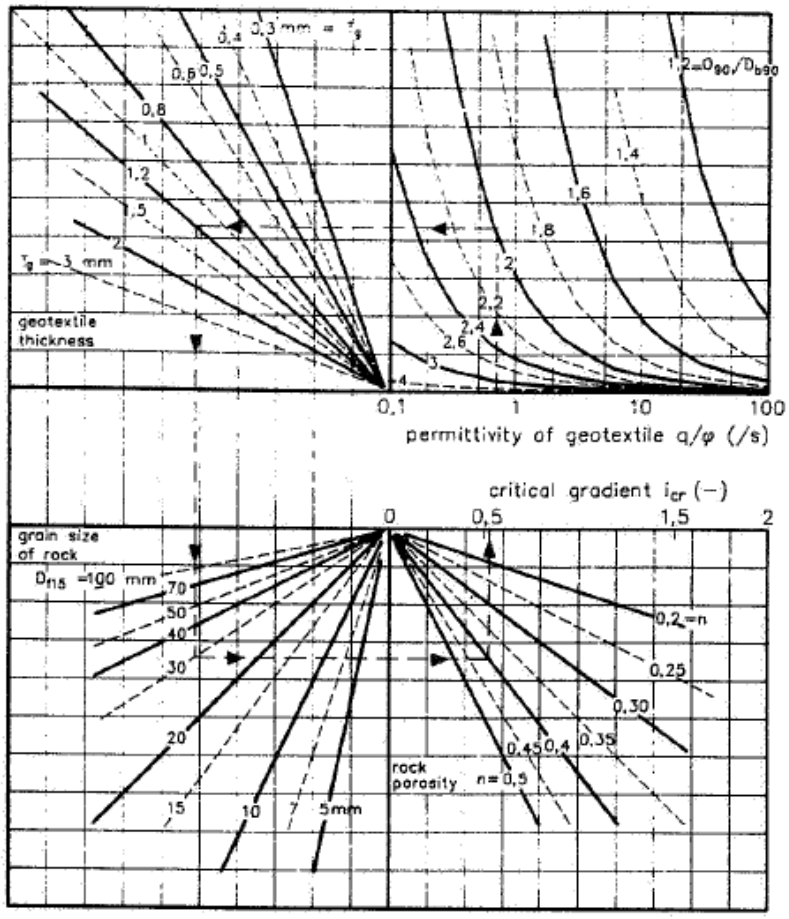

Figure A-2: Design diagram (only valid for woven geotextiles on non-cohesive sand with 0.1 < d_{b50}< 0.2 mm) (Klein Breteler & Verheij, 1990)

With:

n_f = porosity of filter material [-]
i_{cr} = critical gradient in the rock layer, parallel to the geotextile surface [-]
d_{f15} = grain size of filter layer [mm]

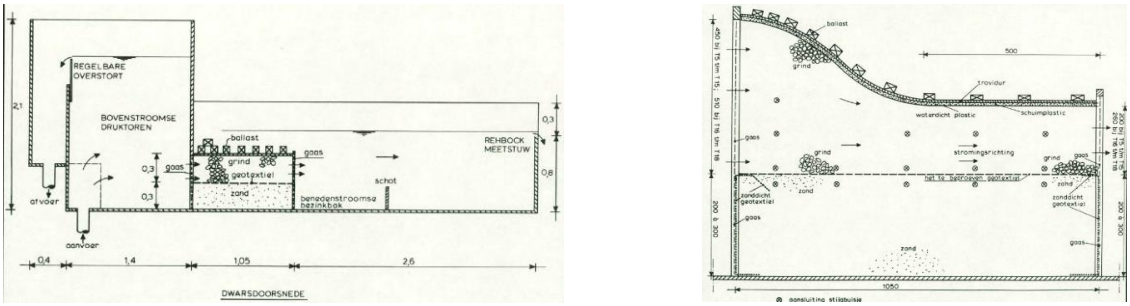

Figure A-3: Test set-up, experiments 1-3 (left) and Test set-up, experiments 5-18 (Klein Breteler, 1988)

proefnummer	geotextiel			filter	zand	watertemp.	i	v_f	s
	nr.	type	O_{90}/D_{b90}	$D_{fmin}-D_{fmax}$	D_{b50}				
				mm	mm	°C	%	mm/s	gr/s/m
T1	N66339	G	1,82	17-35	0,15			24,4	0,013
								38,0	0,028
								46,7	0,012
								53,0	0,034
								57,3	0,061
								57,3	0,034
								60,3	0,06
								60,3	0,11
								66,0	0,18
								74,7	0,44
								82,7	0,68
T2	N66336	G	1,68	17-35	0,15			27,3	0,015
								41,0	0,015
								52,0	0,054
								60,7	0,20
								60,7	0,14
								65,7	0,31
								69,3	0,43
								76,7	0,67
								86,0	0,73
								86,0	0,32
T3	N66339	G	1,82	17-35	0,15	12		45,0	0,025
								52,7	0,05
								59,3	0,18
								68,0	0,63
								68,0	0,44
								75,3	0,73
								82,7	0,68
								82,7	0,35
								82,7	0,23
								86,7	0,34
T5	N66373	G	2,36	17-35	0,15	12	23	52	0,33
								68	4,93
T6	N66336	G	1,68	17-35	0,15	11	14	36	0,020
							26	51	0,071
							42	67	0,27
							53	75	0,75
							65	86	1,62
							65	86	1,02
							65	86	0,69
T7	N66339	G	1,82	17-35	0,15	11	12	35	0,013
							24	54	0,035
							37	67	0,20
							50	75	0,65
							57	85	1,84
							57	85	1,14
							57	85	0,63
T8	N66373	G	2,36	17-35	0,15	10	7	24	0,008
							13	37	0,005
							20	46	0,018
							24	53	0,20
							29	57	0,60
							32	62	1,05
							32	62	0,74
							32	62	0,46
T9	R425	B	2,00	17-35	0,15	9½	65	90	0,02
							71	96	0
							79	102	0,02
							88	108	0,03

proefnummer	geotextiel			filter	zand	watertemp.	i	v_f	s
	nr.	type	O_{90}/D_{b90}	$D_{fmin}-D_{fmax}$	D_{b50}				
				mm	mm	°C	%	mm/s	gr/s/m
T10	N66373	G	2,36	8-20	0,15	9	20	36	0,03
							24	40	0,04
							29	44	0,09
							32	48	0,16
							36	52	0,30
							42	55	0,78
							52	62	1,50
							52	62	0,81
							52	62	0,36
T11	G8147	M	3,00	17-35	0,15	8½	29	62	0,02
							40	73	0,10
							53	84	0,33
							69	97	0,68
							80	105	0,38
							87	110	0,15
T12	-	-	-	17-35	0,15	7½	4,2	16	0
							5,2	20	0,01
							7,5	23	0,34
							8,2	27	1,55
							8,2	27	1,13
							8,2	27	0,99
T13	R425	B	2,00	50-100	0,15	7	39	134	0,04
							51	152	0,07
							63	170	0,07
							75	183	0,10
							86	195	0,15
							100	212	0,24
T14	R425	B	3,38	17-35	0,096	7	12	38	0
							23	54	0,44
							29	62	0,7
							36	70	0,9
							43	76	1,3
							49	82	0,8
							60	90	0,6
T15	-	-	-	17-35	0,096	7	2,0	13	0
							3,5	16	0,06
							4,25	19	0,37
							5,5	22	0,92
							6,5	25	1,55
T16	N66373	G	4,00	17-35	0,096	10	3,5	17	0
							6	23	0
							8	28	0
							11	33	0,13
							14	37	0,28
							18	40	0,85
T18	P6066	B	2,38	45-70	0,096	12	36	105	0
							45	124	0,010
							57	138	0,017
							69	150	0,027
							80	160	0,038
							85	165	0,059

G = gaas
B = bandjesweefsel
M = mat
- = geen geotextiel

Figure A-4: Test results (Klein Breteler, 1988)

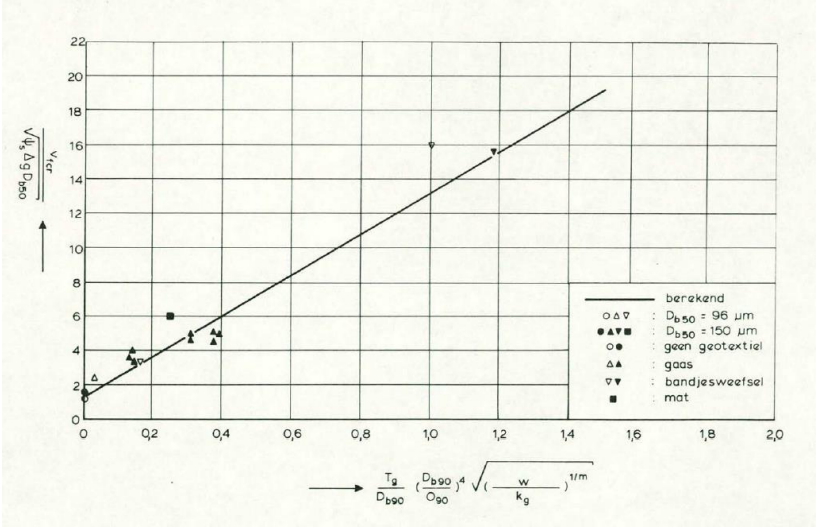

Figure A-5: Comparison of calculated and measured values (Klein Breteler, 1988)

A.2.1 Important test results from 1986 and 1988

- 6 tests with same geotextile
  - Tests T3, T4 and T8 with same base material “A” and filter material “A”
  - Tests T4 and T11 with same base material “A” and filter material “B”
  - T16 with finer sand and filter material “A”

A summary of the most important tests from 1986 and 1988 is presented below. These tests are executed with the same geotextile with 2 different types of filter materials and 2 different base materials. In the table below it is clearly visible that the test T3 from 1986 is equal to the tests T5 & T8 from 1988. Test T4 of 1986 is equal to test T10 from 1988. In both studies no other tests are done with the same geotextile and base material and different filter materials. From the results shown in the table below, it can be concluded that there is an indication that the filter material is independent for the critical filter velocity for woven geotextiles on sand. However, there are only 2 tests to substantiate this statement, so no conclusive conclusion can be drawn as to whether this hypothesis is correct. This means that there are more tests needed to determine if the critical gradient or the critical filter velocity can be indicated as the critical load for geotextiles.

Table A-3: Most important tests 1986 and 1988 with the same geotextile

Test	Geotextile							Base material		Filter		Parameters			Results	
	number	type	O_{90} [mm]	O_{98} [mm]	t_g [mm]	k_g [mm/s]	m [-]	d_{b50} [mm]	d_{b90} [mm]	d_{f15} [mm]	n_f [-]	$\frac{O_{90}}{d_{b90}}$	$\frac{t_g}{d_{b90}}$	$\left(\frac{w}{k_g}\right)^{\frac{1}{m}}$	$u_{f,cr}$ [mm/s]	i_{cr} [-]
T3 (1986)	N66373	G	0.52	0.55	0.68	5.0	1.0	0.15	0.22	20 **	0.425	2.36	3.1	-	52	0.23
T4 (1986)	N66373	G	0.52	0.55	0.68	5.0	1.0	0.15	0.22	11**	0.425	2.36	3.1	-	49	0.32
T5 (1988)	N66373	G	0.52	0.55	0.68	5.0	1.0	0.15	0.22	20	0.425	2.4	3.1	1.8	51	0.23
T8 (1988)	N66373	G	0.52	0.55	0.68	5.0	1.0	0.15	0.22	20	0.425	2.4	3.1	1.8	53	0.24
T10 (1988)	N66373	G	0.52	0.55	0.68	5.0	1.0	0.15	0.22	11	0.425	2.4	3.1	1.8	49	0.33*
T16 (1988)	N66373	G	0.52	0.55	0.68	5.0	1.0	0.096	0.13	20	0.425	4.0	5.2	1.0	35	0.13

* a value of 0.49 was mentioned in the report of 1988, but this value is not in accordance with the data in table 1
** The given d_{f50} in the report of 1986 corresponds with the d_{f50} of the filter material used in 1988 so the assumption has been made that the d_{f15} of 1986 is equal to the d_{f15} of 1988. In both studies the same grain size range was used (8-20 mm and 17-35 mm).

The tests of 1986 and 1988 have resulted in an empirical formula:

$$u_{f,cr} = \left(C_1 \left(\frac{t_g}{d_{b90}}\right)^{C_2} \left(\frac{d_{b90}}{O_{90}}\right)^{C_3} \left(\frac{w}{k_g}\right)^{\frac{C_4}{m}} + \frac{n_f}{e} \right) \sqrt{\psi_s \Delta_b g d_{b50}} \qquad (A.3)$$

With C_1 =12, C_2 =1, C_3 =4, C_4=1/2:

$$u_{f,cr} = \left(12 \left(\frac{t_g}{d_{b90}}\right) \left(\frac{d_{b90}}{O_{90}}\right)^{4} \left(\frac{w}{k_g}\right)^{\frac{1}{2m}} + \frac{n_f}{e} \right) \sqrt{\psi_s \Delta_b g d_{b50}} \qquad (A.4)$$

The coefficients of these formulas have been determined with relatively few tests and is valid for woven geotextiles on a fine sandbed and should not be used outside the range: 0.1<d_{b50}<0.2 mm.

To convert the critical filter velocity into a critical gradient, the Forchheimer equation can be used:

$$i_{cr} = a u_{f,cr} + b u_{f,cr} |u_{f,cr}| \qquad (A.5)$$

With:

$$a = \alpha \frac{(1-n_f)^2}{n_f^3} \frac{v_w}{g d_{fn50}^2} \quad \text{(A.6)}$$

and,

$$b = \beta \frac{(1-n)}{n_f^3} \frac{1}{g d_{fn50}} \quad \text{(A.7)}$$

Van Gent recommended to use an alpha value of 1000 and a beta value of 1.1 (Van Gent, 1992). The value of these two coefficients depends on the type of flow, the grading and shape of the grains and have to be determined experimentally.

The tests from 1986 and 1988 were recalculated to see whether the formula is sufficiently accurate with the formula of Klein Breteler and the Forchheimer equation:

Table A-4: Test results and calculated values with dimensions of geotextile

Test	Geotextile						Base material			Filter			Parameters			Measured results		Calculated from characteristics geotextile	
	number	type	O_{90} [mm]	t_g [mm]	k_g [mm/s]	m [-]	d_{b15} [mm]	d_{b50} [mm]	d_{b90} [mm]	d_{f15} [mm]	d_{f50} [mm]	n_f [-]	$\frac{O_{90}}{d_{b90}}$	$\frac{t_g}{d_{b90}}$	$\left(\frac{w}{k_n}\right)^{\frac{1}{m}}$	$u_{f,cr}$ [mm/s]	i_{cr} [-]	$u_{f,cr}$ [mm/s]	i_{cr} [-]
T3 (1986)	N66373	G	0.52	0.68	5.0	1.0	0.115	0.15	0.22	20**	24	0.42	2.36	3.1	-	52	0.23	46.7	0.16
T4 (1986)	N66373	G	0.52	0.68	5.0	1.0	0.115	0.15	0.22	11**	14.3	0.42	2.36	3.1	-	49	0.32	43.3	0.30
T5 (1988)	N66373	G	0.52	0.68	5.0	1.0	0.115	0.15	0.22	20	24.5	0.42	2.4	3.1	1.8	51	0.23	47.5	0.15
T8 (1988)	N66373	G	0.52	0.68	5.0	1.0	0.115	0.15	0.22	20	24.5	0.42	2.4	3.1	1.8	53	0.24	46.6	0.15
T10 (1988)	N66373	G	0.52	0.68	5.0	1.0	0.115	0.15	0.22	11	14.5	0.42	2.4	3.1	1.8	49	0.33*	42.7	0.30
T16 (1988)	N66373	G	0.52	0.68	5.0	1.0	0.078	0.096	0.13	20	24.5	0.42	4.0	5.2	1.0	35	0.13	23.1	0.05

A.2.2 Conclusion

The calculated critical filter velocities of the various tests result in an underestimate of 10% compared to the measured critical filter velocities. This can be clearly seen by comparing Figure A-6and Figure A-7. Figure A-6 shows the tests in which critical filter velocity was calculated using the characteristics of the geotextiles. It is clearly visible that the calculated value is an underestimate of the measured value. If this value is converted into a critical gradient using the Forchheimer equation, this results in a 35% lower value than the measured value. The underestimation of the critical filter velocity affects the critical gradient.

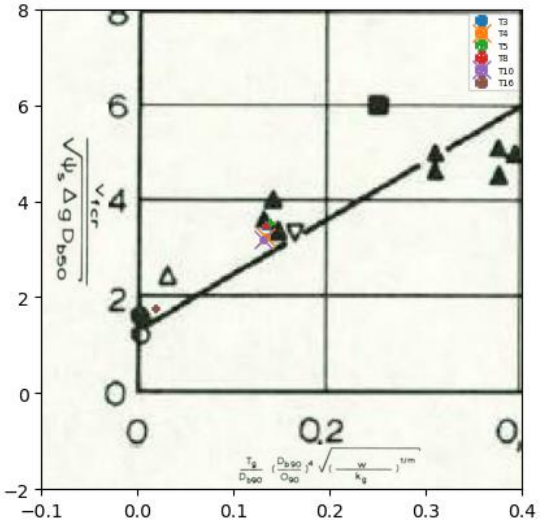

Figure A-6: Results with calculated $u_{f,cr}$ with Klein-Breteler formula

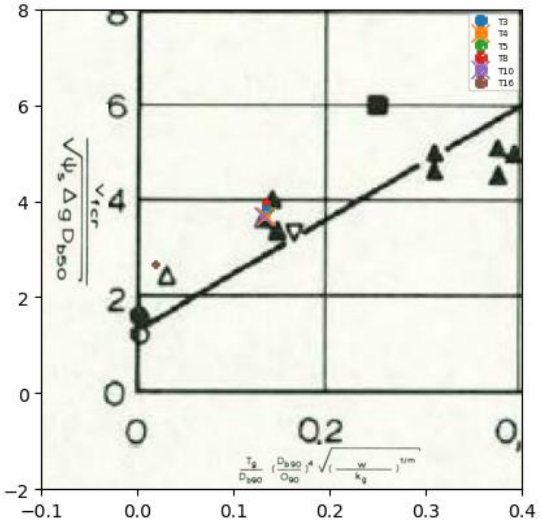

Figure A-7: Measured test results

A.2.3 Influence of method of testing on sand transport

The table and graphs below clearly show that the method of raising influences the amount of sand transport when reaching the critical load. Klein Breteler gives two possible reasons for this:

1) Increasing the filter velocity increases sand transport

2) The formation of erosion canals or erosion pits inhibits sand transport

Table A-5: Test results 1986 and 1988 with the same base material, geotextile and filter material (Klein Breteler, 1988)

Test	Geotextile							Base material		Filter		Parameters			Results	
	number	type	O_{90} [mm]	O_{98} [mm]	t_g [mm]	k_g [mm/s]	m [-]	d_{b50} [mm]	d_{b90} [mm]	d_{f15} [mm]	n_f [-]	$\frac{O_{90}}{d_{b90}}$	$\frac{t_g}{d_{b90}}$	$\left(\frac{w}{k_g}\right)^{\frac{1}{m}}$	$u_{f,cr}$ [mm/s]	i_{cr} [-]
T2 (1988)	N66336	G	0.37	0.39	0.45	6.8	1.0	0.15	0.22	20	0.425	1.7	2.1	1.3	61	-
T6 (1988)	N66336	G	0.37	0.39	0.45	6.8	1.0	0.15	0.22	20	0.425	1.7	2.1	1.3	62	-
T2 (1986)	N66339	G	0.40	0.42	0.72	6.0	1.0	0.15	0.22	20	0.425	1.8	3.3	1.5	63	0.35
T1 (1988)	N66339	G	0.40	0.42	0.72	6.0	1.0	0.15	0.22	20	0.425	1.8	3.3	1.5	67	-
T3 (1988)	N66339	G	0.40	0.42	0.72	6.0	1.0	0.15	0.22	20	0.425	1.8	3.3	1.5	62	-
T7 (1988)	N66339	G	0.40	0.42	0.72	6.0	1.0	0.15	0.22	20	0.425	1.8	3.3	1.5	67	0.37

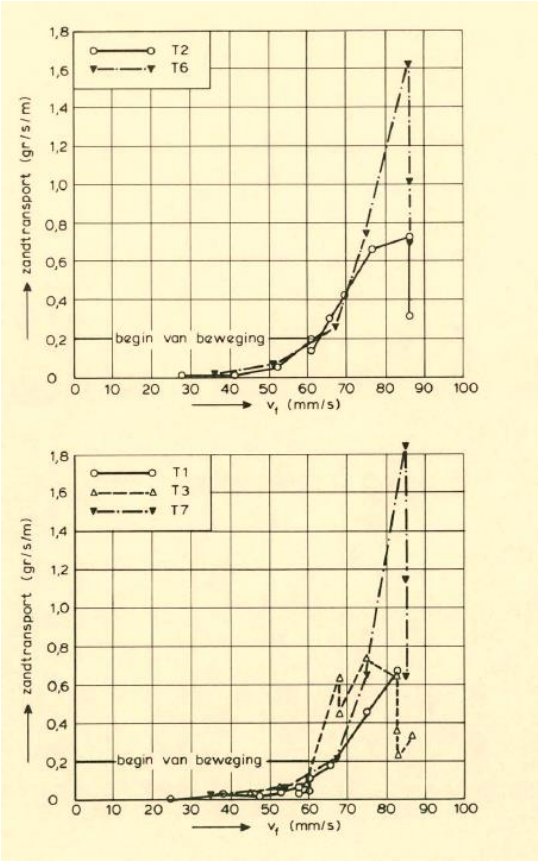

Figure A-8: Influence of model set-up and method of testing (Klein Breteler, 1988)

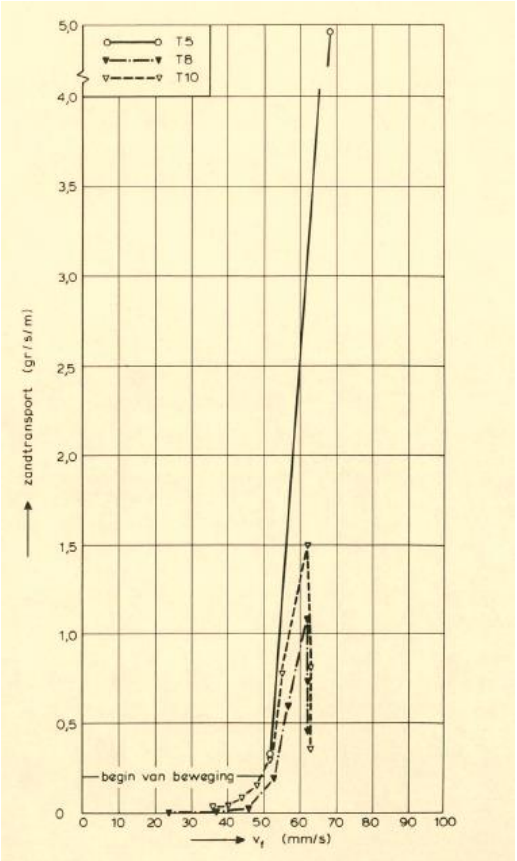

Figure A-9: influence of model set-up and method of testing (Klein Breteler, 1988)

A.2.4 Influence of structure of geotextile on critical load

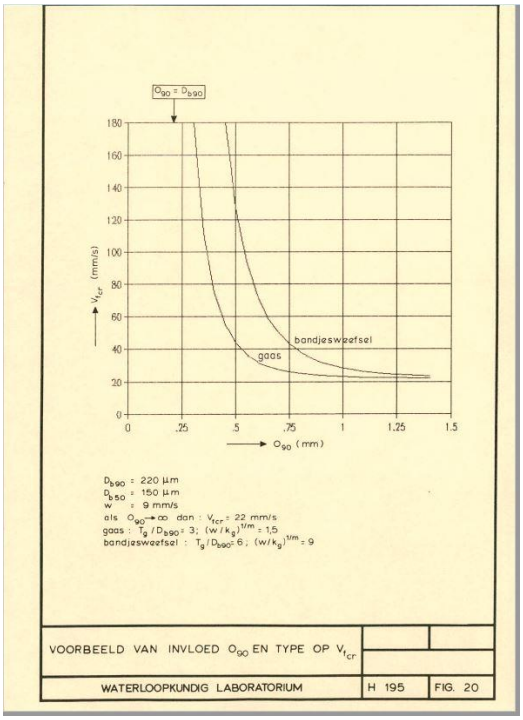

Figure A-10: Influence of structure of geotextile on critical load (Klein Breteler, 1988)

A.3 Past study: Performance of geotextiles on clay and fine sand in bed and bank protections (1994)

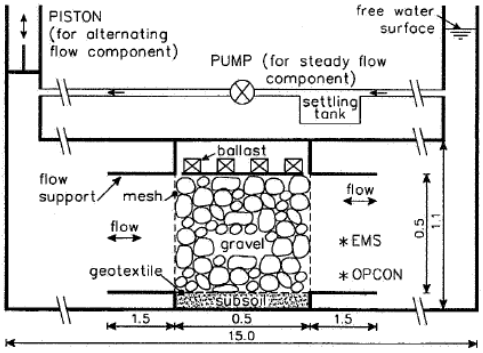

Figure A-11: Test set-up (Klein Breteler et al., 1994)

subsoil	geotextile	$O_{90,d}$ (μm)	t_{GT} (mm)	k_n (mm/s)	test	i_{cr} (%)	q_{cr} (m/s)
good clay <2 μm: 39% d_{50} = 9 μm d_{90} = 80 μm	P6014	185	1.5	0.9	1	450	0.54
	NF180	185	0.7	1.5	2	>300	>0.5
	NH625	209	2.1	0.7	3	300	0.47
	none	-	-	-	4	10	0.06
medium clay <2 μm: 22% d_{50} = 42 μm d_{90} = 100 μm	P6014	185	1.5	0.9	5	220	0.40
					6	150	0.32
	NF180	185	0.7	1.5	7	150	0.32
	NH625	209	2.1	0.7	8	110	0.27
	FF3S	105	1.6	2.1	9	130	0.30
	S201	161	3.3	5.1	10	190	0.37
	PHB3	144	1.3	4.2	11	280	0.46
					12	150	0.32
			4		13	120	0.28
poor clay <2 μm: 20% d_{50} = 130 μm d_{90} = 400 μm	P6014	185	1.5	0.9	14	140	0.31
	NH625	209	2.1	0.7	15	120	0.28
	S201	161	3.3	5.1	16	110	0.27
			10		17	380	0.54
	PHB3	144	1.3	4.2	18	120	0.28
	T3407	144	0.5	1.1	19	150	0.32
fine sand d_{10} = 65 μm d_{50} = 90 μm d_{90} = 105 μm	NF180	185	0.7	1.5	20	8	0.05
	R425	297	1.3	2.1	21	12	0.07
	PHB3	144	1.3	4.2	22	10	0.06

$O_{90,d}$ = O_{90} determined with dry sieving test (m)
q_{cr} = filter velocity in the rock layer, parallel to the geotextile, at which the subsoil starts to wash out (m/s)
i_{cr} = (pressure potential) gradient in the rock layer, parallel to the geotextile, at which the subsoil starts to wash out (-)
t_{GT} = geotextile thickness (m)
k_n = permeability of geotextile: $k_n = (\phi_t/T_g)^n/q_t$ (m/s)
ϕ_t = pressure potential over geotextile during permeability test (m)
q_t = filter velocity through geotextile during permeability test (m/s)

Figure A-12: Test programme and results (Klein Breteler et al., 1994)

A.4 Past study: Applied geotextile research (1995)

In 1994 and 1995, research was also conducted into woven and non-woven geotextiles on clay (Table A-6). These results show that for clay the critical filter velocity does show a dependence on the grain size of the filter material. However, the properties of clay cannot be compared with those of sand as cohesion plays a significant role in clay.

Table A-6: Most important tests 1995 with the same geotextile

Test	Geotextile					Base material		Filter		Results	
	number	O_{90} [mm]	t_g [mm]	k_g [mm/s]	m [-]	d_{b50} [mm]	d_{b90} [mm]	d_{f50} [mm]	n_f [-]	$u_{f,cr}$ [m/s]	i_{cr} [-]
102	S201-3 (nw)	0.130	0.68	172	0.96	0.15	0.22	75	0.425	0.35	2.2
105	NF180 (w)	0.183	0.68	49	0.73	0.15	0.22	75	0.425	0.40	2.6
301	S201-3 (nw)	0.130	2.7	172	0.96	0.15	0.22	8	0.425	0.20	Approx 6.5
302	NF180 (w)	0.183	0.68	49	0.73	0.15	0.22	22	0.425	0.30	Approx 6
303	NF180 (w)	0.183	0.68	49	0.73	0.15	0.22	145	0.425	0.32	1.5

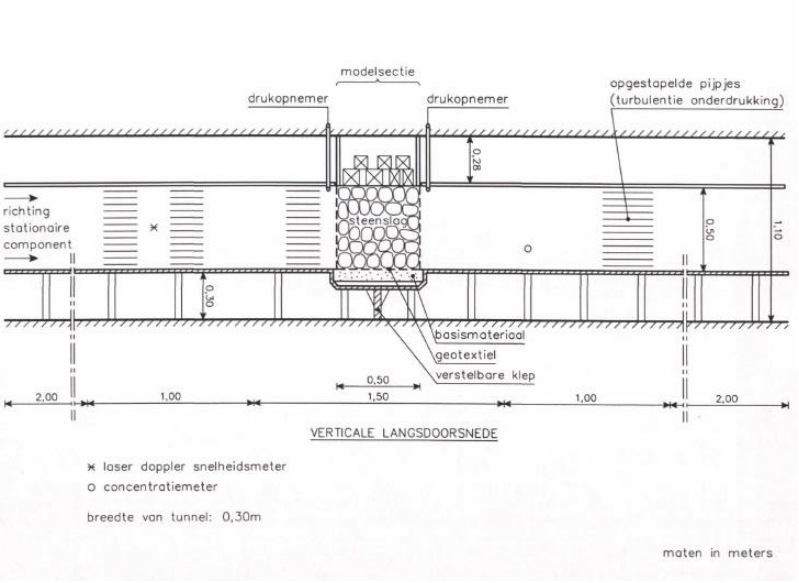

Figure A-13: Test set-up (Van Der Meulen & Smith, 1995)

Proefnummer	Geotextiel	Basismateriaal	i_{cr}	v_{for} (m/s)
101	F3S non-woven (nw)	klei	1,8	0,34
102	S201-3 (nw)	klei	2,2	0,35
103d	F300 woven (w)	klei	1,5	0,33
104	S351 (nw)	klei	2,2	0,39
105	NF180 (w)	klei	2,6	0,40
106	R400/50 (w)	klei	1,0	0,25
107	T600 (nw)	klei	2,0	0,35
108	S1004 (nw)	klei	1,8	0,31
109	F3S (nw)	zand	0,7	0,21
110	S351 (nw)	zand	2,0	0,33
111	T600 (nw)	zand	2,5	0,36
112	S1004 (nw)	zand	2,0	0,32
301	S201-3 (nw) Filter 8 mm	klei	circa 6,5	0,20
302	NF180 (w) Filter 22 mm	klei	circa 6	0,30
303	NF180 (w) Filter 145 mm	klei	1,5	0,32
401/402	NF180 (W) vooraf geul in basis aangebracht	klei	0,8	0,23
403/404	S201-3 (nw) vooraf geul in basis aangebracht	klei	1,0	0,24
501c 501d	NF 180 (w) steenzetting met 8.5 mm geul	klei	4,5 3,4	nvt
503	S201-3 (nw) steenzetting met 8.5 mm geul	klei	2,4	nvt

nvt = niet van toepassing

Figure A-14: Test results (Van Der Meulen & Smith, 1995)

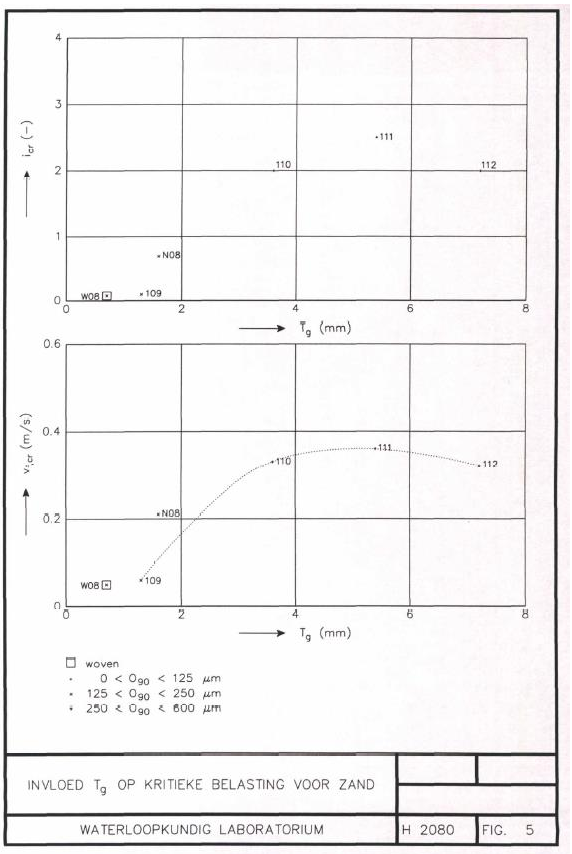

Figure A-15: Influence of t_g at the critical load for sand (Van Der Meulen & Smith, 1995)

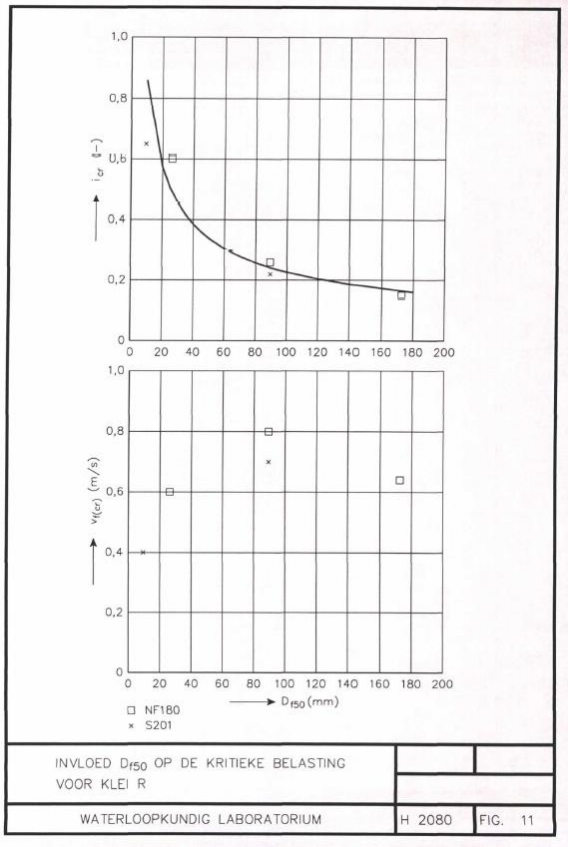

Figure A-16: Influence of d_{f50} at the critical load for clay (Van Der Meulen & Smith, 1995)

The tests 110, 111, 112 had geotextiles with a small O_{90} which can be considered as geometrically closed.

A.5 Lemmens (1996)

In 1996, Lemmens already conducted research into the critical gradient of natural geotextiles and three synthetic geotextiles. In this study, only the critical gradient was measured. The table below shows the data of the woven synthetic geotextiles used in Lemmens' study. No data is included in the report for natural geotextiles, and data of the used synthetic geotextiles is provided or can be found in the literature. To make the calculation, a number of assumptions were made: the thickness of two geotextiles, the porosity of the filter layer, and the Forchheimer coefficients. The porosity of the filter layer is assumed to be 42% and an alpha value of 1000 and a beta value of 1.1 is assumed for the Forchheimer equation.

The critical filter velocity was determined using the Klein Breteler formula with the data of the three geotextiles. These calculated values are utilized to determine the critical gradient with the Forchheimer equation. The results are shown Table A-7. The calculated critical gradient is 15% more than the measured critical gradient by Lemmens for the F180 geotextile. The calculated critical gradient of the geotextile 6G/120/SA is twice the measured gradient. With geotextile C10.341, the difference is even three times higher than the measured value.

Table A-7: Test results Lemmens (1996) and calculated critical gradient with the Klein Breteler formula

Geotextile					Base material			Filter			Parameters			Results	Calculated from characteristics geotextile and filter layer		Calculated from measured i_{cr} to $u_{f,cr}$ [mm/s]
Type	O_{90} [mm]	t_g [mm]	k_g [mm/s]	m [-]	d_{b15} [mm]	d_{b50} [mm]	d_{b90} [mm]	d_{f15} [m]	d_{fn50} [m]	n_f [-]	$\frac{O_{90}}{d_{b90}}$	$\frac{t_g}{d_{b90}}$	$\left(\frac{w}{k_g}\right)^{\frac{1}{m}}$	i_{cr} [-]	$u_{f,cr}$ [mm/s]	i_{cr} [-]	$u_{f,cr}$ [mm/s]
F180 (235 gr/m²)	0.180	0.7	50	1.0	0.095	0.145	0.19	0.10**	0.15**	0.42*	0.95	3.68	0.13	0.59	314.6	0.68	293.2
6G/120/SA (120 gr/m²)	0.200	0.35*	12	1.0	0.095	0.145	0.19	0.10**	0.15**	0.42*	1.05	1.84	0.52	0.16	225.1	0.35	151.4
C10.341 (240 gr/m²)	0.200	0.6*	25	1.0	0.095	0.145	0.19	0.10**	0.15**	0.42*	1.05	3.68	0.25	0.14	259.3	0.46	141.5

* Assumptions
** Assumption made with (Laan, Het gebruik van steen in waterbouwkundige constructies, 1996)

A.5.1 Uncertainties

As can be seen from the table above, it is clearly visible that the calculated critical gradients deviate from the critical gradients measured by Lemmens. A sensitivity analysis was performed to check whether the assumptions for the unknown data have a major influence on the outcome. The sensitivity of the porosity, the Forchheimer coefficients and the unknown thickness of 2 geotextiles are discussed below.

Uncertainty porosity

The graph below (Figure A-17) clearly shows that the porosity influences the calculated critical gradient. A porosity of 42% was assumed as a starting point. If this parameter is varied between 40% and 45%, it has a significant influence on the outcome. Lemmens did not measure the porosity, but he did try to keep it the same for all his tests.

Lemmens used a fascine mattress and two different stone sizes in his test set-up: large stones in the centre of the flume (80-200 mm) and small stones (30-40 mm) along the sides of the flume. This makes it difficult to make a good assumption about the porosity.

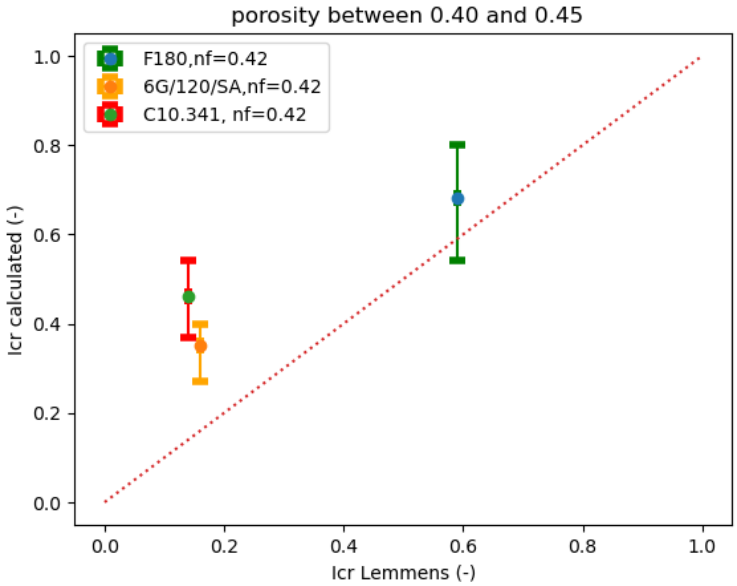

Figure A-17: Uncertainty porosity

Uncertainty Forchheimer coefficients

As can be seen in the figures below (Figure A-18 & Figure A-19), the beta value in the Forchheimer equation have a major influence on the outcome. While the alpha coefficient has almost no influence.

The model constants a and b of the Forchheimer relation can be determined based on the experimental relationship between the gradient and the filter velocity. This is possible by plotting the measured gradient against the filter velocity and fitting a line through these points (i_{cr}=a*u+b*u^2). Because Lemmens did not measure the filter velocities, the constants a and b of the Forchheimer equation cannot be determined.

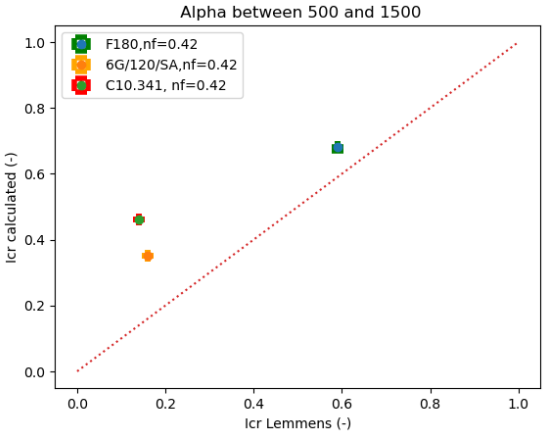

Figure A-18: Uncertainty Alpha coefficient Forchheimer

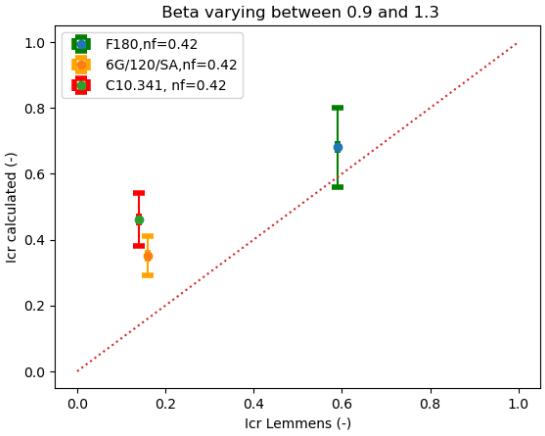

Figure A-19: Uncertainty Beta coefficient Forchheimer

Uncertainty thickness geotextile

Another major uncertainty is the thickness of the geotextile. For two geotextiles, an estimate has been made based on their weight. The geotextile 6G/120/SA is half as heavy as the F180 geotextile, which has a known thickness of 0.7 mm. Therefore, it is assumed that the thickness of the 6G/120/SA geotextile is approximately 0.35 mm. The geotextile C10.341 has approximately the same weight as the geotextile F180, but Lemmens mentions in his report that it has a small thickness. The geotextile is made from polyester, which has a higher density than polypropylene and polyamide. Hence, it is assumed that the thickness of the C10.341 geotextile is 0.6 mm. This assumption is likely on the negative side.

Figure A-20, clearly shows that the C10.341 geotextile is more sensitive to thickness than the 6G/120/SA geotextile. If both geotextiles have a fictitious thickness of 0.25 mm, the 6G/120/SA geotextile will remain above the measured point, while the C10.341 geotextile would be below the measured point.

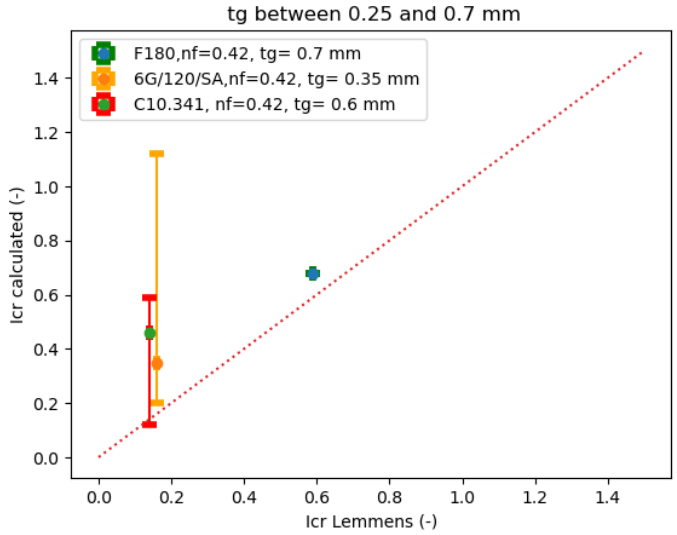

Figure A-20: Uncertainty of unknown thickness of geotextiles

A.5.2 Conclusion

This study applying Klein Breteler's formula with the independent data from Lemmens demonstrates that the formula can provide a rough indication of the actually measured critical gradient. However, the formula is highly sensitive when certain parameters are unknown and need to be estimated. Because the thickness and the Forchheimer coefficients in particular are not known, it is not possible to draw a good conclusion as to whether the formula also provides a good prediction in other situations. Accordingly, it is crucial to accurately determine all important parameters in the Klein-Breteler formula to establish its usefulness in designing open geotextile filters made of natural materials.

Furthermore, this study highlights that the beta coefficient of the Forchheimer coefficient has a significant influence on converting the critical filter velocity to the critical gradient. Therefore, it is necessary to determine this coefficient for the different filter materials which are going to be used in the tests. This can be done by measuring the gradient and filter velocity at several moments during the tests and by plotting the measured gradient against the filter velocity and fitting a line through these points (i_{cr}=a*u+b*u^2).

Appendix B Determining water permeability of geotextiles

Since the water permeability of the various geotextiles is unknown, it has been determined on the basis of the European standard NEN-EN-ISO 11058 with a simplified version (Figure B-1). This simplified version is less accurate than the official test in a laboratory, but sufficient to get a good indication of the order of magnitude. In this test the head loss is measured at 50 mm. The result of this test is the so-called Velocity Index, the flow rate through the geotextile at a gradient of 50 mm. During each test, it was measured how long it takes to get 1 litre of water through the geotextile. With these parameters in combination with the known surface area of the geotextile in the test set-up, the velocity can be calculated. This velocity can be converted into water permeability using the formulas below:

$$V_{H50} = \frac{R_T * V}{A \cdot t} \; with \; R_T = \frac{1.762}{1 + 0.0337T + 0.00022T^2} \tag{B.1}$$

$$\psi = 20 * V_{H50} \tag{B.2}$$

$$k_g = t_g * \psi \tag{B.3}$$

(a) Test set-up

(b) Test set-up

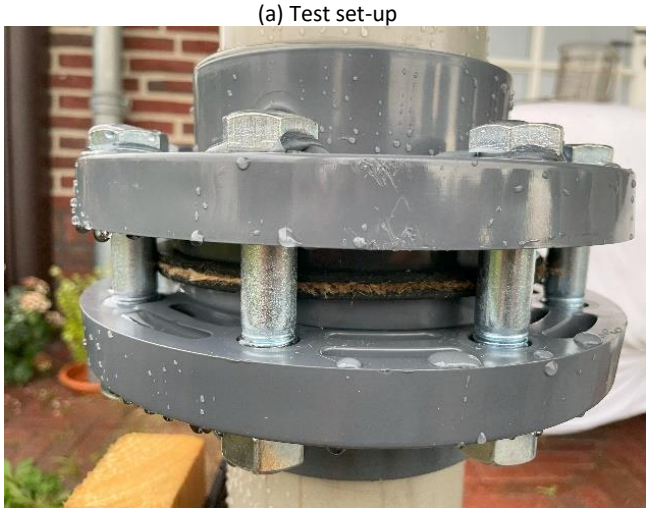

(c) Clamped geotextile

(d) Geotextile after test

Figure B-1: Pictures of water permeability tests

B.1 Results

B.1.1 Woven geotextiles

In the tables below, the results of the permeability tests for each woven geotextile are shown.

J4 geotextile

Table B-1: Results permeability test J4

Test	Volume [m³]	Area [m²]	Temperature [°c]	Thickness [m]	Time [s]	k_g [m/s]	k_g [mm/s]
Test 1	0.001	0.010207	11.9	0.00145	4.56	0.000767	0.76655
Test 2	0.001	0.010207	11.9	0.00145	4.01	0.000872	0.871688
Test 3	0.001	0.010207	11.9	0.00145	4.48	0.00078	0.780239
Test 4	0.001	0.010207	11.9	0.00145	3.81	0.000917	0.917446
Test 5	0.001	0.010207	11.9	0.00145	4.30	0.000813	0.8129
Test 6	0.001	0.010207	11.9	0.00145	4.11	0.00085	0.850479
Test 7	0.001	0.010207	11.9	0.00145	3.99	0.000876	0.876057
Test 8	0.001	0.010207	11.9	0.00145	3.93	0.000889	0.889432
Test 9	0.001	0.010207	11.9	0.00145	4.78	0.000731	0.73127
Average	0.001	0.010207	11.9	0.00145	4.218889	0.000833	0.832896

J5 geotextile

Table B-2: Results permeability test J5

Test	Volume [m³]	Area [m²]	Temperature [°c]	Thickness [m]	Time [s]	k_g [m/s]	k_g [mm/s]
Test 1	0.001	0.010207	10.1	0.00177	5.1	0.000879	0.87923
Test 2	0.001	0.010207	10.1	0.00177	5.2	0.000862	0.86232
Test 3	0.001	0.010207	10.1	0.00177	4.85	0.000925	0.92455
Test 4	0.001	0.010207	10.1	0.00177	4.92	0.000911	0.91140
Test 5	0.001	0.010207	10.1	0.00177	5.03	0.000891	0.89147
Test 6	0.001	0.010207	10.1	0.00177	4.97	0.000902	0.90223
Test 7	0.001	0.010207	10.1	0.00177	4.97	0.000902	0.90223
Test 8	0.001	0.010207	10.1	0.00177	4.93	0.000910	0.90955
Average	0.001	0.010207	10.1	0.00177	4.99625	0.000898	0.89787

J7 geotextile double

Table B-3: Results permeability test J7

Test	Volume [m³]	Area [m²]	Temperature [°c]	Thickness [m]	Time [s]	k_g [m/s]	k_g [mm/s]
Test 1	0.001	0.010207	11.9	0.00195	10.16	0.000462677	0.46268
Test 2	0.001	0.010207	11.9	0.00195	8.92	0.000526996	0.52670
Test 3	0.001	0.010207	11.9	0.00195	8.7	0.000540322	0.54032
Test 4	0.001	0.010207	11.9	0.00195	8.85	0.000531164	0.53116
Test 5	0.001	0.010207	11.9	0.00195	8.98	0.000523475	0.52347
Test 6	0.001	0.010207	11.9	0.00195	9.15	0.000513749	0.51375
Test 7	0.001	0.010207	11.9	0.00195	9.27	0.000507098	0.50710
Average	0.001	0.010207	11.9	0.00195	9.147143	0.000515069	0.51507

J9 geotextile

Table B-4: Results permeability test J9

Test	Volume [m³]	Area [m²]	Temperature [°c]	Thickness [m]	Time [s]	k_g [m/s]	k_g [mm/s]
Test 1	0.001	0.010207	13.4	0.00223	64.16	0.000080	0.08048
Test 2	0.001	0.010207	13.4	0.00223	72.11	0.000072	0.07161
Test 3	0.001	0.010207	13.4	0.00223	69.61	0.000074	0.07418
Test 4	0.001	0.010207	13.4	0.00223	71.4	0.000072	0.07232
Average	0.001	0.010207	13.4	0.00223	69.32	0.000075	0.07464

B.1.2 Non-woven geotextiles

In the tables below, the results of the permeability tests for each non-woven geotextile are shown.

Hemp on jute

Table B-5: Results permeability test hemp on jute

Test	Volume [m^3]	Area [m^2]	Temperature [°c]	Thickness [m]	Time [s]	k_g [m/s]	k_g [mm/s]
Test 1	0.001	0.010207	11.9	0.00258	12.43	0.00050	0.49998
Test 2	0.001	0.010207	11.9	0.00258	11.6	0.00054	0.53575
Test 3	0.001	0.010207	11.9	0.00258	11.7	0.00053	0.53117
Test 4	0.001	0.010207	11.9	0.00258	12.05	0.00052	0.51574
Test 5	0.001	0.010207	11.9	0.00258	12.16	0.00051	0.51108
Average	0.001	0.010207	11.9	0.00258	11.988	0.00052	0.51874

Recycled jute on jute

Table B-6: Results permeability test recycled jute on jute

Test	Volume [m^3]	Area [m^2]	Temperature [°c]	Thickness [m]	Time [s]	k_g [m/s]	k_g [mm/s]
Test 1	0.001	0.010207	11.9	0.00341	6.96	0.001182	1.181782
Test 2	0.001	0.010207	11.9	0.00341	7.56	0.001088	1.087989
Test 3	0.001	0.010207	11.9	0.00341	7.79	0.001056	1.055866
Test 4	0.001	0.010207	11.9	0.00341	7.85	0.001048	1.047796
Test 5	0.001	0.010207	11.9	0.00341	7.41	0.00111	1.110013
Test 6	0.001	0.010207	11.9	0.00341	8.63	0.000953	0.953094
Test 7	0.001	0.010207	11.9	0.00341	8.42	0.000977	0.976865
Test 8	0.001	0.010207	11.9	0.00341	8.92	0.000922	0.922108
Test 9	0.001	0.010207	11.9	0.00341	7.21	0.001141	1.140804
Average	0.001	0.010207	11.9	0.00341	7.861111	0.001053	1.052924

Wool on jute

Table B-7: Results permeability test wool on jute

Test	Volume [m^3]	Area [m^2]	Temperature [°c]	Thickness [m]	Time [s]	k_g [m/s]	k_g [mm/s]
Test 1	0.001	0.010207	11.9	0.00278	4.2	0.001593	1.593337
Test 2	0.001	0.010207	11.9	0.00278	4.15	0.001613	1.612534
Test 3	0.001	0.010207	11.9	0.00278	4.08	0.00164	1.6402
Test 4	0.001	0.010207	11.9	0.00278	4.16	0.001609	1.608657
Test 5	0.001	0.010207	11.9	0.00278	4.05	0.001652	1.652349
Test 6	0.001	0.010207	11.9	0.00278	4.1	0.001632	1.632199
Test 7	0.001	0.010207	11.9	0.00278	4.2	0.001593	1.593337
Test 8	0.001	0.010207	11.9	0.00278	4.01	0.001669	1.668832
Test 9	0.001	0.010207	11.9	0.00278	4.2	0.001593	1.593337
Average	0.001	0.010207	11.9	0.00278	4.127778	0.001622	1.621642

B.1.3 Cross-section test set-up permeability test

Below (Figure B-2) a cross section of the test set-up is shown.

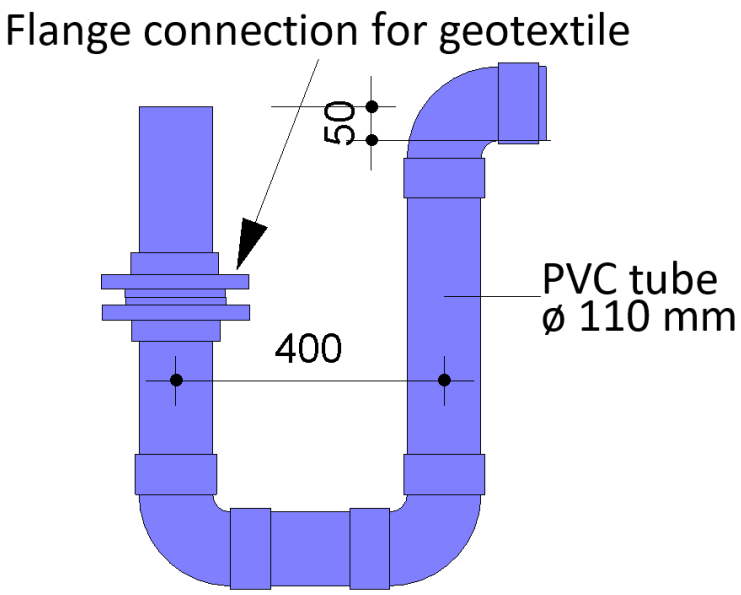

Figure B-2: Cross-section test set-up water permeability test

Appendix C Material properties

C.1 Base material

Dimensions of the base material

The base material is sieved in the lab to determine the sieve curve. The amount of sand collected in each sieve are given in Table C-1. The sieve curve is presented in Figure C-1.

Table C-1: Results sieving base material: M34

Sieve [mm]	Amount of sand [gr]	Amount of sand [%]	Percentage smaller than the sieve diameter [%]
0.3	0.8	0.60	99.40
0.25	1.8	1.35	98.05
0.212	53.2	39.88	58.17
0.18	10.8	8.10	50.07
0.15	44.8	33.58	16.49
0.125	12.2	9.15	7.35
0.09	8.2	6.15	1.20
0.063	1.6	1.20	0.00

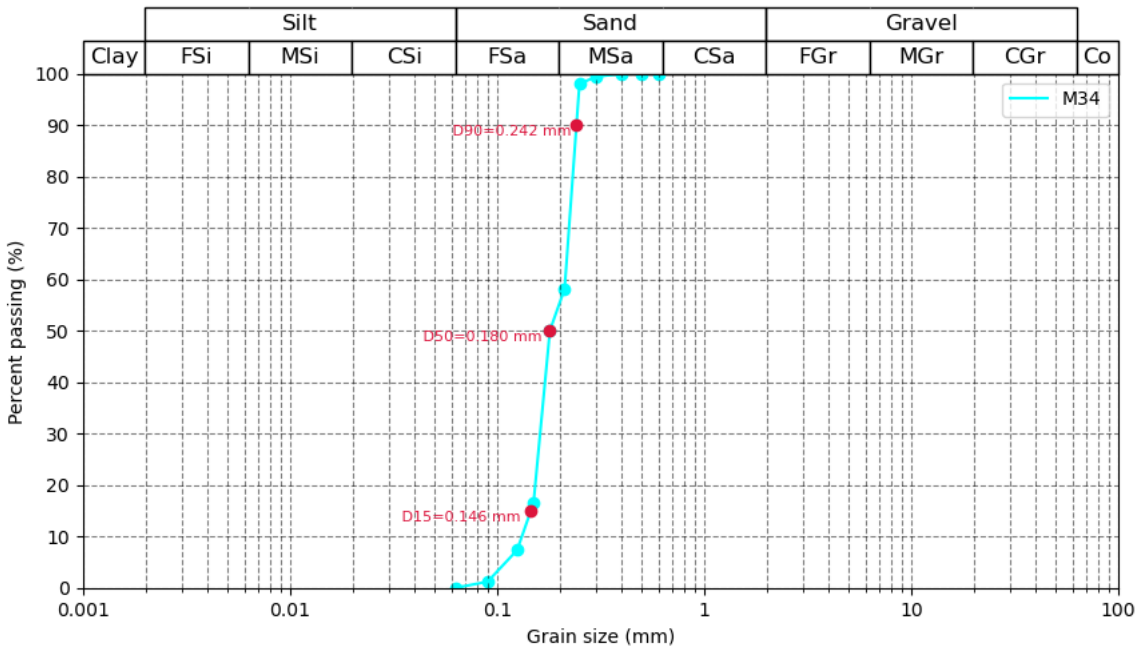

Figure C-1: Grain size distribution of base material

Overview base material

The main properties of the base materials are given in Table C-2.

Table C-2: Main properties of base material

Type	d_{b15} [mm]	d_{b50} [mm]	d_{b90} [mm]	ρ_b [kg/m^3]
M34	0.146	0.180	0.242	2650

C.2 Geotextile

A total of 7 different geotextiles are tested. An overview of the tested geotextiles is presented below (Table C-3):

Table C-3: Overview of geotextiles

Type	**Material**	**Woven or non-woven**	**Weight [gr/m²]**	**Amount of warp threads *[-]***	**Amount of weft threads *[-]***	**O_{90} [µm]**	**t_g [mm]**	**k_g [mm/s]**	***m* [-]**
J4	Jute	Woven	422	1	1	516.1	1.45	0.83*	1
J5	Jute	Woven	518	2	2	819.0	1.77	0.90*	1
J7	Jute	Woven	-	2	2	-	2.01**	0.52*	1
J9	Jute	Woven	963	2	2	283.2	2.23	0.075*	1
Hemp on jute	Hemp on jute	Non-woven	500	-	-	-	2.58**	0.52*	-
Recycled jute on jute	Recycled jute on jute	Non-woven	500	-	-	-	3.41**	1.05*	-
Wool on jute	Wool on jute	Non-woven	500	-	-	-	2.78**	1.62*	-

* Assumption with simplified test with deviation of ± 20%
** Measured with calliper

Thickness of non-woven geotextiles and geotextile J7

The thickness of the non-woven geotextiles and the geotextile J7 has not been investigated at this time. To determine this thickness, it was measured 10 times with a caliper, and the average value was taken. The table below (Table C-4) shows the results.

Table C-4: Thickness non-woven geotextiles

	Thickness hemp on jute [mm]	**Thickness wool on jute [mm]**	**Thickness jute on jute [mm]**	**Thickness J7 [mm]**
Measurement 1	2.44	2.70	3.50	1.98
Measurement 2	3.02	2.82	3.54	2.00
Measurement 3	2.50	2.76	3.30	1.98
Measurement 4	2.58	2.94	3.74	2.18
Measurement 5	2.70	2.96	3.24	2.12
Measurement 6	2.40	2.38	3.32	2.10
Measurement 7	2.58	2.72	3.12	1.96
Measurement 8	2.52	2.54	3.30	1.96
Measurement 9	2.56	2.80	3.60	1.90
Measurement 10	2.48	3.14	3.46	1.92
Average	**2.58**	**2.78**	**3.41**	**2.01**

C.3 Filter material

Density of Filter material

Before the start of the tests, the density of the filter material is determined. Thereafter, the porosity of all 3 types of filter material will be determined. In addition, a grain size distribution will be made for each type of filter material to determine the d_{f15} and d_{fn50}. The densities and grading curves of these individual stone sizes were determined.

The density of the three filter materials is determined with the following step-by-step procedure:

1. A stone is taken out of the big bag.
2. Each stone is weighed using a weighing scale and the weight is recorded in grams (kg).
3. Determine the volume of the sample by submerging it in water and measuring the displacement it causes.
4. Record the volume in cubic meters (m^3).
5. Calculate the density of the sample by dividing the dry weight (kg) by the volume (m^3) (equation (C.1)).
6. Repeat steps 1-5 for a total of 12 times to obtain multiple density measurements.
7. Calculate the average density by adding up all the density values and dividing the sum by the total number of measurements.

$$\rho_f = \frac{W}{V} \tag{C.1}$$

The density of the two different filter materials is based on 12 measurements. The measurements and average density are given in Table C-5.

Table C-5: Density filter material

	Density Grauwacke stones [kg/m³]	**Density Basalt [kg/m³]**
Measurement 1	2531.429	2870.476
Measurement 2	2641.667	2863.333
Measurement 3	2581.176	2874.286
Measurement 4	2556.8	2872.5
Measurement 5	2589.524	2964
Measurement 6	2581.429	2785
Measurement 7	2634	3027.619
Measurement 8	2578.333	2698
Measurement 9	2574.286	2903.636
Measurement 10	2644.286	2727.778
Measurement 11	2692.174	2737.6
Measurement 12	2620	3170
Average	**2602.092**	**2874.519**

Grading curve

After obtaining the average density of the filter materials, samples were taken from the big bags to determine a grain size distribution. All stones that are used in the tests are weighed to determine with equation below (C.2) their nominal diameter.

$$d_n = \left(\frac{W}{\rho_f}\right)^{\frac{1}{3}} \tag{C.2}$$

$$d_n = 0.84 \cdot d \tag{C.3}$$

During the tests, 3 types of filter materials are used. The standard filter material is a grading of 45/125 mm of the type Grauwacke. This grading is the smallest that is used to dump on geotextiles. The second type of material is a grading with a range of 40/70 mm. Two tests are carried out with a grading with a d_{f50} which is equal to the standard grading, but with a d_{f15}/d_{f85} ratio of approximately 1.4. This type of filter material can be seen as a narrow grading (Table C-7). The 3 types of filter

material are shown in Table C-6. The indicative grading curve of the filter materials are presented in Figure C-2.

Table C-6: Main properties of filter material

Type	Range	d_{f15} [mm]	d_{f50} [mm]	d_{f85} [mm]	d_{f85}/d_{f15} [-]	d_{fn50} [mm]	ρ_f [kg/m^3]	Total weight [kg]	Total volume [m^3]
CP45/125* (Wide)	45/125 mm	51.20	73.56	108.75	2.12	61.79	2602.09	109.086*	0.0419
40-70 mm	40/70 mm	45.13	54.44	62.38	1.38	45.73	2874.52	114.218*	0.0397
CP45/125* (Narrow)	60-90 mm	62.46	73.21	87.82	1.41	61.50	2602.09	106.675*	0.0410
*Included 2 endoscope stones of basalt with a total weight of 0.9732 kg and a volume of 0.339 dm^3									

Table C-7: Recommended grading widths (Schiereck, 2012)

	$\left(\frac{W_{85}}{W_{15}}\right)^{\frac{1}{3}}$ or d_{85}/d_{15}	W_{85}/W_{15}
Narrow gradation	Less than 1.5	1.7-2.7
Wide gradation	1.5-2.5	2.7-16.0
Very wide gradation	2.5-5.0+	16.0-125+

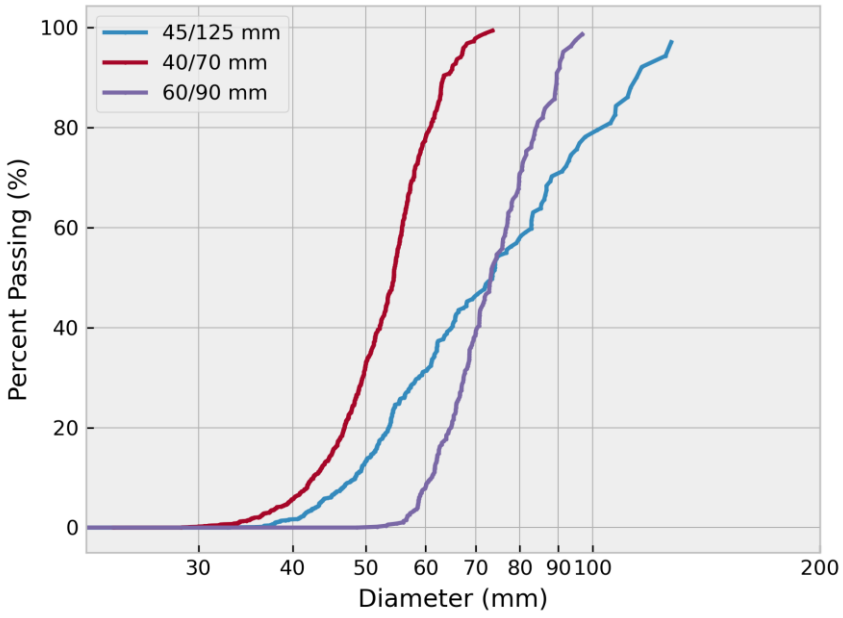

Figure C-2: Grading curve of filter material

C.3.1 Thickness of rubber foam

Volume rubber foam

To determine the volume of the rubber foam, first measure the surface area of the foam rubber on both sides of the flume. This is done by scaling a photo from the side to actual size (see Figure C-3 for an example). Since the length of the glass is 81 cm and the entire filter layer has a length of 100 cm, the surface area is multiplied by a factor of 1.23 (100/81). This is done for both sides of the flume to get an average volume of rubber foam.

Figure C-3: Surface area rubber foam

In the tables below, the average thickness of the rubber foam from the different tests is presented.

Table C-8: Thickness of rubber foam filter material A

Test	Surface area rubber foam right side [cm^2]	Surface area rubber foam left side [cm^2]	Average surface area rubber foam [cm^2]	Volume Rubber foam [m^3]	Average thickness rubber foam [m]
test 1.1	268.259	307.889	288.074	0.011523	0.0288
test 1.3	337.745	339.385	338.565	0.013543	0.0339
test 2.1	317.519	285.617	301.568	0.012063	0.0302
test 2.2	354.185	249.877	302.031	0.012081	0.0302
test 2.3	355.066	323.993	339.530	0.013581	0.0340
test 3.1	330.432	355.395	342.914	0.013717	0.0343
test 3.2	342.358	323.862	333.110	0.013324	0.0333
test 4	360.633	324.510	342.572	0.013703	0.0343
test 10	360.383	283.062	321.722	0.012869	0.0322
test 11	296.358	310.136	303.247	0.01213	0.0303
test 12	222.222	216.123	219.173	0.008767	0.0219

Table C-9: Thickness of rubber foam filter material B

Test	Surface area rubber foam right side [cm^2]	Surface area rubber foam left side [cm^2]	Average surface area rubber foam [cm^2]	Volume Rubber foam [m^3]	Average thickness rubber foam [m]
test 5.1	292.543		292.543	0.011702	0.0293
test 5.2	364.716	228.654	296.685	0.011867	0.0297
test 6	295.716	247.133	271.425	0.010857	0.0271
test 7	293.802	277.864	285.833	0.011433	0.0286

Table C-10: Thickness of rubber foam filter material C

Test	Surface area rubber foam right side [cm^2]	Surface area rubber foam left side [cm^2]	Average surface area rubber foam [cm^2]	Volume Rubber foam [m^3]	Average thickness rubber foam [m]
test 8	351.259	276.185	313.722	0.012549	0.0314
test 9.1	282.852	326.963	304.907	0.012196	0.0305
Test 9.2	358.653	268.140	313.396	0.012536	0.0313

Appendix D Test facility

In this appendix, some technical drawings of the test set-up, including some details of the test set-up are presented.

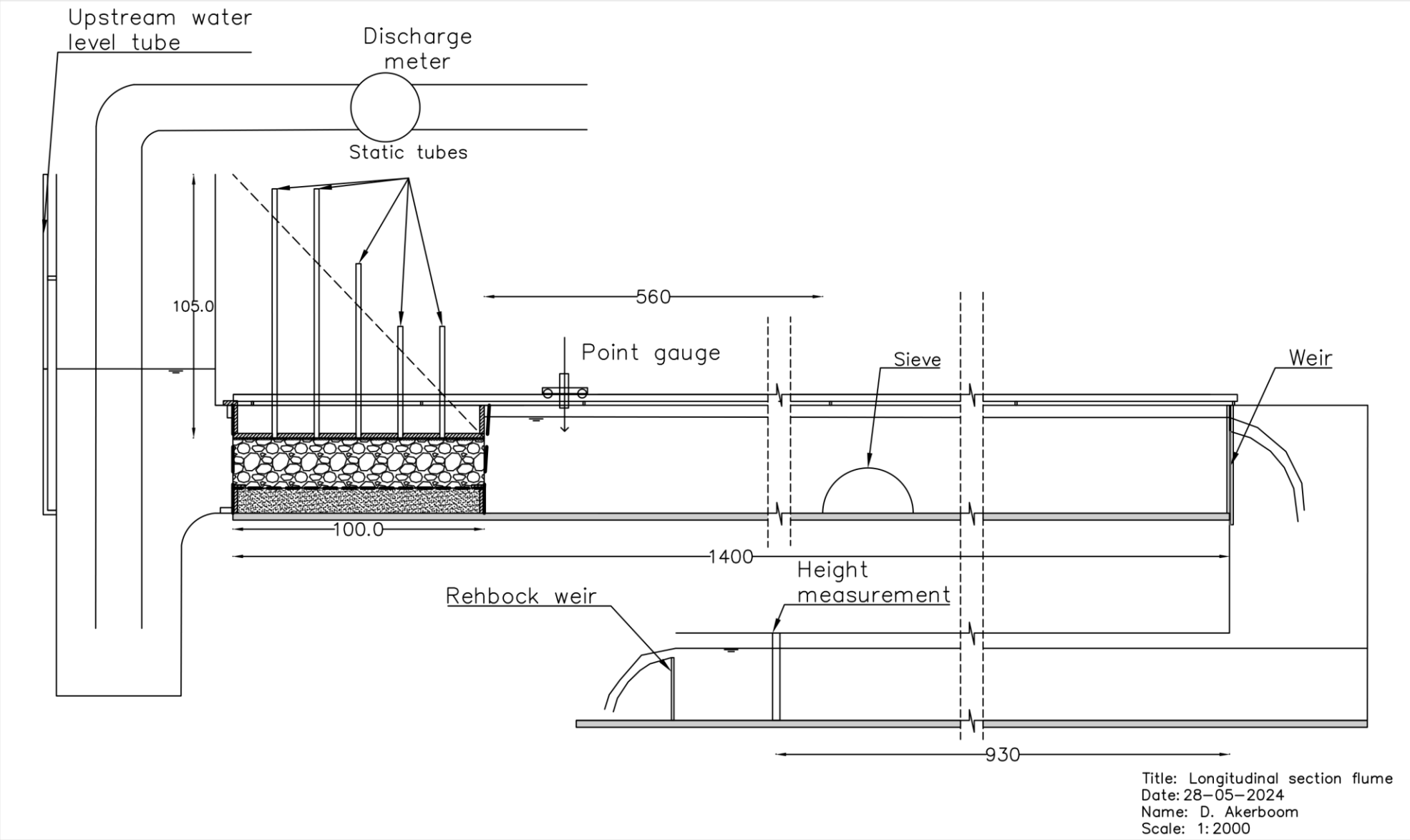

Figure D-1: Longitudinal view flume with test set-up (dimensions in cm)

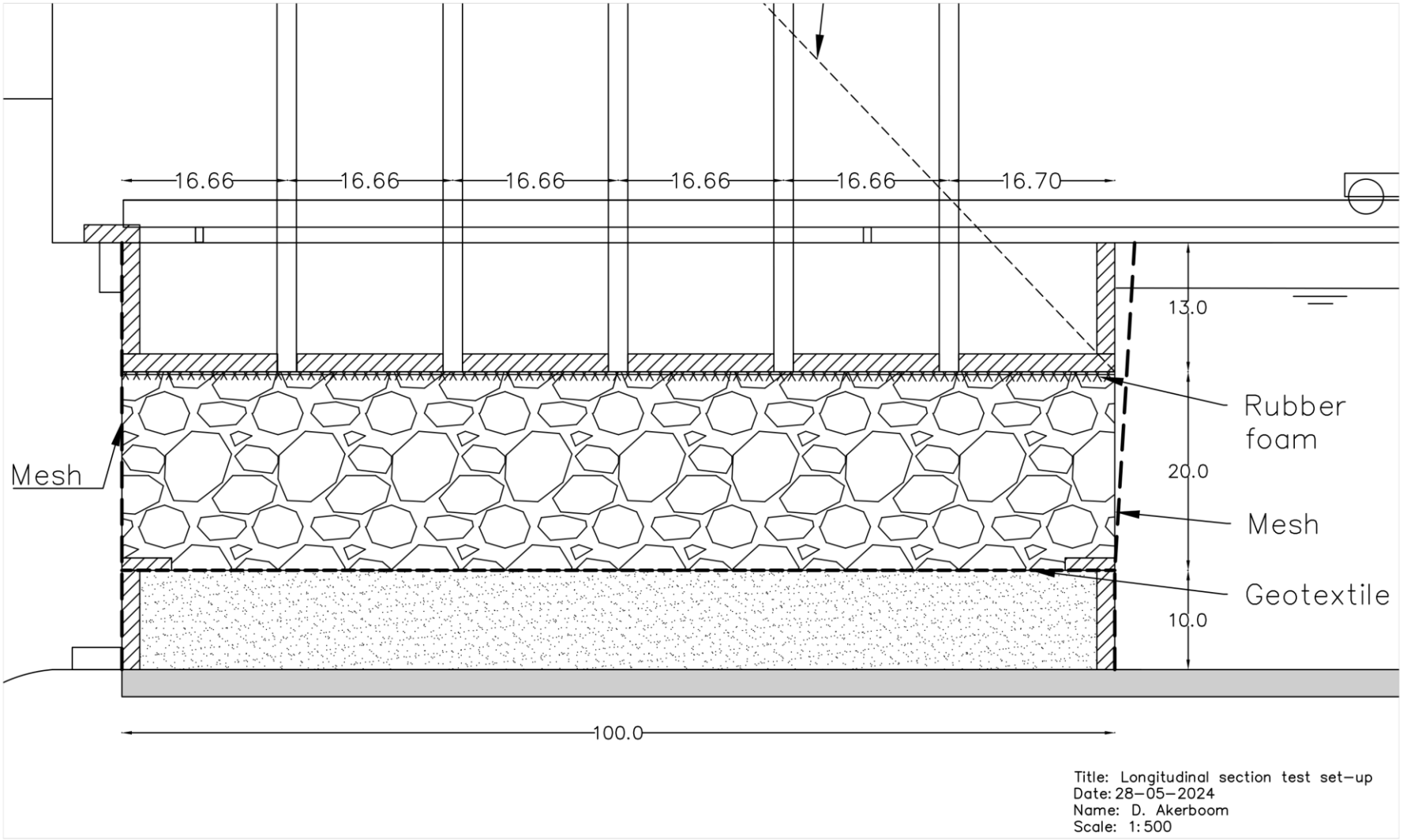

Figure D-2: Longitudinal view test set-up (dimensions in cm)

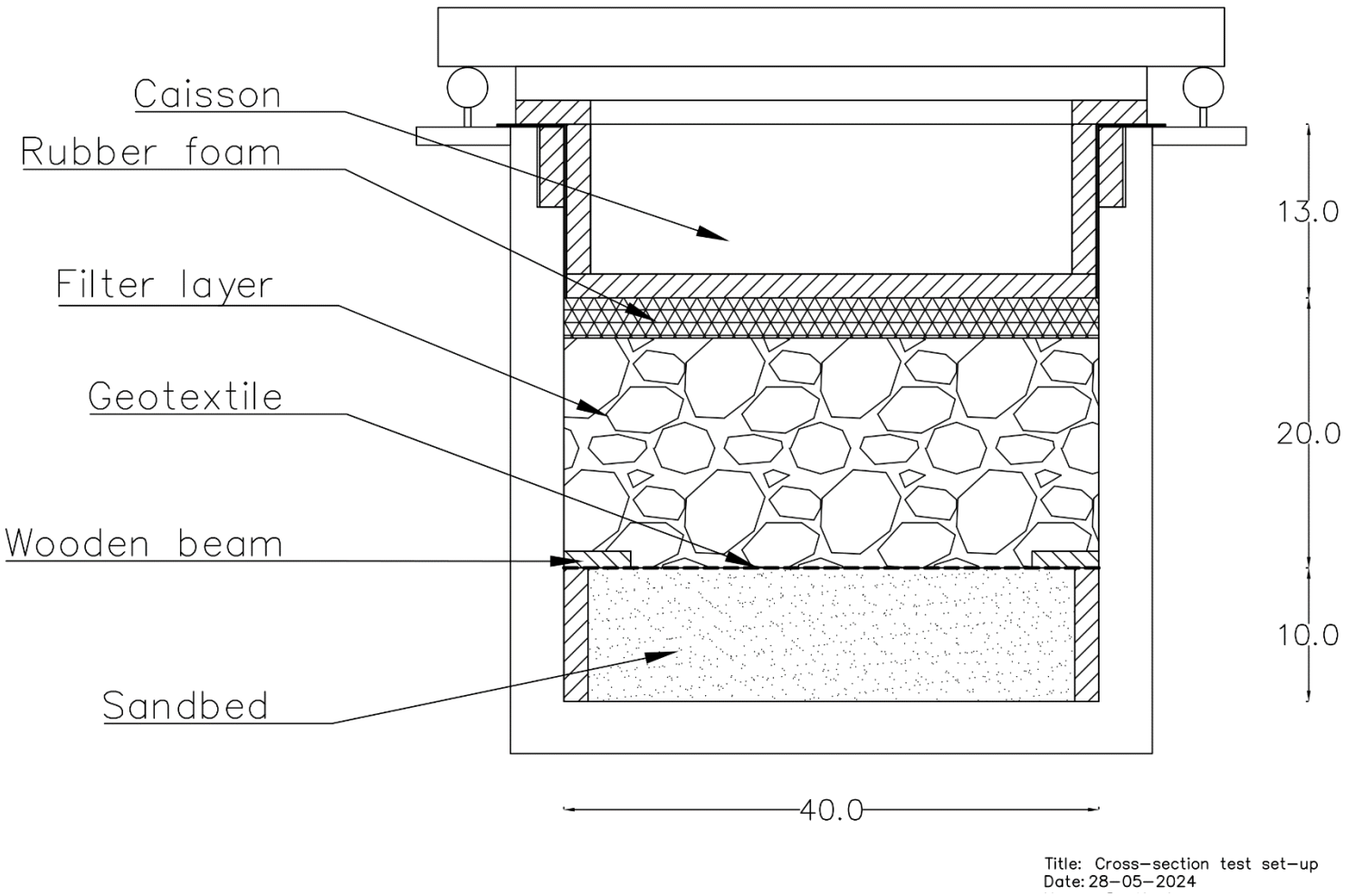

Figure D-3: Cross-section test set-up (dimensions in cm)

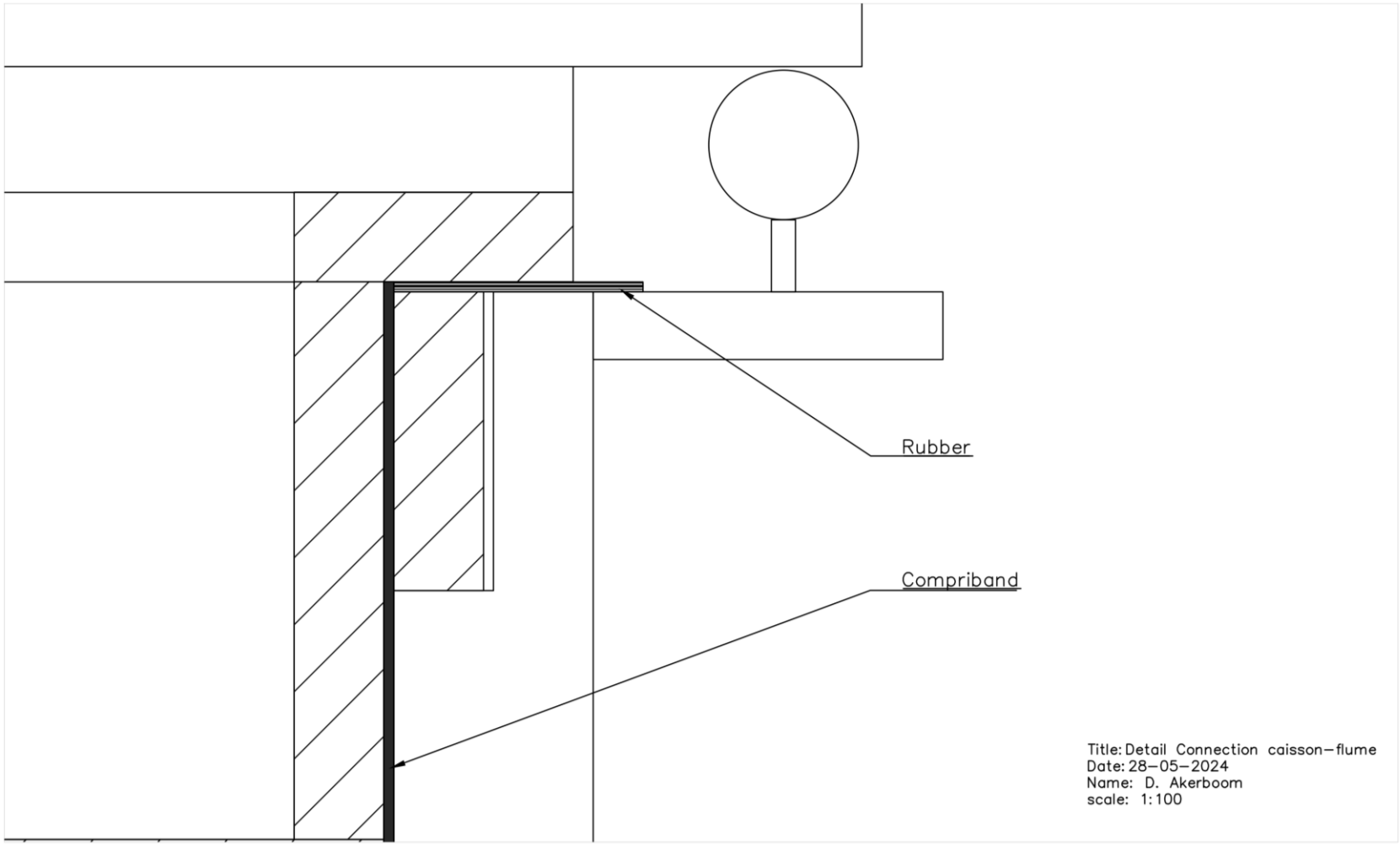

Figure D-4: Detail connection caisson-flume

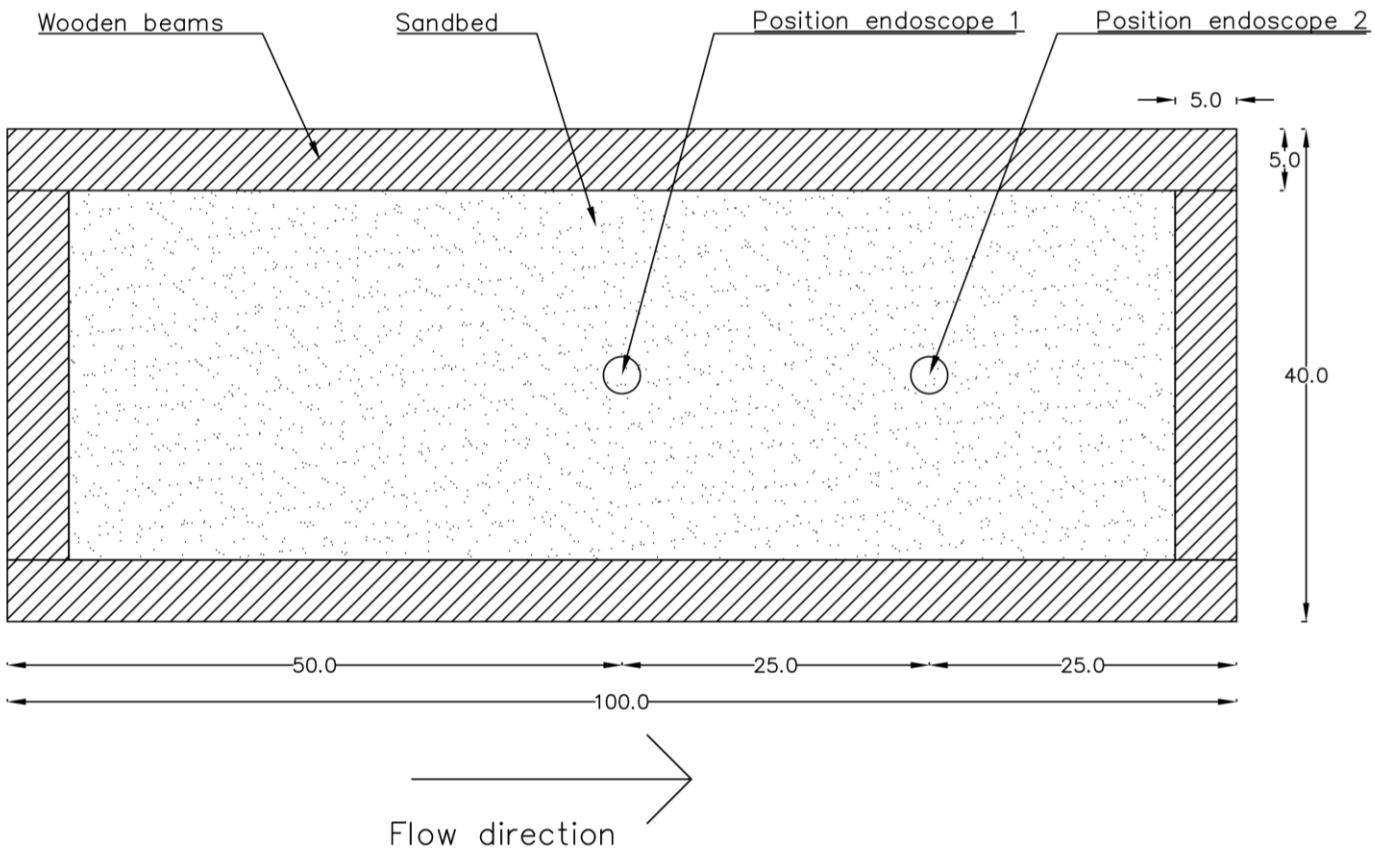

Figure D-5: Top view test set-up (dimensions in cm)

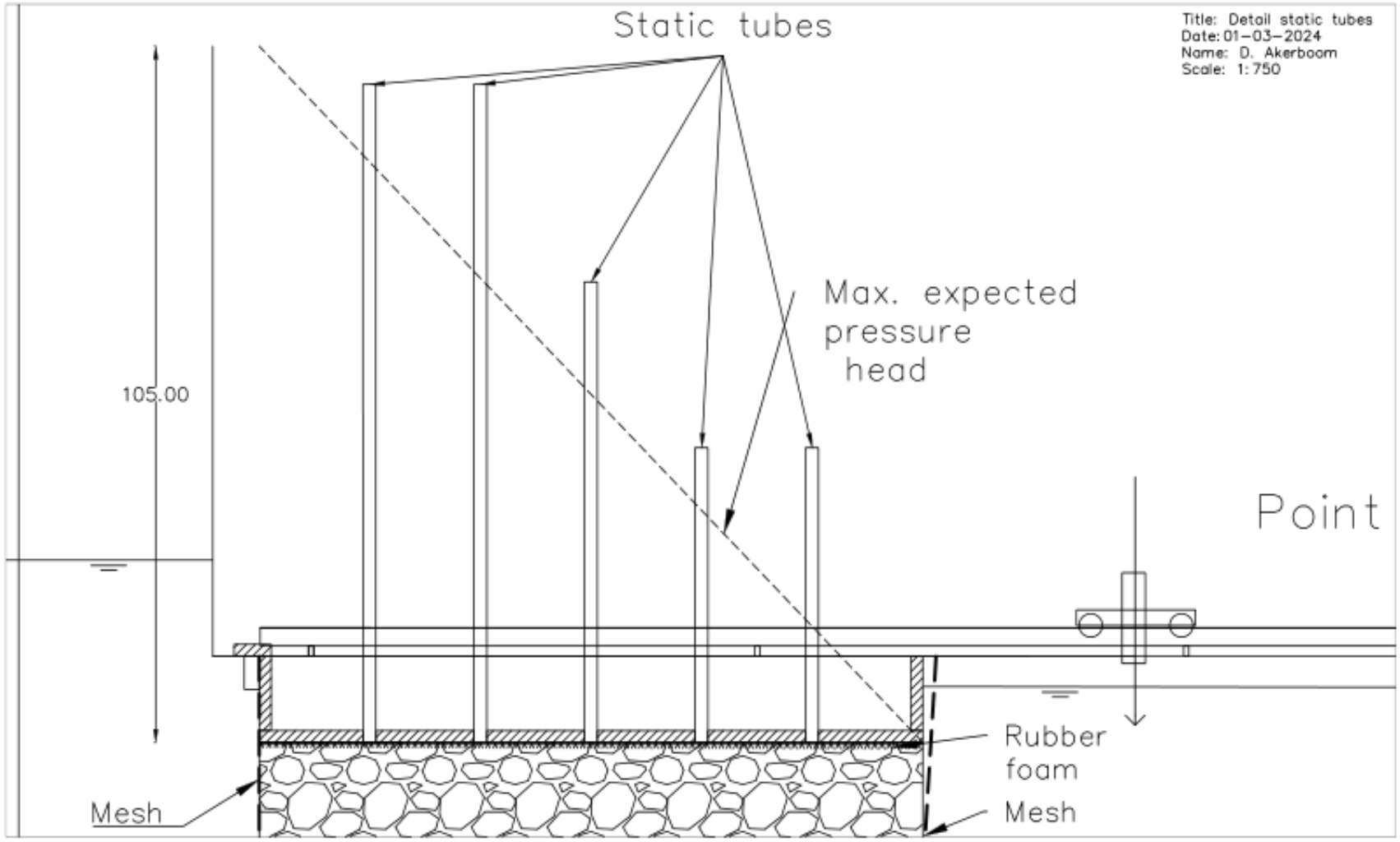

Figure D-6: Detail static tubes (dimensions in cm)

D.1 Test protocol

(a) Smoothen sandbed and if necessary, adding sand

(b) Cutting geotextile to size

(c) Placement of geotextile

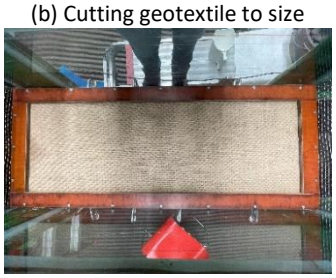

(d) Mounting the wooden slats with screws

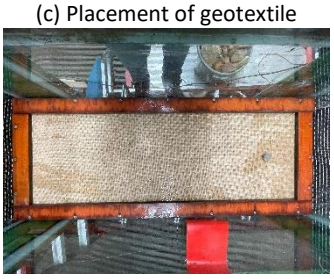

(e) Placement of magnet

(f) Placement of first part filter layer

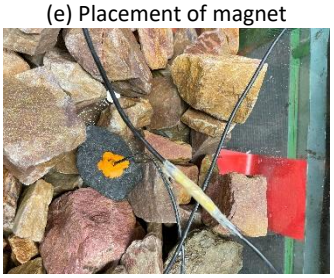

(g) Installing cameras in filter layer

(h) Finishing filter layer

(i) Placement of rubber foam

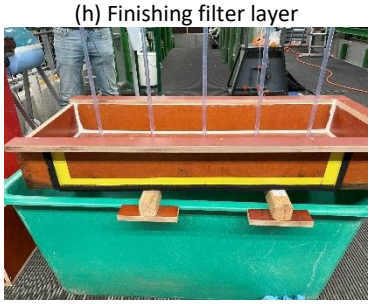

(j) Placement of compriband

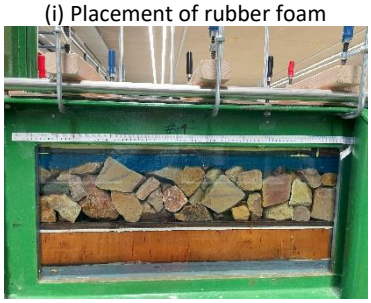

(k) Placing caisson in the flume and pressing with screw clamps

(k) Sieving sand after test

Figure D-7: Setting up the test set-up

Appendix E Calibration figures

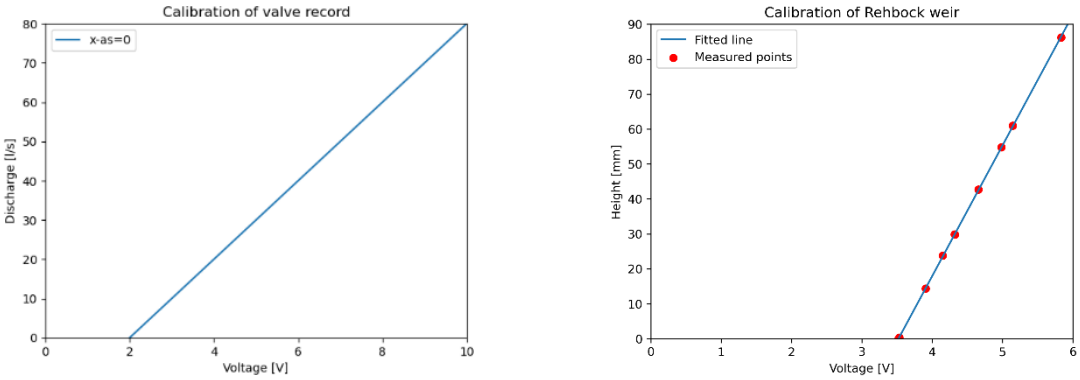

(a) Valve Recorder (b) Rehbock weir

Figure E-1: Calibration graphs discharge

The graph below (Figure E-2) shows the discharge graph created during the calibration test.

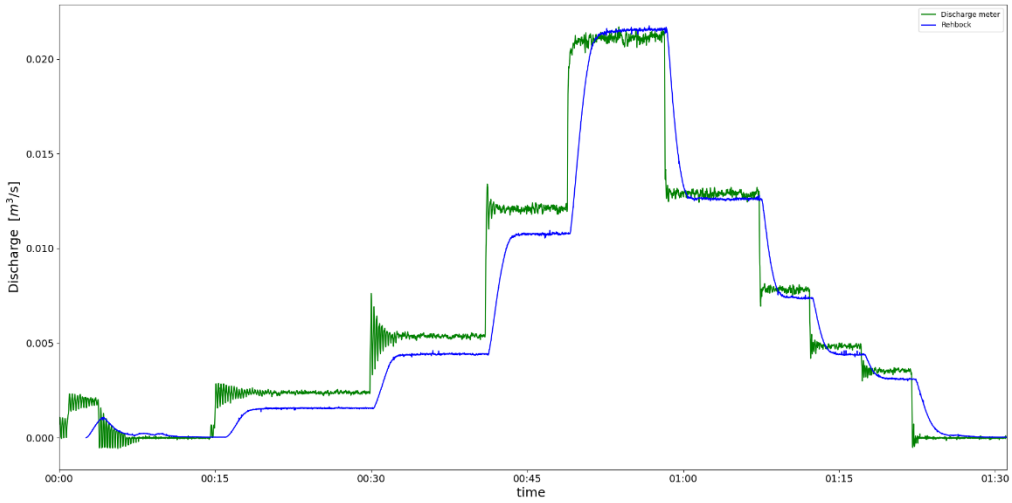

Figure E-2: Discharge graph calibration test

Figure E-3: Calibration test set-up

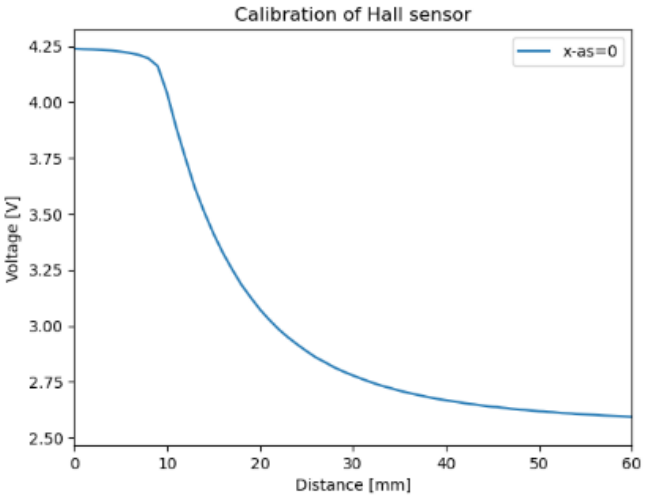

Figure E-4: Calibration of Hall sensor

Appendix F Results model tests

This appendix presents additional results of the tests.

F.1 Overview hydraulic condition results and sediment transport results per test

All results of the hydraulic conditions and sediment transport results per test are shown in the tables below.

Table F-1: Summary of test results of T1.1

Test	Geotextile			Filter	Step	Duration	Q	i	u_f	Erosion state	W	S
	Nr.	Type	O_{90}/d_{b90}	range		[s]	[m³/s]	[-]	[m/s]		[gr]	[gr/s/m²]
T1.1	J4	W	2.13	45/125 mm	1	600	0.0014	0.03	0.0240	Non-erosion	-	-
					2	716	0.0021	0.06	0.0357	Non-erosion		
					3	952	0.0028	0.10	0.0488	Non-erosion		
					4	1038	0.0043	0.15	0.0734	Non-erosion		
					5	832	0.0048	0.19	0.0827	Non-erosion		
					6	800	0.0056	0.24	0.0954	Non-erosion		
					7	1632	0.0062	0.29	0.1062	Steady		
					8	724	0.0065	0.32	0.1115	Steady		
					9	860	0.0071	0.38	0.1225	Steady		
					10	990	0.0076	0.42	0.1299	Failure		
					11	984	0.0081	0.48	0.1398	Failure		
					12	804	0.0086	0.52	0.1471	Failure		
					13	1138	0.0090	0.58	0.1552	Failure		
					14	954	0.0094	0.62	0.1613	Failure		
					15	1794	0.0096	0.65	0.1653	Failure		
					16	3562	0.0101	0.70	0.1729	Failure		
					Total						159	

Table F-2: Summary of test results of T1.2

Test	Geotextile			Filter	Step	Duration	Q	i	u_f	Erosion state	W	S
	Nr.	Type	O_{90}/d_{b90}	range		[s]	[m³/s]	[-]	[m/s]		[gr]	[gr/s/m²]
T1.2	J4	W	2.13	45/125 mm	1	906	0.0046	0.13	0.0797	Non-erosion	-	-
					2	914	0.0059	0.21	0.1014	Steady		
					3	1048	0.0066	0.25	0.1136	Failure		
					4	1092	0.0073	0.30	0.1249	Failure		
					5	1438	0.0082	0.37	0.1403	Failure		
					6	1666	0.0088	0.42	0.1519	Failure		
					7	2334	0.0092	0.46	0.1585	Failure		
					8	2198	0.0100	0.53	0.1719	Failure		
					9	1866	0.0110	0.63	0.1886	Failure		
					10	1788	0.0115	0.68	0.1979	Failure		
					Total						601	

Table F-3: Summary of test results of T1.3

Test	Geotextile			Filter	Step	Duration	Q	i	u_f	Erosion state	W	S
	Nr.	Type	O_{90}/d_{90}	range		[s]	[m³/s]	[-]	[m/s]		[gr]	[gr/s/m²]
T1.3	J4	W	2.13	45/125 mm	1	1884	0.0043	0.11	0.0731	Non-erosion	2	0.003932
					2	1748	0.0057	0.19	0.0983	Steady	1.4	0.002966
					3	1916	0.0067	0.25	0.1147	Failure	5.8	0.011212
					4	1941	0.0074	0.31	0.1280	Failure	26.4	0.050375
					5	1824	0.0083	0.37	0.1429	Failure	33.4	0.06782
					6	2060	0.0090	0.43	0.1542	Failure	79.2	0.142395
					7	2183	0.0095	0.48	0.1639	Failure	95	0.161178
					8	1796	0.0102	0.54	0.1755	Failure	264.4	0.545245
					9	2027	0.0109	0.62	0.1871	Failure	213	0.38919
					10	1315	0.0116	0.68	0.1986	Failure	187.2	0.52725
					Total						907.8	

Table F-4: summary of test results of T2.1

Test	Geotextile			Filter	Step	Duration	Q	i	u_f	Erosion state	W	S
	Nr.	Type	O_{90}/d_{90}	range		[s]	[m³/s]	[-]	[m/s]		[gr]	[gr/s/m²]
T2.1	J5	W	3.38	45/125 mm	1	972	0.0021	0.05	0.0312	Non-erosion	-	-
					2	910	0.0045	0.13	0.0688	Non-erosion		
					3	1080	0.0056	0.19	0.0852			
					4	1122	0.0071	0.28	0.1081			
					5	2178	0.0077	0.33	0.1169			
					6	1430	0.0083	0.38	0.1262			
					7	672	0.0090	0.44	0.1368			
					8	1266	0.0096	0.49	0.1462	Failure		
					9	776	0.0103	0.55	0.1556	Failure		
					10	746	0.0109	0.61	0.1650	Failure		
					11	2164	0.0113	0.65	0.1708	Failure		
					12	658	0.0113	0.66	0.1716	Failure		
					13	748	0.0122	0.75	0.1842	Failure		
					14	730	0.0125	0.78	0.1899	Failure		
					15	1056	0.0129	0.82	0.1950	Failure		
					16	784	0.0133	0.87	0.2016	Failure		
					17	1376	0.0138	0.93	0.2092	Failure		
					18	532	0.0138	0.94	0.2098	Failure		
					19	2692	0.0142	0.98	0.2147	Failure		
					20	790	0.0144	1.00	0.2176	Failure		
					Total						124	

Table F-5: Summary of test results of T2.2

Test	Geotextile			Filter	Step	Duration	Q	i	u_f	Erosion state	W	S
	Nr.	Type	O_{90}/d_{90}	range		[s]	[m³/s]	[-]	[m/s]		[gr]	[gr/s/m²]
T2.2	J5	W	3.38	45/125 mm	1	1020	0.0036	0.09	0.0627	Non-erosion	-	-
					2	684	0.0055	0.19	0.0940	Non-erosion		
					3	1154	0.0065	0.26	0.1127	Non-erosion		
					4	1980	0.0073	0.31	0.1258	Steady		
					5	786	0.0086	0.42	0.1476	Failure		
					6	1070	0.0096	0.52	0.1658	Failure		
					7	1560	0.0103	0.58	0.1779	Failure		
					8	1178	0.0108	0.63	0.1860	Failure		
					9	1680	0.0115	0.71	0.1976	Failure		
					10	1502	0.0122	0.78	0.2095	Failure		
					11	1110	0.0127	0.85	0.2195	Failure		
					12	880	0.0132	0.90	0.2266	Failure		
					13	1186	0.0135	0.95	0.2330	Failure		
					14	216	0.0136	0.97	0.2345	Failure		
					15	1080	0.0138	0.99	0.2381	Failure		
					Total						154	

Table F-6: Summary of test results of T2.3

Test	Geotextile			Filter	Step	Duration	Q	i	u_f	Erosion state	W	S
	Nr.	Type	O_{90}/d_{90}	range		[s]	[m³/s]	[-]	[m/s]		[gr]	[gr/s/m²]
T2.3	J5	W	3.38	45/125 mm	1	2050	0.0039	0.09	0.0670	Non-erosion	1.2	0.0022
					2	1720	0.0057	0.18	0.0982	Non-erosion	0.6	0.0013
					3	2306	0.0069	0.26	0.1183	Non-erosion	0.2	0.0003
					4	1632	0.0076	0.31	0.1316	Steady	1	0.0023
					5	2227	0.0090	0.42	0.1558	Steady	5.8	0.0096
					6	2103	0.0101	0.51	0.1734	Failure	15.8	0.0278
					7	2065	0.0107	0.58	0.1849	Failure	22	0.0395
					8	1919	0.0111	0.62	0.1918	Failure	15.8	0.0305
					9	1738	0.0120	0.71	0.2070	Failure	32.8	0.0699
					10	1631	0.0127	0.78	0.2180	Failure	29.2	0.0663
					11	1886	0.0133	0.86	0.2292	Failure	40.2	0.0789
					12	1046	0.0136	0.90	0.2347	Failure	26.8	0.0949
					Total						191.4	

Table F-7: Summary of test results of T3.1

Test	Geotextile			Filter	Step	Duration	Q	i	u_f	Erosion state	W	S
	Nr.	Type	O_{90}/d_{90}	range		[s]	[m³/s]	[-]	[m/s]		[gr]	[gr/s/m²]
T3.1	J7	W		45/125 mm	1	780	0.0019	0.04	0.0326	Non-erosion	-	-
					2	774	0.0043	0.12	0.0735	Non-erosion		
					3	992	0.0059	0.21	0.1014	Non-erosion		
					4	662	0.0072	0.30	0.1236	Failure		
					5	852	0.0085	0.41	0.1458	Failure		
					6	744	0.0094	0.49	0.1629	Failure		
					7	946	0.0100	0.55	0.1730	Failure		
					8	1630	0.0108	0.62	0.1860	Failure		
					9	1200	0.0113	0.68	0.1951	Failure		
					10	1172	0.0119	0.74	0.2047	Failure		
					11	916	0.0125	0.81	0.2150	Failure		
					12	1108	0.0129	0.86	0.2224	Failure		
					13	1102	0.0132	0.90	0.2284	Failure		
					14	3532	0.0136	0.95	0.2342	Failure		
					Total						459	

Table F-8: Summary of test results of T3.2

Test	Geotextile			Filter	Step	Duration	Q	i	u_f	Erosion state	W	S
	Nr.	Type	O_{90}/d_{90}	range		[s]	[m³/s]	[-]	[m/s]		[gr]	[gr/s/m²]
T3.2	J7	W		45/125 mm	1	1611	0.0022	0.04	0.0383	Non-erosion	0.6	0.001379
					2	1786	0.0043	0.12	0.0739	Non-erosion	1	0.002074
					3	1772	0.0059	0.21	0.1020	Non-erosion	0.6	0.001254
					4	2181	0.0073	0.30	0.1258	Steady	2.4	0.004076
					5	1887	0.0085	0.40	0.1467	Steady	10.2	0.02002
					6	1902	0.0095	0.50	0.1646	Failure	17.6	0.034272
					7	2121	0.0100	0.54	0.1725	Failure	28.8	0.050291
					8	1976	0.0107	0.61	0.1843	Failure	44	0.082471
					9	1999	0.0113	0.68	0.1950	Failure	61	0.113019
					10	2029	0.0118	0.74	0.2042	Failure	75.6	0.137999
					11	1528	0.0124	0.81	0.2141	Failure	73.8	0.178883
					Total						315.6	

Table F-9: Summary of test results of T4

Test	Geotextile			Filter	Step	Duration	Q	i	u_f	Erosion state	W	S
	Nr.	Type	O_{90}/d_{90}	range		[s]	[m³/s]	[-]	[m/s]		[gr]	[gr/s/m²]
T4	J9	W		45/125 mm	1	1411	0.0026	0.05	0.0442	Non-erosion		
					2	1444	0.0047	0.14	0.0809	Non-erosion		
					3	1241	0.0064	0.24	0.1111	Non-erosion		
					4	1256	0.0076	0.33	0.1318	Non-erosion		
					5	1345	0.0088	0.43	0.1521	Non-erosion		
					6	1641	0.0099	0.53	0.1710	Non-erosion		
					7	1202	0.0110	0.64	0.1898	Non-erosion		
					8	1109	0.0118	0.72	0.2039	Non-erosion		
					9	1079	0.0129	0.85	0.2228	Non-erosion		
					10	1549	0.0137	0.95	0.2368	Non-erosion		
					Total						14.8	

Table F-10: Summary of test results of T5.1

Test	Geotextile			Filter	Step	Duration	Q	i	u_f	Erosion state	W	S
	Nr.	Type	O_{90}/d_{90}	range		[s]	[m³/s]	[-]	[m/s]		[gr]	[gr/s/m²]
T5.1	J4	W	2.13	40/70mm	1	900	0.0015	0.03	0.0255	Non-erosion	-	-
					2	900	0.0025	0.08	0.0438	Non-erosion		
					3	1200	0.0039	0.12	0.0669	Non-erosion		
					4	1200	0.0047	0.17	0.0813	Non-erosion		
					5	1500	0.0055	0.21	0.0941			
					6	1200	0.0060	0.25	0.1039			
					7	1200	0.0067	0.30	0.1144			
					8	2100	0.0073	0.35	0.1248			
					9	900	0.0078	0.40	0.1346	Failure		
					10	1200	0.0083	0.44	0.1424	Failure		
					11	900	0.0089	0.50	0.1522	Failure		
					12	900	0.0092	0.54	0.1589	Failure		
					13	1200	0.0102	0.64	0.1760	Failure		
					14	1080	0.0106	0.69	0.1830	Failure		
					15	720	0.0111	0.74	0.1902	Failure		
					Total						134	

Table F-11: Summary of test results of T5.2

Test	Geotextile			Filter	Step	Duration	Q	i	u_f	Erosion state	W	S
	Nr.	Type	O_{90}/d_{90}	range		[s]	[m³/s]	[-]	[m/s]		[gr]	[gr/s/m²]
T5.2	J4	W	2.13	40/70mm	1	644	0.0030	0.09	0.0520	Non-erosion	-	-
					2	668	0.0052	0.17	0.0900	Non-erosion		
					3	1196	0.0068	0.27	0.1164	Failure		
					4	1664	0.0074	0.32	0.1274	Failure		
					5	2312	0.0082	0.38	0.1404	Failure		
					6	1562	0.0086	0.42	0.1485	Failure		
					7	1766	0.0094	0.48	0.1612	Failure		
					8	1530	0.0097	0.51	0.1669	Failure		
					9	1288	0.0100	0.54	0.1722	Failure		
					10	2722	0.0104	0.58	0.1785	Failure		
					Total						195	

Table F-12: Summary of test results of T6

Test	Geotextile			Filter	Step	Duration	Q	i	u_f	Erosion state	W	S
	Nr.	Type	O_{90}/d_{90}	range		[s]	[m³/s]	[-]	[m/s]		[gr]	[gr/s/m²]
T6	J5	W	3.38	40/70mm	1	900	0.0007	0.01	0.0123	Non-erosion	-	-
					2	1140	0.0015	0.03	0.0253	Non-erosion		
					3	1080	0.0022	0.06	0.0373	Non-erosion		
					4	1020	0.0033	0.10	0.0561	Non-erosion		
					5	1020	0.0041	0.14	0.0700	Non-erosion		
					6	1200	0.0048	0.19	0.0826	Non-erosion		
					7	1020	0.0055	0.24	0.0955	Non-erosion		
					8	1200	0.0061	0.29	0.1049			
					9	1080	0.0065	0.33	0.1121			
					10	1140	0.0071	0.38	0.1220			
					11	900	0.0076	0.42	0.1304			
					12	1080	0.0080	0.47	0.1381			
					13	960	0.0086	0.53	0.1478			
					14	1020	0.0089	0.42	0.1309			
					15	1740	0.0094	0.62	0.1621			
					16	1620	0.0098	0.66	0.1690			
					17	1680	0.0101	0.70	0.1744			
					18	2100	0.0106	0.75	0.1822			
					19	1920	0.0109	0.79	0.1870			
					20	3054	0.0111	0.81	0.1906			
					21	1730	0.0115	0.87	0.1978			
					22	1368	0.0118	0.91	0.2030			
					23	600	0.0118	0.91	0.2030			
					24	2484	0.0122	0.98	0.2110			
					Total						76	

Table F-13: Summary of test results of T7

Test	Geotextile			Filter	Step	Duration	Q	i	u_f	Erosion state	W	S
	Nr.	Type	O_{90}/d_{90}	range		[s]	[m³/s]	[-]	[m/s]		[gr]	[gr/s/m²]
T7	-	-	-	40/70mm	1	710	0.0004	0.005	0.0066	Non-erosion	-	-
					2	858	0.0009	0.015	0.0144	Non-erosion		
					3	558	0.0011	0.021	0.0174	Steady		
					4	3708	0.0014	0.030	0.0230	Failure		
					Total						1656	

Table F-14: Summary of test results of T8

Test	Geotextile			Filter	Step	Duration	Q	i	u_f	Erosion state	W	S
	Nr.	Type	O_{90}/d_{90}	range		[s]	[m³/s]	[-]	[m/s]		[gr]	[gr/s/m²]
T8	J4	W	2.13	60/90mm	1	1242	0.0039	0.08	0.0663	Non-erosion	-	-
					2	826	0.0056	0.14	0.0971	Non-erosion		
					3	832	0.0071	0.22	0.1225	Failure		
					4	616	0.0080	0.26	0.1371	Failure		
					5	986	0.0087	0.31	0.1504	Failure		
					6	4482	0.0095	0.36	0.1636	Failure		
					7	1902	0.0107	0.45	0.1837	Failure		
					8	1526	0.0113	0.49	0.1942	Failure		
					9	1676	0.0121	0.56	0.2080	Failure		
					10	1312	0.0129	0.63	0.2219	Failure		
					11	1726	0.0136	0.69	0.2343	Failure		
					Total						585	

Table F-15: Summary of test results of T9.1

Test	Geotextile			Filter	Step	Duration	Q	i	u_f	Erosion state	W	S
	Nr.	Type	O_{90}/d_{90}	range		[s]	[m³/s]	[-]	[m/s]		[gr]	[gr/s/m²]
T9.1	J5	W	3.38	60/90mm	1	654	0.0054	0.13	0.0924		-	-
					2	716	0.0067	0.19	0.1157			
					3	706	0.0081	0.26	0.1393			
					4	796	0.0089	0.31	0.1532			
					5	1006	0.0101	0.40	0.1748			
					6	874	0.0110	0.46	0.1896			
					7	722	0.0116	0.51	0.2004			
					8	890	0.0123	0.57	0.2116			
					9	930	0.0129	0.62	0.2225			
					10	1266	0.0138	0.70	0.2376			
					11	1530	0.0145	0.77	0.2504			
					12	694	0.0147	0.79	0.2535			
					13	544	0.0148	0.80	0.2543			
					14	832	0.0153	0.85	0.2636			
					15	740	0.0159	0.91	0.2733			
					16	3404	0.0164	0.96	0.2823			
					Total						171	

Table F-16: Summary of test results of T9.2

Test	Geotextile			Filter	Step	Duration	Q	i	u_f	Erosion state	W	S
	Nr.	Type	O_{90}/d_{90}	range		[s]	[m³/s]	[-]	[m/s]		[gr]	[gr/s/m²]
T9.2	J5	W	3.38	60/90mm	1	2069	0.0047	0.11	0.0808	Non-erosion	1.4	0.0025
					2	1969	0.0061	0.17	0.1054	Non-erosion	0.4	0.0008
					3	1841	0.0076	0.26	0.1315	Steady	0.8	0.0016
					4	1832	0.0085	0.31	0.1465	Steady	3.2	0.0065
					5	1886	0.0097	0.40	0.1664	Failure	8.8	0.0173
					6	1846	0.0106	0.46	0.1826	Failure	19	0.0381
					7	1856	0.0111	0.50	0.1911	Failure	26.4	0.0527
					8	1847	0.0117	0.57	0.2023	Failure	25.2	0.0505
					9	1768	0.0125	0.62	0.2146	Failure	35	0.0733
					10	1288	0.0133	0.70	0.2290	Failure	31	0.0891
					Total						151.2	

Table F-17: Summary of test results of T10

Test	Geotextile			Filter	Step	Duration	Q	i	u_f	Erosion state	W	S
	Nr.	Type	O_{90}/d_{90}	range		[s]	[m³/s]	[-]	[m/s]		[gr]	[gr/s/m²]
T10	Hemp on jute	NW	-	45/125 mm	1	958	0.0027	0.07	0.0474	Non-erosion	-	-
					2	720	0.0040	0.11	0.0697	Non-erosion		
					3	694	0.0046	0.14	0.0796	Non-erosion		
					4	604	0.0055	0.19	0.0949	Non-erosion		
					5	640	0.0066	0.26	0.1140	Non-erosion		
					6	820	0.0081	0.37	0.1395	Non-erosion		
					7	830	0.0089	0.44	0.1538	Non-erosion		
					8	700	0.0102	0.56	0.1770	Non-erosion		
					9	1094	0.0112	0.67	0.1939	Non-erosion		
					10	1046	0.0118	0.74	0.2047	Non-erosion		
					11	996	0.0124	0.81	0.2151	Non-erosion		
					12	604	0.0128	0.86	0.2219	Non-erosion		
					13	960	0.0134	0.92	0.2314	Non-erosion		
					14	384	0.0134	0.93	0.2327	Non-erosion		
					15	2756	0.0138	0.98	0.2385	Non-erosion		
					Total						17	

Table F-18: Summary of test results of T11

Test	Geotextile			Filter	Step	Duration	Q	i	u_f	Erosion state	W	S
	Nr.	Type	O_{90}/d_{90}	range		[s]	[m³/s]	[-]	[m/s]		[gr]	[gr/s/m²]
T11	Jute on jute	NW	-	45/125 mm	1	530	0.0042	0.11	0.0725	Non-erosion	-	-
					2	2112	0.0068	0.26	0.1187	Non-erosion		
					3	790	0.0078	0.33	0.1365	Non-erosion		
					4	934	0.0089	0.42	0.1553	Non-erosion		
					5	872	0.0101	0.53	0.1768	Non-erosion		
					6	914	0.0116	0.68	0.2026	Non-erosion		
					7	920	0.0122	0.73	0.2117	Non-erosion		
					8	786	0.0128	0.80	0.2228	Non-erosion		
					9	1520	0.0137	0.92	0.2395	Non-erosion		
					10	520	0.0139	0.93	0.2414	Non-erosion		
					11	1086	0.0143	0.98	0.2491	Non-erosion		
					Total						7	

Table F-19: Summary of test results of T12

Test	Geotextile			Filter	Step	Duration	Q	i	u_f	Erosion state	W	S
	Nr.	Type	O_{90}/d_{90}	range		[s]	[m³/s]	[-]	[m/s]		[gr]	[gr/s/m²]
T12	Wool on jute	NW	-	45/125 mm	1	876	0.0036	0.09	0.0627	Non-erosion	-	-
					2	606	0.0052	0.16	0.0908	Non-erosion		
					3	944	0.0065	0.24	0.1121	Non-erosion		
					4	996	0.0087	0.40	0.1511	Non-erosion		
					5	1060	0.0101	0.52	0.1748	Non-erosion		
					6	1028	0.0106	0.56	0.1831	Non-erosion		
					7	1458	0.0114	0.65	0.1970	Non-erosion		
					8	994	0.0119	0.70	0.2063	Non-erosion		
					9	928	0.0125	0.77	0.2166	Non-erosion		
					10	1084	0.0133	0.86	0.2307	Non-erosion		
					11	678	0.0139	0.93	0.2405	Non-erosion		
					12	770	0.0140	0.94	0.2421	Non-erosion		
					13	2908	0.0144	0.99	0.2490	Non-erosion		
					Total						10	

F.2 Overview of Forchheimer coefficients per test

The table below shows the alpha and beta value of the Forchheimer equation for the various tests.

Table F-20: Forchheimer coefficients per test with different rubber foam heights

Test				h_{RF}= 2 cm			h_{RF}= 3 cm			h_{RF}= 4 cm		
	coefficient a [s/m]	coefficient b [s²/m²]	d_{fn50} [m]	Porosity [-]	Alpha value [-]	Beta value [-]	Porosity [-]	Alpha value [-]	Beta value [-]	Porosity [-]	Alpha value [-]	Beta value [-]
Test 1.1	0.760	18.964	0.06232	0.374	3548.05	0.97	0.359	2992.89	0.84	0.352	2760.59	0.78
Test 1.2	0.551	14.635	0.06179	0.425	4396.19	1.18	0.412	3829.85	1.06	0.405	3552.84	0.99
Test 1.3	0.500	14.814	0.06179	0.425	3990.21	1.20	0.412	3476.18	1.07	0.405	3224.75	1.00
Test 2.1	0.748	17.746	0.06228	0.412	5284.86	1.29	0.398	4545.19	1.14	0.391	4211.06	1.06
Test 2.2	0.612	14.915	0.06179	0.425	4878.99	1.21	0.412	4250.46	1.08	0.405	3943.03	1.01
Test 2.3	0.503	14.160	0.06179	0.425	4011.21	1.15	0.412	3494.47	1.02	0.405	3241.72	0.96
Test 3.1	0.656	14.463	0.06179	0.425	5232.46	1.17	0.412	4558.39	1.04	0.405	4228.69	0.98
Test 3.2	0.446	15.553	0.06179	0.425	3556.52	1.26	0.412	3098.36	1.12	0.405	2874.26	1.05
Test 4	0.582	14.496	0.06179	0.425	4643.03	1.17	0.412	4044.90	1.05	0.405	3752.33	0.98
Test 5.1	0.697	16.872	0.04573	0.46	4466.70	1.37	0.453	4157.39	1.29	0.453	4157.39	1.29
Test 5.2	0.656	14.480	0.04573	0.46	4120.63	1.17	0.453	3835.29	1.10	0.453	3835.29	1.10
Test 6	0.936	17.534	0.04573	0.46	5882.41	1.42	0.453	5475.06	1.34	0.453	5475.06	1.34
Test 7	0.619	30.167	0.04573	0.46	3728.99	2.54	0.453	3470.77	2.39	0.453	3470.77	2.39
Test 8	0.453	10.709	0.0615	0.437	4056.30	0.96	0.424	3539.60	0.86	0.418	3321.89	0.81
Test 9.1	0.433	10.537	0.0615	0.437	3882.13	0.94	0.424	3387.62	0.84	0.418	3179.25	0.80
Test 9.2	0.472	11.314	0.0615	0.437	4231.07	1.01	0.424	3692.11	0.90	0.418	3465.02	0.86
Test 10	0.588	14.723	0.06179	0.425	4687.55	1.19	0.412	4083.68	1.06	0.405	3788.31	1.00
Test 11	0.618	13.405	0.06179	0.425	4926.71	1.08	0.412	4292.03	0.97	0.405	3981.60	0.91
Test 12	0.552	13.768	0.06179	0.425	4405.64	1.11	0.412	3838.09	0.99	0.405	3560.49	0.93

F.3 Test 1.1

Table F-21: Data test 1.1

Base material (d_{b50})	0.180 (M34)	[mm]
Geotextile	J4	
Filter material	45/125 mm	
d_{fn50}	62.32	[mm]
Weight of stones	118.71	[kg]

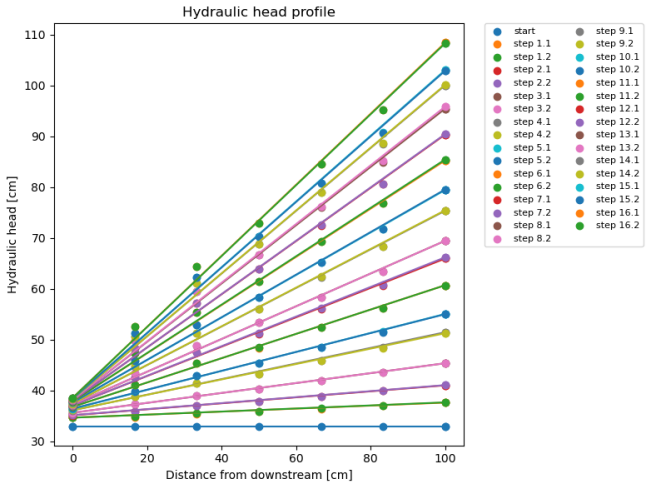

Figure F-1: Hydraulic head profile test 1.1

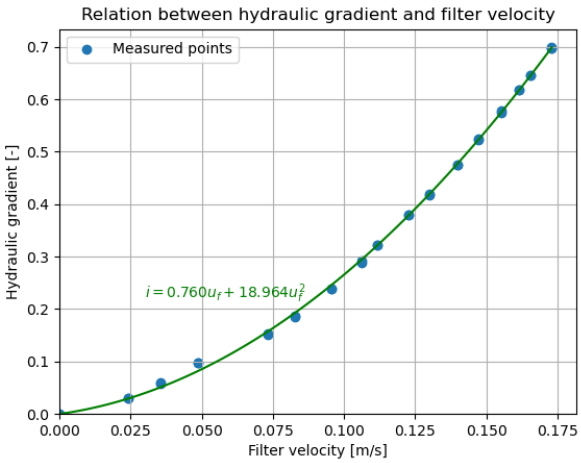

Figure F-2: Forchheimer relation test 1.1

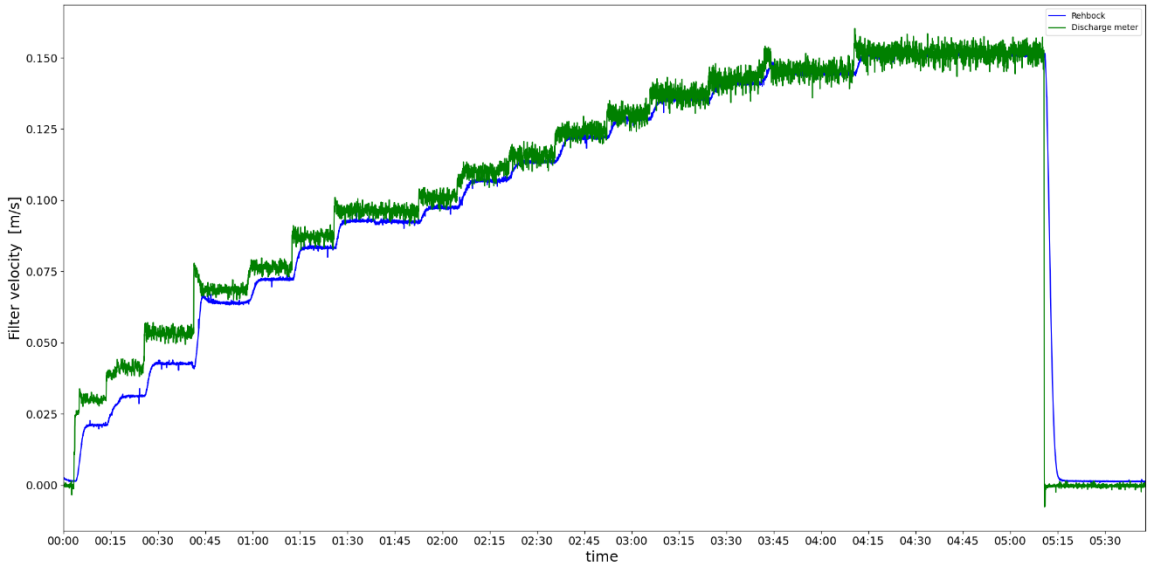

Figure F-3: Filter velocity test 1.1

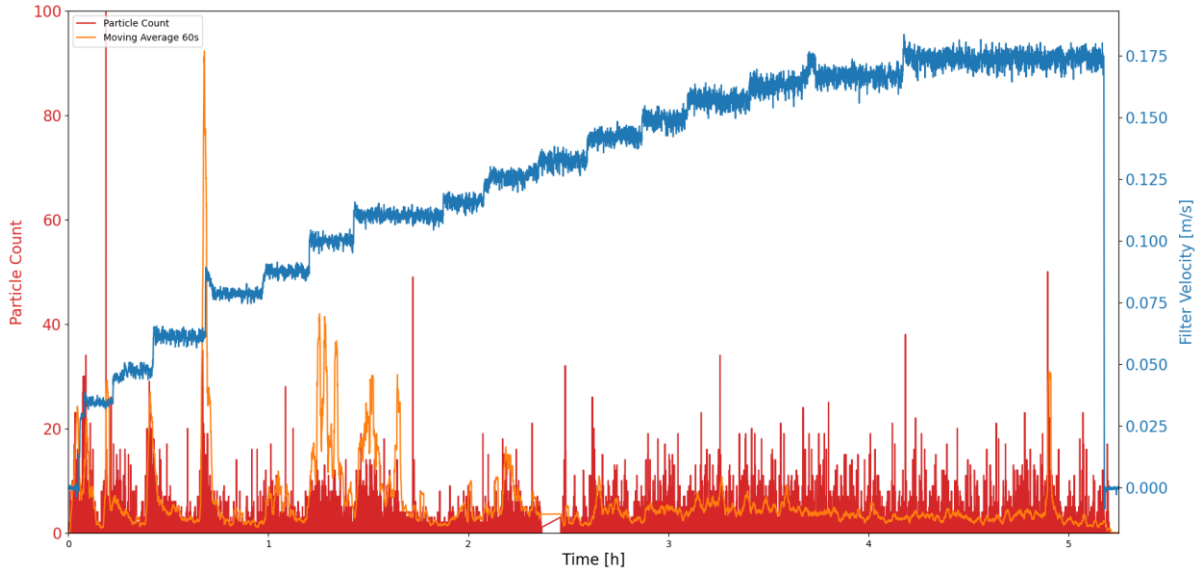

Figure F-4: Sand particles per frame and moving average vs. time, test 1.1 camera 50 cm

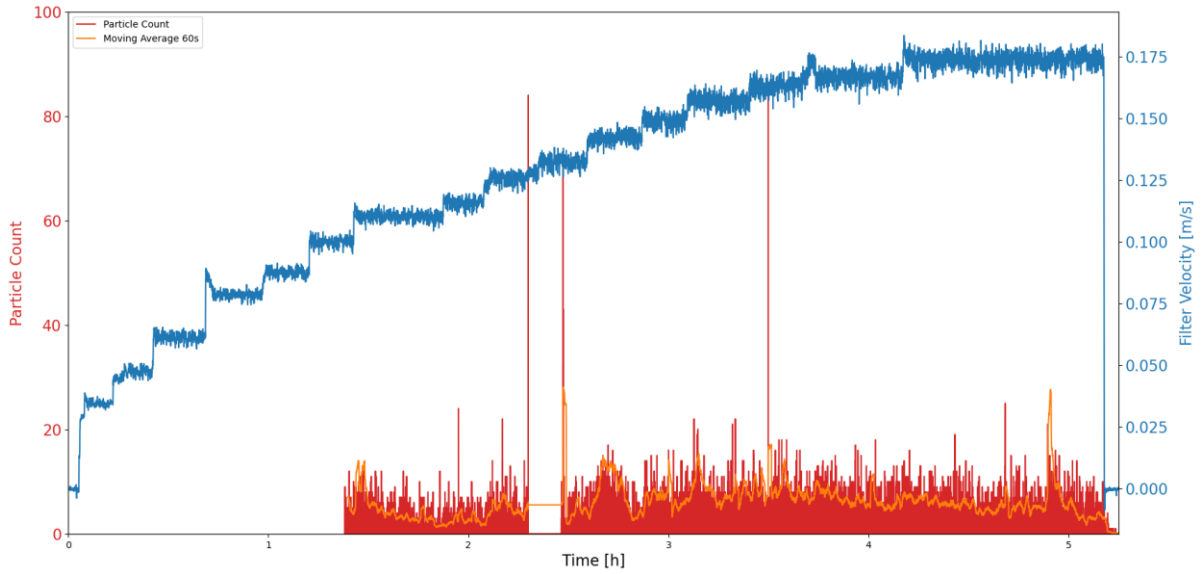

Figure F-5: Sand particles per frame and moving average vs. time, test 1.1 camera 75cm

Geotextile and sandbed after test

Figure F-6: Geotextile after test

Figure F-7: Dry geotextile after test

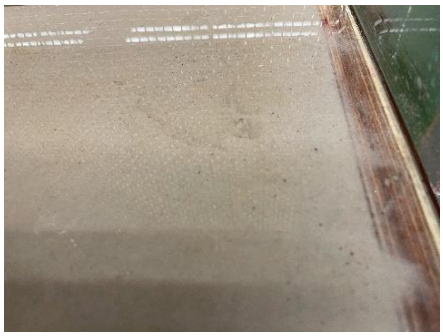

Figure F-8: Sandbed after test

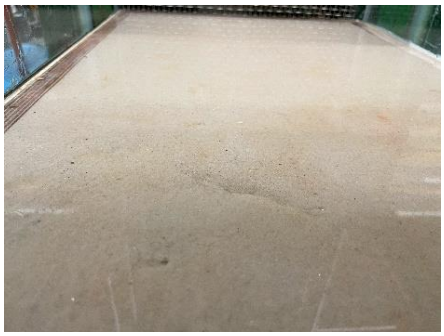

Figure F-9: Sandbed after test

Figure F-10: Sandbed after test

F.4 Test 1.2

Table F-22: Data test 1.2

Base material (d_{b50})	0.180 (M34)	[mm]
Geotextile	J4	
Filter material	45/125 mm	
d_{fn50}	61.79	[mm]
Weight of stones	109.086	[kg]

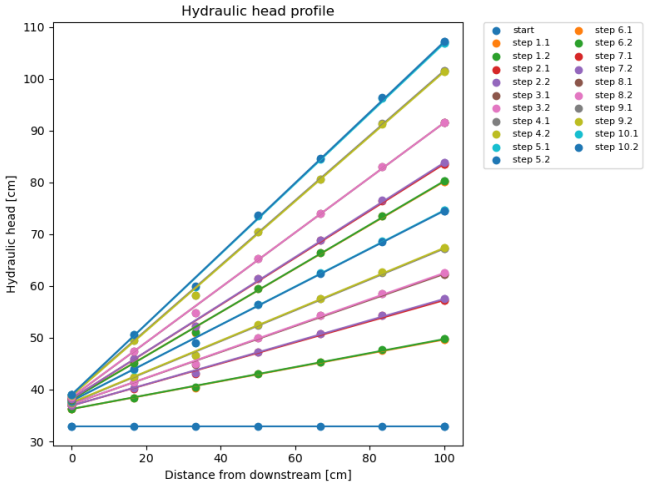

Figure F-11: Hydraulic head profile test 1.2

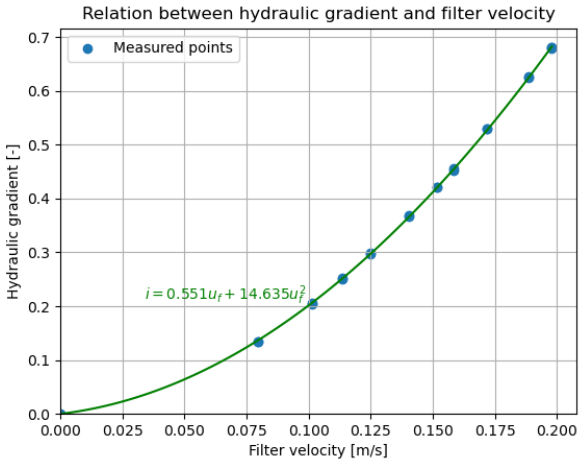

Figure F-12: Forchheimer relation test 1.2

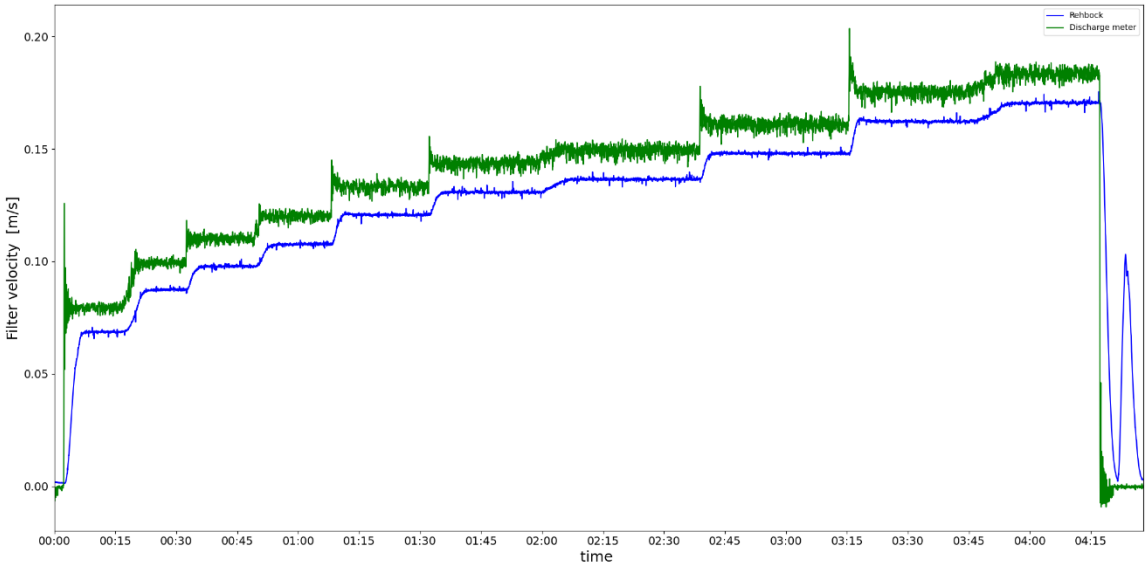

Figure F-13: Filter velocity test 1.2

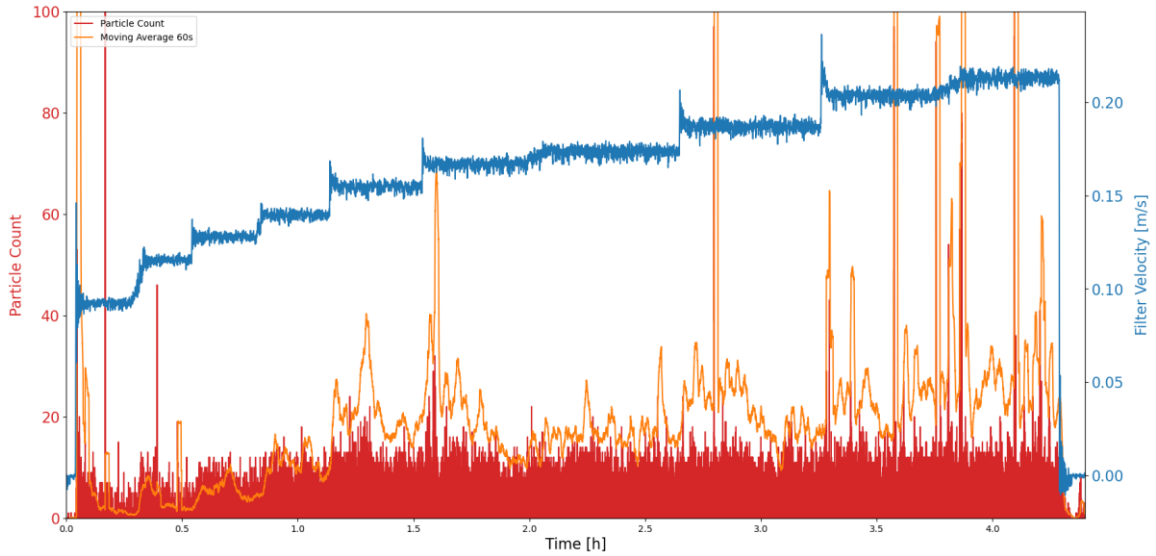

Figure F-14: Sand particles per frame and moving average vs. time, test 1.2 camera 75cm

Geotextile and sandbed after test

Figure F-15: Geotextile after test

Figure F-16: Dry geotextile after test

Figure F-17: Sandbed after test

Figure F-18: Sandbed after test

Figure F-19: Sandbed after test

Figure F-20: Sandbed after test

F.5 Test 1.3

Table F-23: Data test 1.3

Base material (d_{b50})	0.180 (M34)	[mm]
Geotextile	J4	
Filter material	A	
d_{fn50}	61.79	[mm]
Weight of stones	109.086	[kg]

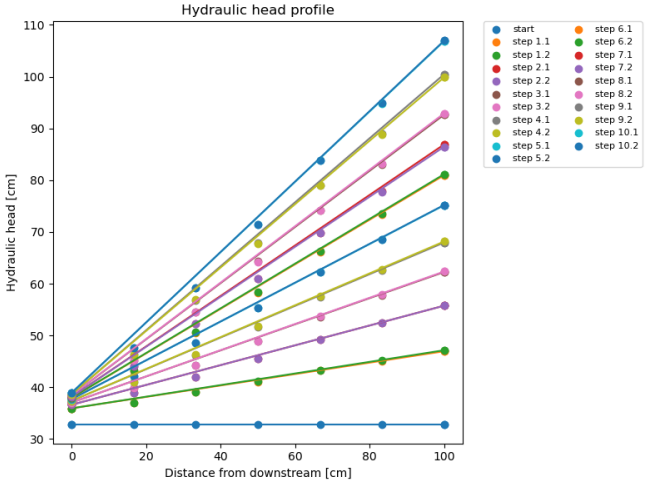

Figure F-21: Hydraulic head profile test 1.3

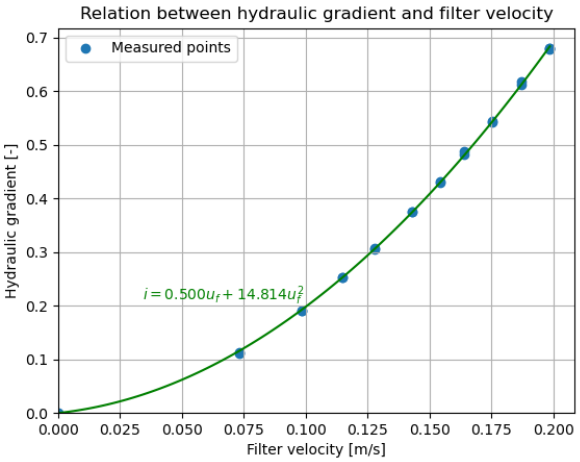

Figure F-22: Forchheimer relation test 1.3

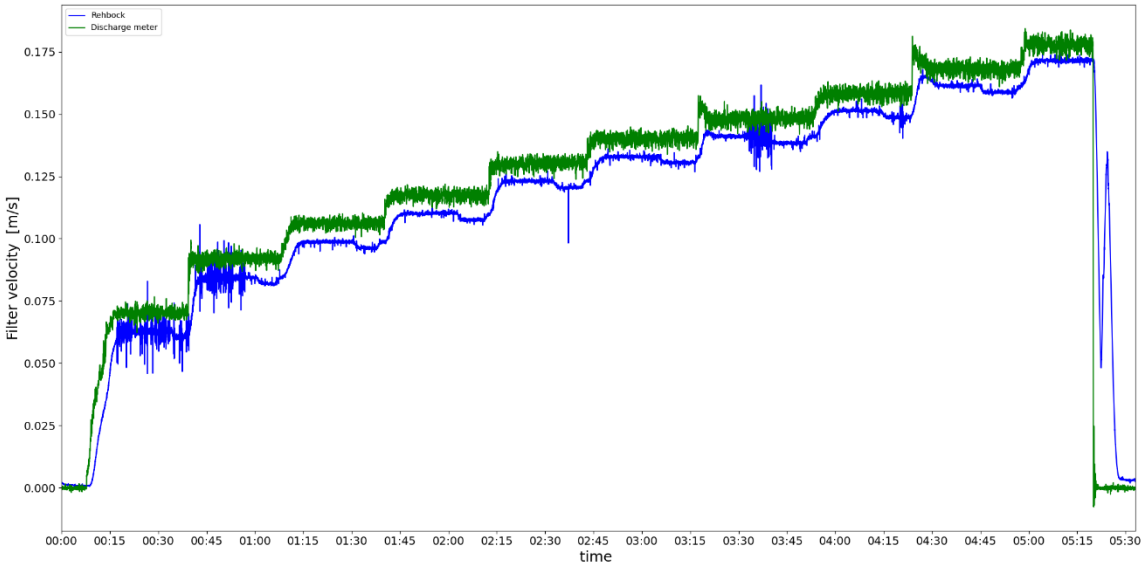

Figure F-23: Filter velocity test 1.3

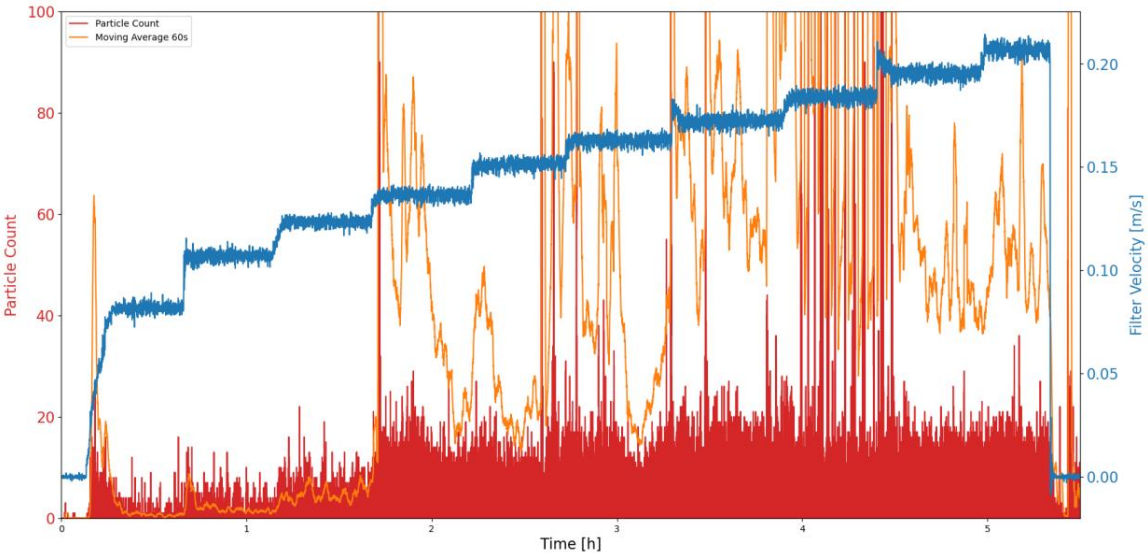

Figure F-24: Sand particles per frame and moving average vs. time, test 1.3 camera 50 cm

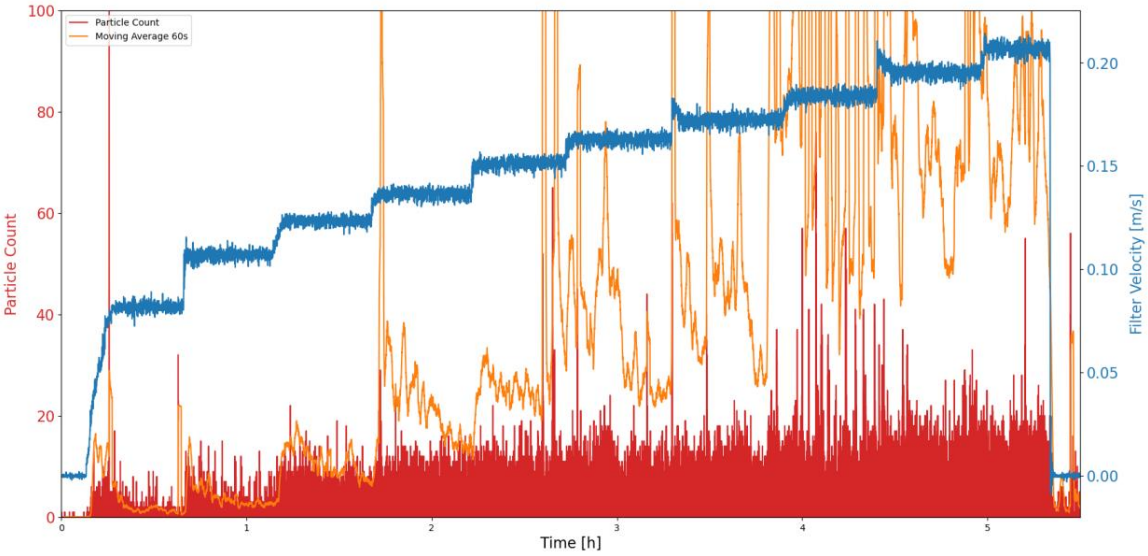

Figure F-25: Sand particles per frame and moving average vs. time, test 1.3 camera 75cm

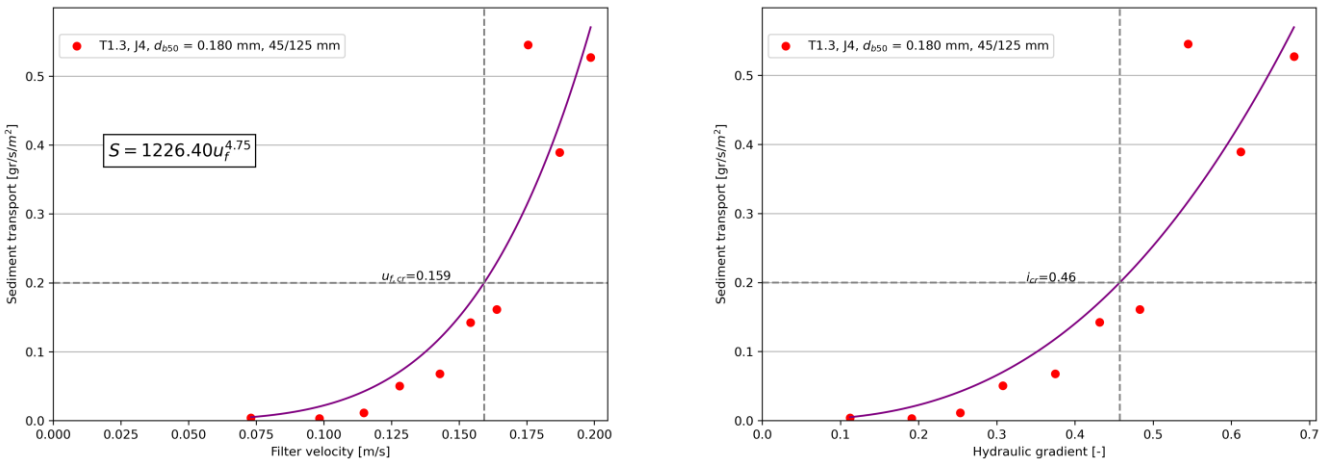

Figure F-26: Transport of base material vs. filter velocity and transport of base material vs hydraulic gradient, test 1.3

Geotextile and sandbed after test

Figure F-27: Geotextile after test

Figure F-28: Geotextile after test

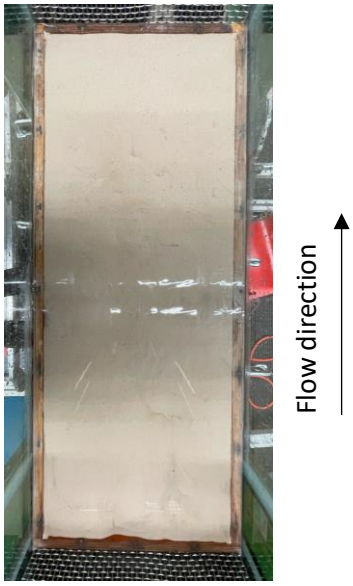

Figure F-29: Sandbed after test

Figure F-30: Sandbed after test at outflow point

Figure F-31: Sandbed after test at middle

Figure F-32: Sandbed after test at inflow point

Figure F-33: Erosion channel

Figure F-34: Erosion channel

F.6 Test 2.1

Table F-24: Data test 2.1

Base material (d_{b50})	0.180 (M34)	[mm]
Geotextile	J5	
Filter material	45/125 mm	
d_{fn50}	62.28	[mm]
Weight of stones	111.48	[kg]

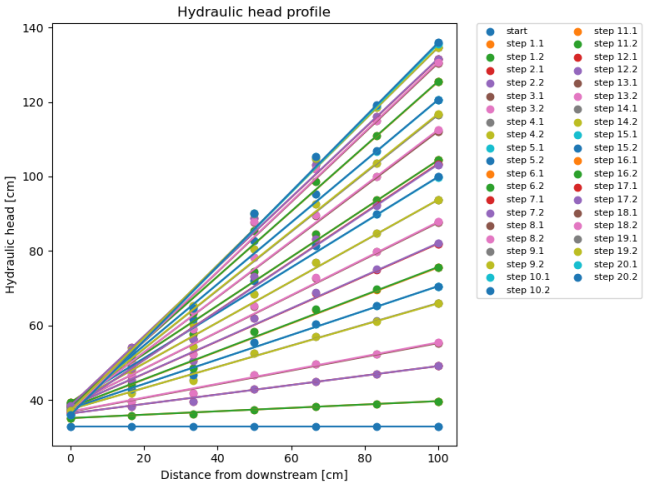

Figure F-35: Hydraulic head profile test 2.1

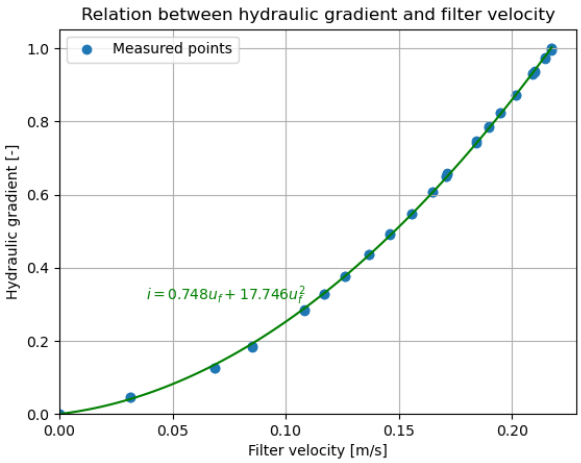

Figure F-36: Forchheimer relation test 2.1

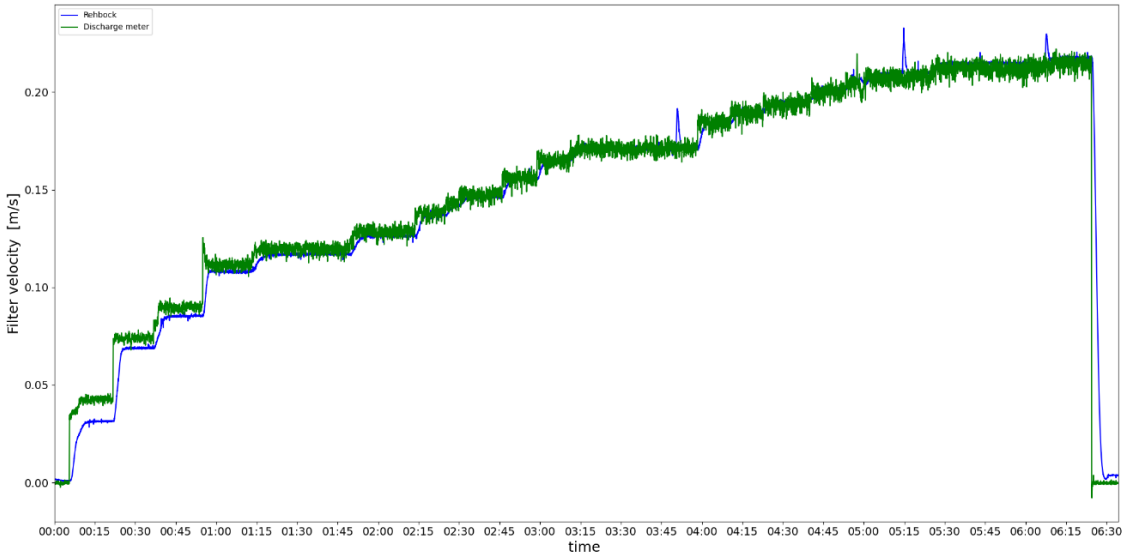

Figure F-37: Filter velocity test 2.1

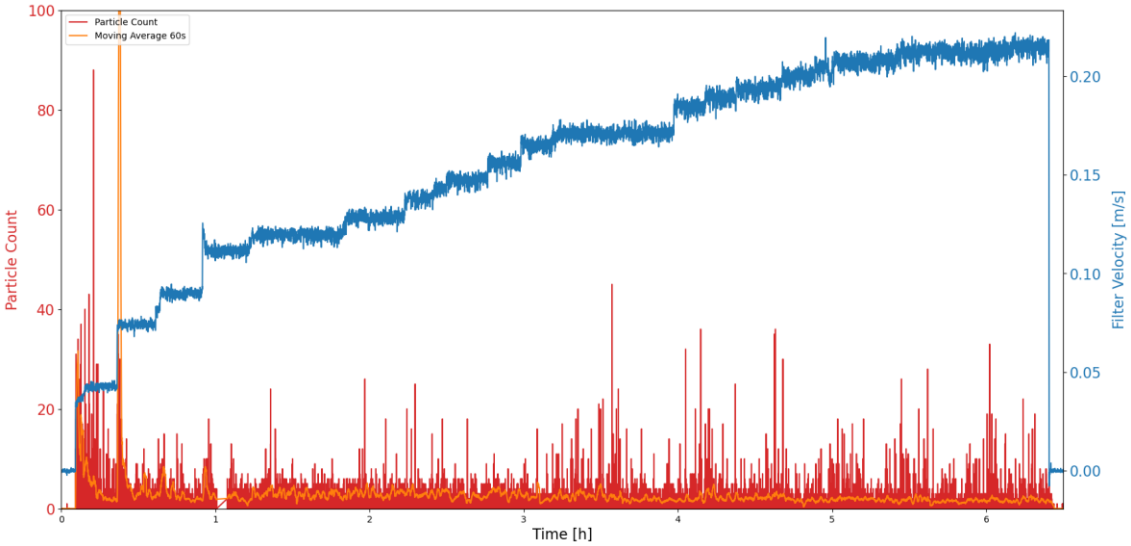

Figure F-38: Sand particles per frame and moving average vs. time, test 2.1 camera 50 cm

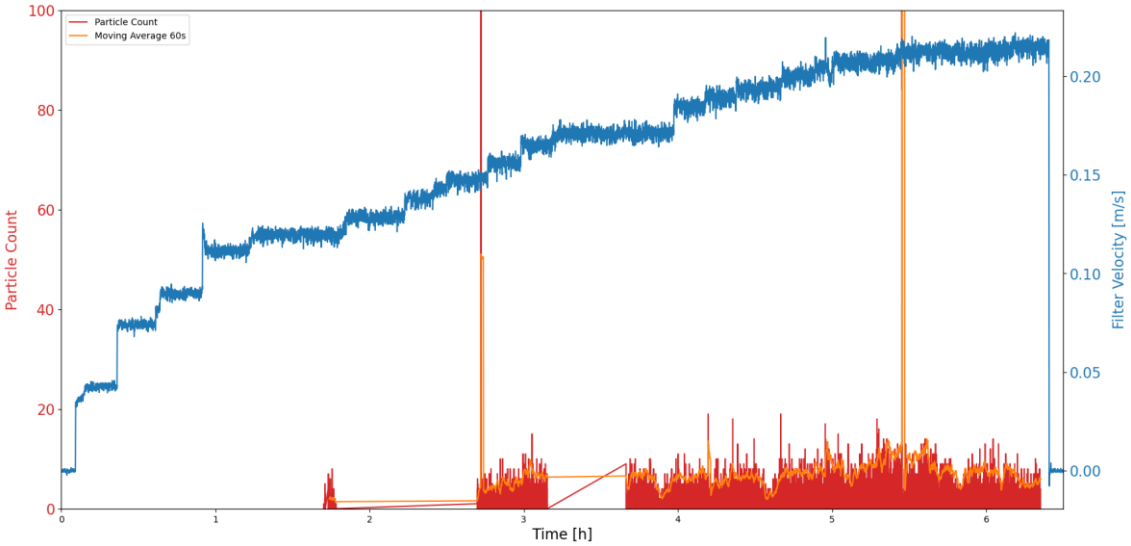

Figure F-39: Sand particles per frame and moving average vs. time, test 2.1 camera 75cm

Geotextile and sandbed after test

Figure F-40: Geotextile after test

Figure F-41: Dry geotextile after test

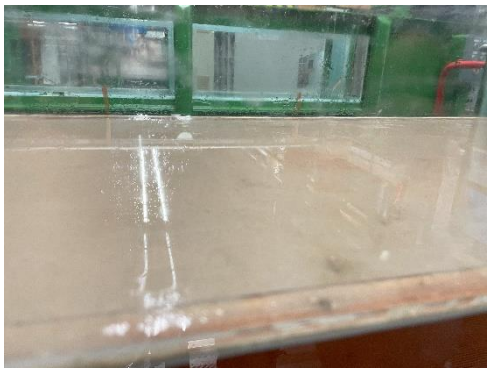

Figure F-42: Sandbed after test

Figure F-43: Sandbed after test

F.7 Test 2.2

Table F-25: Data test 2.2

Base material (d_{b50})	0.180 (M34)	[mm]
Geotextile	J5	
Filter material	45/125 mm	
d_{fn50}	61.79	[mm]
Weight of stones	109.086	[kg]

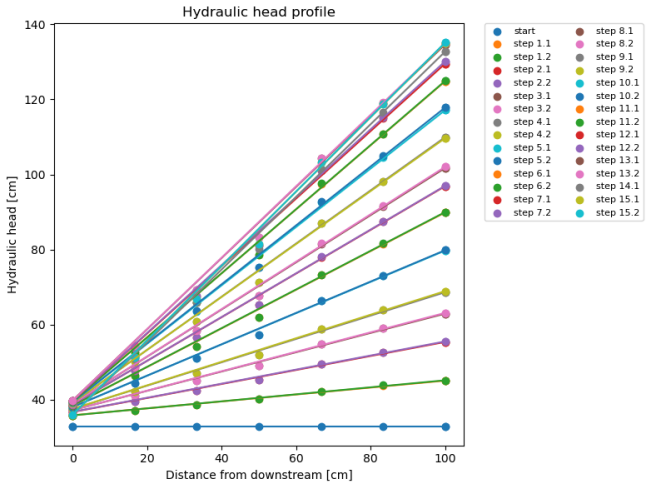

Figure F-44: Hydraulic head profile test 2.2

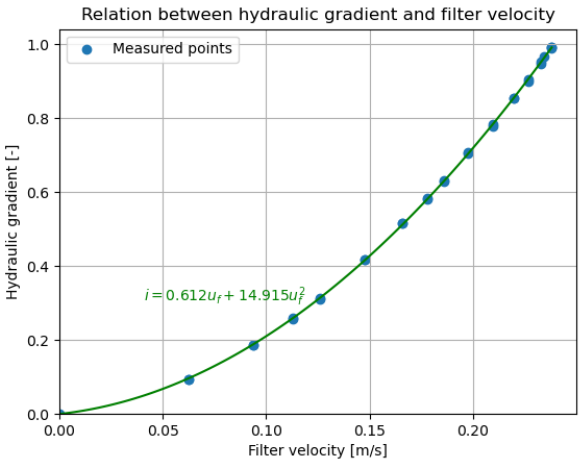

Figure F-45: Forchheimer relation test 2.2

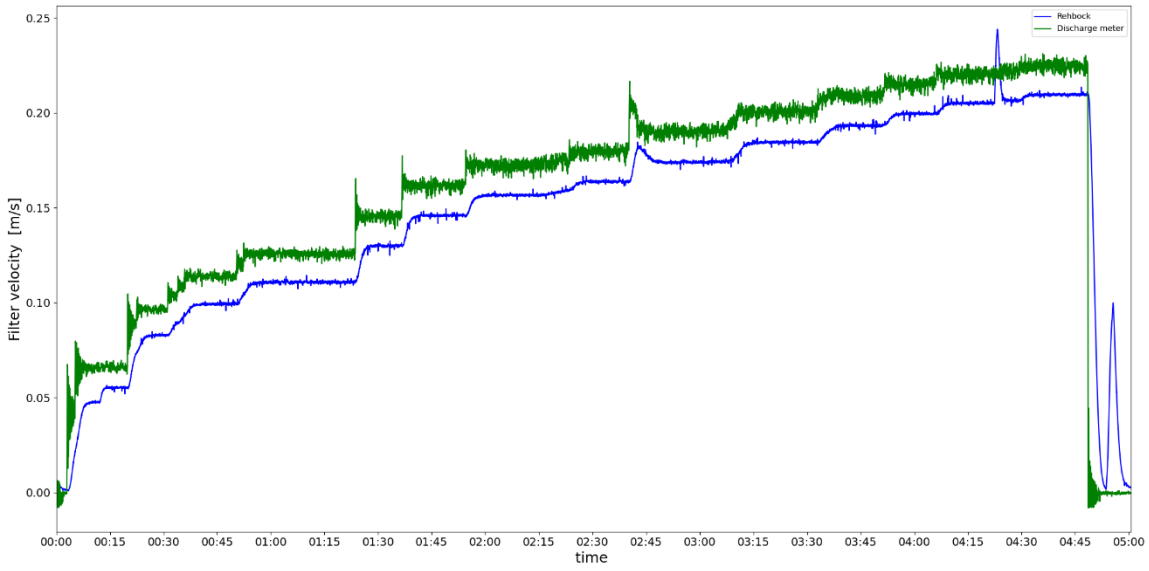

Figure F-46: Filter velocity test 2.2

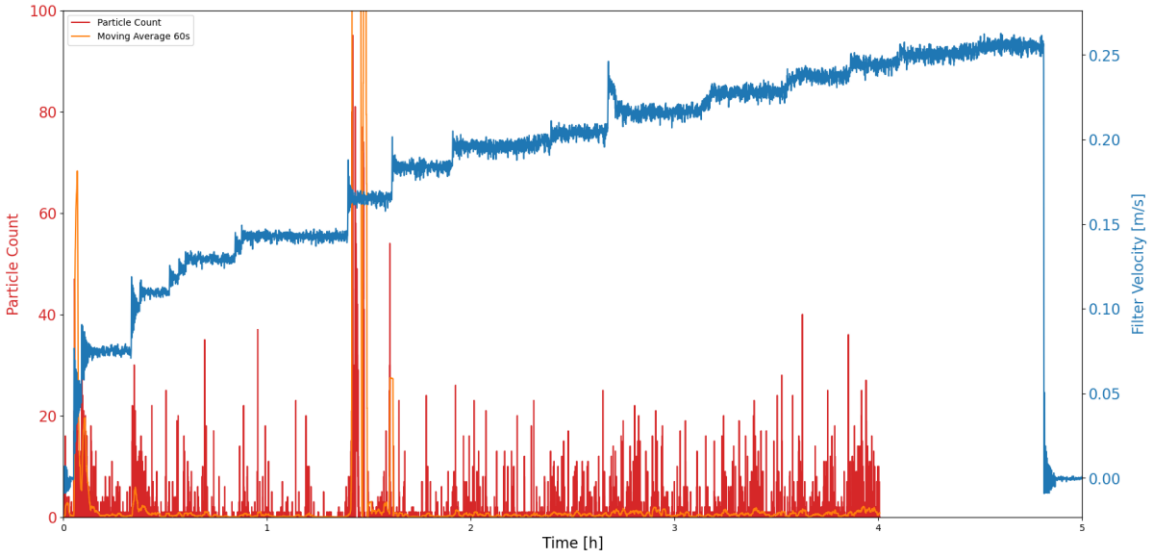

Figure F-47: Sand particles per frame and moving average vs. time, test 2.2 camera 50 cm

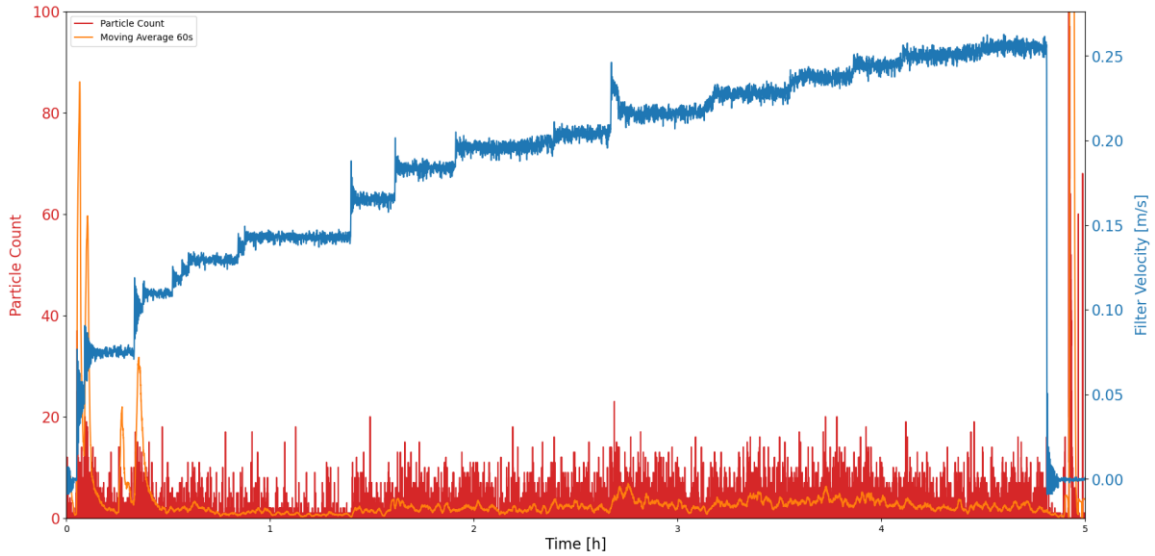

Figure F-48: Sand particles per frame and moving average vs. time, test 2.2 camera 75cm

Geotextile and sandbed after test

Figure F-49: Geotextile after test

Figure F-50: Dry geotextile after test

Figure F-51: Sandbed after test

Figure F-52: Sandbed after test

Figure F-53: Sandbed after test

F.8 Test 2.3

Table F-26: Data test 2.3

Base material (d_{b50})	0.180 (M34)	[mm]
Geotextile	J5	
Filter material	45/125 mm	
d_{fn50}	61.79	[mm]
Weight of stones	109.086	[kg]

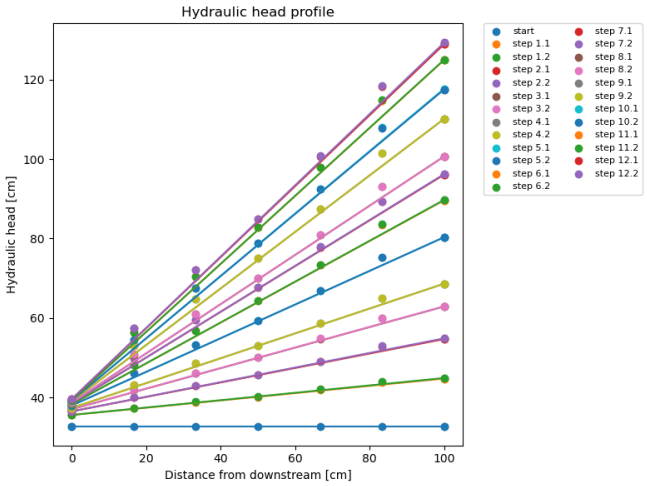

Figure F-54: Hydraulic head profile test 2.3

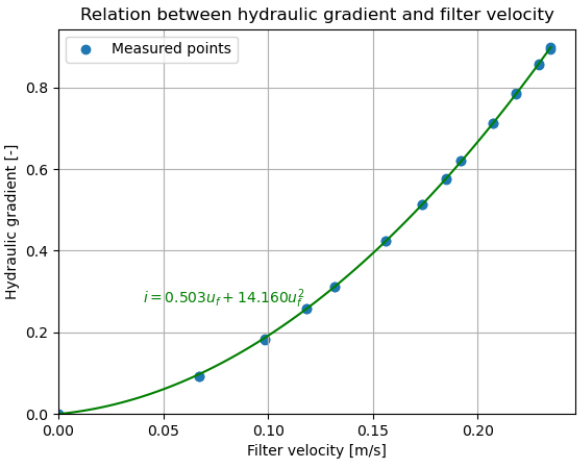

Figure F-55: Forchheimer relation test 2.3

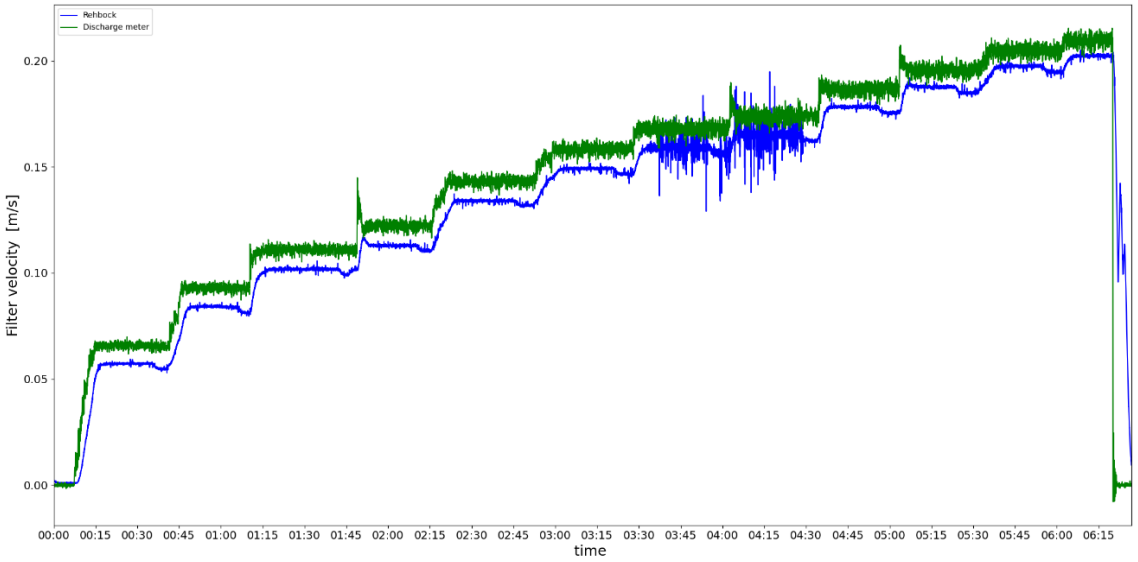

Figure F-56: Filter velocity test 2.3

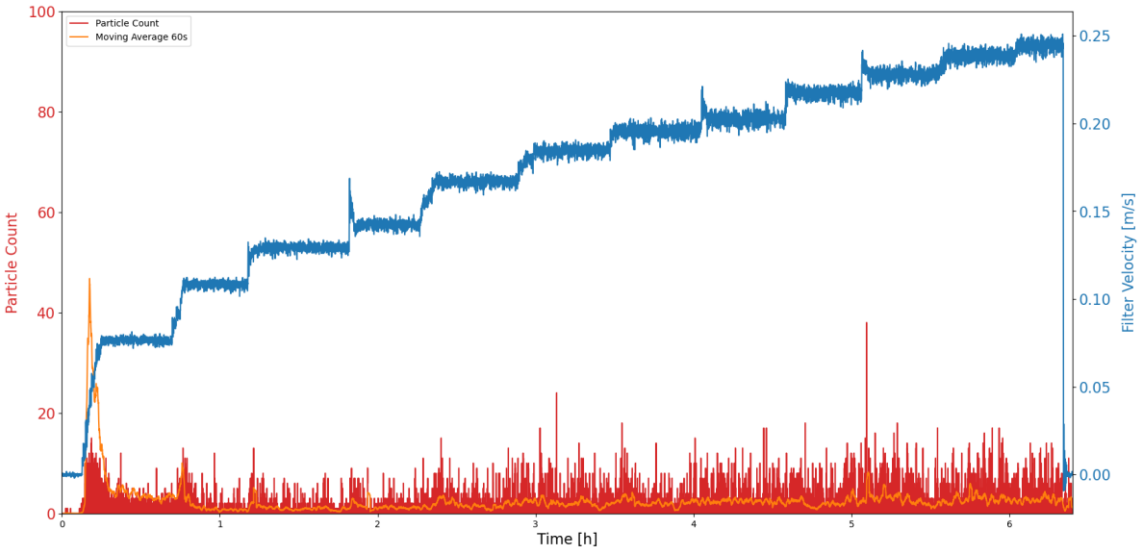

Figure F-57: Sand particles per frame and moving average vs. time, test 2.3 camera 50 cm

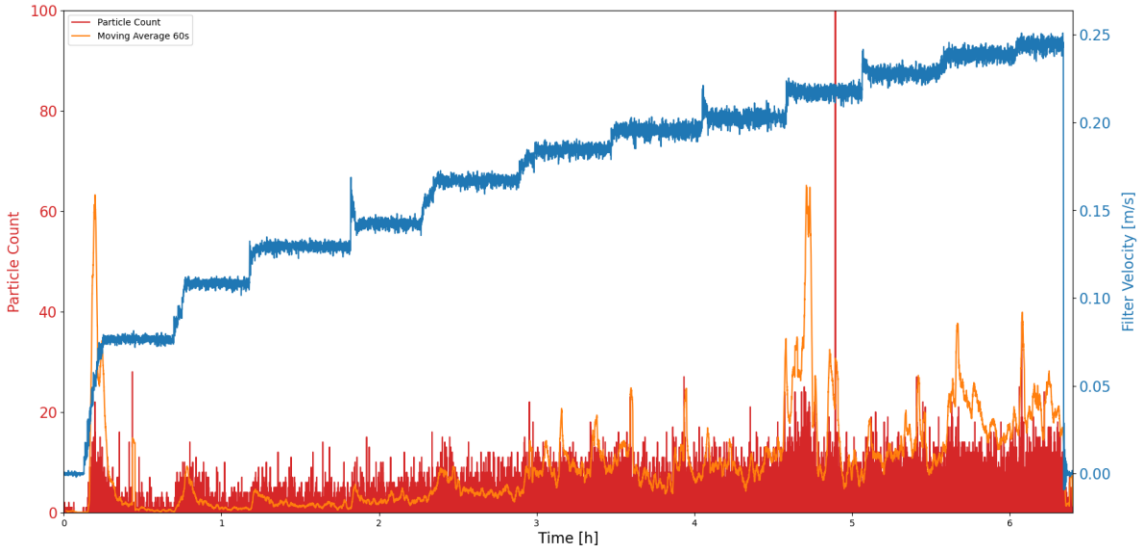

Figure F-58: Sand particles per frame and moving average vs. time, test 2.3 camera 75cm

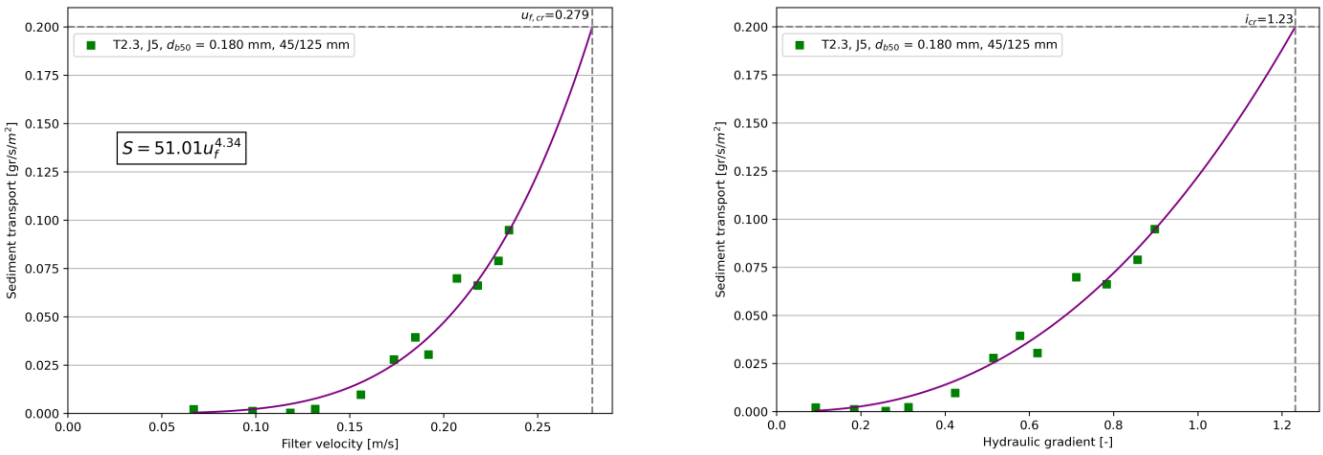

Figure F-59: Transport of base material vs. filter velocity and transport of base material vs hydraulic gradient, test 2.3

Geotextile and sandbed after test

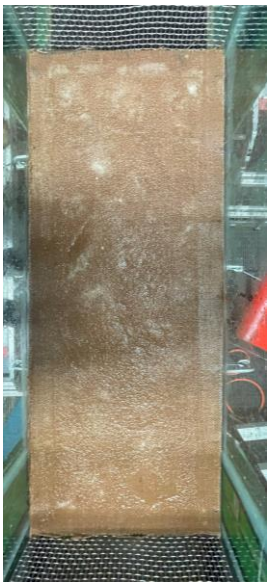

Figure F-60: Geotextile after test

Figure F-61: Dry geotextile after test

Figure F-62: Sandbed after test

Figure F-63: Sandbed after test at outflow point

Figure F-64: Middle of sandbed after test

Figure F-65: Sandbed after test at inflow point

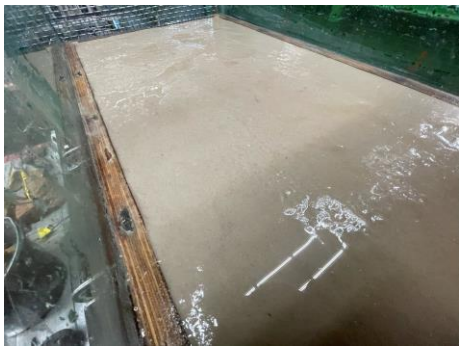

Figure F-66: Sandbed after test

Figure F-67: Sandbed after test

F.9 Test 3.1

Table F-27: Data test 3.1

Base material (d_{b50})	0.180 (M34)	[mm]
Geotextile	J5	
Filter material	45/145 mm	
d_{fn50}	61.79	[mm]
Weight of stones	109.086	[kg]

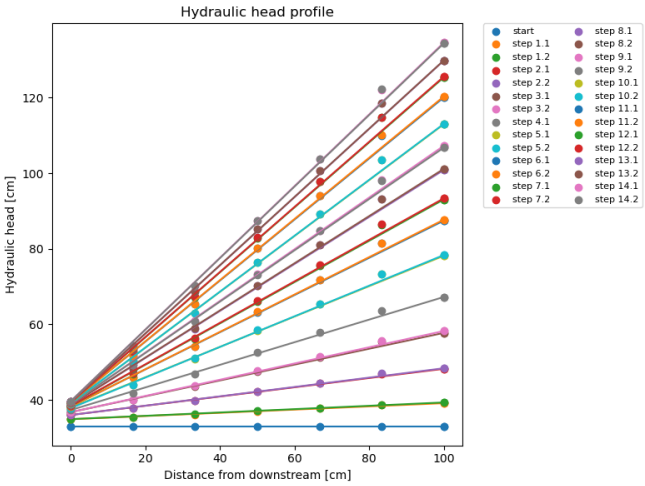

Figure F-68: Hydraulic head profile test 3.1

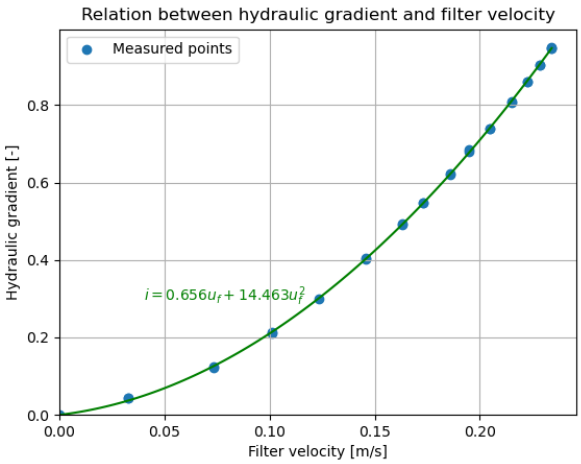

Figure F-69: Forchheimer relation test 3.1

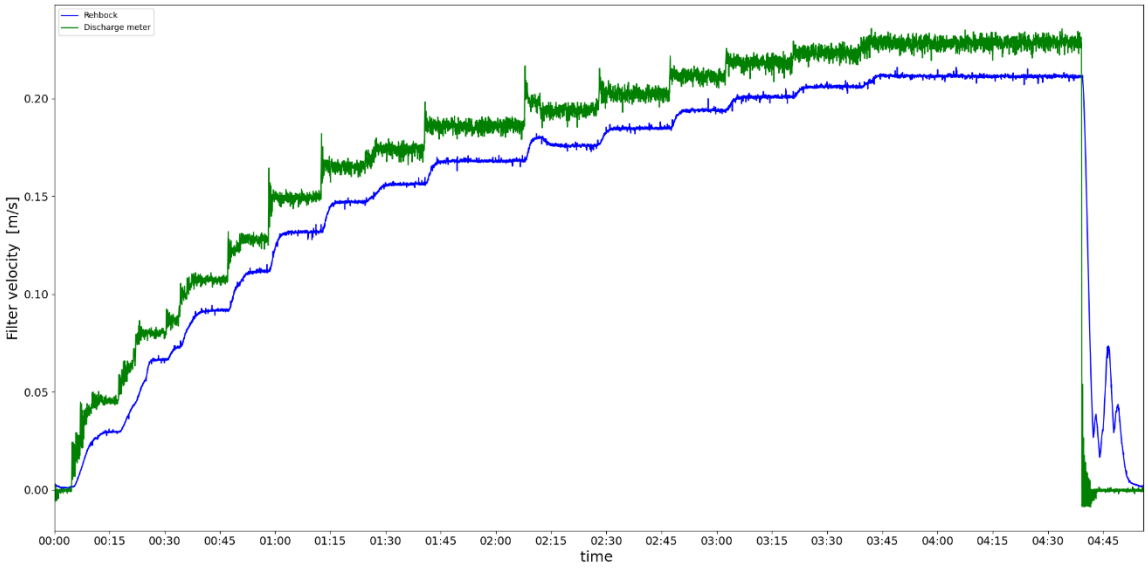

Figure F-70: Filter velocity test 3.1

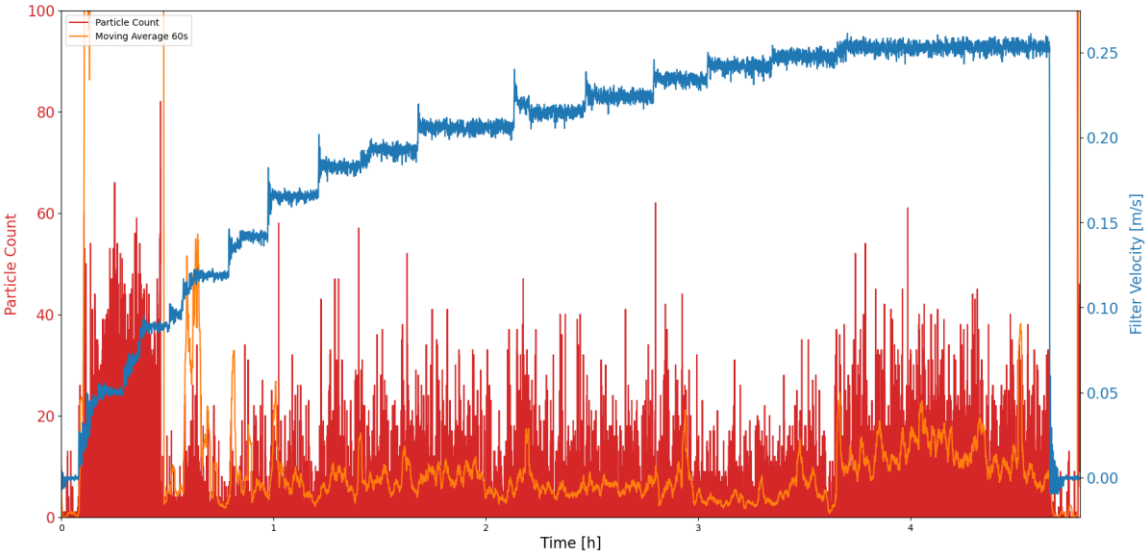

Figure F-71: Sand particles per frame and moving average vs. time, test 3.1 camera 50 cm

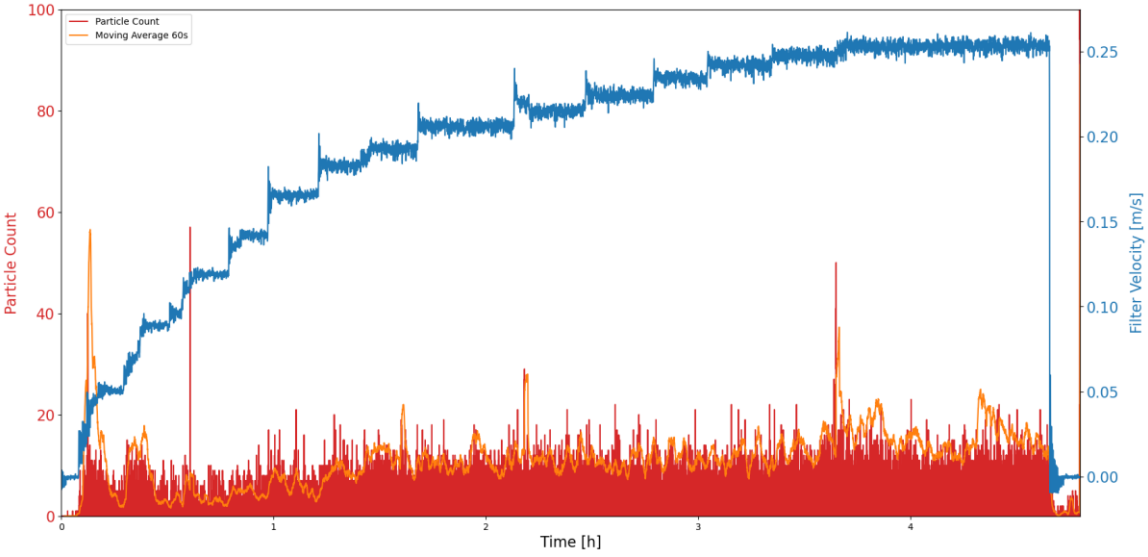

Figure F-72: Sand particles per frame and moving average vs. time, test 3.1 camera 75cm

Images of surface behind test set-up

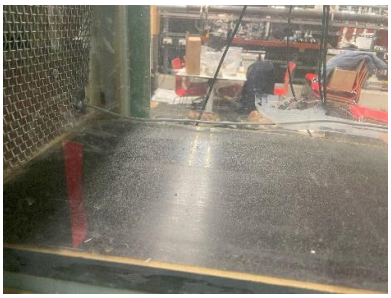

Figure F-73: Surface behind structure at starting point

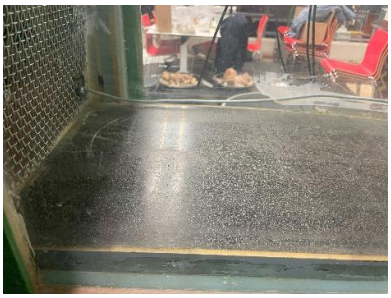

Figure F-74: After step 1

Figure F-75: After step 2

Figure F-76: After step 2

Figure F-77: After step 3

Figure F-78: After step 3

Figure F-79: After step 4

Figure F-80: After step 4

Figure F-81: After step 5

Figure F-82: After step 5

Figure F-83: After step 6

Figure F-84: After step 6

Geotextile and sandbed after test

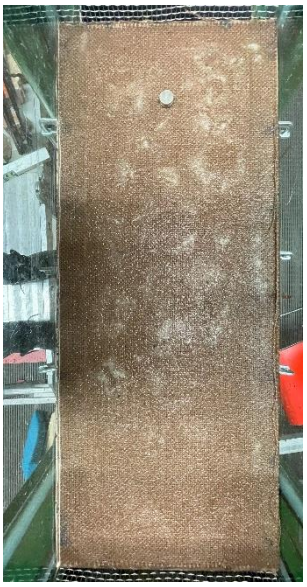

Figure F-85: Geotextile after test

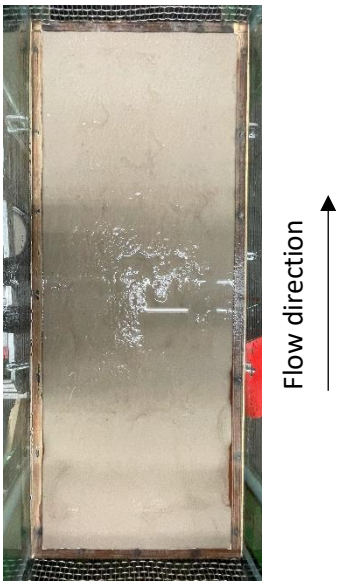

Figure F-86: Sandbed after test

Figure F-87: Sandbed after test at outflow point

Figure F-88: Sandbed after test at middle

Figure F-89: Sandbed after test at inflow point

Figure F-90: Sandbed after test

F.10 Test 3.2

Table F-28: Data test 3.2

Base material (d_{b50})	0.180 (M34)	[mm]
Geotextile	J5	
Filter material	45/125 mm	
d_{fn50}	61.79	[mm]
Weight of stones	109.086	[kg]

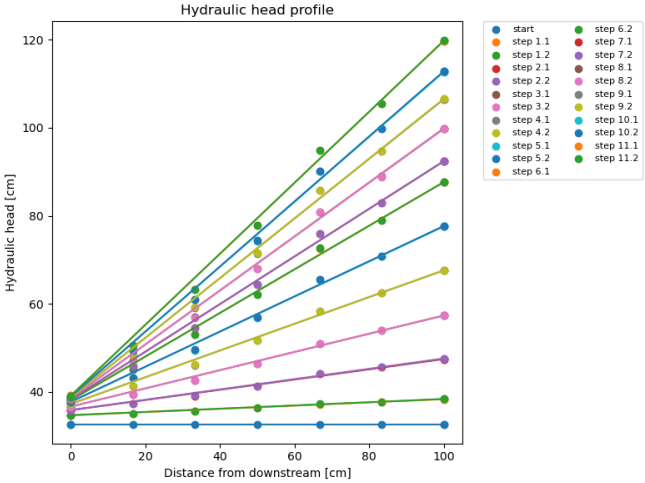

Figure F-91: Hydraulic head profile test 3.2

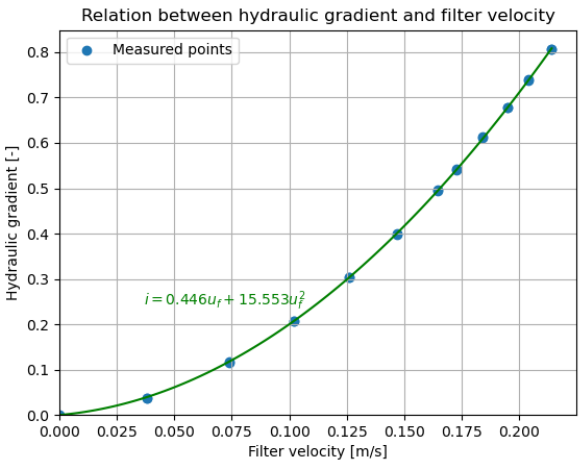

Figure F-92: Forchheimer relation test 3.2

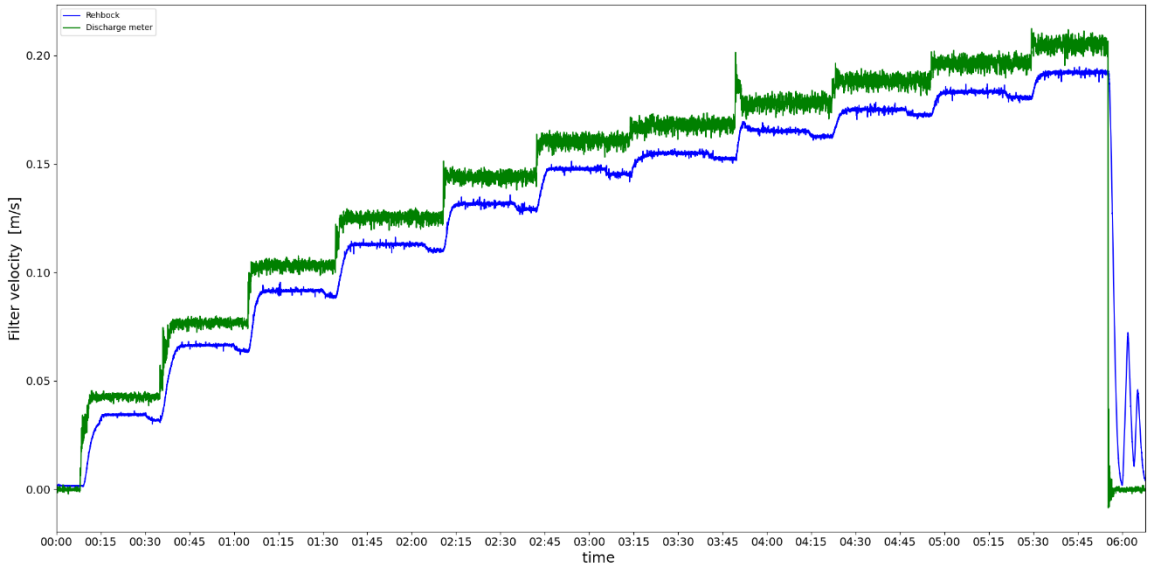

Figure F-93: Filter velocity test 3.2

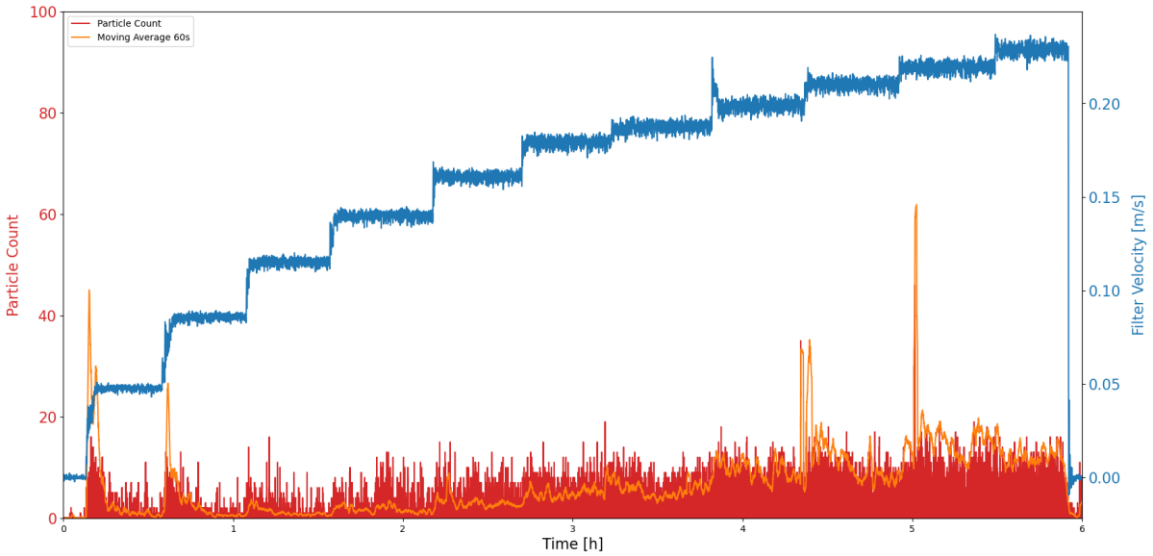

Figure F-94: Sand particles per frame and moving average vs. time, test 3.2 camera 50cm

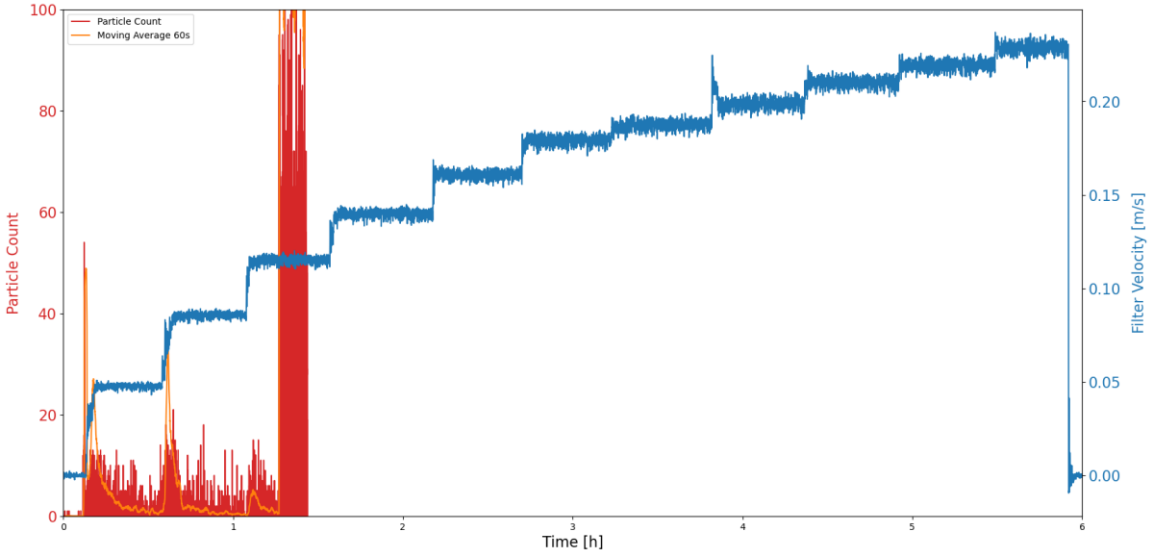

Figure F-95: Sand particles per frame and moving average vs. time, test 3.2 camera 75cm

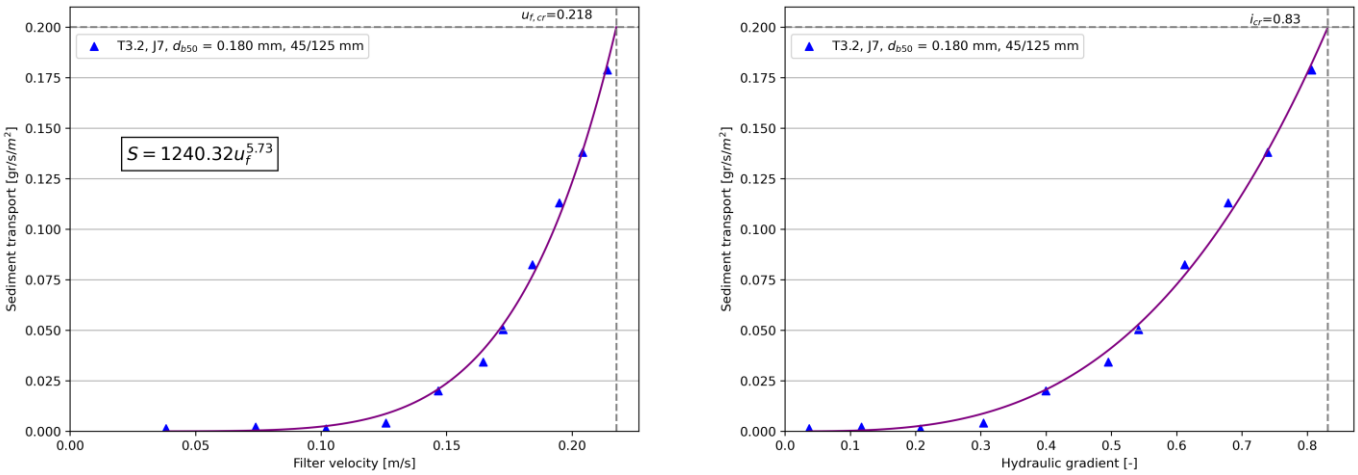

Figure F-96: Transport of base material vs. filter velocity and transport of base material vs hydraulic gradient, test 3.2

Geotextile and sandbed after test

Figure F-97: Geotextile after test

Figure F-98: Dry geotextile after test

Figure F-99: Sandbed after test

Figure F-100: Sandbed after test

Figure F-101: Sandbed after test

Figure F-102: Sandbed after test

Figure F-103: Sandbed after test

F.11 Test 4

Table F-29: Data test 4

Base material (d_{b50})	0.180 (M34)	[mm]
Geotextile	J9	
Filter material	45/125 mm	
d_{fn50}	61.79	[mm]
Weight of stones	109.086	[kg]

During test 4 at 3 points during the test the eroded sand on the bottom of the flume is suctioned. The results are given in the table below (Table F-30).

Table F-30: Eroded sand test 4

Test step	Sand [gr]
After step 2	11.2
After step 6	2.2
After test	1.2

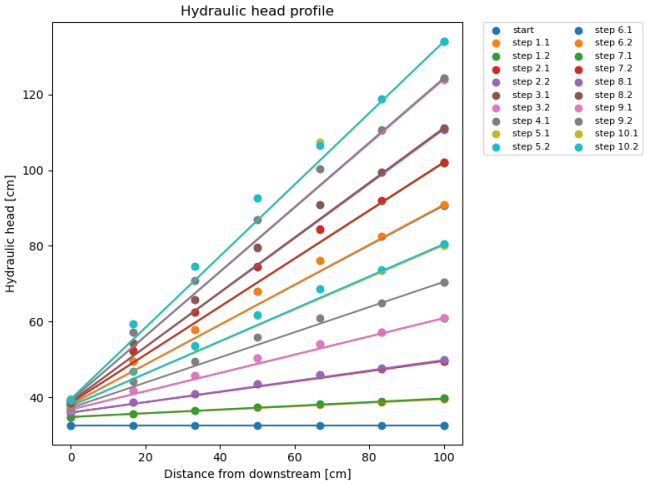

Figure F-104: Hydraulic head profile test 4

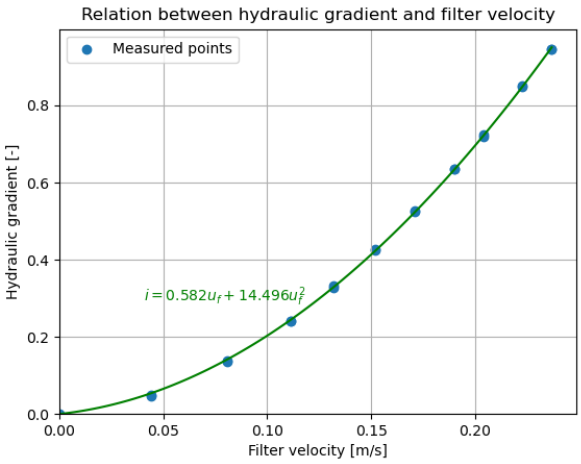

Figure F-105: Forchheimer relation test 4

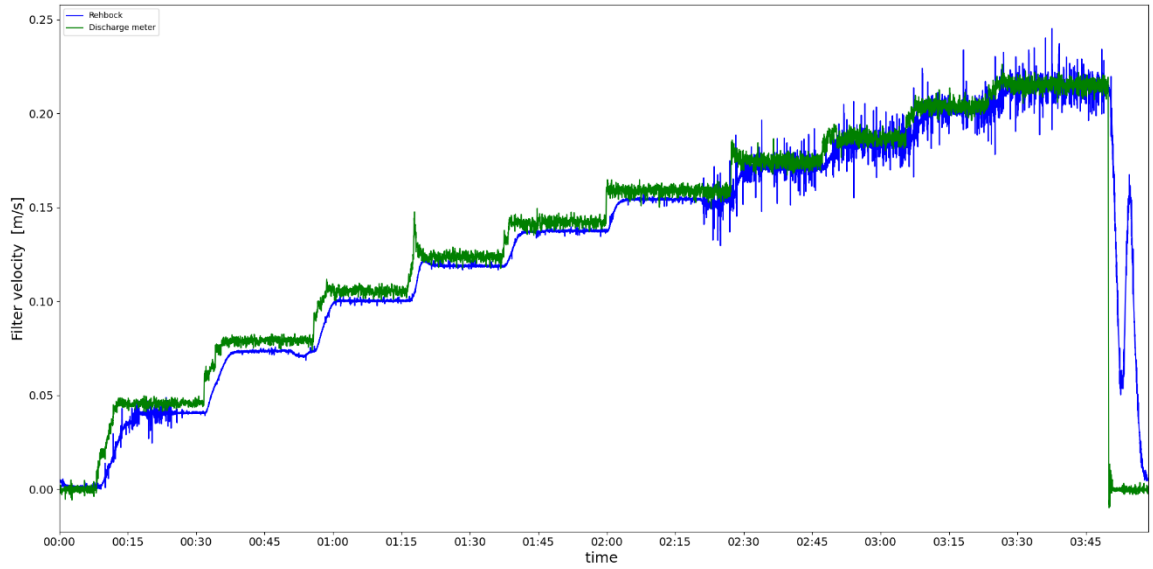

Figure F-106: Filter velocity test 4

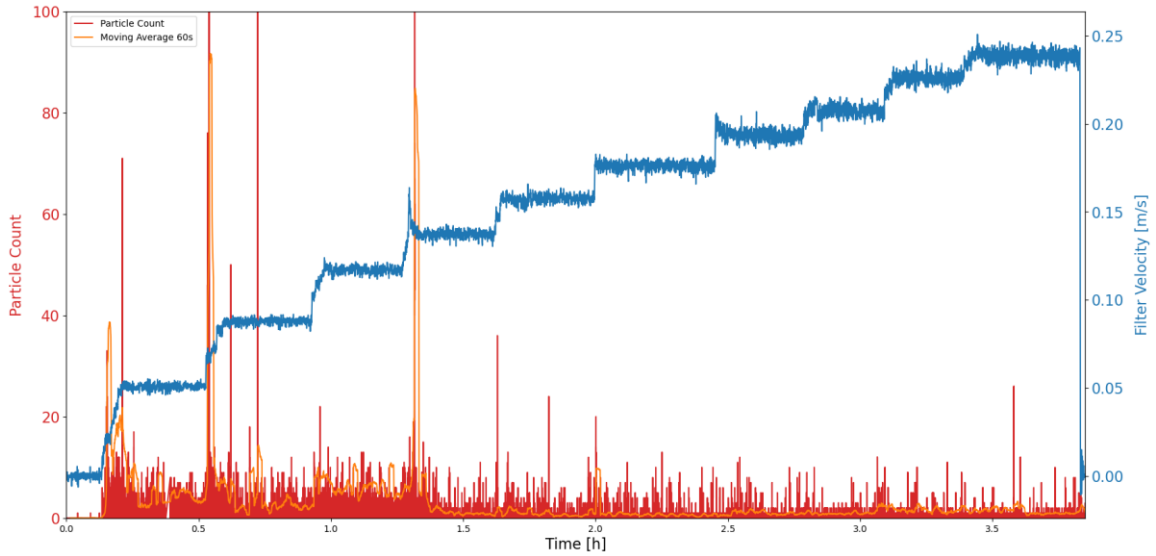

Figure F-107: Sand particles per frame and moving average vs. time, test 4 camera 75cm

Geotextile and sandbed after test

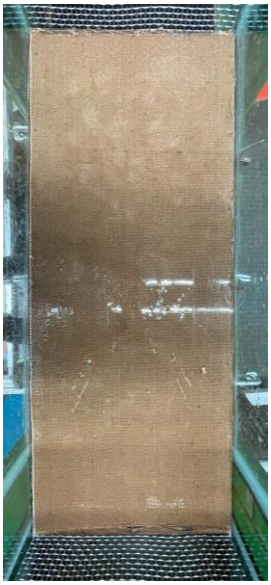

Figure F-108: Geotextile after test

Figure F-109: Dry geotextile

Figure F-110: Sandbed after test

F.12 Test 5.1

Table F-31: Data test 5.1

Base material (d_{b50})	0.180 (M34)	[mm]
Geotextile	J4	
Filter material	40/70 mm	
d_{fn50}	45.73	[mm]
Weight of stones	114.218	[kg]

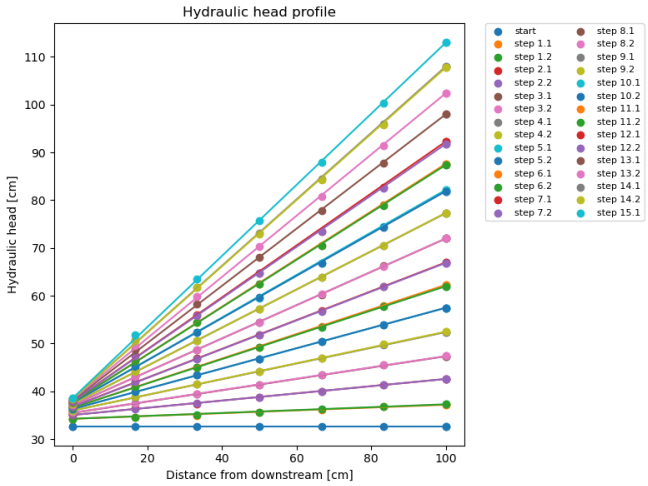

Figure F-111: Hydraulic head profile test 5.1

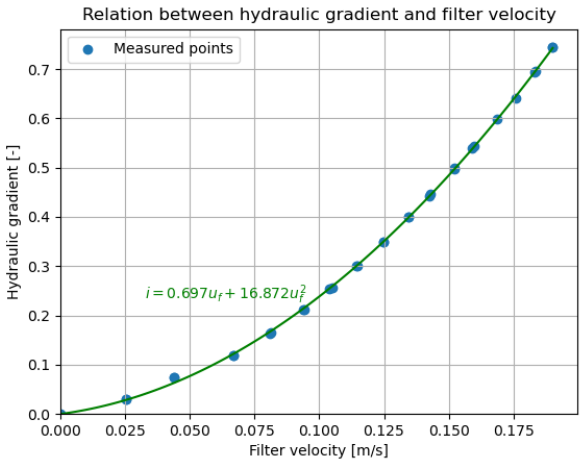

Figure F-112: Forchheimer relation test 5.1

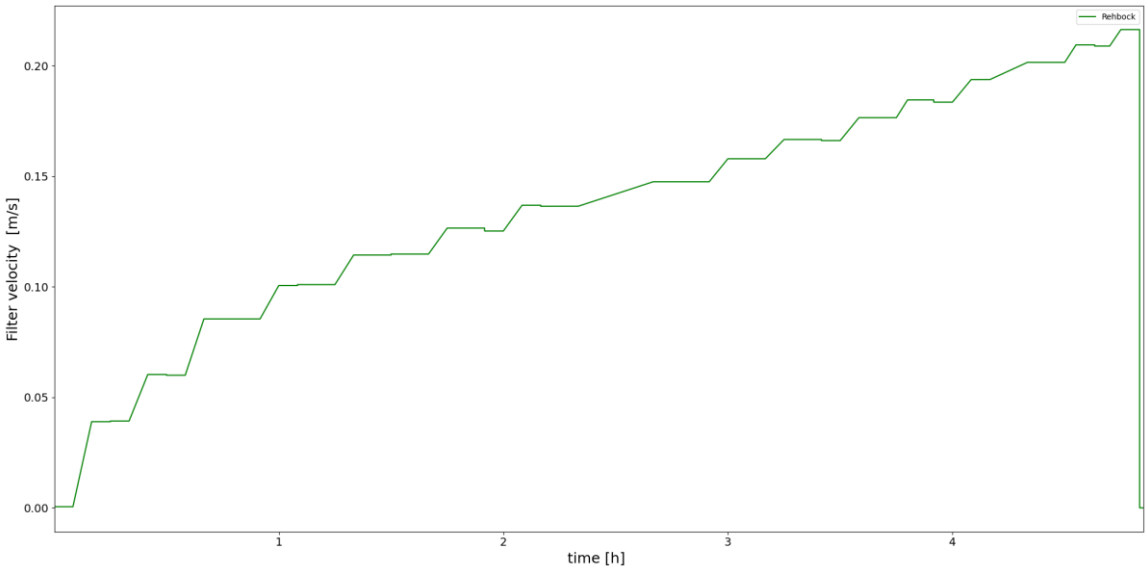

Figure F-113: Filter velocity test 5.1

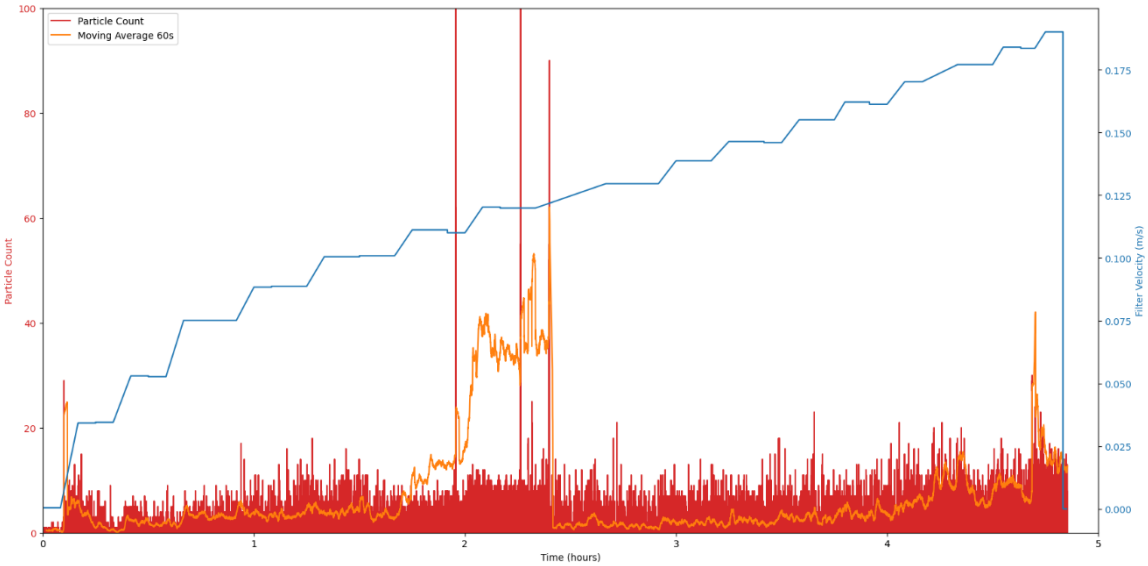

Figure F-114: Sand particles per frame and moving average vs. time, test 5.1 camera 50 cm, the measurements up to 2.5 hours were affected by air bubbles present under the camera.

Geotextile and sandbed after test

Figure F-115: Geotextile after test

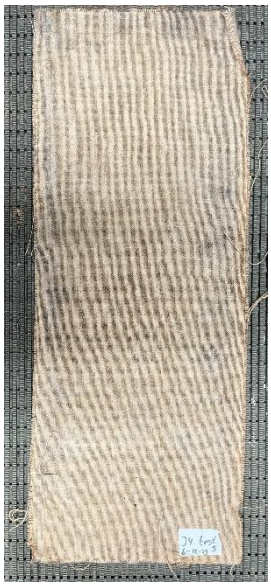

Figure F-116: Dry geotextile after test

Figure F-117: Sandbed after test

Figure F-118: Sandbed after test

Figure F-119: Sandbed after test

F.13 Test 5.2

Table F-32: Data test 5.2

Base material (d_{b50})	0.180 (M34)	[mm]
Geotextile	J4	
Filter material	40/70 mm	
d_{fn50}	45.73	[mm]
Weight of stones	114.218	[kg]

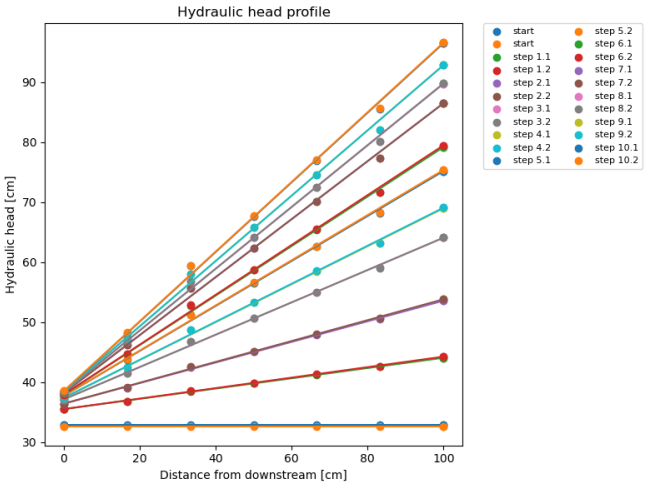

Figure F-120: Hydraulic head profile test 5.2

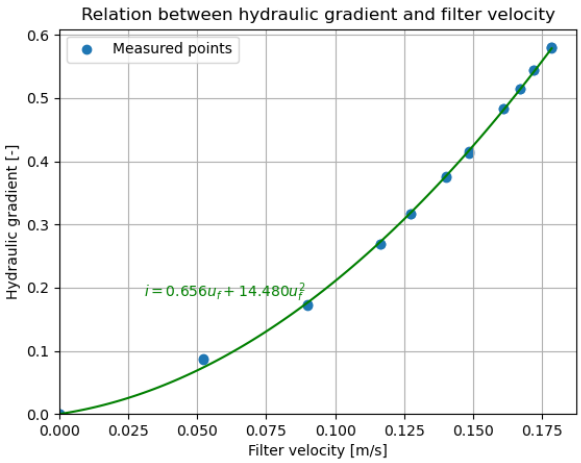

Figure F-121: Forchheimer relation test 5.2

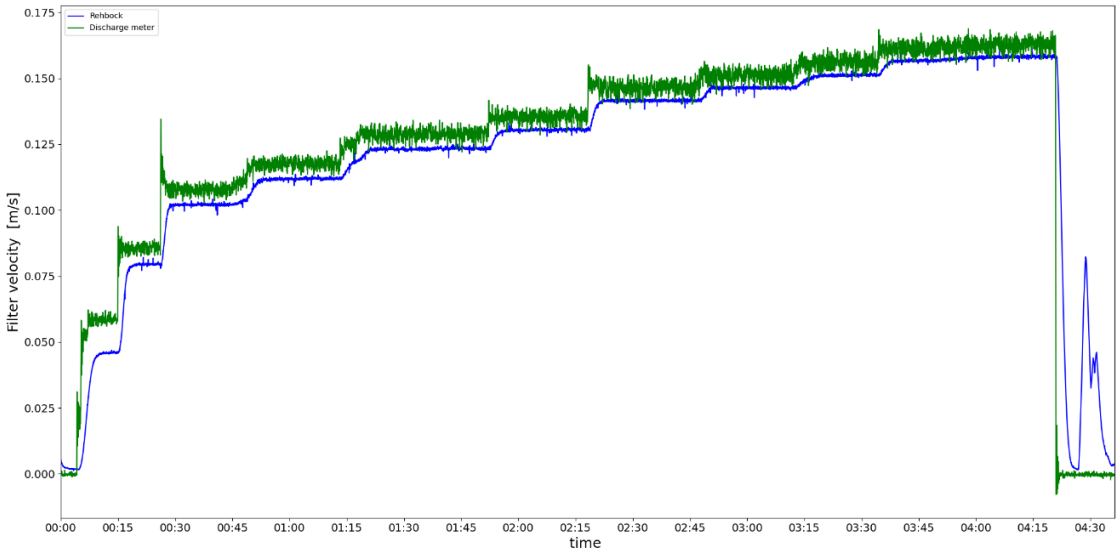

Figure F-122: Filter velocity test 5.2

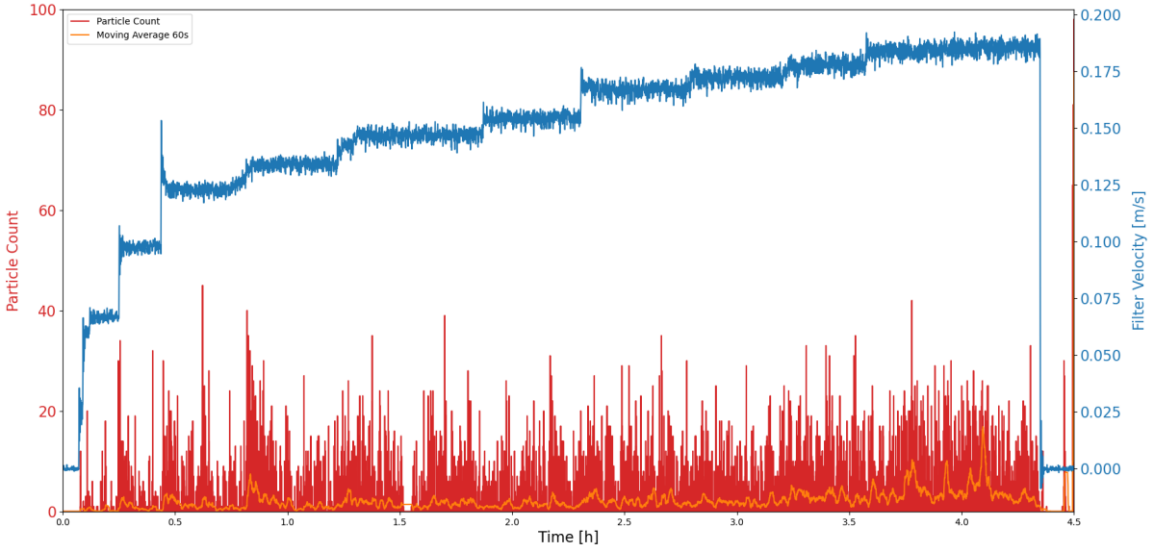

Figure F-123: Sand particles per frame and moving average vs. time, test 5.2 camera 50 cm

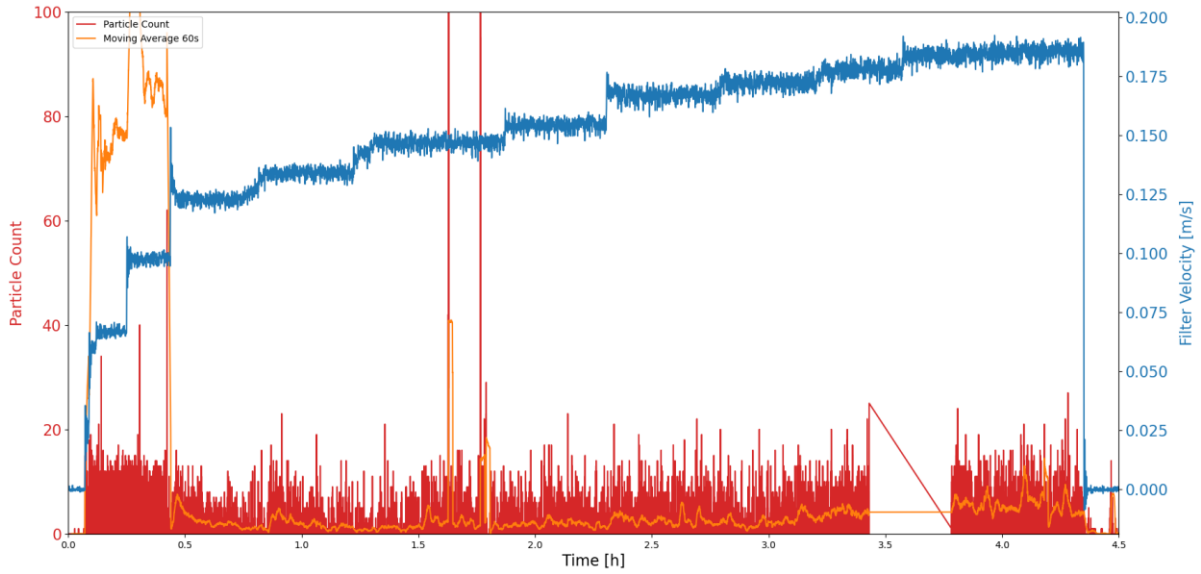

Figure F-124: Sand particles per frame and moving average vs. time, test 5.2 camera 75cm

Geotextile and sandbed after test

Figure F-125: Geotextile after test

Figure F-126: Dry geotextile after test

Figure F-127: Sandbed after test

Figure F-128: Sandbed after test

Figure F-129: Sandbed after test

F.14 Test 6

Table F-33: Data test 6

Base material (d_{b50})	0.180 (M34)	[mm]
Geotextile	J5	
Filter material	40/70 mm	
d_{fn50}	45.73	[mm]
Weight of stones	114.218	[kg]

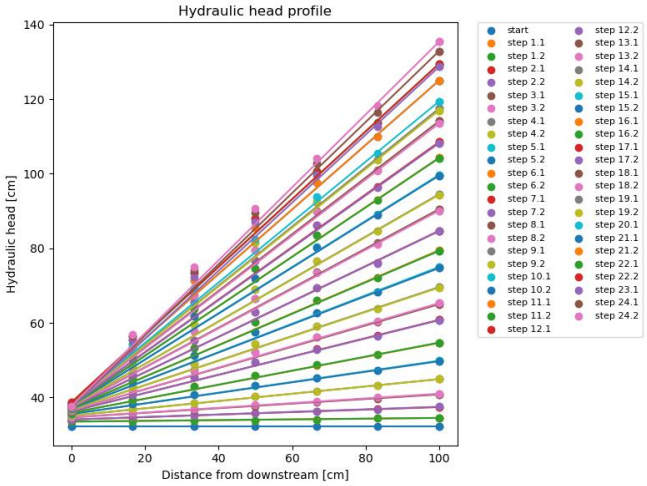

Figure F-130: Hydraulic head profile test 6

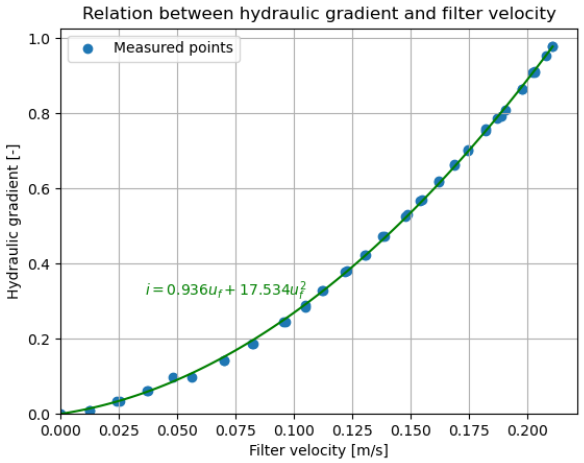

Figure F-131: Forchheimer relation test 6

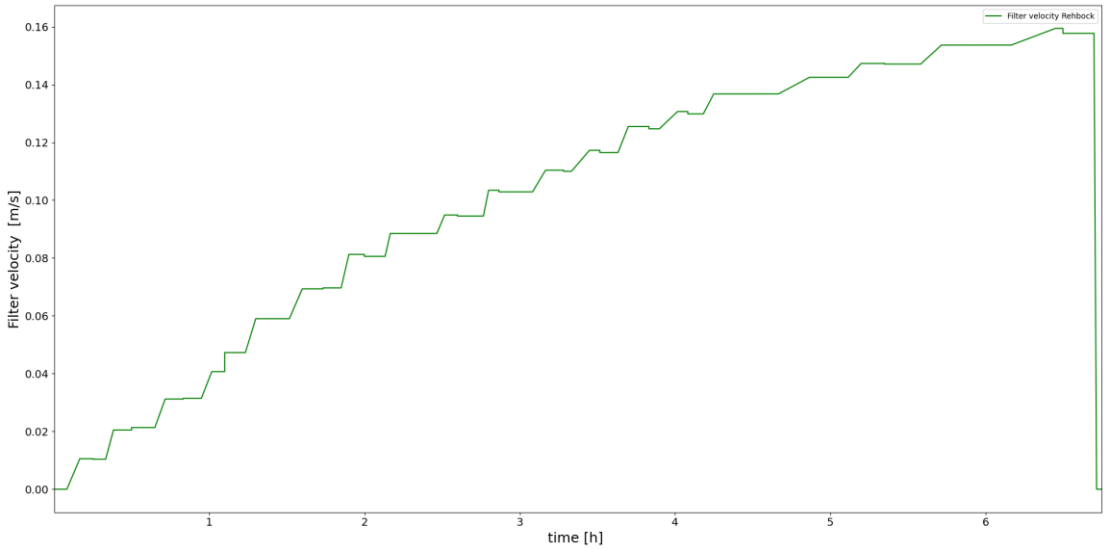

Figure F-132: Filter velocity test 6 day 1

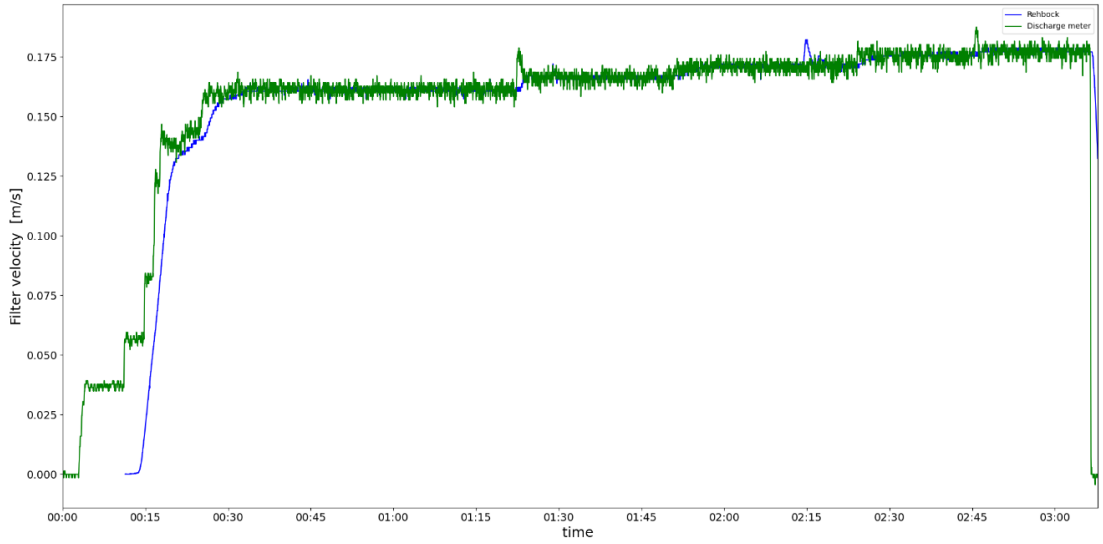

Figure F-133: Filter velocity test 6 day 2

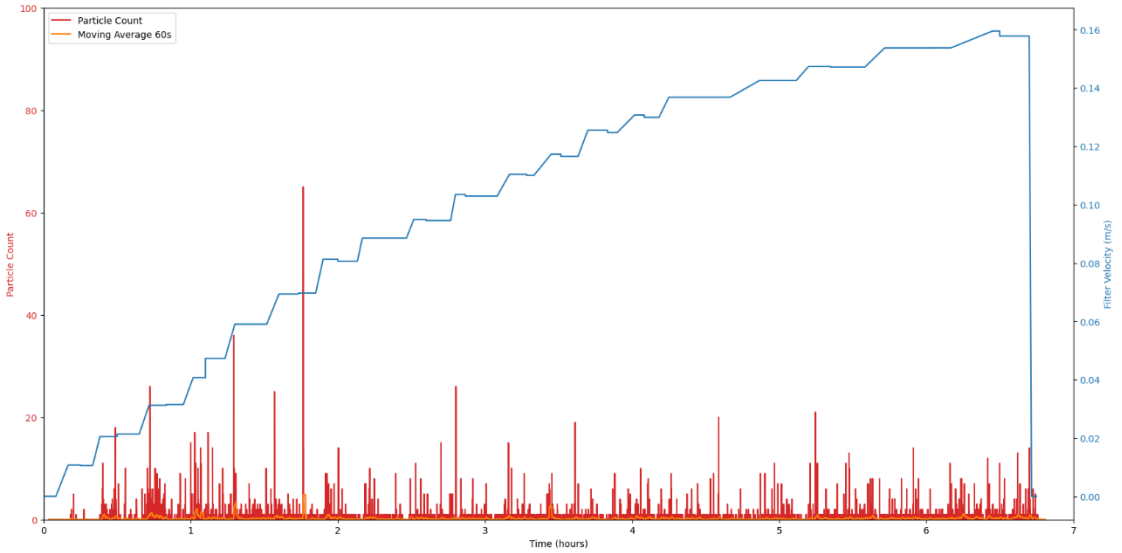

Figure F-134: Sand particles per frame and moving average vs. time, test 6 day 1 camera 50 cm

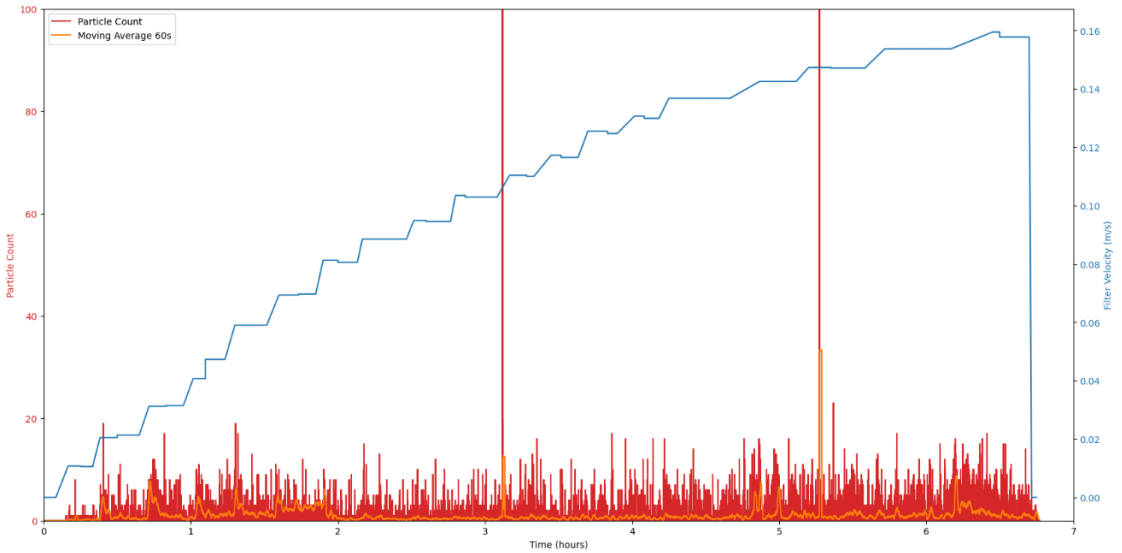

Figure F-135: Sand particles per frame and moving average vs. time, test 6 day 1 camera 75cm

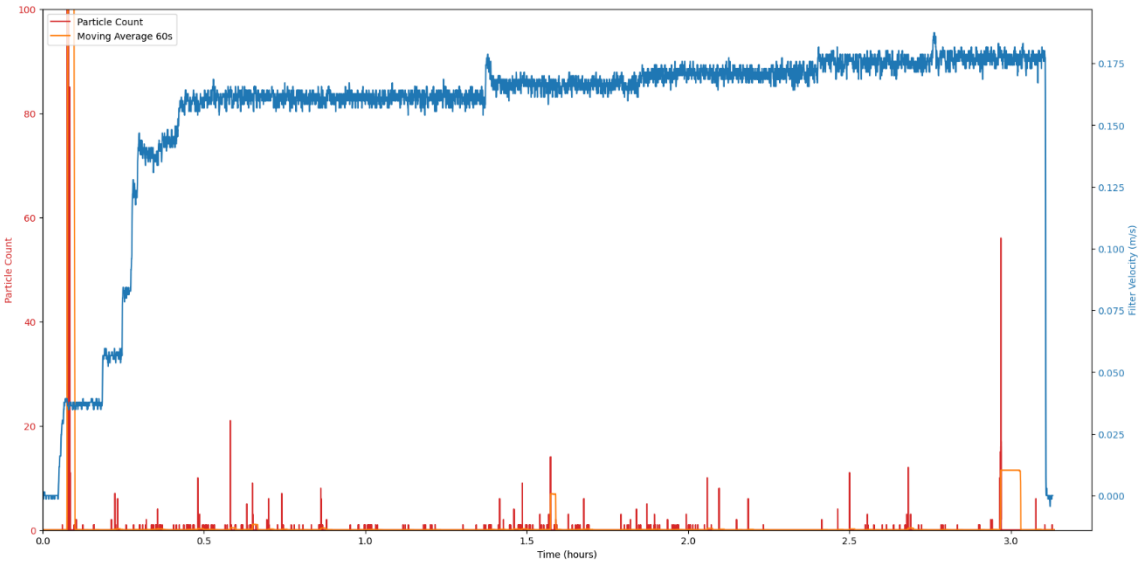

Figure F-136: Sand particles per frame and moving average vs. time, test 6 day 2 camera 50 cm

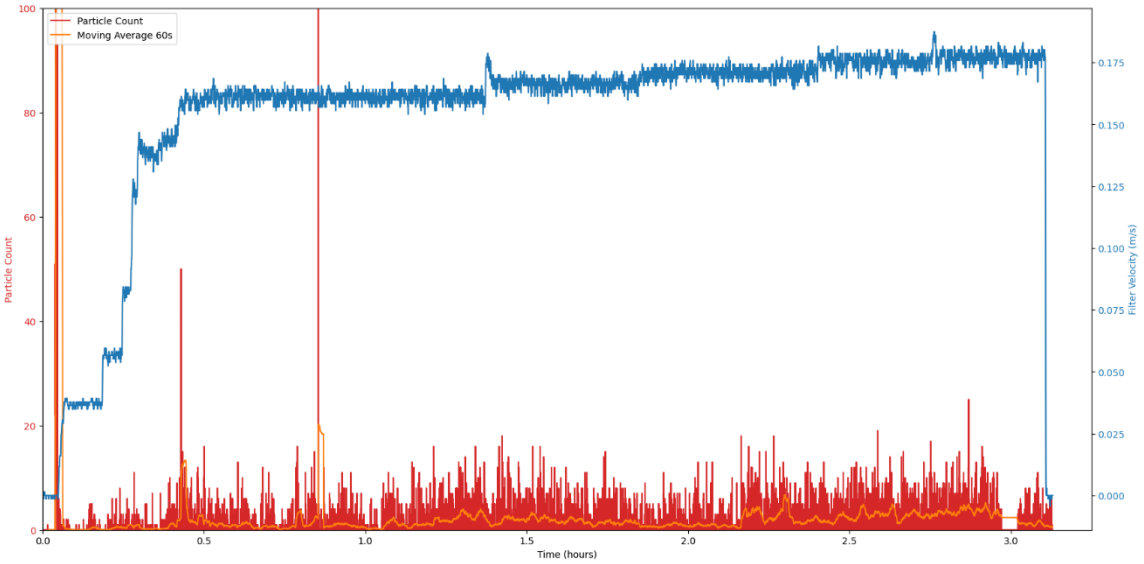

Figure F-137: Sand particles per frame and moving average vs. time, test 6 day 2 camera 75cm

Geotextile and sandbed after test

Figure F-138: Geotextile after test

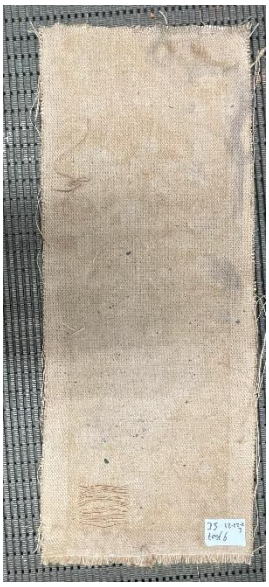

Figure F-139: Dry geotextile after test

Figure F-140: Sandbed after test

F.15 Test 7

Table F-34: Data test 7

Base material (d_{b50})	0.180 (M34)	[mm]
Geotextile	-	
Filter material	40/70 mm	
d_{fn50}	45.73	[mm]
Weight of stones	114.218	[kg]

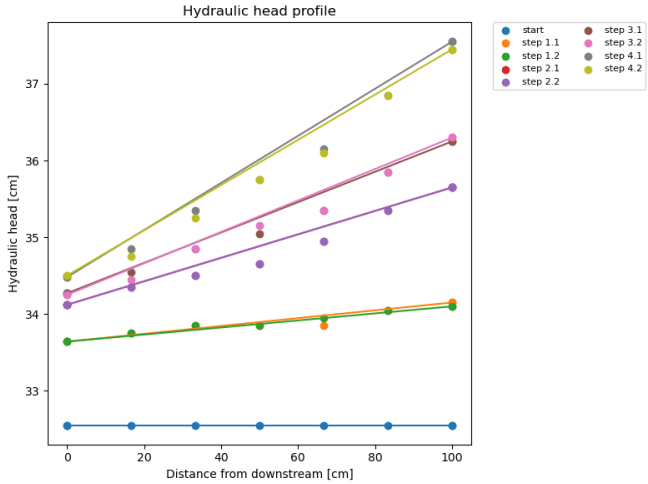

Figure F-141: Hydraulic head profile test 7

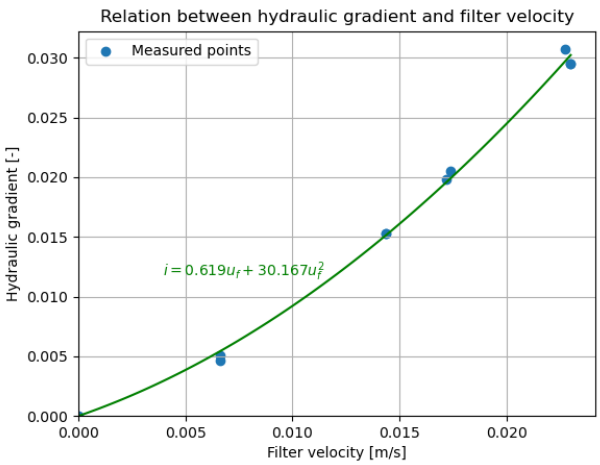

Figure F-142: Forchheimer relation test 7

Due to an error, the flow rate data from this test was recorded with one less decimal place than the other tests, resulting in the graph looking slightly different.

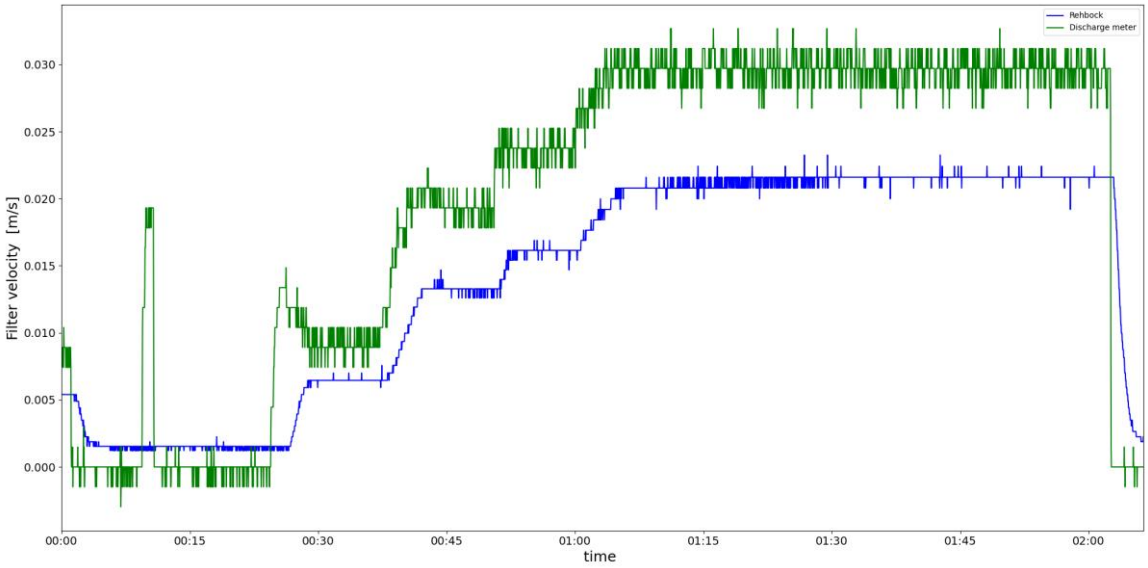

Figure F-143: Filter velocity test 7

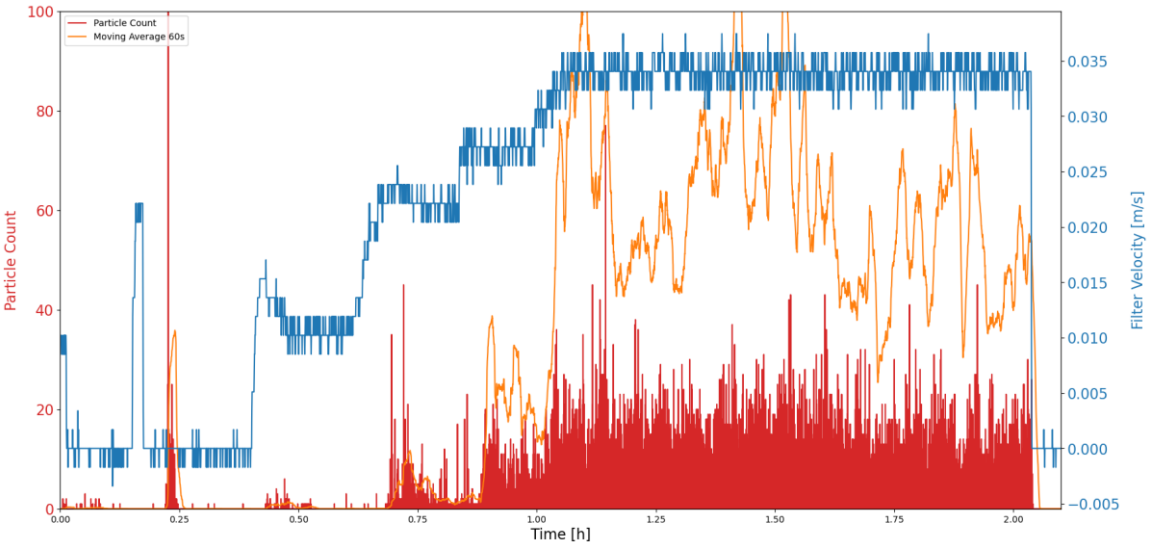

Figure F-144: Sand particles per frame and moving average vs. time, test 7 camera 50 cm

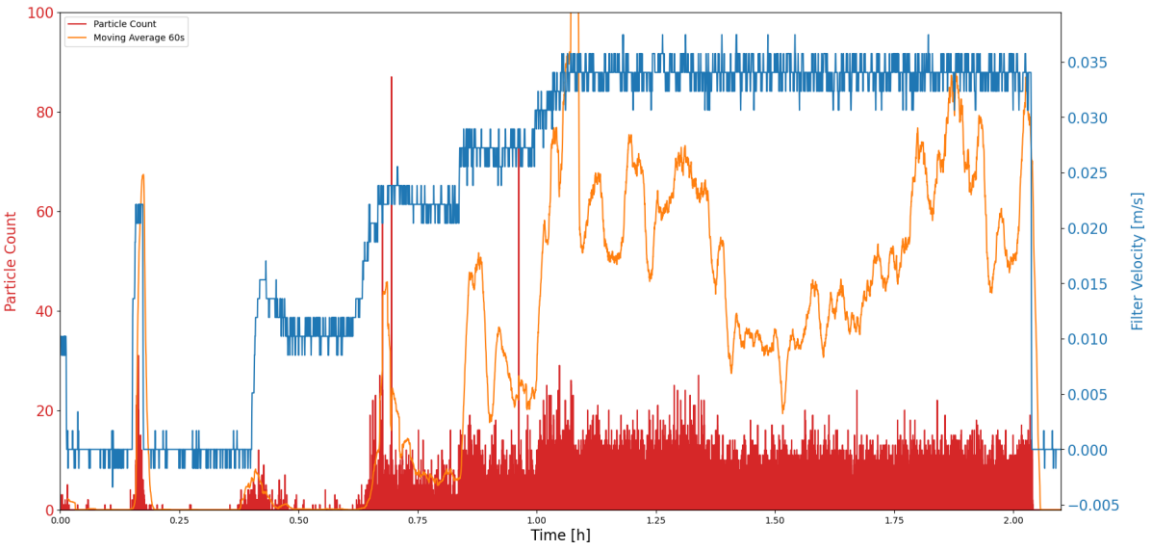

Figure F-145: Sand particles per frame and moving average vs. time, test 7 camera 75cm

Geotextile and sandbed after test

Figure F-146: Sandbed after test

Figure F-147: Sandbed after test

Figure F-148: Sandbed after test

F.16 Test 8

Table F-35: Data test 8

Base material (d_{b50})	0.180 (M34)	[mm]
Geotextile	J4	
Filter material	60-90 mm	
d_{fn50}	61.50	[mm]
Weight of stones	114.218	[kg]

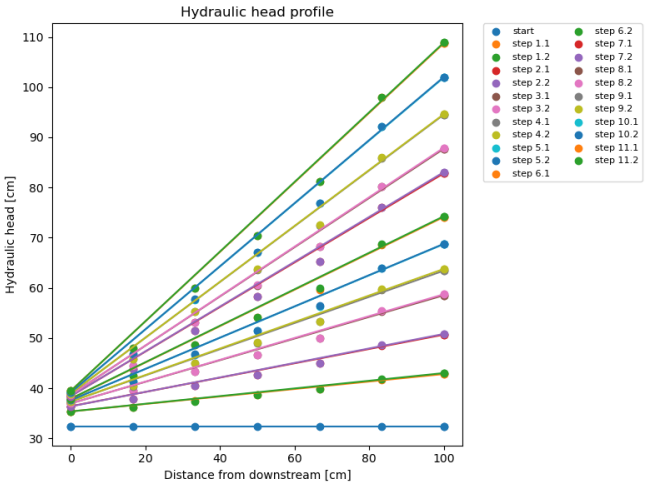

Figure F-149: Hydraulic head profile test 8

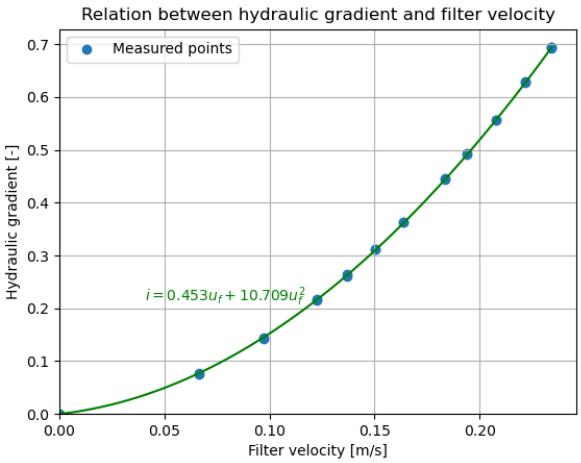

Figure F-150: Forchheimer relation test 8

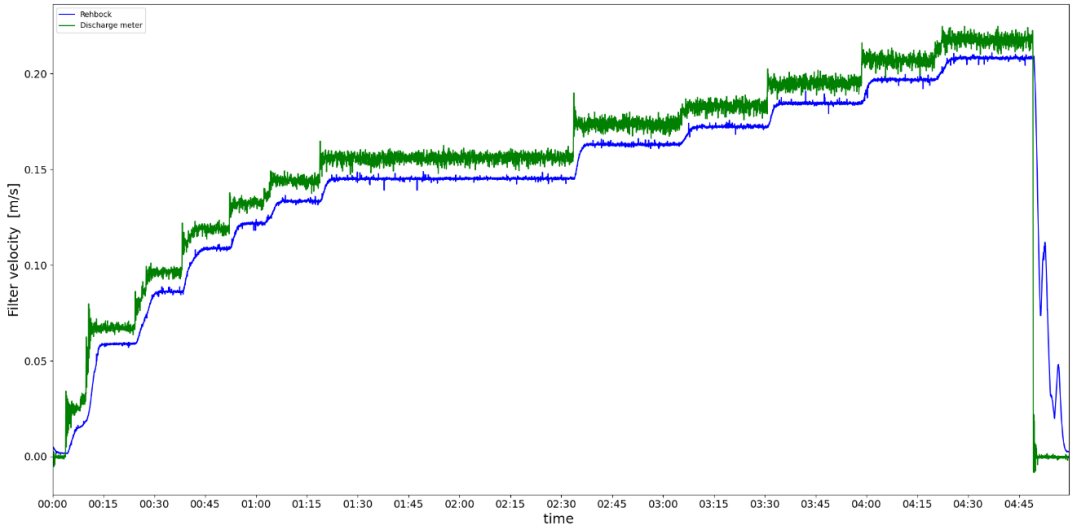

Figure F-151: Filter velocity test 8

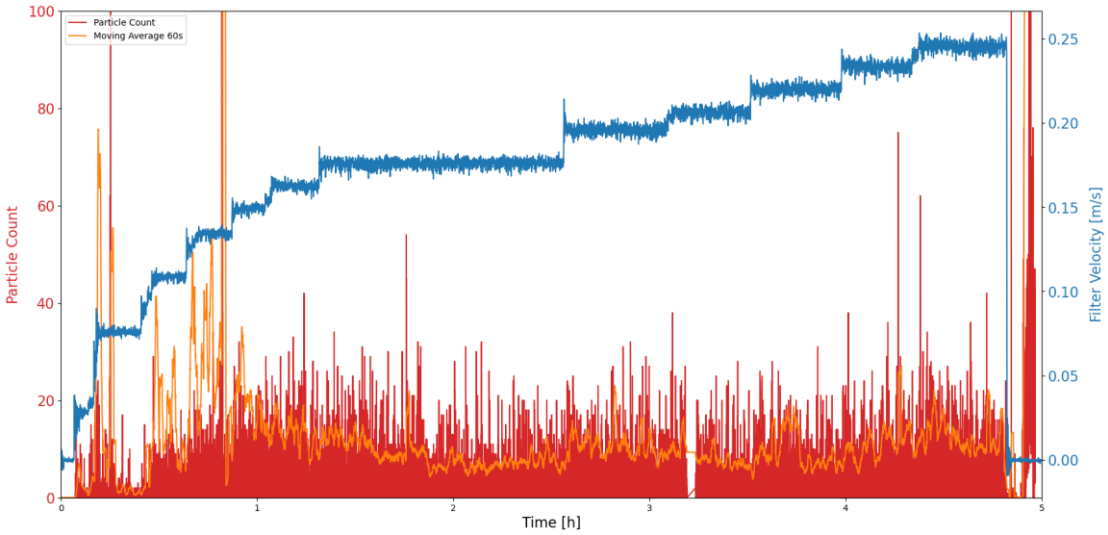

Figure F-152: Sand particles per frame and moving average vs. time, test 8 camera 50 cm

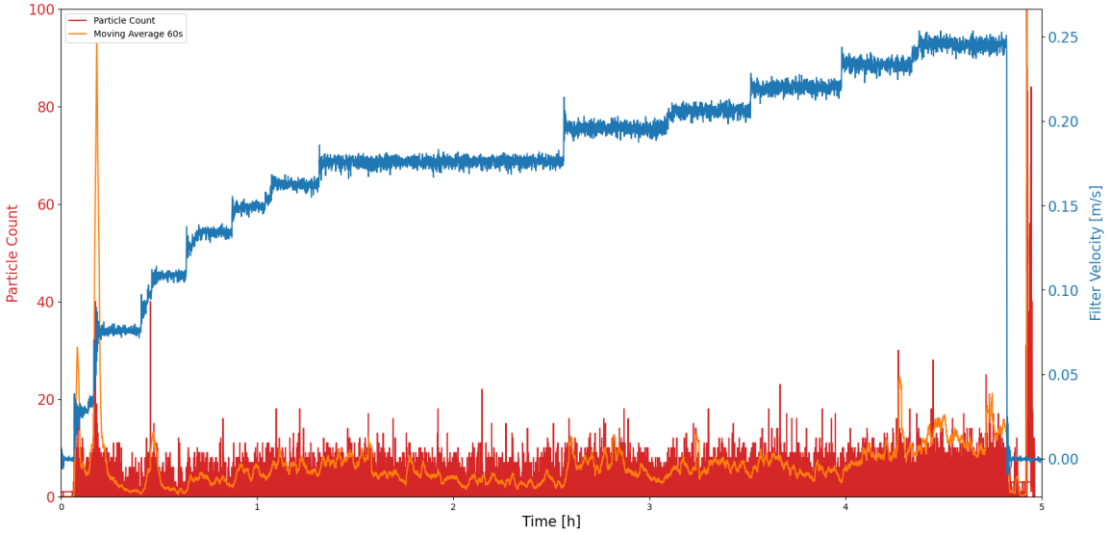

Figure F-153: Sand particles per frame and moving average vs. time, test 8 camera 75cm

Geotextile and sandbed after test

Figure F-154: Geotextile after test

Figure F-155: Dry geotextile after test

Figure F-156: Sandbed after test

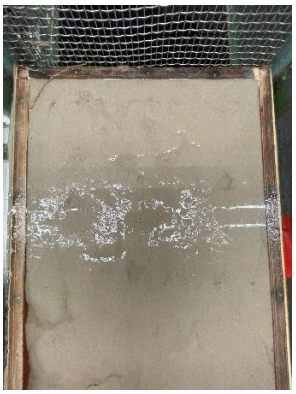

Figure F-157: Sandbed after test at end test set-up

Figure F-158: Sandbed after test at middle test set-up

Figure F-159: Sandbed after test at begin test set-up

F.17 Test 9.1

Table F-36: Data test 9.1

Base material (d_{b50})	0.180 (M34)	[mm]
Geotextile	J4	
Filter material	60-90 mm	
d_{fn50}	61.50	[mm]
Weight of stones	114.218	[kg]

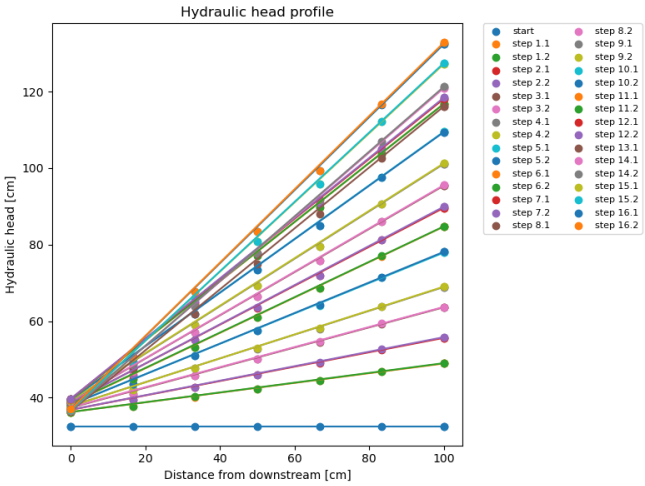

Figure F-160: Hydraulic head profile test 9.1

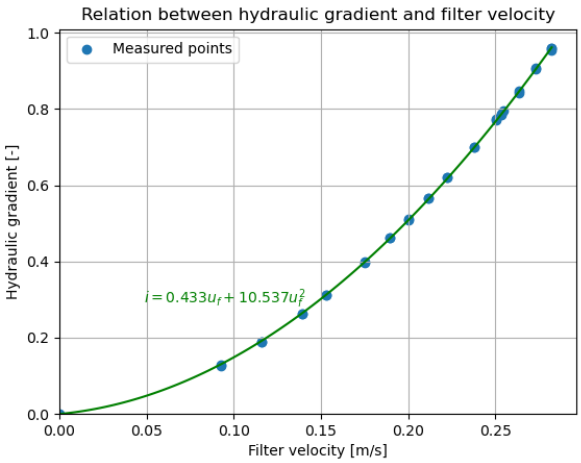

Figure F-161: Forchheimer relation test 9.1

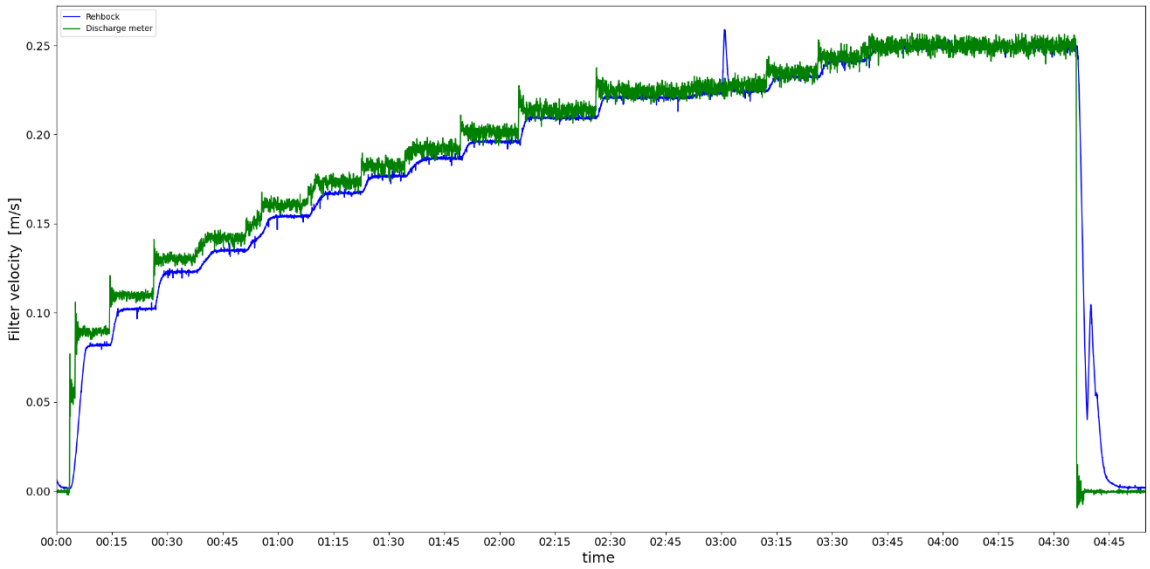

Figure F-162: Filter velocity test 9.1

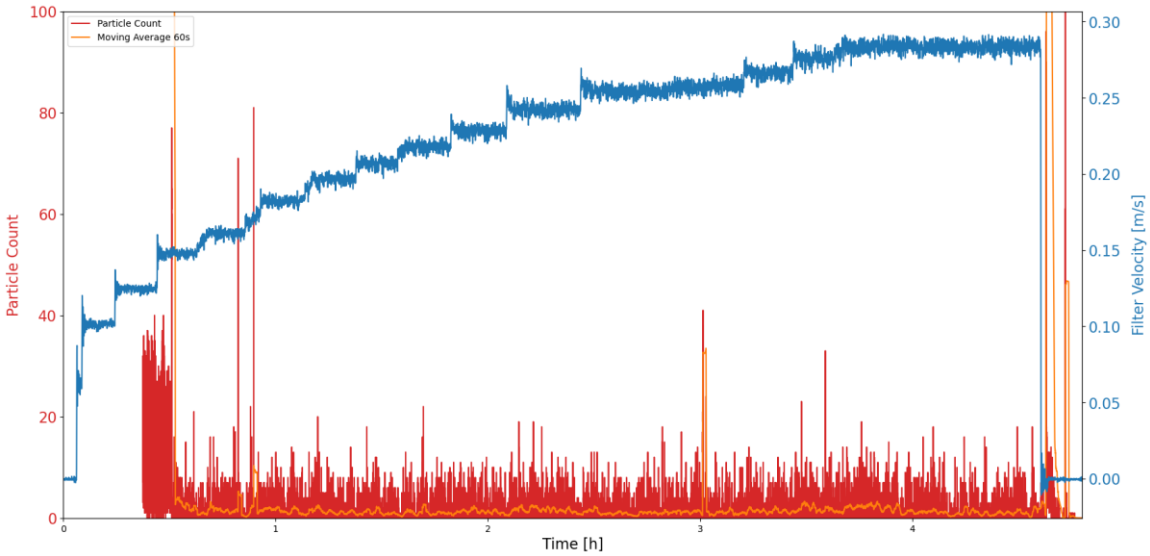

Figure F-163: Sand particles per frame and moving average vs. time, test 9.1 camera 75cm

Geotextile and sandbed after test

Figure F-164: Geotextile after test

Figure F-165: Dry geotextile after test

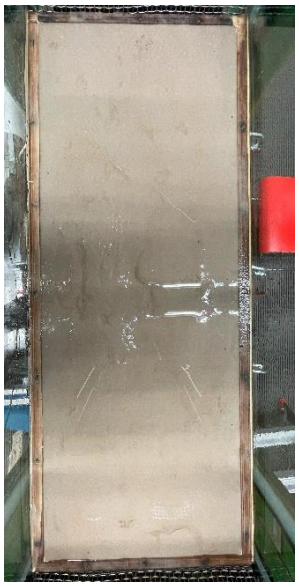

Figure F-166: Sandbed after test

Figure F-167: Sandbed after test at outflow point

Figure F-168: Sandbed after test at middle

Figure F-169: Sandbed after test at inflow point

F.18 Test 9.2

Table F-37: Data test 9.2

Base material (d_{b50})	0.180 (M34)	[mm]
Geotextile	J4	
Filter material	60-90 mm	
d_{fn50}	61.50	[mm]
Weight of stones	114.218	[kg]

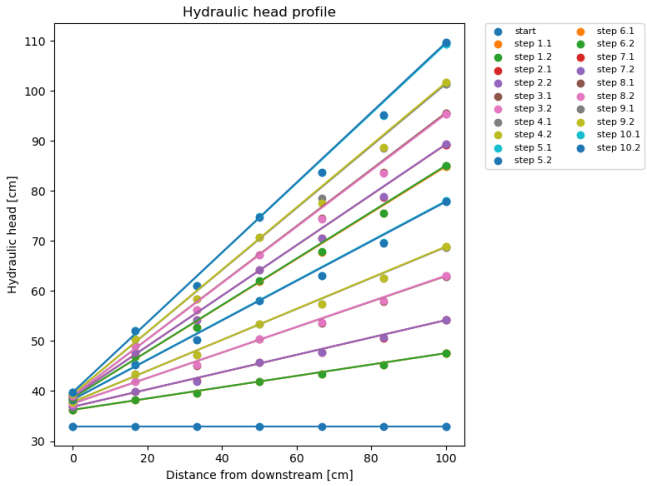

Figure F-170: Hydraulic head profile test 9.2

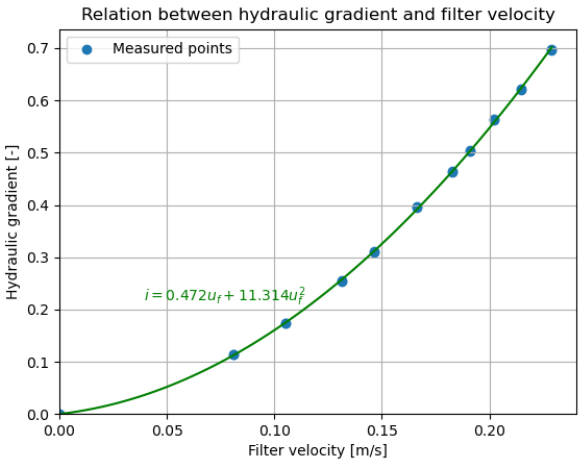

Figure F-171: Forchheimer relation test 9.2

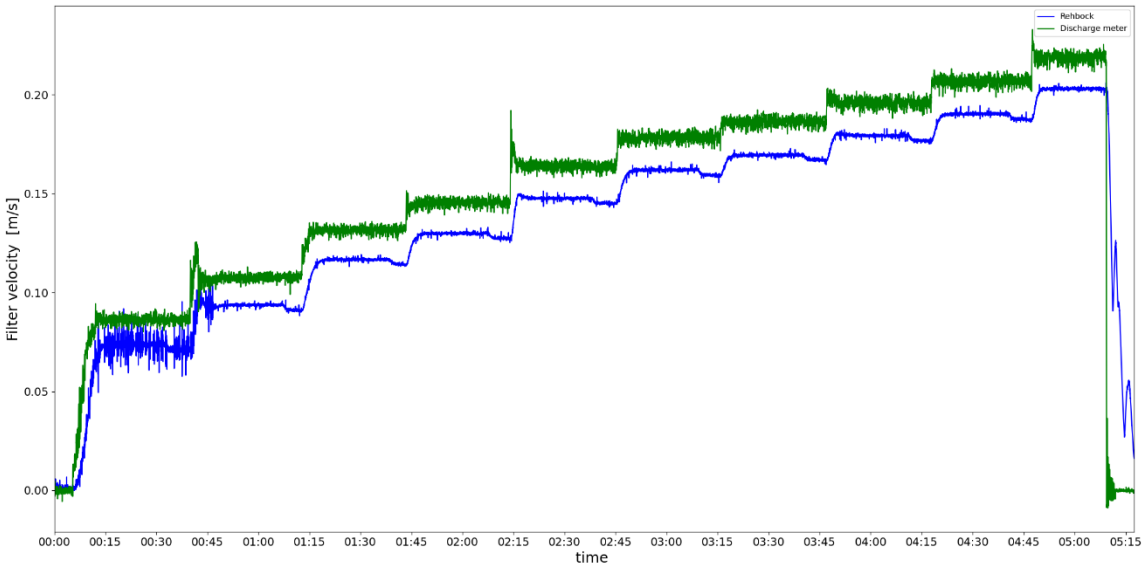

Figure F-172: Filter velocity test 9.2

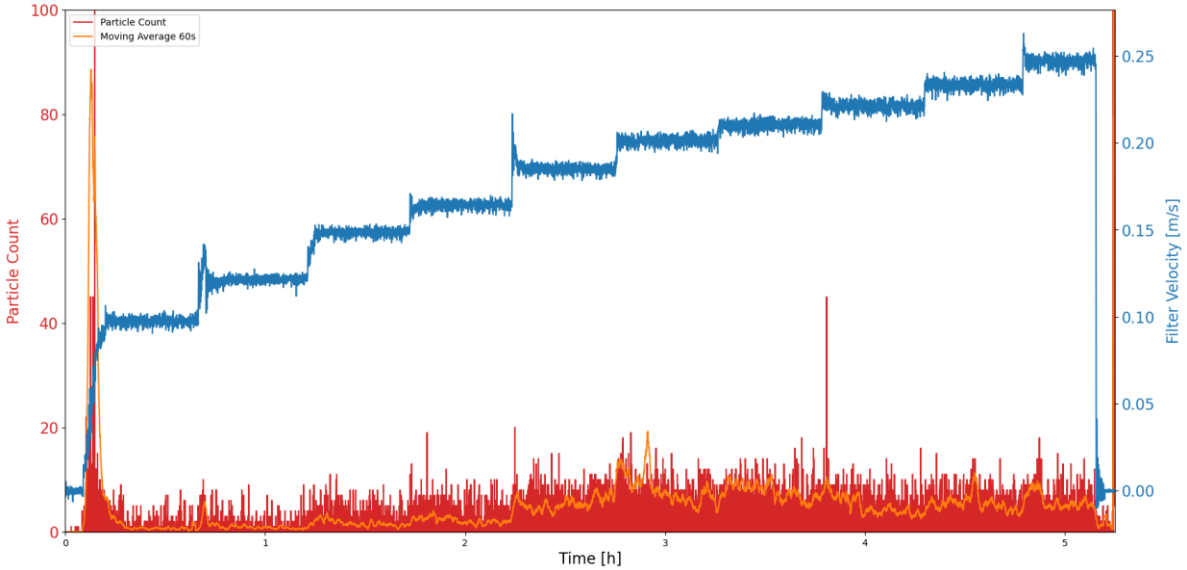

Figure F-173: Sand particles per frame and moving average vs. time, test 9.2 camera 50cm

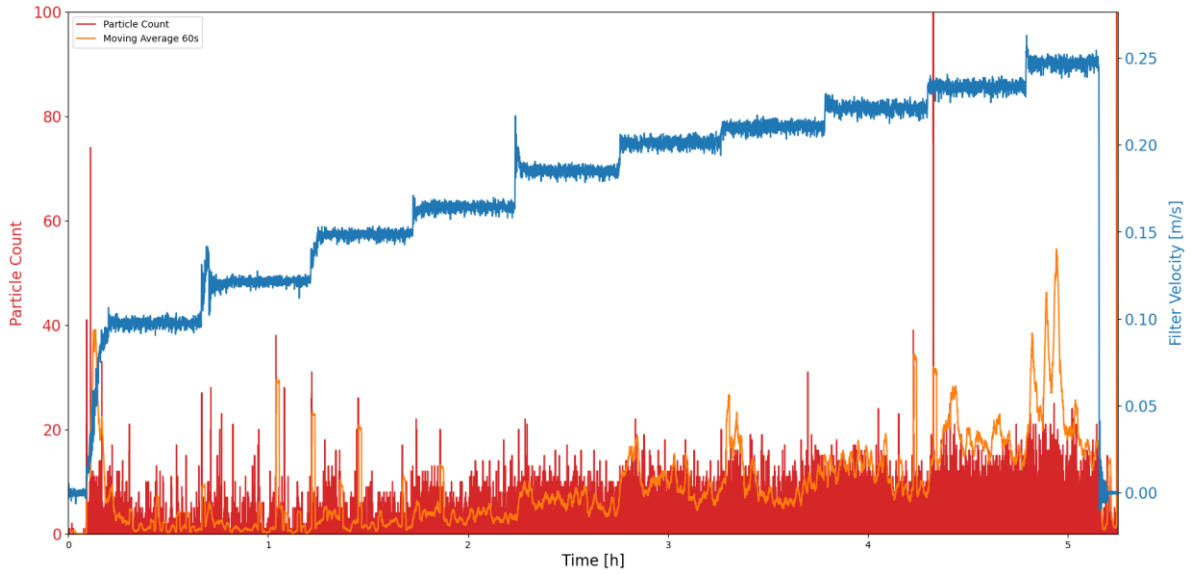

Figure F-174: Sand particles per frame and moving average vs. time, test 9.2 camera 75cm

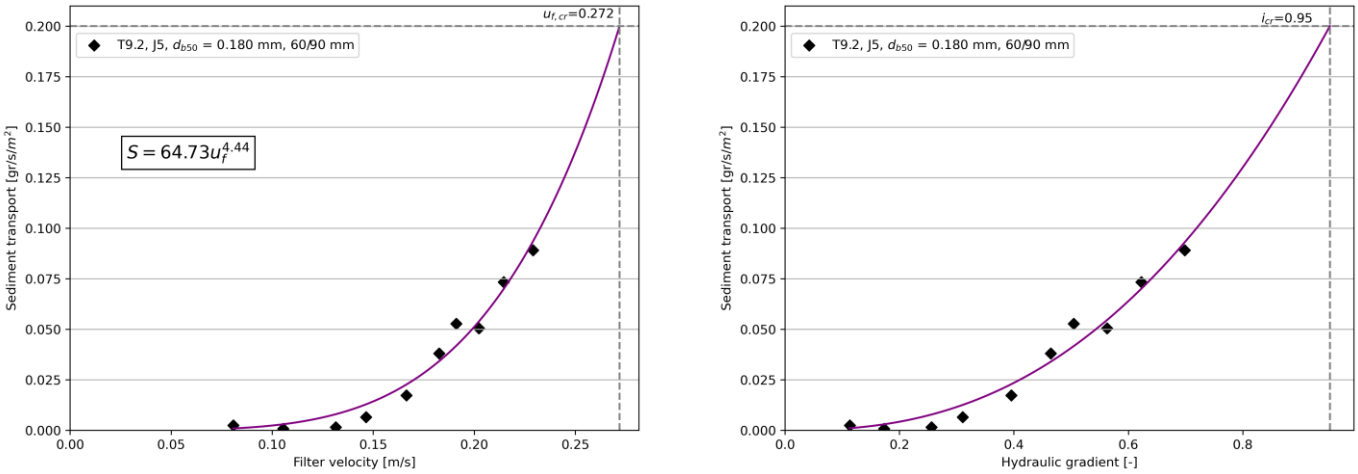

Figure F-175: Transport of base material vs. filter velocity and transport of base material vs hydraulic gradient, test 9.2

Geotextile and sandbed after test

Figure F-176: Geotextile after test

Figure F-177: Dry geotextile after test

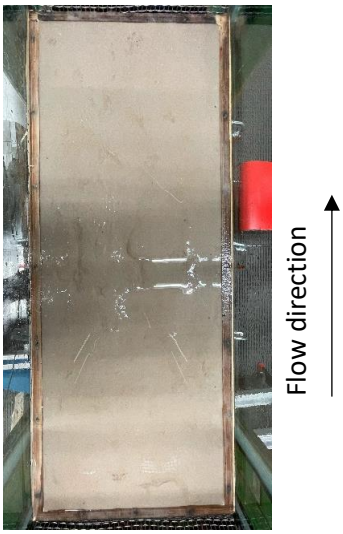

Figure F-178: Sandbed after test

Figure F-179: Sandbed after test at outflow point

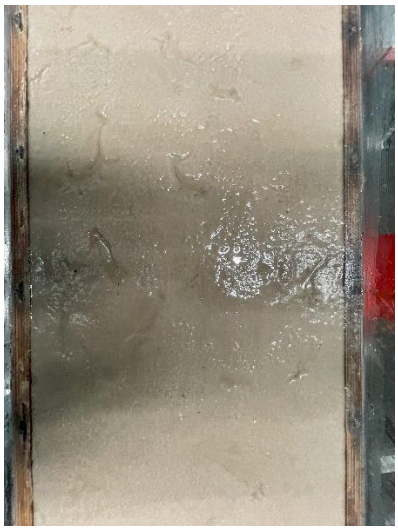

Figure F-180: Sandbed after test at middle

Figure F-181: Sandbed after test at inflow point

F.19 Test 10

Table F-38: Data test 10

Base material (d_{b50})	0.180 (M34)	[mm]
Geotextile	Hemp on jute	
Filter material	45/125 mm	
d_{fn50}	61.79	[mm]
Weight of stones	114.218	[kg]

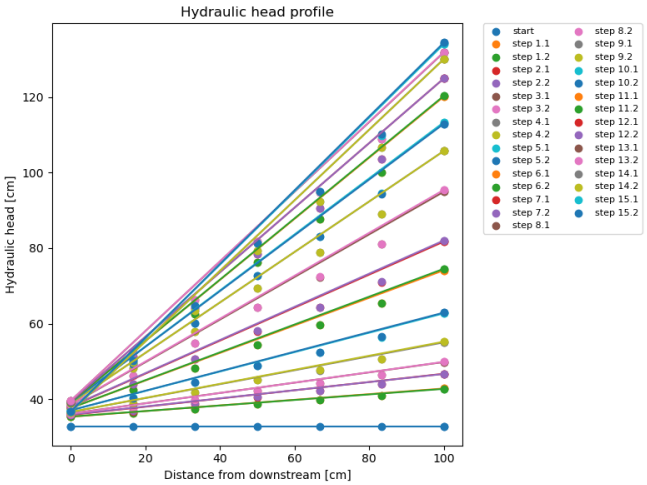

Figure F-182: Hydraulic head profile test 10

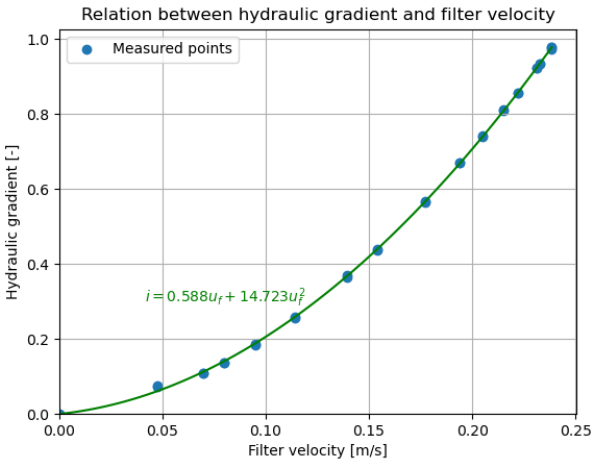

Figure F-183: Forchheimer relation test 10

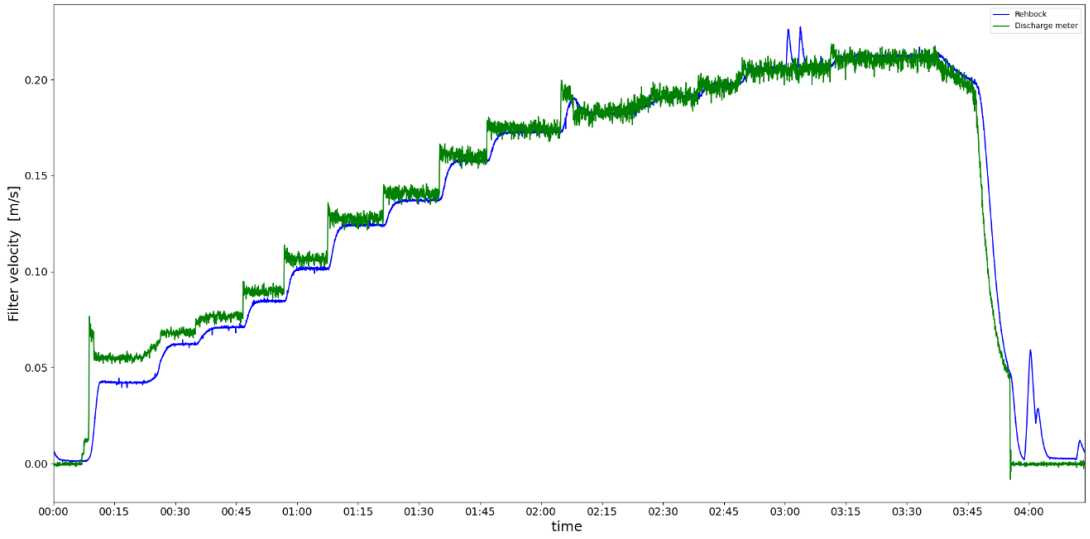

Figure F-184: Filter velocity test 10

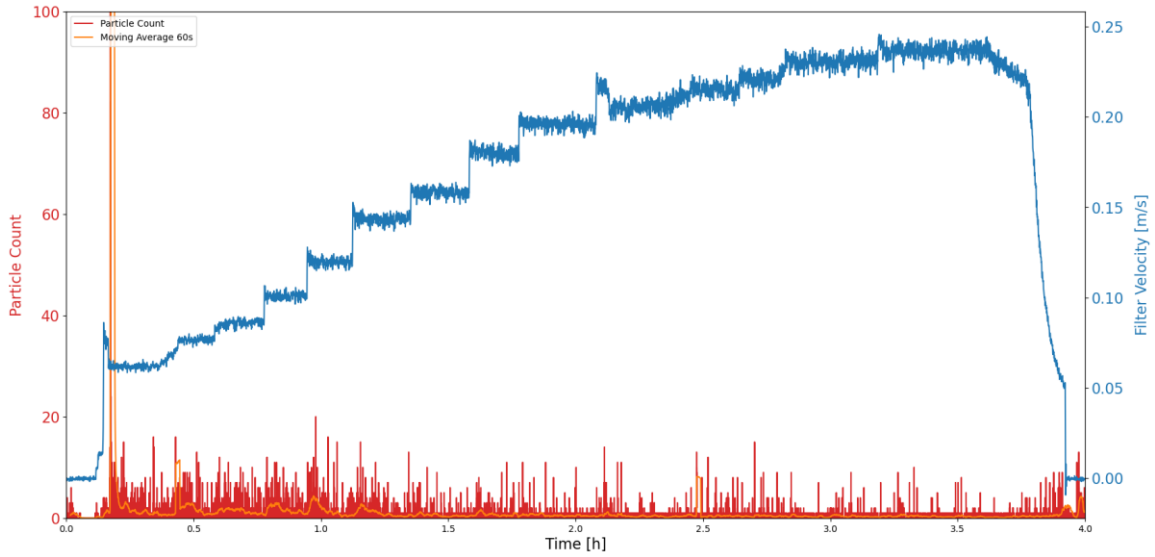

Figure F-185: Sand particles per frame and moving average vs. time, test 10 camera 75cm

Geotextile and sandbed after test

Figure F-186: Geotextile after test

Figure F-187: Sandbed after test

Figure F-188: Sandbed after test

F.20 Test 11

Table F-39: Data test 11

Base material (d_{b50})	0.180 (M34)	[mm]
Geotextile	Jute on jute	
Filter material	45/125 mm	
d_{fn50}	61.79	[mm]
Weight of stones	114.218	[kg]

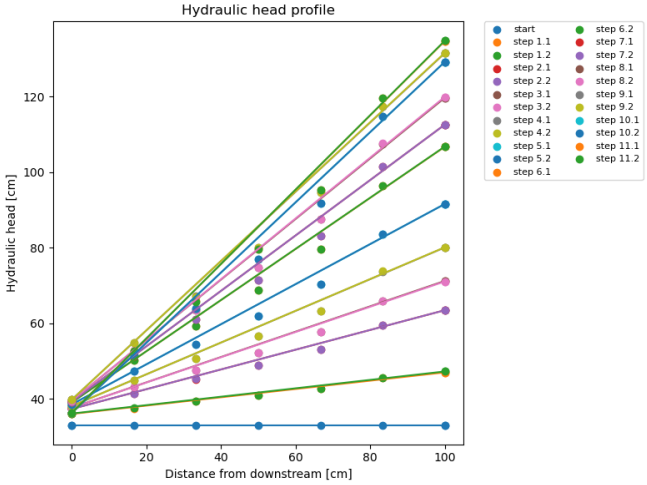

Figure F-189: Hydraulic head profile test 11

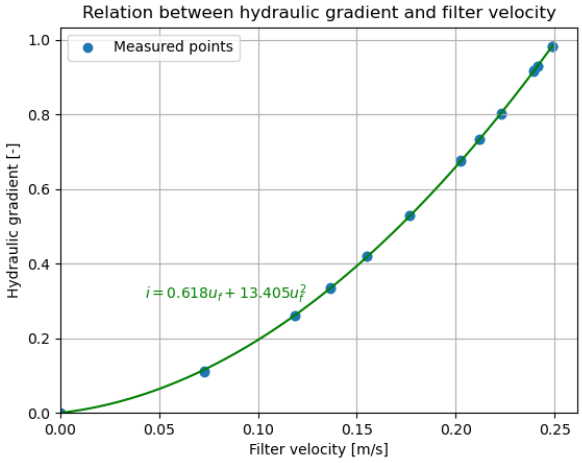

Figure F-190: Forchheimer relation test 11

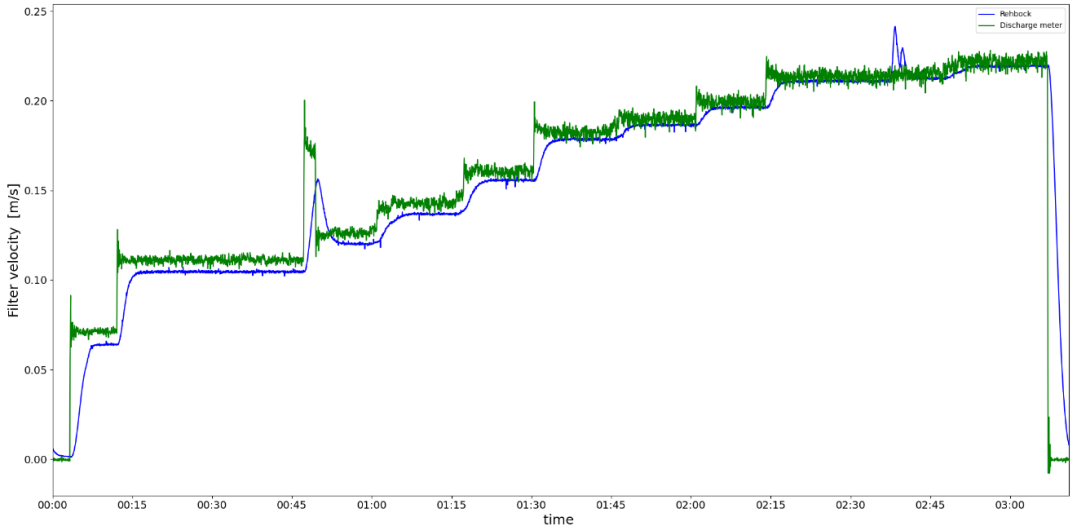

Figure F-191: Filter velocity test 11

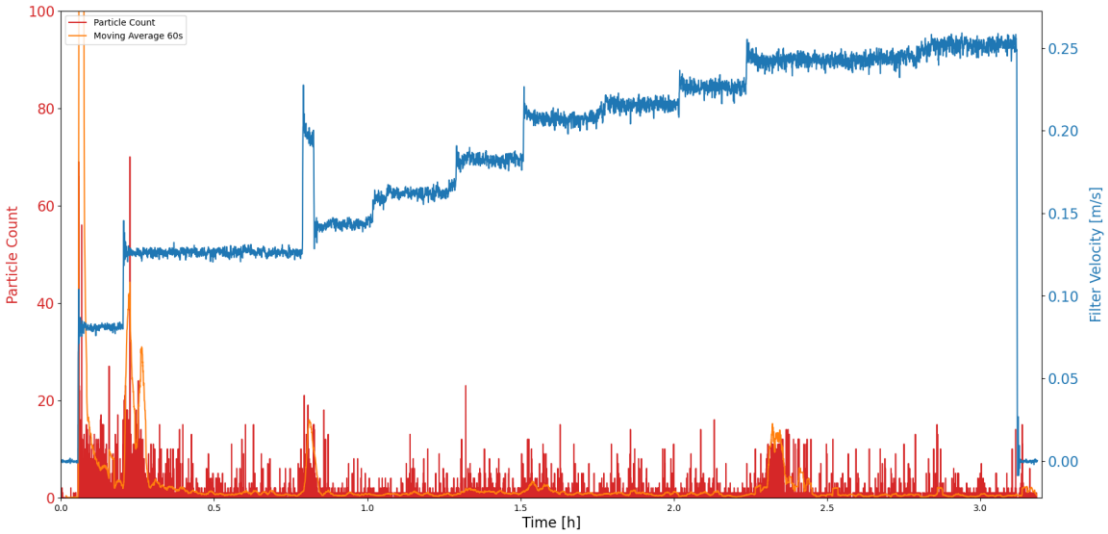

Figure F-192: Sand particles per frame and moving average vs. time, test 11 camera 75cm

Geotextile and sandbed after test

Figure F-193: Geotextile after test

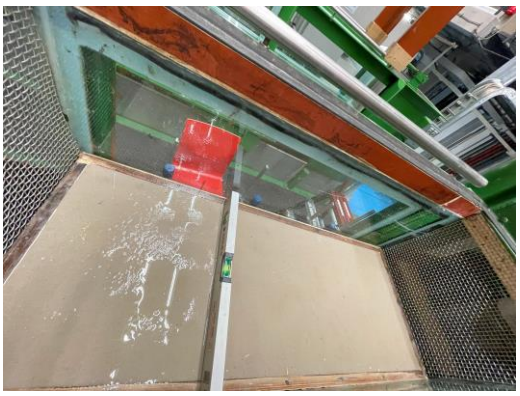

Figure F-194: Sandbed after test

F.21 Test 12

Table F-40: Data test 12

Base material (d_{b50})	0.180 (M34)	[mm]
Geotextile	Wool on jute	
Filter material	45/125 mm	
d_{fn50}	61.79	[mm]
Weight of stones	114.218	[kg]

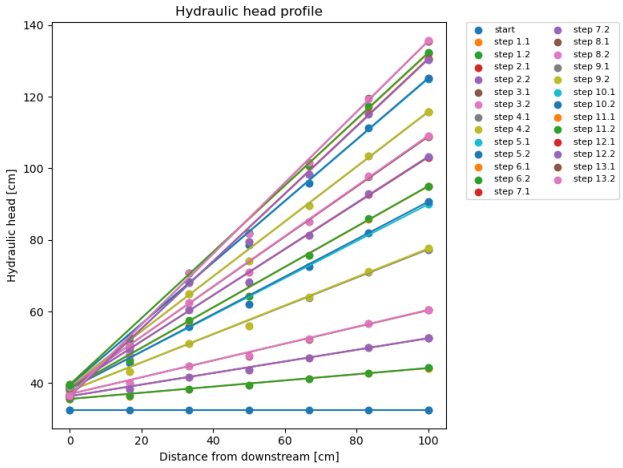

Figure F-195: Hydraulic head profile test 12

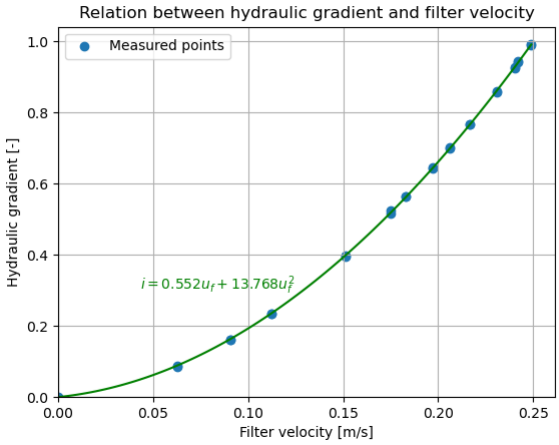

Figure F-196: Forchheimer relation test 12

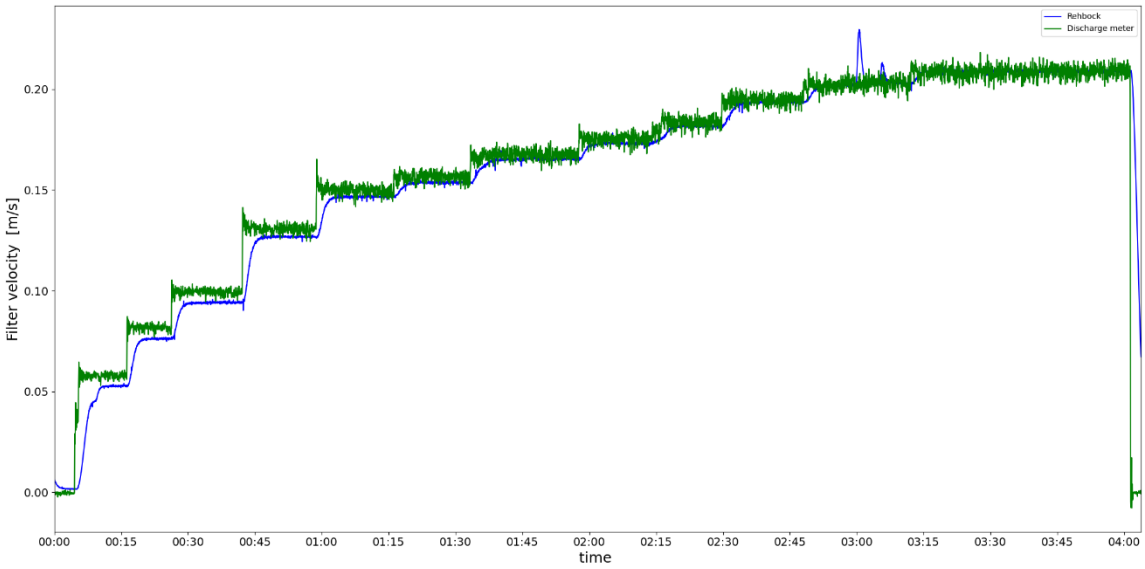

Figure F-197: Filter velocity test 12

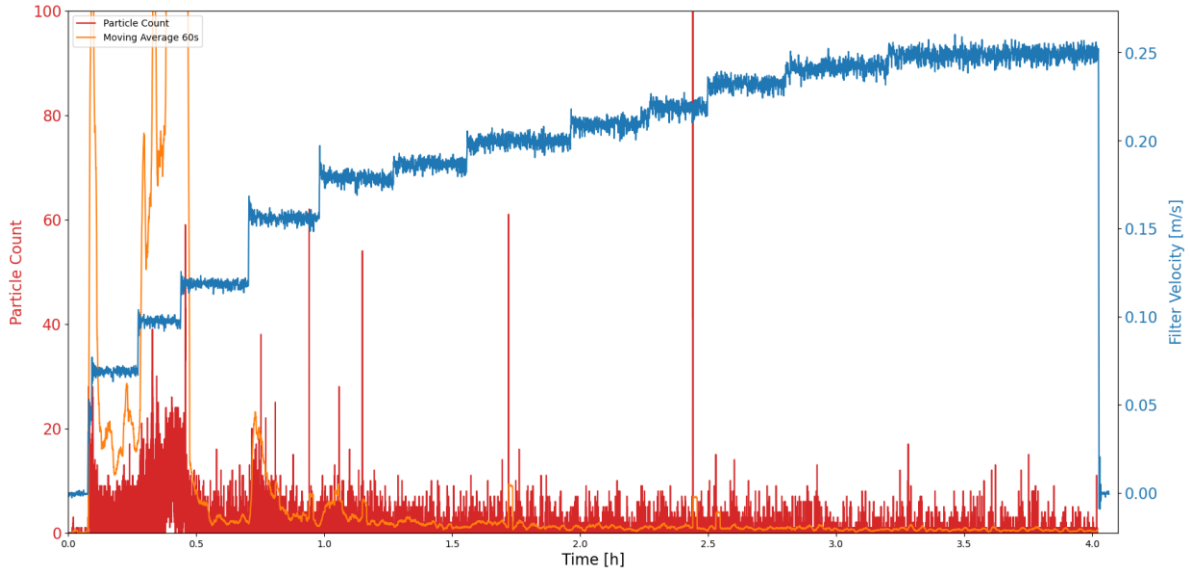

Figure F-198: Sand particles per frame and moving average vs. time, test 12 camera 50cm

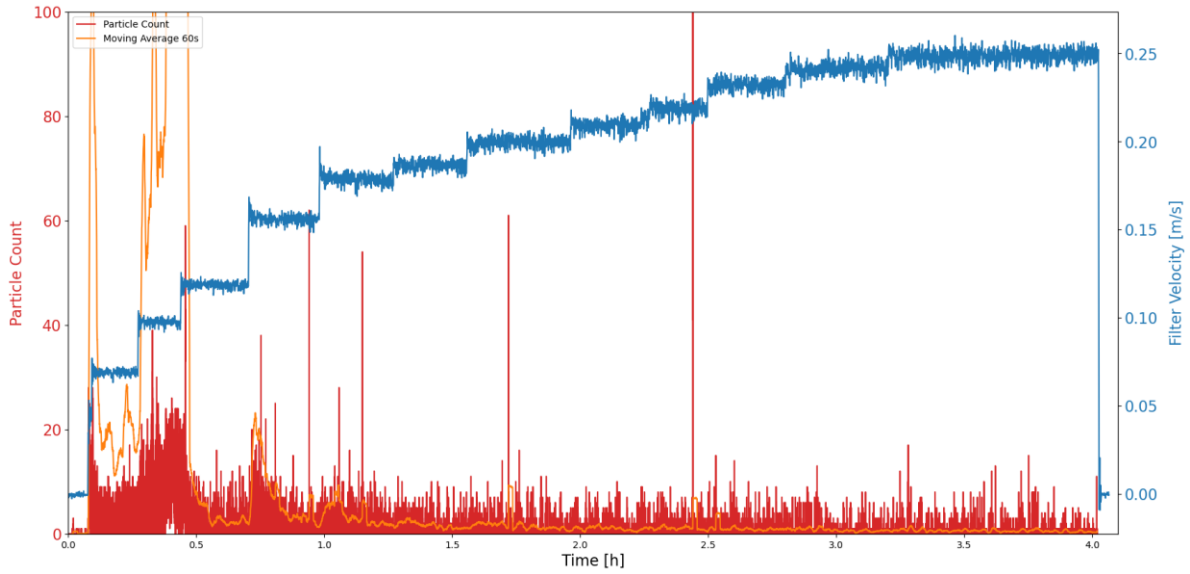

Figure F-199: Sand particles per frame and moving average vs. time, test 12 camera 75cm

Geotextile and sandbed after test

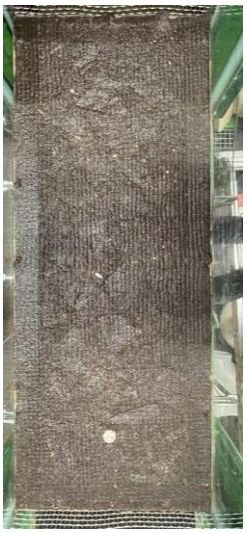

Figure F-200: Geotextile after test

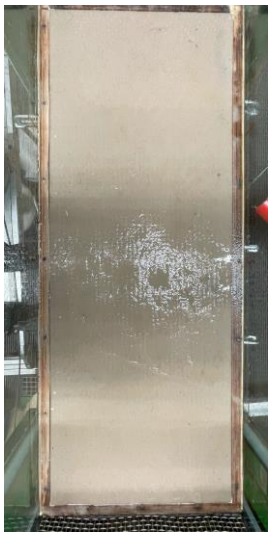

Figure F-201: Sandbed after test

Figure F-202: Sandbed after test

Appendix G Test set-up perpendicular flow

In the figure below (Figure G-1), a 3D impression is shown of a set-up for testing geotextiles with perpendicular flow. In Figure G-2, a cross-section of the set-up is presented.

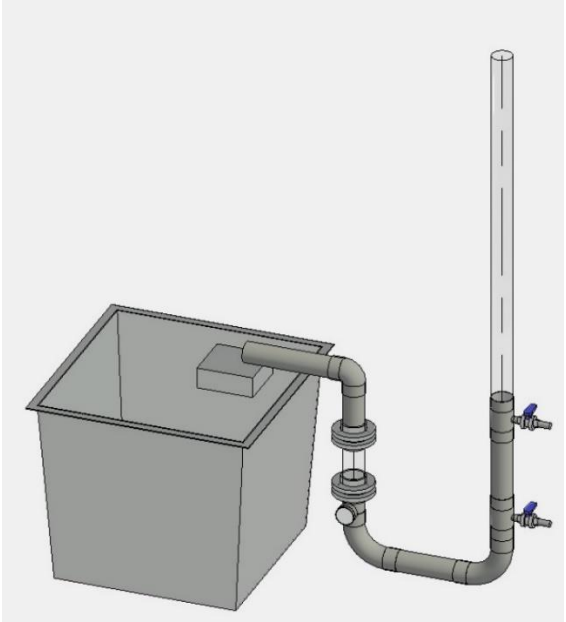

Figure G-1: 3D impression of test set-up perpendicular flow

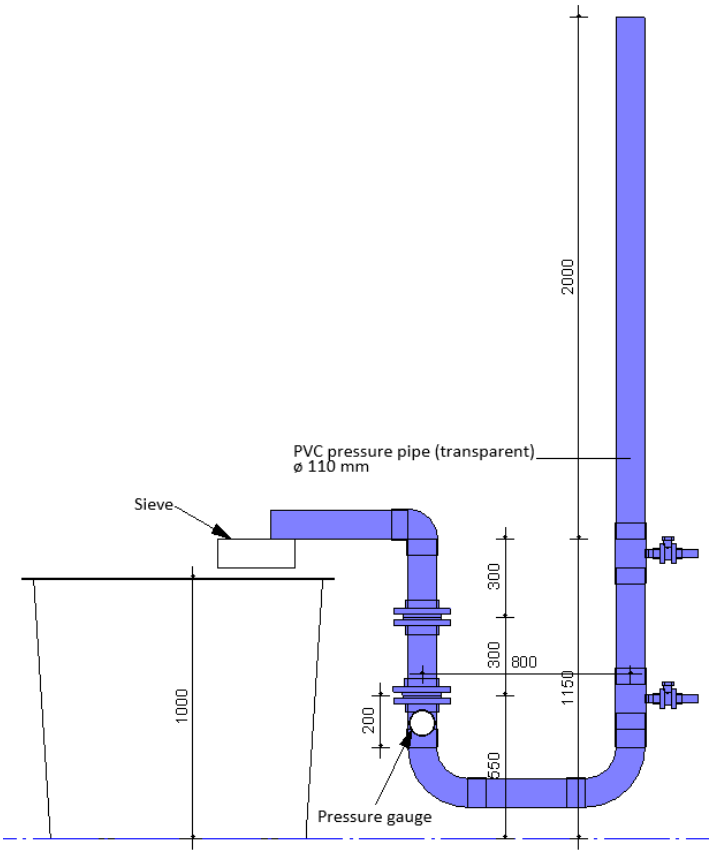

Figure G-2: Cross-section test set-up perpendicular flow